Mechanosensitive Biological Functions: From Membrane Tension to Synthetic Exocytosis

by

Yen-Yu Hsu

A dissertation submitted in partial fulfillment
of the requirements for the degree of
Doctor of Philosophy
(Mechanical Engineering)
in the University of Michigan
2024

Doctoral Committee:

Associate Professor Allen Liu, Chair
Professor Jianping Fu
Assistant Professor Tobias W Giessen
Professor Katsuo Kurabayashi, New York University

Yen-Yu Hsu

yenyu@umich.edu

ORCID iD: 0000-0003-0866-6184

Dedication

To my family, friends, and mentors

Acknowledgements

I am grateful for the unwavering support of my advisor, Dr. Allen Liu, without whom this work would not have come to fruition. I extend my sincere appreciation to Allen for affording me the invaluable opportunity to contribute to his lab's research over the past four years. His consistent guidance has profoundly shaped my growth as a researcher, and I am deeply thankful for his mentorship. Dr. Liu's work ethic and humanity have been a wellspring of inspiration to me. His dedication to scientific inquiry has fostered my admiration, and I am particularly grateful for his unwavering commitment to excellence. I am also indebted to him for his thoughtful recommendations on training and workshops, as well as his generous financial support, which has enhanced my expertise and skill set in this field of study. Working in Liu Lab has been a transformative experience, and I hold Dr. Liu in high esteem as a mentor. His profound impact on my academic journey cannot be overstated.

My gratitude extends to the members of the Liu Lab, both past and present, who have fostered an environment of kindness and support. First of all, I extend my heartfelt thanks to Sagardip for introducing me to experimental research and instilling in me a foundation of good laboratory practices during my initial training. I would like to acknowledge Max and Jophin for their insightful discussions on cell biology, which have greatly enriched my understanding. To my fellow lab members Hossein, Sung-Won, Nadab, and Samuel, whose focus aligns with mine in the realm of synthetic biology, I offer thanks for their valuable insights and the stimulating discourse that has invigorated my work over the past year. Finally, I reserve a special place of gratitude for

Grace, my best friend and closest lab mate since the time we joined the lab. Her unwavering support, thoughtful advice, and even the culinary sustenance she provided during challenging research junctures have been a constant source of solace and encouragement.

Beyond the laboratory, I would also like to thank my committee members, Dr. Jianping Fu, Dr. Katsuo Kurabayashi, and Dr. Tobias Giessen for their valuable feedback on my research and genuine interest in my career development. My sincere thanks also extend to the Department of Mechanical Engineering staff for their prompt and effective resolution of any challenges that crossed my path. To my friend Albert, who stood by me during the arduous process of learning and exploring the sciences, I am profoundly grateful. A heartfelt tribute goes to my sister Catherine for her unflagging emotional and moral support throughout my PhD pursuit.

In the end, I am indebted to my parents, whose unwavering support has played an integral role in shaping the person I am today. Their love and guidance have been my guiding lights. This thesis is dedicated to their well-being and enduring influence.

Table of Contents

List of Tables

List of Figures

Abstract

Cell communication is crucial for coordinating development and facilitating environmental adaptations in biological processes. Cells receive and transmit messages through various chemical or physical signals, including mechanical force, which is transmitted via mechanosensitive (MS) ion channels. These channels convert mechanical inputs into biochemical or electrical signals, regulating cellular behaviors.

Despite the presence of MS channels as natural membrane tension sensors, a lack of suitable measurement tools has hindered the characterization of membrane tension changes in living cells. In Chapter 2, I developed an optical membrane tension reporter using a genetically modified MS channel, MscL, incorporating circularly permuted green fluorescence protein (cpGFP). This reporter serves as an OFF sensor in living cells, with fluorescence negatively correlated to membrane stretching and substrate stiffness, offering a valuable approach for detailed investigations in cellular membrane biophysics.

While many MS channels have been investigated in living cells, studying their molecular mechanisms in response to mechanical force remains challenging due to the complexity of their protein structures, interactions with other cellular components, low expression levels, and toxicity issues in conventional cell culture systems. Therefore, in Chapter 3, I describe the use of cell-free expression (CFE) systems encapsulated inside lipid bilayers vesicles to reconstitute a putative MS channel found in fission yeast, Pkd2, and delved into its function without the involvement of complex cell signaling pathways. By co-encapsulating a cell-free expressed calcium indicator G-

GECO with Pkd2 inside vesicles, I demonstrated that Pkd2 became calcium permeable when vesicle membranes were being stretched by hypo-osmotic shock. Moreover, the peak fluorescence intensities increased proportionally to the strength and duration of hypo-osmotic pressure. Our findings present the potential of using synthetic cells as a useful reconstitution platform for in vitro study of MS channels and other complicated membrane proteins.

Realizing synthetic cells provide a powerful platform to replicate cellular functions, the final goal of my dissertation is to construct synthetic cells capable of intercellular communication, based on mimicking calcium-triggered exocytosis in living cells. It is well known that membrane fusion is an essential process for exocytosis. In Chapter 4, I describe the development of a DNA-mediated membrane fusion system that can be triggered by calcium ions by using surface-bound PEG (polyethylene glycol) chains which are cleavable by calpain, a calcium-activated protease. I demonstrated that membrane interactions and fusions are only observed in the presence of calcium ions, mimicking in vivo SNARE-mediated membrane fusion by recapitulating its calcium-dependent nature. I further showed that this strategy can be integrated into a vesicle-in-vesicle system reconstituted with MS channels for generating force-activated synthetic exocytosis which could enable communication between synthetic cells and natural cells in the future.

In summary, my dissertation established the application of MS channel as an optical membrane tension reporter in living cells. I also advanced knowledge by leveraging encapsulated CFE systems inside synthetic cells for in vitro study of Pkd2p channels. To explore the use of the synthetic cell platform for controlled cell communications, a calcium-dependent membrane fusion strategy was developed and used in vesicle systems for the reconstitution of synthetic exocytosis, which can be integrated with mechanosensing mechanisms using MS channels. By improving the understanding of the biological functions of MS channels, I hope this research can help decipher

the sophisticated mechanism of force-dependent signaling pathways and explore their potential biomedical applications.

Chapter 1 Introduction

1.1 Cellular communication through cell signaling pathways

In the complex symphony of life, cells harmonize through a complex dance of communication, orchestrating fundamental physiological processes essential for the intricate functioning of the human body. Much like a community relies on conversations for smooth operation, individual cells engage in a continuous interaction to coordinate activities such as growth, division, differentiation, migration, and programmed cell death[1]. This dynamic interplay, integral to life itself, constitutes the essence of cell signaling pathways.

The study of cell communication delves into the mechanisms by which a cell both imparts and receives messages, creating a dynamic dialogue with its environment and internally with other cellular components. Survival hinges on the cell's ability to receive and process information from the extracellular cues, whether that information pertains to mechanical, electrical, or chemical stimuli. Cells are not solitary entities; they interact directly, fine-tuning their functions through a myriad of chemical and mechanical signals. In the complex tapestry of multicellular organisms, cell signaling facilitates the specialization of cell groups, enabling the formation of tissues like muscle, blood, and brain tissue. Even in single-celled organisms, signaling coordinates populations of cells, transforming them into a cohesive team capable of achieving tasks beyond the capacity of an individual cell.

The exploration of cell signaling traverses diverse biological disciplines, including developmental biology[2], neurobiology[3], and endocrinology[4]. Two primary domains capture the essence of this communication: membrane signaling and intracellular communication. Membrane

signaling involves intricately shaped proteins, acting as receptors embedded in the cell membrane, connecting external triggers to the dynamic chemistry within the cell[5]. Mechanosensitive (MS) ion channels exemplify this, responding to external mechanical stimuli by altering their pore open probability under increasing plasma membrane tension and, consequently, allowing the passage of selected ions and small molecules, causing biochemical or electrochemical gradient, to regulate cellular behavior[6,7]. For intracellular communication, cells have evolved an array of signaling mechanisms to transmit vital biological information. Diverse instances of this complexity include receptors facilitating ion currents in response to photons, effectively transducing light into chemical messengers within the cone and rod cells of the retina[8]. Metabolites circulating in the blood can activate a cell's receptors, prompting the release of hormones crucial for glucose regulation[9]. Adhesion receptors play a role in conveying tension-generated forces, dictating whether a cell remains stationary or changes its direction of movement[10]. Growth factors engaging with the cell membrane can activate receptors that significantly influence chromatin structure and the modulation of gene expression[11]. Additionally, developmentally regulated receptors play a precise role in guiding the trajectory of migrating cells, ultimately orchestrating the complicated wiring of an entire organism[12,13]. All of the cellular receptors contribute to the intricate web of signaling pathways.

The consequences of disrupted cellular communication are profound, leading to aberrations in processes such as growth, metabolism, and immune response. Conditions like cancer[14], autoimmune disorders[15,16], and developmental abnormalities[17,18] can be attributed to breakdowns in these communication networks. Hence, effective cell communication, with the precise delivery and exchange of signals, allows cells to coordinate development, adapt to their environment, and fulfill their functions. In unraveling the dynamic nature of cell biology systems,

understanding the network of signaling pathways and signal transduction emerges as the crucial initial step. This exploration paves the way for deciphering the intricacies of cellular communication, shedding light on the underlying mechanisms that govern life's convoluted ballet at the cellular level.

1.1.1 Diversity and evolution of cell signaling

Cells intricately communicate through a myriad of mechanical and chemical signals, constituting a complex network of intercellular interactions[19]. Among the diverse signaling messengers, intracellular mediators, including lipids[20], phospholipids[21], proteins[22], amino acids[23], nucleotides[24], neurotransmitters[25], glycoproteins, fatty acid derivatives[26], and even dissolved gases like nitric oxide and carbon monoxide[27], play pivotal roles. These signaling molecules are released into the extracellular environment through various mechanisms, including exocytosis, diffusion through the plasma membrane, or remaining bound to the signaling cell's surface.

Irrespective of the signal's nature, target cells respond to extracellular cues via specific transmembrane proteins such as ion channels or receptors[28]. These proteins sense environmental stimuli or selectively bind to signal molecules, initiating a cascade of responses within the target cell. The initial response activates signaling networks, translating extracellular cues into the reprogramming of biochemical or genetic processes. The onset of cellular signaling occurs when the first messenger, which is usually the ligand, binds to its receptor, inducing conformational changes and initiating a series of controlled reactions by second messengers or signaling intermediates[29].

In multicellular organisms, four categories of chemical signaling facilitate intercellular communication, differing primarily in the distance the signal travels to reach the target cell (**Figure 1-1**). Autocrine signals, produced by signaling cells that can bind to the ligand they release, play

crucial roles in early development, pain sensation regulation, inflammatory responses, and programmed cell death during viral infections[30,31]. Signaling through gap junctions in animals and plasmodesmata in plants allows rapid intercellular communication because of direct contact between signaling and target cells. These water-filled channels permit the selective diffusion of specific small signaling molecules and ions between the two cells, ensuring their independence while facilitating rapid signal transmission, vital for the rapid propagation of electrical activity required for synchronized cardiac contractions and postural reflexes[32]. Paracrine signals act locally between closely spaced cells, ensuring quick responses through diffusion, often exemplified by neurotransmitter transfer across synapses between nerve cells.[33,34] To maintain a localized and prompt response, paracrine ligand molecules are swiftly degraded by enzymes or removed by neighboring cells, which help reestablish the signal concentration gradient for their rapid diffusion through the intracellular space if released again. Endocrine signals, released as hormones from distant endocrine glands, travel through the bloodstream to target cells. Due to their mode of transport, these signals typically elicit a slower response characterized by low concentrations but exert a longer-lasting effect.

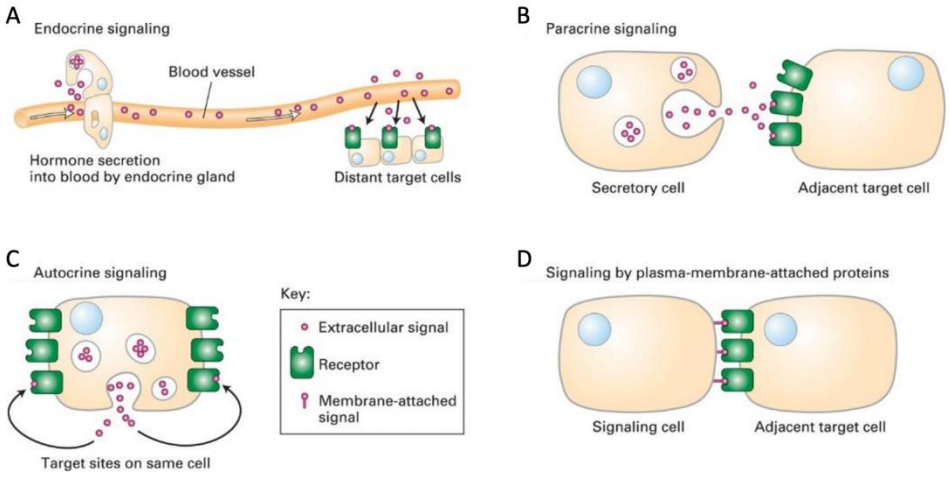

Figure 1-1: Types of cell communication. (A) Endocrine signaling. (B) Paracrine signaling. (C) Autocrine signaling. (D) Juxtacrine signaling.[35]

The intricate cellular signaling networks enable cells to communicate, respond to extracellular stimuli, and maintain regular biological functions while adapting to environmental changes. Dysfunctions in these signaling pathways can lead to pathological conditions, ranging from abnormal cell proliferation to organismal demise[36,37]. Consequently, unraveling the molecular basis of cell signaling provides profound insights into fundamental biological processes such as cell growth, movement, and division, offering promising avenues for potential therapeutic approaches.

1.1.2 Force-activated signaling pathways

Mechanical forces represent pivotal physical stimuli that govern a multitude of cellular processes, including cell proliferation, differentiation, and apoptosis, by instigating intracellular signal transduction pathways[38–40]. Despite their recognized significance, the mechanisms through which cells perceive and respond to mechanical stimuli remain largely elusive. Current research predominantly concentrates on cellular membrane proteins, such as ion channels[6,7,41], integrins[42,43], growth factor receptors[44–46], and transcription factors[7,47,48], as the primary mechanosensory units. These sensors exhibit diverse behaviors in the mechanotransduction process, functioning either independently or cooperatively within interacting networks that finely regulate cell function.

Within the realm of mechanotransducers, mechanosensitive ion channels and receptors have gained prominence due to their involvement in a spectrum of physiological and pathological conditions. Notably, Piezo and TRP (transient receptor potential) ion channels have emerged as extensively studied players in aortic endothelial cells, intimal macrophages, and smooth muscle cells, with documented implications in atherogenesis[49–53]. Disturbed flow-mediated Piezo1-Gaq/Ga11 signaling, for instance, activates NF-κB and proatherogenic inflammatory signaling in endothelial cells[54,55]. In a similar vein, inflammatory contributors to atherosclerosis elevate the

expression of various TRP proteins including TRPC, TRPV and TRPM families[54,56–58] and intracellular ion concentrations of calcium and magnesium in coronary artery smooth muscle cells[59–62].

Beyond atherogenesis, the Piezo1 and TRP families exert significant influence on the proliferation, migration, and invasion of diverse cancer cells through various signaling pathways. For instance, Piezo1 at focal adhesions triggers integrin–FAK signaling, modulating the extracellular matrix and reinforcing tumor tissue stiffening[63,64]. Mechanical activation of Piezo channels induces calcium influx, subsequently activating downstream pathways like Src and extracellular regulated protein kinase (ERK), culminating in the formation of actin-based protrusions called invadopodia capable of degrading the surrounding extracellular matrix[63,65]. In tumors, TRPV4 interacts with the Rho/Rho kinase pathway or the ERK1/2 phosphorylation process, influencing angiogenesis and tumor vessel maturation by modulating tumor epithelial cells' mechanosensitive channels[66,67].

Experimental evidence underscores the role of mechanical force in T cell-antigen presenting cell physiology and the activation of T cell receptors signaling triggered by peptide-MHC complexes[68]. Another key effector in the response to mechanical cues is Yes-associated protein (YAP)/transcriptional coactivator with PDZ-binding motif (TAZ). ECM stiffness, fluid shear stress, cell geometry, density, and substrate adhesion collectively impact YAP/TAZ, regulating tumor and fibrosis progression[69–71]. Besides, integrins are crucial transmembrane receptors that transduce mechanical and biochemical signals from the extracellular matrix (ECM) into cells, facilitating cell-cell communication and influencing cell proliferation, differentiation, migration, and invasion[72,73]. Activation of integrins by increased tissue elasticity initiates the

RhoA/ROCK pathway, enhancing collagen and fibronectin accumulation, as well as the osteogenic differentiation of mesenchymal stem cells[74–76].

In addition to the aforementioned examples, numerous crucial signaling pathways associated with cellular mechanotransduction contribute to diseases related to mechanical cues. These include the TGFβ/Smad signaling pathway in inflammatory bone destruction and lung fibrosis[77–79], Janus kinase (JAK)/STAT signaling pathway in liver fibrosis and multiple sclerosis[80,81], Wnt/β-catenin signaling pathway in renal fibrosis and osteoarthritis[82,83], ERK1/2 signaling pathway in fibro-proliferative disorders[84–86], and epigenetic signaling in tumorigenesis[87–89], aging[90,91], and fibroblast activation[92,93]. These pathways, predominantly implicated in cell proliferation and fibrogenetic processes, are highly interconnected, contributing to intricate intracellular communication and mutual influence.

1.1.3 Intra- and inter-cellular communication through membrane fusion

Membrane fusion is an important biological process that is observed in a wide variety of intra- and intercellular events such as secretion, membrane biogenesis, viral infection, and fertilization[94–99]. It is essential for communication between membrane-delineated compartments in all eukaryotic cells for transporting essential nutrients, synthesizing and delivering vital cellular components, and destructing and removing damaged cellular materials (**Figure 1-2**). For example, the best-studied process involving membrane fusion is exocytosis, whereby vesicles fuse depending on Ca^{2+} and efficient SNARE function assisted by synaptotagmins to release their contents into the extracellular milieu, or to deposit receptors, transporters, channels, or adhesion molecules into the limiting membrane[100]. The fusion of synaptic vesicles, which requires synaptobrevin and neuronal SNAREs SNAP25 and syntaxin-1 and depends on calcium influx, is essential for the release of neurotransmitters and hormones for efficient intercellular

communication[101,102]. Besides the important role in secretory pathway, SNAREs are also essential and are assisted by the Rab5 effector EEA1 in endosome fusion[103,104].

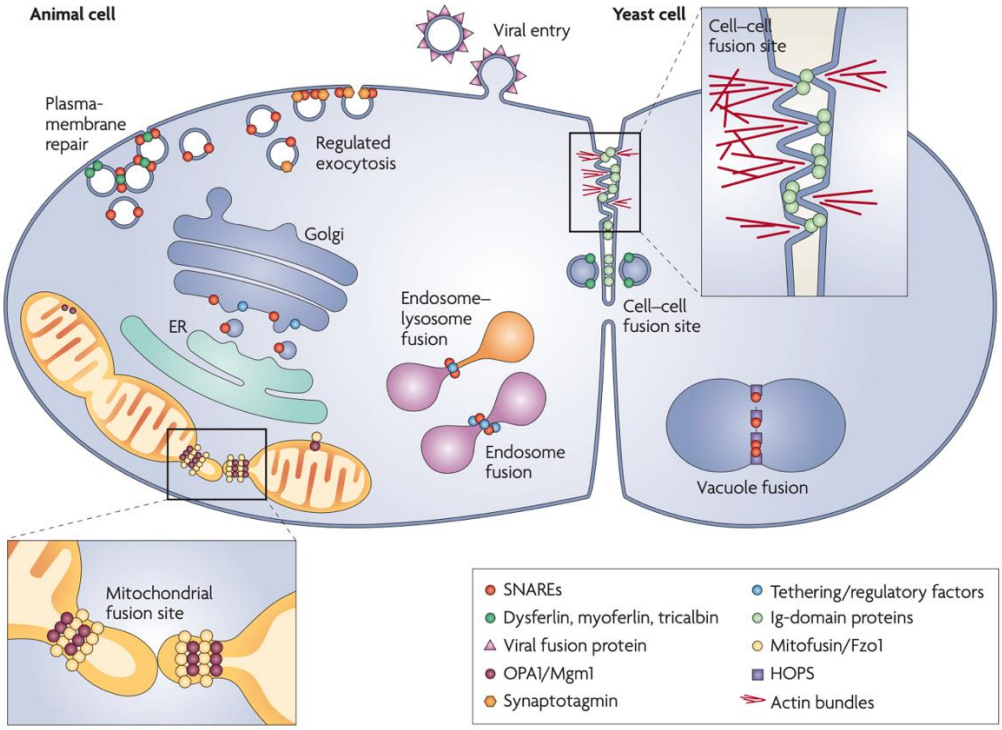

Figure 1-2: The broad spectrum of membrane-fusion events. Membrane fusion, observed ubiquitously, is crucial for intercellular communication by facilitating the merging of lipid bilayer compartments within cells. Membrane fusion in various cellular processes relies on SNAREs, along with assisting factors such as synaptotagmins and EEA1. In viral and cell-cell fusion, different proteins take over this role. The actin cytoskeleton and MC2D proteins also play roles, particularly in cell-cell fusion and plasma membrane repair. Yeast vacuole fusion requires SNAREs and HOPS. Mitochondrial fusion involves mitofusin and OPA1. Plasma membrane repair involves Ca2+ influx and dysferlin. SNARE involvement in plasma membrane repair isn't fully established yet.[105]

Besides mammalian systems, homotypic yeast vacuole fusion during the budding of haploid cells and in zygotes also requires SNARE proteins Vam3, Vam7, Vti1, and Nyv1 with the assistance of Rab GTPases and Rab effectors such as HOPS[106,107]. One of the most common intercellular fusion events is mitochondrial fusion which depends on the dynamin superfamily GTPases OPA1 (optic atrophy protein-1) and mitofusin[108–110]. Mitofusins can tether mitochondria to each other and form an antiparallel coiled structure for membrane fusion. In addition to the tethering, these proteins also promote membrane tubulation as a driving force for fusion.

Apart from intercellular communication, cell-cell fusions play a crucial role in numerous biological processes such as fertilization, development, and immune responses. Proteins with immunoglobulin (Ig)-like domains are shown to play important roles in cell-cell tethering for multiple cell-cell fusion events[111,112]. For example, fusion of myoblasts that requires Drosophila melanogaster proteins DUF, RST and SNS with multiple extracellular Ig-like domains is observed during myotube generation[113,114]. For sperm-egg fusion, CD9, a multiple transmembrane-domain protein on the egg surface, and IZUMO, a single transmembrane-domain protein with an extracellular Ig-like domain on the sperm surface, are required for inducing membrane curvature and facilitating further fusion steps[115,116]. With a similar structure to Ig domains, C2 domains bind Ca^{2+} and are found in proteins that are central to intracellular membrane-fusion events such as signalling and membrane trafficking[117–119]. Other cell-cell fusion events contain fusion of macrophages during osteoclast and 'giant cell' formation[120,121], yeast-cell fusion during mating[122–124], and trophoblast cell-cell fusion that requires syncytins was observed in syncytiotrophoblast formation during placental development[125].

Membrane fusion is also an essential step in the entry and infection of cells by enveloped viruses. Viral-surface fusion proteins, which are structurally classified into three classes α-helical, β-sheets and mixed secondary structure, are involved in the viral fusion processes, where they undergo conformational changes triggered by certain environmental conditions or interaction with specific receptors, and expose fusion peptides or loops for insertion into the target membrane to induce membrane fusion caused by membrane apposition and bilayer disturbance[97,126,127]. One of the best-studied viral fusion proteins is haemagglutinin, which is a class I protein that comes from the influenza virus with its structure determined in a low pH environment[127–130].

Recognizing the pivotal role membrane fusions play in biological processes, they have been extensively reconstituted in synthetic systems. For example, the machinery involved in vesicle transport and membrane fusion, mediated by SNAREs during exocytosis, has been dissected through in vitro reconstitution assays [131]. Further examples will be introduced and discussed in the section titled '1.2.3 Reconstitution of Membrane Fusion Machinery in Synthetic Systems'.

1.2 Cellular biology through bottom-up reconstitution

1.2.1 Exploring mechanism of biological functions through in vitro reconstitution

With the development of advanced experimental techniques in cell biology, a lot of essential cellular processes such as migration, division, endocytosis, exocytosis, and many others have been understood. Traditional cell biology studies were primarily focused on observations of input-output relationships in cells subjected to changes in their environment by the use of top-down approach, a research methodology that starts with studying complex biological systems as a whole and then gradually dissecting them into constituent parts to understand their individual functions and interactions[132,133]. However, complexities and redundancies in different functional units of cells due to self-organization, crosstalk, and feedback mechanisms enable cells to be robust and adaptive to external and internal stimuli, which hinders the investigation of fundamental understanding into the mechanism of a given cellular process through top-down techniques. To address these questions, the field of bottom-up *in vitro* reconstitution[134–137], where individual components or proteins of interest can be assembled under controlled conditions, has gained considerable traction over the past years to elucidate which biomolecular or genetic compositions are constitutive in mediating different cellular functions.

In recent years, several biological systems have been reconstituted using bottom-up synthetic platforms. It is well known that the actin cytoskeleton is involved in a vast number of cellular processes, from shaping cells to their propagation and locomotion[138,139]. Actin cytoskeleton networks have been reconstituted in synthetic supported lipid bilayers or giant unilamellar vesicles (GUVs) for understanding the dynamics, organization and emergent behaviors of membrane–cytoskeleton interactions[140]. The reconstitution of actin networks both inside and outside GUVs demonstrates that actin polymerization, in conjunction with a limited number of actin-binding proteins like crosslinkers and membrane-bound nucleators, is adequate to trigger membrane protrusions resembling biological structures like filopodia[141,142]. Furthermore, distinct overall membrane shapes can be achieved when a branched actin network forms at GUV membranes in the presence of capping protein[143]. Membrane organization and transformation for diverse biological functions such as vesicular trafficking during endocytosis and exocytosis were also studied using *in vitro* reconstitution approaches. For instance, *in vitro* reconstitution of COP-I and COP II, which are required for cargo transport between the endoplasmic reticulum and the Golgi apparatus, on GUVs cause membrane deformations[144,145].

Recent *in vitro* experiments have shown that proteins with Bin/amphiphysin/Rvs (BAR) domains that have intrinsically curved shapes can aid the function of other membrane-remodeling proteins such as dynamin because of their capability of sensing and inducing local membrane deformation[146]. *In vitro* reconstitution has also been a powerful paradigm for studying signaling and signal transduction pathways, which are common biological processes for sensing environmental stimuli and conveying messages through signal amplification mechanisms and signal modulation mechanisms into changes of biological activities of target cells[147–149]. Being pivotal for immune cell function, TCR proximal signaling events are one of the best-studied

juxtracrine signaling processes and have been semi-reconstituted by hybrid interfaces between cell membranes and supported synthetic supported lipid bilayers to study the recruitment of adaptor proteins to cell-surface receptors[150]. The supported synthetic supported lipid bilayers reconstituted with adhesion proteins and specific ligands are used as model membranes which T-cells are allowed to interact with, which serves as a useful platform to probe different parameters of TCR signaling activation such as ligand density, changing contact area and composition of protein clusters[151–154]. Continued efforts were undertaken to reconstitute the adaptor proteins alongside various domains of the T-cell receptor (TCR) such as intracellular TCR domains to delineate the interaction pathway and enhance our comprehension of the enzymatic pathways linked with T-cell activation[155,156].

Recent studies in synthetic biology have produced invaluable insights on regulatory protein networks and gene circuit architecture within artificial cells and explored their application on medicine and biomedical use. For example, a synthetic gene circuit that can produce a self-organized pattern in *E. coli* was developed. This circuit is composed of an activation part containing a positive feedback loop with T7 RNA polymerase (T7 RNAP) and an inhibition part of quorum sensing-mediated lysozyme expression induced by acyl-homoserine lactones (AHLs) from a positive-feedback module[157]. The development of synthetic gene circuits can be further explored to enhance phenotype-based drug discovery and to validate therapeutics in complex cellular systems with the potential for higher precision and sensitivity. The aforementioned discoveries underscore the benefits of *in vitro* reconstitution for unraveling the intricacies of various cellular processes.

1.2.2 Investigation of gating mechanism and ion selectivity of mechanosensitive channels

The ability of cells to sense and respond to their physical environment is ubiquitous and essential in a broad spectrum of biological processes. Mechanically activated ion channels are one of the most essential molecular force sensors and transducers playing important roles in mechanosensation and mechanotransduction, which connect microenvironmental stimuli to cellular responses. MS channels localizing to plasma membranes can detect and be activated by extracellular mechanical forces with their probability of channel pore opening governed by the changes in membrane tension. By regulating the channel permeability which allows molecules and ions to exchange across cell membranes, mechanical cues can be converted into biochemical or electrical signals to regulate many physiological processes associated with mechanosensory transduction, including osmoregulation in plants, fungi, and bacteria as well as hearing, touch, proprioception, and blood flow regulation in mammalian cells[158,159].

Found in all bacteria, mechanosensitive channel of small conductance (MscS) and mechanosensitive channel of large conductance (MscL) are channels with nanoscale protein pores found in the plasma membrane that can protect the bacterial cells from bursting upon a hypo-osmotic shock by quick release of osmolytes through opening channel pores in response to increasing membrane tension resulting from the increase in turgor pressure[160,161]. The importance of the membrane is underscored by the observation that alterations in the thickness of the phospholipid bilayer or the introduction of compounds inducing spontaneous membrane curvature directly influence the tension threshold for the gating and pore opening of MscL[162].

Besides non-selective MS channels, studies have shown that cation-sensitive MS channels play a critical role in cell volume regulation and are involved in regulating membrane potential in mammalian cells. For example, A member of the DEG/ENaC family of ion channels was identified to contribute to regulatory volume increases in brain cells[163,164] while TRPV4 channels were

responsible for regulatory volume decrease in astrocytes following hypo-osmotic stress[164]. Heterologously expressed TREK-1, a two-pore domain K^+ (K2P) channel, responds to membrane stretch in both whole cells and excised patches and it also has a potentially mechanosensitive role in the vascular system with the evidence that vasodilation from mechanical stimuli is decreased in TREK-1 knockout animals[165]. Other K2P channels such as TREK-2(15) and TRAAK also open in response to the addition of volatile anesthetics, polyunsaturated fatty acids, and lysophospholipids, which cause the change in membrane curvature and contribute to the mechanical stress within the lipid bilayer applied to these channels[166,167]. Electrophysiological properties of TRPA1 strongly supported its role as the auditory MS channel responding to sound vibrations[168]. Gain-of-function mutations in human Piezo1 cause hereditary dehydrated stomatocytosis[169]. Recently, the activity of Piezo1-like cationic channels has been recorded in mammalian neocortical and hippocampal pyramidal neurons for triggering spiking of action potentials[170]. All the evidence shows the importance of MS channels' involvement in cellular mechanosensory and transduction processes.

The availability of the three-dimensional (3D) crystal structure and advanced patch clamp technique for electrophysiological recordings allows for detailed structure and function studies of mechanosensitive channels. For instance, while transmembrane helices function as the sensors for membrane tension and are involved in channel voltage sensitivity, MscS cytoplasmic vestibular domain also undergoes significant conformational change upon channel gating and acts as a selectivity filter in MscS-like channels by the structural studies[171–175]. The gating properties and ion selectivity of the MscS have also been studied by examining channel conductance in solutions containing different mono- and divalent cations, where the evidence indicates that divalent cations play a crucial role in MscS' conductive properties by facilitating channel gating at subconducting levels[176]. Besides bacterial MS channels, MEC-4 and MEC-10 found in *C. elegans* were confirmed

as pore-forming subunits of the native sensory mechanotransduction channel by the apparent reduce in mechanoreceptor currents and change in ion selectivity of their missense mutations[163].

In addition to *in vivo* studies, mechanosensitive channels have been extensively investigated through *in vitro* reconstitution in synthetic membranes, enabling a deeper understanding of their structures, gating properties, and ion selectivity. For example, research has demonstrated that the membrane insertion of MscL is mediated by YidC, a protein insertase. Studies have shown that in vitro synthesized MscL can be successfully inserted into YidC-containing proteoliposomes, where it oligomerizes to form a homopentamer. Interestingly, while YidC facilitates the insertion of MscL, its function for ion transport is not entirely dependent on YidC, as channel activity has also been observed in empty liposomes lacking YidC [177]. However, there is some debate regarding the role of insertases like YidC in membrane protein insertion. Evidence suggests that MscL produced by a cell-free system, complemented with preformed liposomes, can insert directly into pure lipid bilayers and exhibit high activity, as recorded by patch-clamp experiments [178]. This challenges the notion that insertases are indispensable for membrane protein insertion and highlights the complexity of the process.

Moreover, the combination of synthetic cells with in vitro cell-free synthesis has emerged as a promising expression system for membrane proteins, including those that may require an insertion machinery in vivo. Synthetic cells, which are cell-like lipid bilayer compartments encapsulating biological systems in isolation, offer an ideal environment for investigating specific biological processes and membrane protein functions [179–181]. By encapsulating bacterial cell-free expression reactions inside synthetic cells, prior work from our lab has successfully reconstituted functional MscL on vesicle membranes. These reconstituted channels can be activated, opening their pore to induce calcium influx in response to hypo-osmotic shocks[182]. The development of in

vitro transcription and translation systems, coupled with the use of synthetic cell systems with artificial lipid bilayers, provides a versatile platform for exploring the mechanosensitivity and functions of mechanosensitive channels. This approach offers insights into the intricate mechanisms underlying channel function and paves the way for future studies on membrane protein biology and biophysics.

1.2.3 Reconstitution of membrane fusion machinery in synthetic systems

Membrane fusion is an essential physiological process observed in many cellular activities including subcellular compartmentalization, cell growth, hormone secretion and neurotransmission. Fusion involves reorganization of lipids within two closely aligned membranes. This process entails the merging of their membrane proteins and lipids, followed by the mixing of their internal contents, all without causing lysis[105,183]. As obligate intracellular pathogens, viruses use intracellular machineries and pathways for efficient replication in their host target cells by mediating cell-cell fusion between infected cells and neighboring non-infected target cells through interactions of viral fusion proteins expressed at the cell surface of the virus-donor cells with surface molecules or receptors involved in virus entry existing on neighboring non-infected cells[126,184]. Membrane fusion in the secretory (exocytic and endocytic) pathways involves initial membrane association requiring Rab GTPases and tethering proteins, followed by Rab-regulated enrichment of fusion proteins and lipids in a microdomain[185–187]. SNARE complexes with additional regulatory proteins SNARE-associated proteins (SM proteins; NSF or Sec18p; SNAP or Sec17p; and others) are then assembled and cooperating with specific lipids to catalyze fusion with mixing of lipid bilayers, membrane proteins and luminal compartments but retention of the barrier between cytoplasm and organellar lumen[188–192].

Besides *in vivo* studies of intracellular fusion events, the fusion of liposomes has been demonstrated by using purified components and explored extensively. Bottom-up reconstitution approaches have been utilized as tools and strategies for creating tailored biological functions from basic biological building blocks. For example, SNARE-mediated membrane fusion triggered by calcium, which is an evolutionarily conserved process responsible for the exocytosis of synaptic, was largely applied in vesicular membrane and content mixing in *in vitro* studies[193,194]. Complementary sets of recombinant SNARE proteins were successfully reconstituted into either the donor or acceptor liposomes to generate a vesicular SNARE (vSNARE)-containing donor vesicle and transport SNARE (tSNARE)-containing acceptor vesicle, and SNARE-driven fusion was observed through increasing kinetics of fluorescence from self-quenching fluorescent lipids, rhodamine-phosphatidylethanolamine and NBD-phosphatidylethanolamine, initially existed in the donor liposome[195]. Studies also show that complexin can bind to trans-SNARE complexes formed by interaction between t-SNARE vesicles and v-SNARE vesicles to stimulate membrane fusion triggered by calcium ions[196], which is verified by lipid mixing with an increase in the FRET efficiency[197]. Experiments involving neuronal SNARE liposomes have demonstrated that fusion requires significantly fewer SNAREs when calcium and synaptotagmin are present[198,199]. A similar system involving membrane fusion is the development of an artificial beta cell with a multicompartmental vesicle-in-vesicle structure with a glucose metabolism system for sensing glucose levels and release insulin-loaded inner small liposomal vesicles by peptide-mediated membrane fusion, a simplified SNARE-mimicking model that used native transmembrane domains linked to coiled-coil peptides, K3-syntaxin and E3-VAMP2[199]. Through such *in vitro* reconstitution platforms, different membrane fusion machineries can be investigated to understand the process of cell-cell fusion involved in a variety of physiological and pathological conditions.

While in vitro membrane fusion strategies have been extensively demonstrated between synthetic lipid bilayer membranes, many of these approaches rely on spontaneous fusion without mechanisms to trigger or regulate the process in response to specific external signals, such as the presence of particular molecules or ions. This has prompted me to consider the development of a membrane fusion strategy activated by calcium ions, one of the most common secondary passengers in stimulus-response reactions of cells. The details of the concepts and demonstrations of the newly developed calcium-dependent membrane fusion system are described in Chapter 4.

1.2.4 In vitro protein reconstitution (Conventional protein purification vs. Cell-free protein expression – coupling in vitro biomolecular translation machinery with bottom-up reconstitution)

To dissect the mechanism of cellular behaviors, targeting the functions of specific proteins is crucial. Since many cellular processes are regulated simultaneously *in vivo*, it is difficult to resolve complex interactions between different proteins and focus on a single cellular function in living cells. Therefore, reducing the complexity of these interactions becomes a primary motivation for reconstitution studies. Towards this goal, the first task is to ensure the extraction of the protein of interest with sufficient purity to enable detection using available techniques, which can be achieved through standard protein purification approaches that are customized based on the physical and chemical properties of individual proteins. This process allows for the isolation of specific proteins from complex cellular mixtures, enabling their detailed characterization and functional analysis. Highly pure protein samples not only allow researchers to gain valuable insights into protein structure, interactions, and biochemical properties but also serve as essential tools for various downstream applications, including enzymatic assays, structural studies, and functional assays.

Usually for cytoplasmic proteins with little or no membrane interaction, purification is the only step required for effective reconstitution. Recombinant proteins of interest can be expressed in a variety of eukaryotic and prokaryotic host systems including mammalian, plant, insect, yeast, fungus, or bacteria[200]. However, purification of almost all soluble proteins is carried out in bacteria due to ease of use, rapid cell growth and low cost of culturing. One of the most common methods for isolating or immobilizing a specific protein is the use of affinity tags, such as polyhistidine, glutathione-S-transferase (GST), and HaloTag. A range of chromatography techniques are available for separating the protein of interest from the rest of the lysate[201]. For affinity-based separation, the peptide tags used to create the protein of interest can be cleaved depending on downstream applications and removed from the solution by dialysis. In addition to cytoplasmic proteins, there is a critical need for the purification of membrane proteins, considering that approximately one-third of human proteins are membrane-bound[202]. Deciphering the function of membrane proteins with reconstitution is indispensable to unravel the complexities of biological systems. Usually, most of the procedures of purifying membrane proteins are quite similar to soluble proteins but the strategy is much more complicated as compared to soluble proteins as their structure, function and mobility are closely intertwined with the structure and composition of membranes and their surrounding environment. Since membrane proteins have hydrophobic residues that can affect protein folding upon exposure to aqueous environment, care must be taken to solubilize the membrane protein of interest after cell lysis. During the solubilization stage, membrane proteins are extracted from the lipid membrane to an aqueous environment by the use of detergents, which act by disintegrating the lipid bilayer while incorporating lipids and proteins in detergent micelles. Depending on the stability of the targeting membrane protein, different types of detergents are used which are primarily non-ionic to prevent denaturation by strong electrostatic

interactions[203–205]. Following lysis, standard chromatographic techniques such as polystyrene adsorbents and chromatography can be used to isolate the protein of interest[206,207]. The challenge in overexpressing membrane proteins lies in facilitating their efficient trafficking to the host membrane following synthesis. If such localization process is not spontaneous, it can lead to the formation of inclusion bodies at high concentrations of the protein of interest. Therefore, to achieve efficient protein purification, choosing the right host for expressing different types of membrane proteins is very important.

Although the tenacious process of protein purification[208,209], several limitations exist for *in vitro* reconstitution. For example, the expression levels of recombinant proteins in conventional cell culture systems might be low and can lead to growth retardation and toxic effects due to the production of heterologous proteins. Overexpression of membrane proteins *in vivo* remains a bigger bottleneck due to their complex structure, hydrophobic transmembrane region, host toxicity, and the time-consuming and low-efficiency refolding steps required[210]. Therefore, apart from the application of traditional protein purification techniques, people have also used cell-free protein expression (CFPS) systems based on prokaryotic and eukaryotic cell lysates for *in vitro* protein studies[211–213]. To produce proteins of interest, CFPS systems harness an ensemble of catalytic components necessary for energy generation and protein synthesis from crude lysates of microbial, plant, or animal cells. Crude lysates contain the necessary elements for transcription, translation, protein folding, and energy metabolism (e.g., ATP, ribosomes, aminoacyl-tRNA synthetases, translation initiation and elongation factors, metabolic enzymes, chaperones, foldases, etc.). Activated catalysts within the cell lysate act as a chemical factory to synthesize and fold desired protein products upon incubation with essential substrates, which include amino acids,

nucleotides, DNA or mRNA template encoding the target protein, energy substrates, cofactors, and salts (**Figure 1-3**).

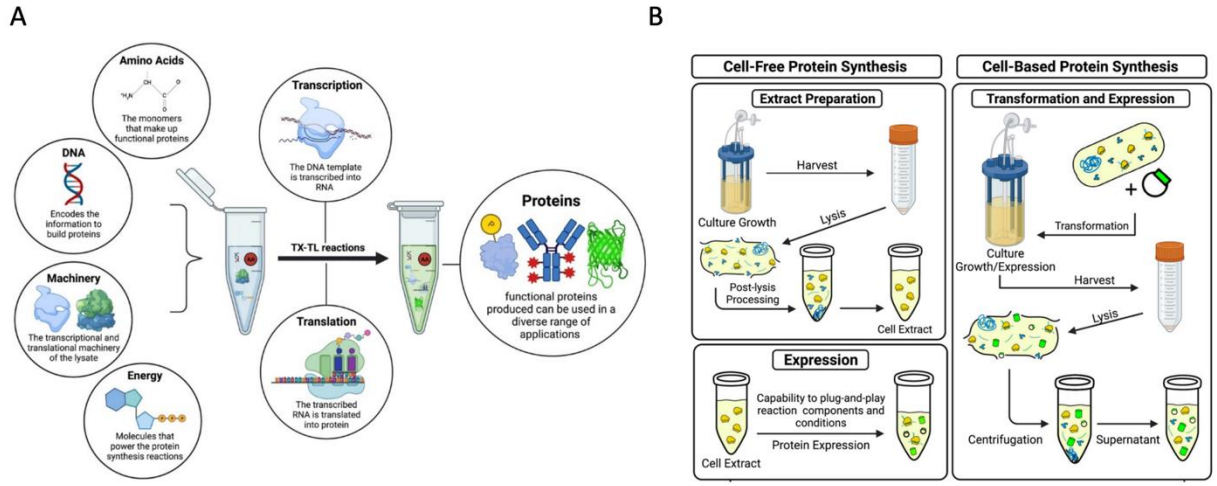

Figure 1-3: (A) The components of a cell-free protein synthesis reaction. (B) The comparison between the cell-free and cell-based protein synthesis systems.[214]

Protein production typically continues until one of the substrates is depleted or byproduct accumulation reaches an inhibitory concentration. The extracts derived from different cells behave very differently. Therefore, things like the yield of protein needed, protein origin and complexity, downstream processing needs, and cost need to be considered for choosing an appropriate source of extract when producing a protein of interest using CFPS. So far, the most common cell-free translation systems include extracts from *E. coli*, wheat germ, insect cells, and rabbit reticulocytes. The prokaryotic *E. coli* system is most popular for simple extract preparation and high protein yields with low cost. However, the main barrier is the inability to produce functional eukaryotic membrane proteins due to the lack of necessary components such as molecular chaperons and post-translational modifications [215,216]. Therefore, wheat germ, insect cells and rabbit reticulocytes become the most widely used eukaryotic CFPS systems for *de novo* production of complex proteins. For example, microsomal bodies present in the cell-free lysates of Sf-21 insect cells have been isolated to facilitate the integration of the pH-sensitive bacterial membrane protein KcsA[217].

In terms of protein yields among eukaryotic CFPS systems, wheat germ prepared from isolated wheat seed embryos[218,219] is the most productive but it is not readily suitable for some post-translational processing like glycosylation[220]. On this front, rabbit reticulocytes and insect cells have shown more versatility for isoprenylation[221,222], acetylation[223], N-myristoylation[223], phosphorylation[224], ubiquitin-conjugation[225], signal peptide processing[226], and core glycosylation[220,226]. Beyond the platforms listed above, eukaryotic CFPS systems based on yeast[227,228] and mammalian cells[229–231] have also been developed. For instance, the cell-free protein synthesis system based on HeLa cells emerges as an excellent choice for membrane protein production, given its inclusion of endogenous microsomal structures that facilitate the direct translocation and post-translational modifications of newly synthesized proteins[229,232,233]. Although eukaryotic CFPS systems show several characteristics that are beneficial for the production of eukaryotic and complex proteins, they generally are more costly and have lower protein yields in batch reactions due to more complicated laborious extract preparation procedures as compared to the bacteria systems. Hence, trade-offs between yield, cost, and post-translational modification requirements must be carefully considered.

With the advances in CFPS coupling transcription and translation reactions, higher efficiency of protein production and translational control can be achieved as compared with cell-based expression. Cell-free synthetic systems could also decrease sensitivity to product toxicity and is more flexible to work with different mutants over *in vivo* protein expression systems. Multiple supplements like molecular chaperones, membrane compartments, and radioisotope labels can be added and desired post-translational modifications achieved based on the protein of interest. The modularity of CFPS makes it a powerful biotechnology for simultaneous multiple protein synthesis and investigation.

1.2.5 Development of synthetic cells mimicking biological functions

The scope of applications for CFE systems has expanded over the past years including the utility of CFE for *in vitro* reconstitution studies. Leveraging CFPS, the bottom-up construction of cell-sized compartments, also known as synthetic cells, that encapsulate CFE reactions in lipid bilayer vesicles have been established as one of the most popular experimental platforms to characterize biological functions in isolation as they encompass both cellular compartmentalization and the central biological dogma of transcription and translation in a minimalistic fashion[234–237]. By encapsulating multiple DNAs with CFPS within liposomes, proteins with diverse functions can be simultaneously reconstituted[238] (**Figure 1-4**). Therefore, with an appropriate choice of proteins, synthetic cells can be capacitated with specific biological functions with desirable physical and chemical properties. Because multiple variants of proteins can be easily expressed by tweaking their genes, a library of desirable mutants can be screened in such synthetic cell systems with high efficiency.

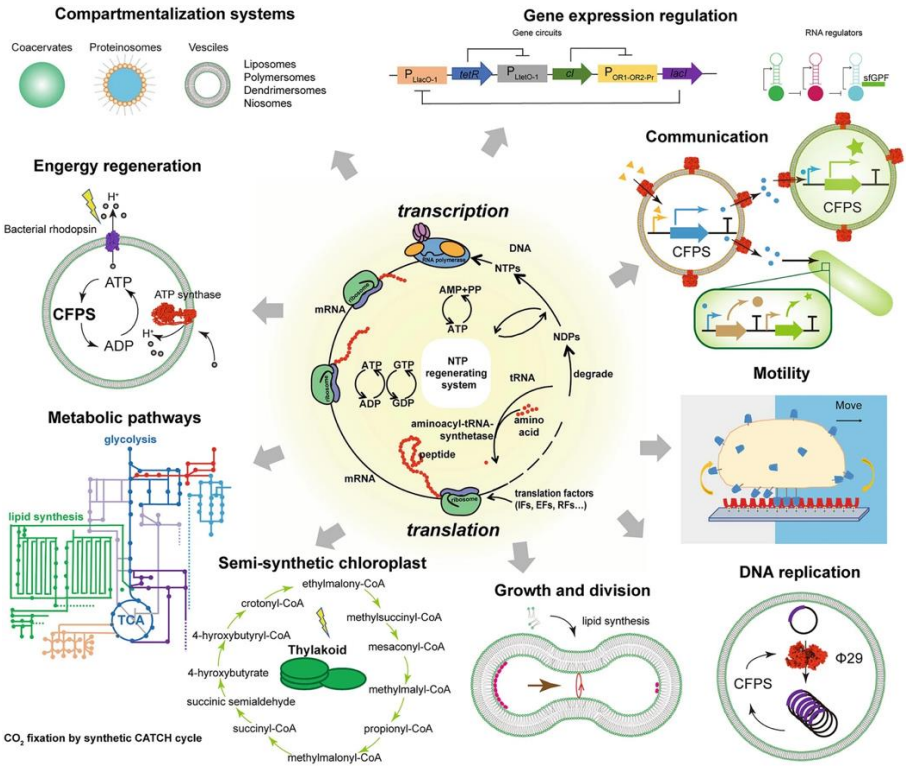

Figure 1-4: Bottom-up construction of synthetic cell systems using the CFPS system. Various modules were created, encompassing compartmentalization, regulation of gene expression, energy regeneration, metabolic pathways, semi-synthetic chloroplasts, growth and division mechanisms, communication systems, motility functions, and self-enhanced DNA replication.[239]

Past studies have employed different techniques to achieve reconstitution at cellular scales using synthetic cells. One such study has successfully synthesized phospholipids from multiple *E. coli* enzymes produced from a cell-free gene expression system encapsulated within liposomes[240]. Some other works have demonstrated communication between synthetic cells by employing gene regulatory networks in CFE systems. For example, cell-free riboswitches that can respond to histamine have been engineered and applied to chemical communication between cell-sized droplets[241]. Another work developed genetic circuit-containing synthetic minimal cells that include multiple-part genetic cascades which can be controlled by external signals as well as inter-liposomal communication without crosstalk. Incompatible reactions can be combined via different genetic cascades within liposomes[242]. To explore the possibility of self-replication and self-reproduction of synthetic cells, functional bacterial ribosomes were synthesized inside synthetic

cells from a self-catalyzed enzymatic reaction with natural RNA[243,244]. Further extrapolation of similar work led to the development of synthetic cells capable of self-replication of DNA through the reconstitution of autocatalytic DNA replication cycle for expressing functional proteins[245]. Recent development of synthetic cells that encapsulate CFPS also offers alternative approach to advance disease treatments. Cell-free expressed proteins encapsulated in polymer membranes were delivered into the body with long survival time while ameliorating chronic conditions such as diabetes[246–248], neurological diseases[249], hemophilia[250], or cancer[251]. Schroeder and colleagues pioneered synthetic cell therapy by demonstrating that liposomes containing transcription and translation systems could be used to synthesize anti-cancer proteins such as *Pseudomonas* exotoxin A inside tumors can kill most cancer cells in culture and cause robust apoptosis when injected into 4T1 tumors in mice[252]. These studies illustrate the potential of CFE to reconstitute complex cell-like molecular interactions *in vitro* through the use of synthetic cell models.

Besides the aforementioned achievements, CFE reactions encapsulated within synthetic cell-like compartments also work as advanced platforms for *in vitro* studies of membrane proteins as they provide lipid bilayer substrates necessary for membrane proteins[253,254]. Also, the innate endogenous microsomal structures in eukaryotic CFE systems enable newly synthesized membrane proteins to insert directly into the natural endoplasmic reticulum (ER)-based lipid bilayers without detergents, which significantly reduces the potential for membrane protein denaturation and favors their proper folding in vitro [233,255,256]. So far, synthetic cells displaying cell-like organization, behavior, and complexity with reconstituted ion channels have been used to recreate several cell functions. For example, the bacterial mechanosensitive channel MscL is expressed by encapsulating CFE reactions in giant unilamellar vesicles (GUVs) and has been shown to sense physical stimuli[182]. Here, such advanced engineering platforms are exploited in

this dissertation to study and reconstitute the functions of mechanosensitive proteins, which sense and convert mechanical stimuli into biochemical signals involved in different cellular phenomena.

1.3 Dissertation outline

Cell communication is a crucial cog in organizing synchronization and differentiation of cellular activities in response to mechanical stimuli, including mechanical deformations generated by hydrostatic forces or a change in the mechanical properties of the ECM induced by a neighboring cell. Speaking to force-dependent cell signaling, MS ion channels are to date the best-characterized biological force-sensing systems that respond to membrane tension by altering their conformation between an open state and a closed state for transport of small molecules in regulating cell behaviors. Based on their characteristic of protein structural change under membrane tension, in Chapter 2, I develop a fluorescence-based optical tension reporter using a bacterial MS channel MscL and demonstrate its feasibility in investigating spatial and temporal dynamics of membrane tension in different cell types. Besides *in vivo* application, I also explore *in vitro* studies of a newly found MS channel in fission yeast, Pkd2. I investigated the topology and mechanosensititvity of Pkd2 by reconstituting it in synthetic membranes using CFE systems with lipid-coated beads and lipid bilayer vesicles and tested its channel permeability under hypo-osmotic pressures. The technique of bottom-up reconstitution of MS channels on GUV membranes can be used to generate synthetic cells capable of communicating mechanically with each other or even with natural cells by performing exocytosis triggered by mechanical force. In Chapter 4, I develop an *in vitro* DNA-mediated membrane fusion strategy mimicking *in vivo* SNARE-mediated membrane fusion by recapitulating its calcium-dependent nature and demonstrating its application in lipid bilayer vesicles. The calcium-induced membrane fusion strategy is then integrated into a

vesicle-in-vesicle system (small unilamellar vesicles inside GUVs) and functionalized with mechanosensing mechanisms by reconstitution of MscL in GUV membranes. Such systems provide the potential for controlled synthetic exocytosis triggered by mechanical stimuli, enabling force-activated communication between synthetic cells and natural cells in the future. More comprehensive perspective about the future research and potential applications on medical use will be described in more details in Chapter 5.

Chapter 2 Development of Mechanosensitive Channel-Based Optical Membrane Tension Reporter

The results of this chapter have been published in Hsu et al. *ACS Sensors*, 2023. Y.Y.H., A.P.L. and J.F. contributed to the conception and design of conceived the study. Y.Y.H., A.P.L. designed the experiments. Y.Y.H. performed the experiments. A.M.R. wrote the codes for image processing. Y.Y.H. and A.M.R. carried out image processing. Y.Y.H., A.M.R. and A.P.L. wrote the paper. All authors contributed to the manuscript revision and approved the final version. A.P.L. and J.F. provided supervision and administered the project.

2.1 Abstract

Plasma membrane tension has been recognized as a global physical organizer of cellular activities. Technical limitations of current membrane tension measurement techniques have hampered in-depth investigation of cellular membrane biophysics and the role of plasma membrane tension in regulating cellular processes. Here, we develop an optical membrane tension biosensor by repurposing an E. coli mechanosensitive channel via insertion of circularly permuted GFP (cpGFP), which undergoes a large conformational rearrangement associated with channel activation and thus fluorescence intensity changes under increased membrane tension.

2.2 Introduction

The plasma membrane is the initial medium through which a cell detects and reacts to external physical stimuli. As a global mechanical regulator, plasma membrane tension coordinates

a number of cellular behaviors[257–259]. For instance, membrane tension governs the homeostasis between exocytosis and endocytosis, where high membrane tension promotes exocytosis while low membrane tension supports endocytosis by enhancing vesicle trafficking[260,261]. In addition, actin-based protrusions have also been suggested to be regulated by plasma membrane tension wherein low membrane tension facilitates polymerization of actin filaments, which generates lamellipodium-like protrusions at the leading edge during cell spreading[262]. Moreover, plasma membrane coordinates cytoskeletal tension for force transmission to control cell polarity and movement[263].

Although membrane tension has been shown to play critical roles in regulating cell behaviors, the molecular mechanisms by which cells actively regulate membrane tension remain largely unknown. Studies have shown that certain membrane proteins can sense extracellular mechanical forces and convert them into intracellular biochemical signals dubbed as mechanotransduction to modulate cell activities. For example, changes in membrane tension can be recognized and be affected by the activity of membrane-to-cortex proteins, which act as a linker between cellular membranes and actin filaments[264]. Mechanosensitive (MS) channels are another membrane tension sensor with their channel pore opening controlled by changes in plasma membrane tension[6]. Found in all bacteria, mechanosensitive channel of large conductance (MscL) is one of the most studied non-selective MS channels for transporting molecules and ions across the membrane in response to physical stimuli[162]. It is also believed to function as a pressure regulator to prevent lysis of bacterial membrane resulting from the sudden increase of membrane tension during osmotic down-shock[161]. Other eukaryotic MS proteins such as transient receptor potential (TRP) channels[265] and Piezo1[266] are found to mediate a variety of sensations including hearing, touch, and thermo- and osmo-sensation.

Despite the above-mentioned proteins identified as natural membrane tension sensors, a lack of suitable membrane tension measurement tools has hindered detailed studies of the effect of membrane tension on cellular processes. Therefore, development of molecular sensors that report membrane tension of live cells is of significant interest. One of the most widely used technologies for membrane tension quantification is micropipette aspiration[267], in which surface tension is deduced by measured radius of the pipette and cells subjected to suction pressure applied by the micropipette using the Laplace law. The use of optical tweezers[268] or atomic force microscopy[269] is another option for indirect membrane tension measurement. However, these methods require special technical expertise and instrumentation. In recent years, several new methods have been developed to measure molecular tension. The development of fluorescence resonance energy transfer (FRET)-based biosensors has revolutionized the imaging of molecular signals with high spatiotemporal resolution[270,271]. However, the limitations in sensitivity and specificity have hindered their broader applications. In addition, current FRET-based tension biosensors focus on the tension change in the actin cytoskeleton or focal adhesion proteins rather than on plasma membrane tension[272]. Although fluorescent membrane tension probes using small molecules such as Laurdan and Flipper-TR have been used in the past few years[273,274], their functions and sensitivities are highly dependent on lipid and chemical environments. To overcome the above-mentioned technical barriers, herein we report the development of an optical membrane tension reporter using genetically modified MscL. Given that MscL opens a pore in response to elevated membrane tension, our membrane tension reporter acts both as a sensor and as an actuator.

2.3 Materials and Methods

2.3.1 Materials and Reagents

NIH3T3 cells were purchased from American Type Culture Collection. Human mesenchymal stem cells (hMSCs) and MSCGM™ Mesenchymal Stem Cell Growth Medium BulletKit™were purchased from Lonza Pharma and Biotech. Gibco Dulbecco's Modified Eagle Medium (DMEM), trypsin-EDTA (0.25%), and phosphate-buffered saline (PBS, 1X) were purchased from Thermo Fisher Scientific. Fetal bovine serum (FBS) was purchased from Gibco. Human fibronectin, Pluronic® F-127, and Trichloro (1H,1H,2H,2H-perfluorooctyl) silane were purchased from Sigma-Aldrich. SYLGARD™ 184 Silicone Elastomer Kit (polydimethylsiloxane (PDMS) base & curing agent) was purchased from Dow. All primers for cloning were purchased from Eurofins Scientific.

2.3.2 DNA Constructs

pDisplay-SpyCatcher was a kind gift from Dr. Taekjip Ha, Johns Hopkins University. Linear HaloTag-encapsulin dsDNA was a kind gift from Dr. Tobias Giessen, University of Michigan. P70-G-GECO was used in our previous study[182]. mCherry/EGFP-P2A-MscL G22S in a pLVX-puro-based vector was used in a separate previous study[275].

To generate MscL G22S-cpGFP construct as a membrane tension reporter for cell transfection, the MscL G22S construct from our prior study was used as a template for Gibson assembly cloning. The primers used in the study are included in **Table 2-1**. First, cpGFP was amplified from P70-G-GECO construct using the primers cpGFP – F and cpGFP – R with Phusion High-Fidelity DNA polymerase. Next, cpGFP was inserted into MscL G22S after amino acid 61 in the mCherry-P2A-MscL G22S construct. To amplify the backbone, mCherry-MscL G22S, primers MscL61 G22S-F and MscL61 G22S-R were used with Phusion High- Fidelity DNA polymerase for PCR amplification. Afterwards, the resulting PCR products, cpGFP and mCherry-P2A-MscL G22S were digested with DpnI for 1 hour at 37 °C and subsequently purified with the

QIAquick Gel Extraction Kit, and then ligated together with homemade Gibson Master Mix (**Table 2-2**) to create mCherry-P2A-MscL61 G22S-cpGFP construct.

MscL G22S -cpGFP construct with ER export signal sequence, TTTTGCTATGAAAATGAAGTT, was generated to increase MscL's membrane localization. mCherry-P2A-MscL(G22S)61-cpGFP or EGFP-P2A-MscL(G22S)61-cpGFP was used as a template respectively for Gibson assembly cloning. To encode ER export signal after MscL(G22S)61-cpGFP, ER export signal sequence was designed to be included within the primer ERexp – R. Combined with the primer ERexp – F, MscL61 G22S with cpGFP inserted and followed by the ER export signal sequence, referred to as MscL61 G22S-cpGFP-ERexp, was produced and amplified by PCR. The rest of the part of the template, which was mCherry-P2APuro or EGFP-P2A, was defined as the backbones and was amplified using the primers MscL61 G22S – cpGFP-F and MscL61 G22S – cpGFP-R. Again, the resulting PCR products were digested with DpnI, subsequently purified, and then ligated to create mCherry-P2AMscL(G22S)61-cpGFP-ERexp and EGFP-P2A-MscL(G22S)61-cpGFP-ERexp construct.

To remove mCherry-P2A from the mCherry-P2A-MscL(G22S)61-cpGFP construct, or to remove EGFP-P2A from the EGFP-P2A-MscL(G22S)61-cpGFP construct, primers DelmCherry/EGFP-MscL-F and Del-mCherry/EGFP- MscL-R were used to amplify the vector without mCherry or EGFP, which contains MscL(G22S)61 with cpGFP and ER export signal. The resulting PCR products were digested with DpnI, subsequently purified, and then ligated to create MscL(G22S)61-cpGFP-ERexp, which is the final version of our MscL membrane tension reporter. For the control, cpGFP was removed and GFP was fused to the C terminus of MscL G22S to generate MscL G22S-c-term-GFP-ERexp construct. To replace MscL(G22S)61-cpGFP with MscL (G22S)-c-term-GFP, primers MscL-GFP-F and MscL-GFP-R were used to amplify

MscL(G22S)-GFP from EGFP-P2A-MscL G22S construct. Primers Puro-F and Puro-R were also used to amplify the Puro-containing vector as the backbone. The resulting PCR products were digested with DpnI, subsequently purified, and then ligated to create MscL(G22S)61-GFPERexp construct.

MscL G22S-c-term-cpGFP-ERexp, where cpGFP is fused to the C terminus of MscL G22S, and Glu70-ERexp-cpGFP, where cpGFP is inserted into the extracellular domain of the glutamine transporter GluR0 after amino acid 70, were designed as other controls. To generate MscL G22S-c-term-cpGFP-ERexp construct, primers Control-cpGFP-F and Control-cpGFP-R were used to amplify the insert fragment MscL G22S-c-term-cpGFP-ERexp, which is purchased from Twist Bioscience. For Glu70-ERexp-cpGFP construct, primers Glu-F and Glu-R (same as Control-cpGFP-R) were used to amplify the insert fragment Glu70-ERexp, which is purchased from Twist Bioscience. Primers Puro-F and Puro-R were used to amplify Puro-containing vector as the backbone for both control constructs.

To label cell membranes, TMD-HaloTag construct was generated by encoding HaloTag, into the transmembrane domain of transferrin receptor (TfR) in pDisplay-SpyCatcher construct, a gift from Dr. Taekjip Ha at Johns Hopkins University, by Gibson assembly cloning. The linear DNA construct HaloTag-encapsulin with HaloTag fused to the T. maritima encapsulin capsid is a gift from Dr. Tobias Giessen at the University of Michigan. Initially, HaloTag was amplified from HaloTag-encapsulin using the primers HaloTag – F and HaloTag – R. To localize HaloTag to the cell membrane, it is fused to the transmembrane domain of TfR by replacing sfGFP with HaloTag in the pDisplay-SpyCatcher construct. To remove sfGFP from pDisplay-SpyCatcher construct as the backbone, primers xCatch-F and xCatch-R were used for PCR amplification. The resulting PCR products, HaloTag and pDisplay-SpyCatcher without sfGFP were digested with DpnI,

subsequently purified, and ligated to create TMD-HaloTag construct. All constructs created in this study are summarized in **Table 2-3**.

Table 2-1: List of primers used in this study. (Extended)

cpGFP – F	GATTTTAAACAGTTTGCTGTCACGAGCAAGGGCGAGGAGCTG
cpGFP – R	GATATCCCCCTGCGCATCGCGTAGGTTGTACTCCAGCTTGTGCCCCAG
MscL61 G22S-F	GCACAAGCTGGAGTACAACCTACGCGATGCGCAGGGGGATATC
MscL61 G22S -R	CAGCTCCTCGCCCTTGCTCGTGACAGCAAACTGTTTAAAATCGATCCCG
ERexp – F	CATGGACGAGCTGTACAAGGGAAGCGGAGCTACTAACTTCAGCCTGCTGAAGC
ERexp – R	CTACCCGGTAGAATTATCTAGATTAAACTTCATTTTCATAGCAAAAAGAGCGG
MscL61 G22S – cpGFP-F	TAATCTAGATAATTCTACCGGGTAGGGGAG
MscL61 G22S – cpGFP-R	TCCGCTTCCCTTGTACAGCTCG
MscL-GFP-F	CAGATCTCGAGCTCAAGCTTCGAATTCATGAGCATTATTAAAGAATTTCGCG
MscL-GFP-R	CTCCCCTACCCGGTAGAATTATCTAGATTACACTTCGTTTTCATAGCAAAAGCT
pLVX-Puro-F	TAATCTAGATAATTCTACCGGGTAGG
pLVX-Puro-R	GAATTCGAAGCTTGAGCTCGAG
HaloTag – F	ATCGGCACGGGCTTTCCGTTTG
HaloTag – R	TTCCAGCCCGGAGATCTCCAGTG
xCatch-F	CTGGAGATCTCCGGGCTGGAAGAATTCCTCGAGGCGGCCGC
xCatch-R	CAAACGGAAAGCCCGTGCCGATCCCGGATCCTCCGCTTCCATAG
Del-mCherry/EGFP-MscL-F	CTACCGGACTCAGATCTCGAGCTCAAGCTTCGAATTCATGAGCATTATTAAAGAATTTCGCGAATTTG
Del-mCherry/EGFP-MscL-R	CATCGCAAATTCGCGAAATTCTTTAATAATGCTCATGAATTCGAAGCTTGAGCTCGAGATCTG

Table 2-2: 2X homemade Gibson master mix for 20 reactions.

5X isothermal reaction buffer	40 µl
10U/µl T5 exonuclease	0.1µl
2U/µl Phusion polymerase	2.5 µl
40U/µl Taq DNA ligase	20 µl
UltraPure DNase/RNase-Free Distilled Water	37.4µl
Total	100 µl

Note: The mixture is split in 5 µl aliquots for each reaction and should be froze immediately with liquid nitrogen. The reactions can be stored at -80°*C* for up to 3 months.

Table 2-3: List of plasmids used in this study.

Content	**Description**
pLVX-mCherry-P2A-MscL G22S-Puro	MscL G22S separated from mCherry
pLVX-GFP-P2A-MscL G22S-Puro	MscL G22S separated from GFP
pLVX-mCherry-P2A-MscL61 G22S-cpGFP-ERexp-Puro	cpGFP inserted after amino acid 61 of MscL G22S, separated from mCherry, with addition of ER export signal at its C terminus
pLVX- MscL G22S-GFP-ERexp-Puro	GFP connected to MscL G22S
pLVX- MscL G22S-cpGFP- Puro	Membrane tension sensor version 1
pLVX- MscL G22S-cpGFP-ERexp-Puro	Membrane tension sensor version 2

2.3.3 Cell Culture and Transfection

NIH3T3 cells were cultured in 2 ml of growth medium (DMEM supplemented with 2 mM L-glutamine, 1 mM sodium pyruvate, and 10% fetal bovine serum (Gibco) and seeded onto 35 mm glass-bottom dishes (MatTek) for 2 days before transfection. For transfection, cells at 50% confluency were co-transfected with the desired DNA constructs (~500 ng/µl), MscL tension reporters version 1 or 2 (MscL(G22S)61-cpGFP or MscL(G22S)61-cpGFP-ERexp), or control plasmids (GFP-P2A-MscL G22S-ERexp, MscL G22S-c-term-GFP-ERexp, MscL G22Sc-term-cpGFP-ERexp, Glu70-cpGFP-ERexp) along with TMD-HaloTag, using Lipofectamine 3000

transfection reagent (Invitrogen) for 2 days before they were subjected to osmotic pressure experiments. Constructs used for transfections are listed in **Table 2-4**.

hMSCs were cultured in 2 ml of growth medium and seeded onto 6-well culture plate for 2 days before transfection. For transfection, cells at 70% confluency were co-transfected with the desired DNA constructs (~500 ng/µl), MscL tension reporters (MscL(G22S)61-cpGFP-ERexp) or control plasmids (MscL G22S-c-term-GFP-ERexp or GFP-P2A-MscL G22S-ERexp) along with TMD-HaloTag, using Lipofectamine 3000 transfection reagent for 1 day. The transfected cells were then trypsinized and reseeded on the micropost arrays at a density of 1500 cells/cm2. hMSCs were allowed to attach and spread on the micropost for at least 2 hours before imaging.

Table 2-4: List of plasmids used for transfection in each experiment.

	DNA construct	**DNA amount in 2ml media**
Version 1	pLVX-MscL G22S-cpGFP-Puro (1) + TMD-HaloTag (2)	(1) 1.25 µg (2) 1.25 µg
Version 2	pLVX-MscL G22S-cpGFP-ERexp-Puro (1) + TMD-HaloTag (2)	(1) 1.25 µg (2) 1.25 µg
Control 1	pLVX-MscL G22S-GFP-ERexp-Puro (1) + TMD-HaloTag (2)	(1) 1.25 µg (2) 1.25 µg
Control 2	pLVX-EGFP-P2A-MscL G22S-ERexp-Puro (1) + TMD-HaloTag (2)	(1) 1.25 µg (2) 1.25 µg

2.3.4 Membrane Labeling with HaloTag Fluorescent ligands

10 µl of 1 mg/ml JF594i-HaloTag ligand (obtained from Janelia Research Campus) was added to the 35 mm glass bottom dish with or without micropost arrays containing 2 ml of growth medium with cells transfected with TMD-HaloTag. The plate was incubated for 10 min at 37°C before washing with 2 ml of 1X PBS, pH 7.4 three times to remove the residual ligands.

Afterwards, 1.5 ml of the fresh culture medium (DMEM supplemented with 10% fetal bovine serum) was added to the plate and incubated for 20 min at 37°C with 5% CO2 before imaging.

2.3.5 Application of Hypo-Osmotic/ Hyper-Osmotic Shock and Pressure Cycle Test

The osmolarity of DMEM supplemented with 10% FBS was measured by the vapor pressured osmometer (ELITech Group) to be around 330 mOsm. In the osmotic pressure test, the osmolarity of the growth medium in the dish was progressively decreased from 330 to 108 mOsm or increased from 330 to 552 mOsm (step by step) by adding water or 10X PBS in order to apply increasing or decreasing osmotic shock to the cells, which stay in the desired osmotic condition for 4 minutes before image acquisition and the next addition of water/ 10X PBS. To achieve a targeted osmolarity, different amount of ultrapure water/10X PBS was added to 1 ml growth medium as shown in **Table 2-5**.

For the pressure cycle test, the osmolarity of the growth medium was alternated between ~330 mOsm (iso-osmotic condition) and ~165 mOsm (hypo-osmotic condition). Cells were subjected to two times of hypo-osmotic shocks in between three times of iso-osmotic conditions. First, 1000 µl ultrapure water was added to 1 ml growth medium to create hypo-osmotic solution, and then 127 µl 10X PBS solution (~2930 mOsm) was added back to the growth medium to increase the osmolarity back to 330 mOsm for creating iso-osmotic environment. To apply second osmotic shock to cells, 2127 µl ultrapure water was added to the medium. For the last step, addition of 270 µl 10X PBS solution returned the sample to iso-osmotic condition again. The stepwise procedures for the amount of PBS solution and water added to the growth medium is summarized in **Table 2-6**.

Table 2-5: Osmolarity of iso-osmotic and hypo-osmotic solutions added sequentially to an initial 1 mL volume for hypo-osmotic pressure test.

Osmolarity of medium (mOsm)	Medium condition	Addition of water (µl)
330	Iso-osmotic	0
240	Hypo-osmotic	375
165	Hypo-osmotic	1000
108	Hypo-osmotic	2055.5

Table 2-6: The amount of water or 10X PBS added to an initial 1 mL volume for cyclic osmotic pressure test.

Osmolarity of medium (mOsm)	Medium condition	Addition of water (µl)	Addition of 10X PBS (µl)
330	Iso-osmotic	X	X
165	Hypo-osmotic	1000	X
330	Iso-osmotic	X	127
165	Hypo-osmotic	2127	X
330	Iso-osmotic	X	270

2.3.6 Micropost Array Fabrication

2.3.6.1 Replica Molding of Micropost Arrays

Soft lithography was used to fabricate patterned PDMS stamps from silicon molds fabricated using photolithography and deep reactive-ion etching, as described previously[276]. First, the PDMS base and crosslinker were mixed at a 10:1 ratio and degassed under vacuum for 0.5 hr to remove bubbles. The uncured PDMS mixture was poured over the SU-8 silicon master in an aluminum boat before baking at 110 °C for 20 minutes in the oven. The partially cured PDMS negative molds were then peeled away from silicon master slowly, treated with oxygen plasma for 90 seconds to activate the surface, and left overnight to silanize in a desiccator using trichlorosilane. For positive casting, a droplet of 10:1 w/w PDMS was placed onto each PDMS

mold and topped by a plasma-treated 18 mm-diameter round glass coverslip. The assembled PDMS molds were then placed in an oven at 110°C for 20 hrs to fully cure. After curing, the negative PDMS molds were slowly peeled away from the glass coverslips and inspected for collapsed posts. To restore micropost integrity, the patterned coverslips were immersed in 100% ethanol, sonicated for 1 minute, and subjected to dry-release in a critical point drier (Tousimis Samdri-PVT-3D). The micropost array-containing coverslips were then adhered onto bottomless 12-well plates with the use of 10:1 w/w PDMS.

2.3.6.2 PDMS Stamps for Microcontact Printing

Microcontact printing was carried out on the micropost array to control the shape or spreading of cells. First, stamps were generated by pouring PDMS (10:1 mixture of PDMS base and crosslinker) into a 150 mm Petri dish and cured at 65 °C for at least 2 hours. The PDMS was then peeled from the wafer, cut into blocks with dimensions comparable to the micropost arrays, and coated with 100 μl of 50 μg/mL fibronectin 1 hour. Finally, the stamps were washed with DI water and dried with nitrogen gas. The micropost substrates were ozone treated for 7 minutes to activate the surface for stamping. The fibronectin-coated stamps were gently lowered and placed in conformal contact with the micropost arrays, lightly tapping the top with tweezers while being careful to avoid post collapse. The stamps were then carefully removed with tweezers. The microposts were then sterilized using submersion in 100% ethanol followed by submersion in 70% ethanol for 15 seconds each. Finally, the substrate was washed with DI water three times. After washing, the micropost substrates were submerged in 0.2% Pluronic F-127 (SigmaAldrich) for 30 minutes in order to prevent the adsorption of additional proteins to areas outside of the stamped pattern. The substrates were then rinsed with DI water three times and stored in DI water at 4°C for up to one week.

2.3.6.3 Cell Seeding

To seed hMSCs onto the microposts, we first replaced the DI water in the wells with mesenchymal stem cell growth medium. hMSCs were washed with Dulbecco's phosphate buffered saline and trypsinized with 0.25% trypsin-EDTA at 37°C for 5 minutes. The cell solution was then centrifuged at 1.5k rpm for 5 minutes. After removing trypsin-EDTA, the cells were resuspended in the growth medium and a density of approximately 1,500 cells/cm^2 was pipetted into each micropost array well. The dish was then placed in the incubator for at least 2 hours to allow cells to adhere and spread onto the adhesive islands of the micropost arrays.

2.3.7 Fluorescence Imaging

All images were acquired using an oil immersion 60×/1.4 NA Plan-Apochromat objective with an Olympus IX-81 inverted fluorescence microscope (Olympus, Japan) controlled by MetaMorph software (Molecular Devices) equipped with a CSU-X1 spinning disk confocal head (Yokogawa, Japan), AOTF-controlled solid-state lasers (Andor, Ireland) or via a custom controller, and an iXON3 EMCCD camera (Andor). Images of cpGFP/GFP fluorescence and HaloTag fluorescence were acquired with 488 nm laser excitation at an exposure time of 500 ms and with 561 nm laser excitation at an exposure time of 200 ms, respectively. Each acquired image contained 1-3 cells. For an individual experiment, at least three images with nine cells in total were taken at different locations across a well. Three independent repeats were carried out for each experimental condition. Cells were stained with JF594i-HaloTag ligand for 10 minutes at 37°C prior to imaging.

2.3.8 Data Analysis and Image Processing

Images were processed in Python with the use of OpenCV. The membrane signal was isolated using a multi-step background subtraction pipeline. For the first background subtraction step, a binary threshold (cv2.threshold) was applied to the JF594i-HaloTag signal (561 channel) to obtain a background mask (**Figure 2-1**B). Background noise was eliminated by finding the connected components (cv2.connectedComponentsWithStats) and filtering them out by size. The mask was further smoothed using closing (cv2.MORPH_CLOSE) and opening (cv2.MORPH_OPEN) operations. Following this step, the component filtering process was repeated. This background mask was then used as a mask to eliminate background noise (**Figure 2-1**C). For the second background subtraction step, this output image with reduced background noise was subjected to adaptive Gaussian thresholding (**Figure 2-1**D). This new binary image was then used as a mask to accurately capture the membrane signal from the 488-channel reporting the tension response (**Figure 2-1**F). Total pixel intensity was measured and compared between different osmotic pressures. For the micropost array assay, average membrane signal of the membrane tension reporter was measured for each condition. For this process, the membrane signal was isolated using the previously explained process, and the total signal intensity was divided by the number of pixels in the membrane to account for different cell sizes.

To better visualize the membrane cpGFP or GFP signal expressed in cells, the confocal images were adjusted using the lookup table function with orange hot selection built in Image J. However, the raw data captured by the confocal microscope was used for all data analysis and fluorescence calculation.

For fluorescence intensity of membrane pixels corresponding to osmolarity in **Figure 2-3**, **Figure 2-4**, **Figure 2-5**, **Figure 2-6**, **Figure 2-7**, **Figure 2-8**, **Figure 2-9**, and cell spreading areas and average fluorescent intensity of membrane pixels in **Figure 2-10**, the statistical analyses were

verified by one-way ANOVA test to determine the p values. The convention of p values of *: $p < 0.05$; **: $p < 0.01$; ***: $p < 0.001$. $p < 0.05$ was considered statistically significant. Every experiment was performed three times with data collected from nine cells in each replicate.

For fluorescence intensity of membrane pixels analysis with cyclic osmolarity changes in **Figure 2-3**, **Figure 2-4**, **Figure 2-5**, **Figure 2-6**, **Figure 2-7**, **Figure 2-8**, **Figure 2-9**, statistical analysis was performed using a two-tailed t-test with a significance level of 0.05. The quantitative data was compared/analyzed within individual groups (within cells transfected with the MscL membrane tension reporters or control cells) between iso- and hypoosmotic conditions. *: $p < 0.05$; **: $p < 0.01$; ***: $p < 0.001$. $p < 0.05$ was considered statistically significant. Every experiment was performed three times with data collected from nine cells in each replicate.

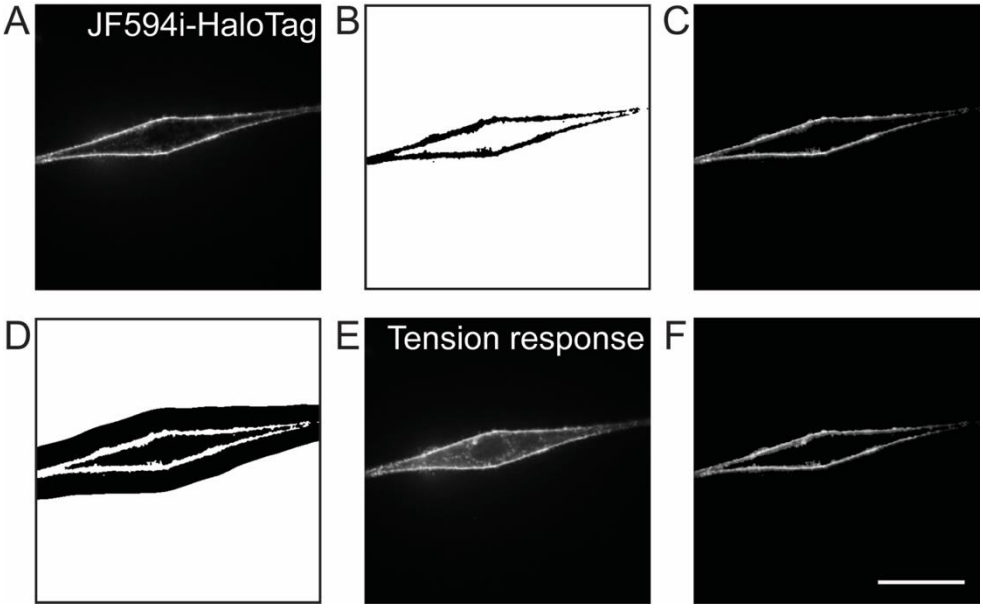

Figure 2-1: Multi-step background subtraction pipeline for tension signal measurement. (A) JF594i-HaloTag signal (561 channel). (B) Mask created by the application of a binary threshold to the JF594i-HaloTag signal. (C) JF594i-HaloTag signal with applied background mask. (D) Mask created from subjecting masked JF594i-HaloTag signal to adaptive Gaussian thresholding. (E) Tension response (488 channel). (F) Tension response with applied background mask resulting from adaptive Gaussian thresholding. Scale bar: 10 μm.

2.4 Results

2.4.1 Repurposing MscL as A Membrane Tension Reporter with Insertion of Circularly Permuted GFP

Specifically, our approach involves the development of a membrane tension OFF sensor, by inserting circularly permuted green fluorescence protein (cpGFP), whose optical property depends on its structure, into the extracellular domain of MscL G22S. As a gain-of-function mutant of MscL, MscL G22S has a ~50% lower tension activation threshold (5–6 mN/m) than wild-type (WT) MscL[277]. MscL G22S is used instead of WT MscL given the increased sensitivity to mechanical stimuli. An increase in membrane tension causes the tilting of MscL G22S's transmembrane helices and triggers channel opening. Since MscL is activated solely by increased membrane tension, a MscL conformation reporter is a proxy for reporting relative membrane tension increases. We hypothesize that structural rearrangement of MscL G22S caused by membrane tension would be transferred to the connected cpGFP, leading to a conformational change that gives rise to a change in its fluorescence (**Figure 2-2**A). A similar concept has been recently utilized for the successful development of a fluorescent voltage sensor[278].

To generate the membrane tension reporter DNA construct, we first encoded MscL G22S with cpGFP fused to its extracellular loop domain after amino acid 61 into a plasmid vector, under the control of CMV promoter as version 1 (**Figure 2-2**B). However, transfection of NIH3T3 cells leads to expression of the reporter version 1 and their notable intracellular accumulation but poor membrane localization (**Figure 2-2**C). We speculate a lack of a mammalian-specific export signal, which inhibits heterologous protein retention in the endoplasmic reticulum (ER), is responsible for MscL cytoplasmic accumulation. To overcome this, we next appended the Kir2.1 ER export signal (FCYENEV), which is known to mediate protein export from the ER to the Golgi complex to the

plasma membrane, [279] to the C terminus of MscL G22S as version 2 (**Figure 2-2**B). This strategy has previously been shown to promote MscL membrane expression in neurons[280]. To examine the localization of the MscL tension reporters, we co-transfected cells with either reporter design along with a membrane-targeted HaloTag construct (TMD-Halo), where HaloTag was linked to the transmembrane domain of transferrin receptor (TfR) for membrane localization.

As shown in **Figure 2-2**C, reduction of cytoplasmic aggregation and enhancement of membrane expression of the version 2 reporter was confirmed by the stronger cpGFP signal observed in the plasma membrane targeted with TMD-Halo as compared to the case of the version 1 reporter. Therefore, the version 2 reporter (MscL(G22S)61-cpGFP) is referred to as the final version of our MscL tension reporter and is used for the remaining experiments.

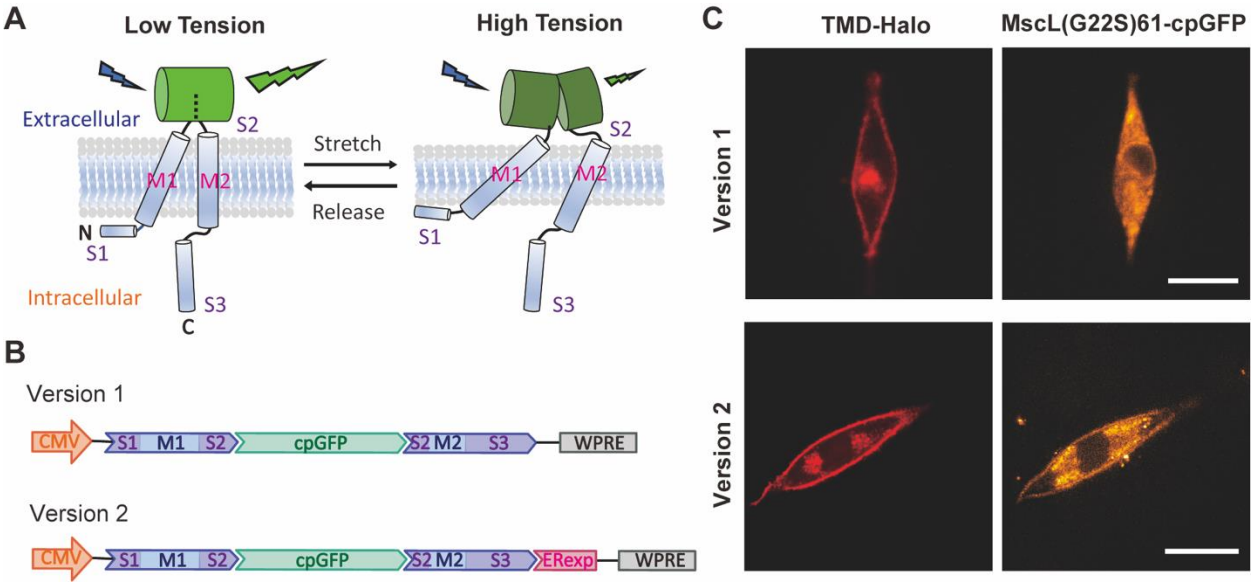

Figure 2-2: Schematics of the structure of the MscL membrane tension reporter and its expression in living cells. (A) The schematic of engineering MscL as a membrane tension reporter using cpGFP. The substantial conformational changes of the extracellular domain S2 caused by the tilting of the transmembrane domain M1 and M2 under high tension leads to a decrease in fluorescence while cpGFP stays fluorescent under low tension. For simplicity, only a monomer is illustrated with S1, M1, S2, M2, and S3 domains shown. (B) The DNA constructs of the version 1 (top) and version 2 (bottom) MscL membrane tension reporters. For both constructs, cpGFP was inserted into the sensory domain of MscL G22S after amino acid 61 as an OFF sensor. Version 2 is optimized with the addition of the Kir2.1 ER export signal (ER exp) for enhancement of membrane localization. (C) Confocal fluorescence images showing the expression of version 1 (top) and version 2 (bottom) constructs in NIH3T3 cells. Scale bar: 10 μm.

2.4.2 Application of The MscL Membrane Tension Sensor in cells in Response to Osmotic Pressure

To test MscL tension reporter sensitivity, we applied an osmotic pressure test, with increasing osmotic shock to cells transfected with the MscL tension reporter. The hypo-osmotic condition is a well-accepted means to increase membrane tension. Previously, we have shown the influx of small molecules into mammalian cells expressing MscL in an osmotic pressure-dependent manner[275,281]. In the osmotic pressure test, the osmolarity of the culture medium was gradually decreased from 330 to 108 mOsm. As shown in **Figure 2-3**Ai, MscL tension reporters were found on the membrane as indicated by TMD-Halo in NIH3T3 cells over the range of hypo-osmotic conditions. MscL(G22S)61-cpGFP fluorescence decreased as the osmolarity of culture medium decreased, supporting that the MscL tension reporters function properly in living cells.

To verify that the declining fluorescence intensity in **Figure 2-3**Ai was not caused mainly by photobleaching, we fused GFP to the C-terminus of MscL G22S as a control (MscL(G22S)-c-term-GFP) and carried out the same osmotic pressure test. While the membrane localization of the control sensor was similar to that of the MscL tension reporter, no significant change in the green fluorescence intensity at the plasma membrane was detected as the osmolarity of culture medium decreased (**Figure 2-3**Aii). We analyzed the fluorescence intensity by normalizing the fluorescence with the initial fluorescence intensity localized to the plasma membranes (using a mask generated from the TMD-Halo image) of cells under iso-osmotic condition (**Figure 2-1**). Cells with MscL tension reporters displayed a substantial decrease in fluorescence in response to increasing osmotic pressure. For example, osmotic pressure with an osmolarity difference of 222 mOsm reduced fluorescence intensity by about 23%, whereas cells expressing the control sensors manifested only 5% fluorescence reductions under the same osmolarity difference (**Figure 2-3**B).

This is also evident from normalized fluorescence of MscL tension reporters in individual cells for both conditions (**Figure 2-3**C). Besides MscL(G22S)-c-term-GFP, we also generated three other controls. The first construct is GFP-P2A-MscL(G22S), in which we used a bicistronic construct with self-cleaving peptide P2A to express MscL G22S and GFP. To rule out the influence of different environmental sensitivities and photostabilities between GFP and cpGFP on the fluorescence change in response to osmolarity, we created another control MscL G22S-c-term-cpGFP, where cpGFP is fused to the C-terminus of MscL G22S. In addition, we also inserted cpGFP into the extracellular domain after amino acid 70 of a glutamine transporter GluR0, an ion channel which is not mechanosensitive, as Glu70-cpGFP. With all three control constructs, we found that GFP/cpGFP fluorescence at the membrane (GFP-P2A-MscL(G22S), MscL(G22S)-c-term-cpGFP, and Glu70-cpGFP) did not reduce with increasing osmolarity difference (**Figure 2-4**, **Figure 2-5**, **Figure 2-6**), suggesting that volume changes of cells due to osmotic downshock did not appreciably change the fluorescence of these control constructs at the membrane.

Besides testing hypotonic conditions, we also applied increasing hyper-osmotic shocks to cells by adding different amounts of 10X PBS to the cell culture medium and found that no appreciable cpGFP membrane fluorescence changes were observed during the test (**Figure 2-7**), consistent with the fact that the hypertonic state does not change the protein structure of MscL, and MscL remains closed under hyper-osmotic conditions as in iso-osmotic conditions.

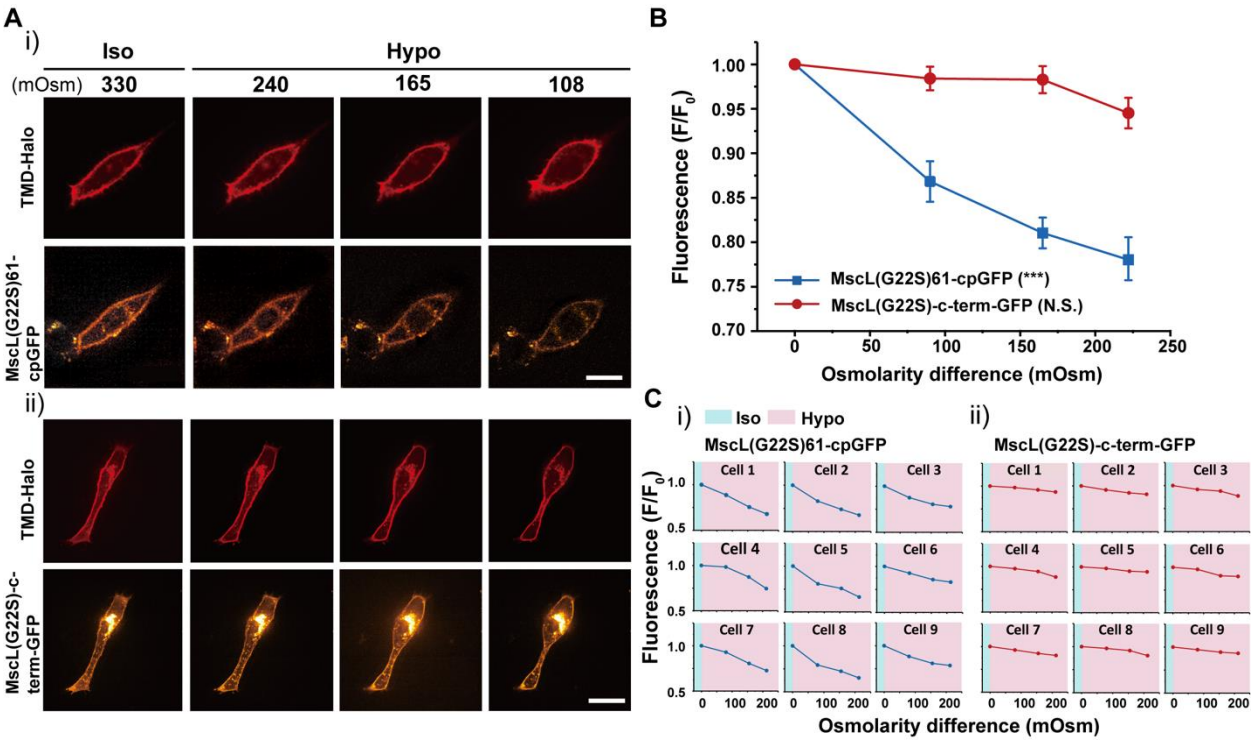

Figure 2-3: NIH3T3 cells transfected with the MscL tension reporter in response to osmotic pressure. (A) (i) Confocal images showing the membrane localization of the MscL(G22S)61-cpGFP in NIH3T3 cells in response to different osmotic shocks. Transfected cells were cultured in iso-osmotic condition for 2 days, and then DI water was sequentially added to the cell culture media to create increasing hypo-osmotic environments. Each image was taken 4 min after the addition of DI water. (ii) Confocal images showing the NIH3T3 cells transfected with the MscL(G22S)-c-term-GFP construct as a control in response to different osmotic shocks. The experiment followed the same method as mentioned in (i). (B) Normalized fluorescence intensities of the cell membranes of NIH3T3 cells transfected with the MscL tension reporter (MscL(G22S)61-cpGFP) or MscL(G22S)-c-term-GFP under different osmotic conditions corresponding to the experiment mentioned in (A). (C) Normalized fluorescence intensities of the MscL tension reporter (i) and MscL(G22S)-c-term-GFP control (ii) localizing on cell membranes of nine different NIH3T3 cells, from three separate experiments, at increasing osmotic pressures. Scale bars: 10 μm. The error bars denote standard error. ***: $p < 0.001$.

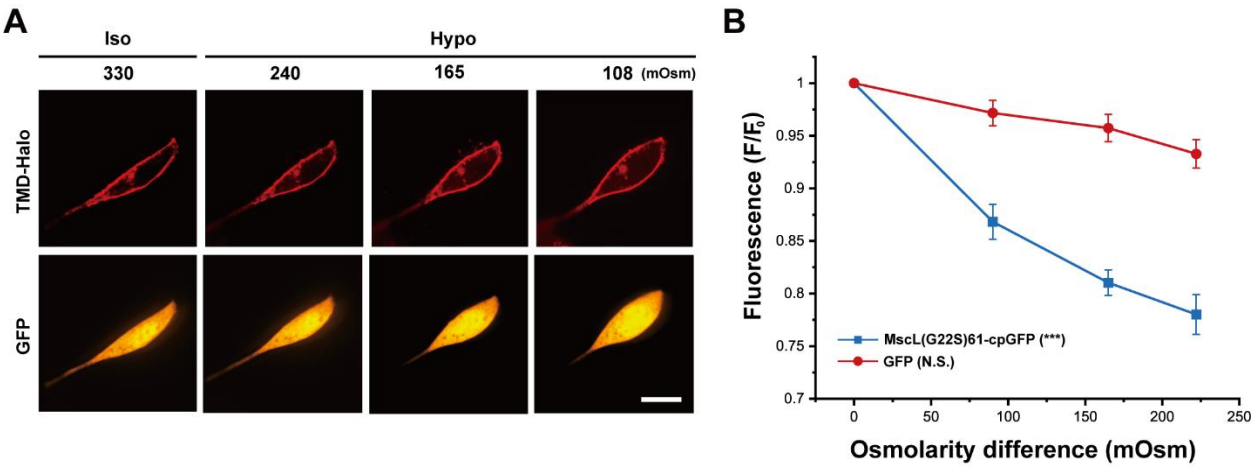

Figure 2-4: NIH3T3 cells expressing MscL G22S and GFP in response to hypo-osmotic pressure. (A) Confocal images showing the NIH3T3 cells transfected with the GFP-P2A-MscL(G22S) construct as a control in response to

different osmotic shocks. Transfected cells were cultured in iso-osmotic condition for 2 days and then DI water was sequentially added to the cell culture media to create increasing hypo-osmotic environments. Each image was taken four minutes after the addition of DI water. (B) Normalized fluorescence intensities (MscL-cpGFP or GFP) of the cell membranes of NIH3T3 cells transfected with the MscL tension reporter or GFP-P2A-MscL(G22S) under different osmotic conditions corresponding to the experiment mentioned in (A). Nine cells were analyzed for each condition from three independent experiments. Scale bars: 10 μm. ***: $p < 0.001$.

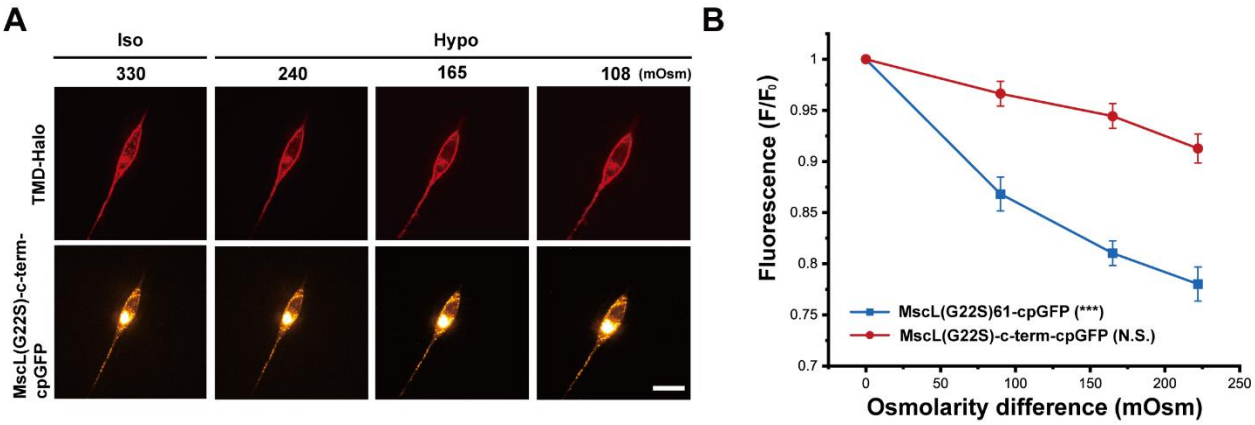

Figure 2-5: NIH3T3 cells expressing cpGFP fused to the c-terminus of MscL G22S in response to hypo-osmotic pressure. (A) Confocal images showing the NIH3T3 cells transfected with MscL(G22S)-c-term-cpGFP construct as a control in response to different osmotic shocks. Transfected cells were cultured in iso-osmotic condition for 2 days and then DI water was sequentially added to the cell culture media to create increasing hypo-osmotic environments. Each image was taken four minutes after the addition of DI water. (B) Normalized fluorescence intensities of the cell membranes of NIH3T3 cells transfected with the MscL tension reporter or MscL(G22S)-c-term-cpGFP under different osmotic conditions corresponding to the experiment mentioned in (A). Nine cells were analyzed for each condition from three independent experiments. Scale bars: 10 μm. ***: $p < 0.001$.

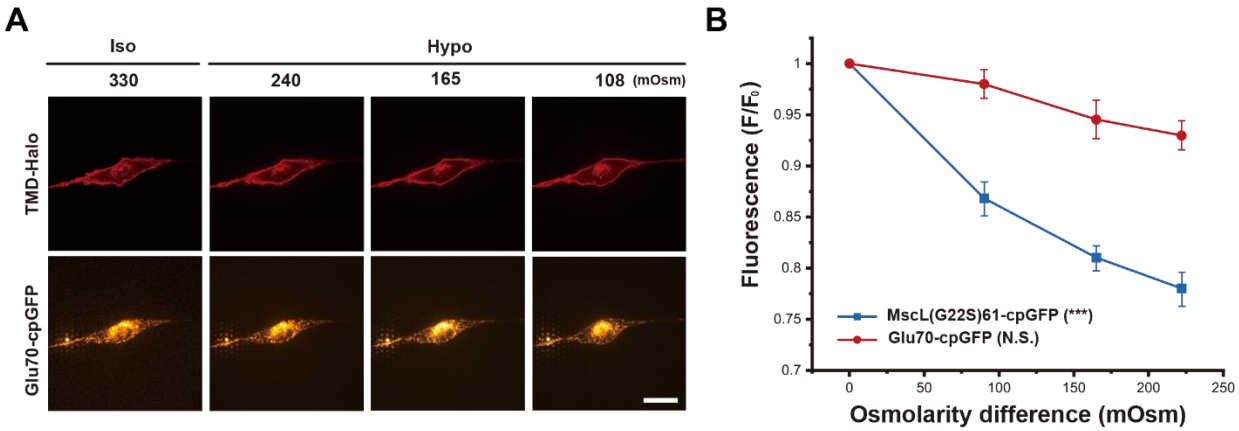

Figure 2-6: NIH3T3 cells expressing GluR0 with cpGFP inserted into its extracellular loop in response to hypo-osmotic pressure. (A) Confocal images showing the NIH3T3 cells transfected with the Glu70-cpGFP construct as a control in response to increasing osmotic downshock. Transfected cells were cultured in iso-osmotic condition for 2 days and then DI water was sequentially added to the cell culture media to create increasing hypo-osmotic environments. Each confocal image was taken four minutes after the addition of DI water. (B) Normalized fluorescence intensities of the cell membranes of NIH3T3 cells transfected with the MscL tension reporter or Glu70-cpGFP construct corresponding to the experiment mentioned in (A). Nine cells were analyzed from three independent experiments. Scale bars: 10 μm. ***: $p < 0.001$.

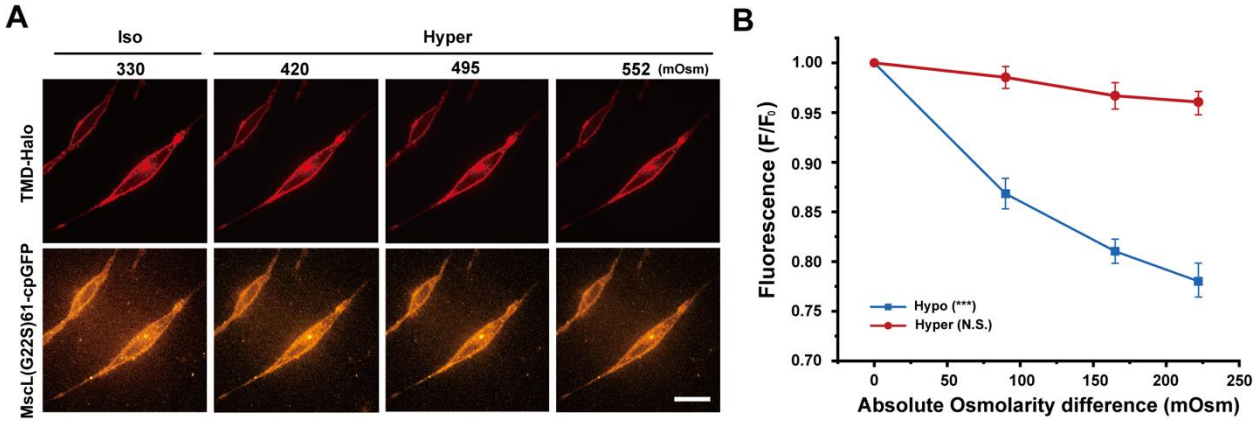

Figure 2-7: NIH3T3 cells expressing MscL(G22S)61-cpGFP in response to hyper-osmotic pressure. (A) Confocal images showing the NIH3T3 cells transfected with the MscL(G22S)61-cpGFP construct in response to different hyper-osmotic shocks. Transfected cells were cultured in iso-osmotic condition for 2 days and then 10X PBS solution was sequentially added to the cell culture media to create increasing hyper-osmotic environments. Each image was taken four minutes after the addition of DI water. (B) Normalized fluorescence intensities (hypo- or hyper-osmotic conditions) of the cell membranes of NIH3T3 cells transfected with the MscL tension reporter under different osmotic conditions corresponding to the experiment mentioned in (A). Hypo-osmotic conditions were described in Figure S4. Osmotic difference is higher external osmolarity for hyper-osmotic condition and lower external osmolarity for hypo-osmotic condition. Nine cells were analyzed for each condition from three independent experiments. Scale bars: 10 μm. ***: $p < 0.001$.

To further verify the sensitivity of the fluorescence shift of the MscL tension reporter in response to changes in membrane tension, we performed the cyclic osmotic test on NIH3T3 cells co-transfected with the MscL tension reporter and TMD-Halo. The osmolarity was repeatedly switched between iso-osmotic (~330 mOsm) and hypo-osmotic conditions (~165 mOsm) to generate alternating "resting" and elevated membrane tension. As shown in **Figure 2-8**A, the MscL tension reporter was located on a plasma membrane as expected. MscL(G22S)61-cpGFP fluorescence intensity varied depending on membrane tensions resulting from the cyclic iso-osmotic and hypo-osmotic conditions. We observed an alternating pattern of high and low fluorescence in iso-osmotic and hypo-osmotic conditions, respectively.

When quantified as before, fluorescence intensities of the MscL tension reporter displayed a 'W' shape trend (**Figure 2-8**B, Ci). A similar cyclical test was also conducted on NIH 3T3 cells transfected with MscL-(G22S)-c-term-GFP as a control, in which no obvious trend of MscL

fluorescence could be correlated to the osmolarity changes (**Figure 2-8**Aii, B, Cii). Our other controls GFP-P2A-MscL(G22S), MscL(G22S)-c-term-cpGFP, and Glu70-cpGFP also lacked such a trend (**Figure 2-9**, **Figure 2-10**, **Figure 2-11**). Together, these results demonstrate the reversibility of the MscL tension reporter.

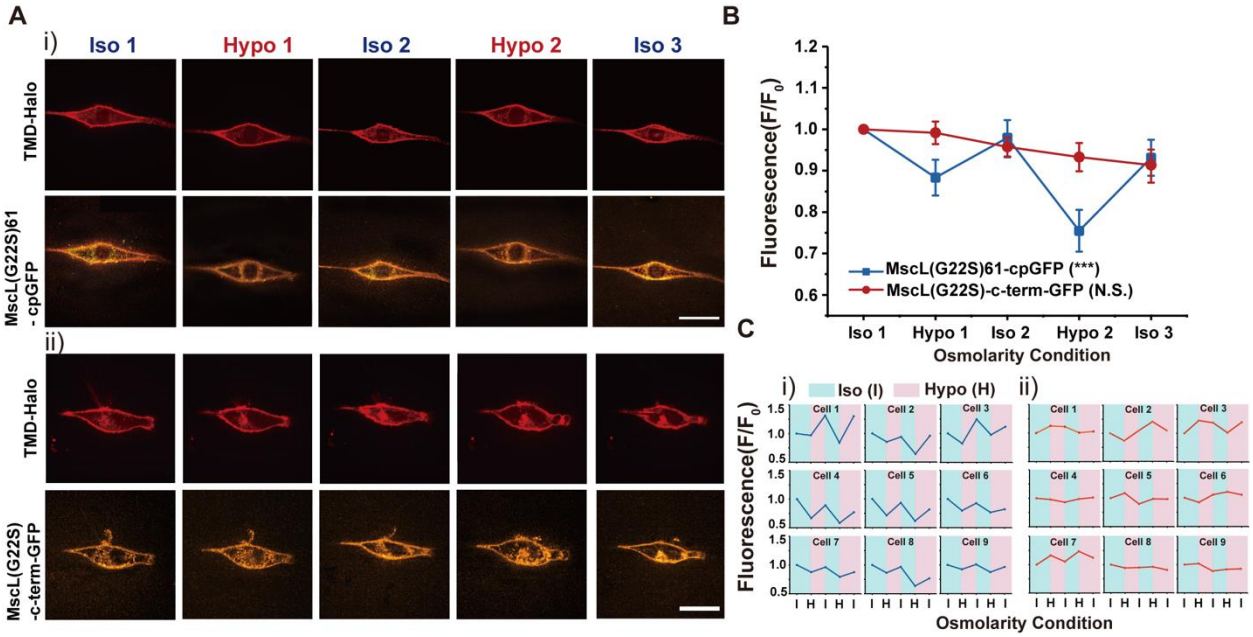

Figure 2-8: NIH3T3 cells transfected with the MscL tension reporter in response to cyclic pressure (A) (i) Confocal images showing the membrane localization of MscL tension reporter in NIH3T3 cells in response to the cyclic pressure test, which was carried out by alternating between iso-osmotic and hypo-osmotic conditions repeatedly. Transfected cells were cultured in iso-osmotic condition for 2 days. DI water was first added to the cell culture media to create hypo-osmotic environments, and then 10X PBS solution was added back to the media to increase the osmolarity for iso-osmotic environments. The osmolarity of the media is ~330 mOsm for iso-osmotic conditions and ~165 mOsm for hypo-osmotic conditions. Each confocal image was taken 4 min after the addition of DI water or PBS solution. (ii) The confocal images showing the NIH3T3 cells transfected with the MscL(G22S)-c-term-GFP construct as a control in response to the same cyclic pressure test as mentioned in (i). (B) Normalized fluorescence intensities of the cell membranes of NIH3T3 cells transfected with the MscL tension reporter and MscL(G22S)-c-term-GFP construct corresponding to the cyclic pressure cycle test. Nine cells were analyzed for each condition from three independent experiments. (C) (i) Fluorescence intensity traces of MscL(G22S)61-cpGFP on cell membranes of nine different NIH3T3 cells during the cyclic osmotic tests (ii) Fluorescence intensity traces of MscL(G22S)-c-term-GFP on cell membranes of nine different NIH3T3 cells as a control. Scale bars: 10 μm. The error bars denote standard error. ***: $p < 0.001$.

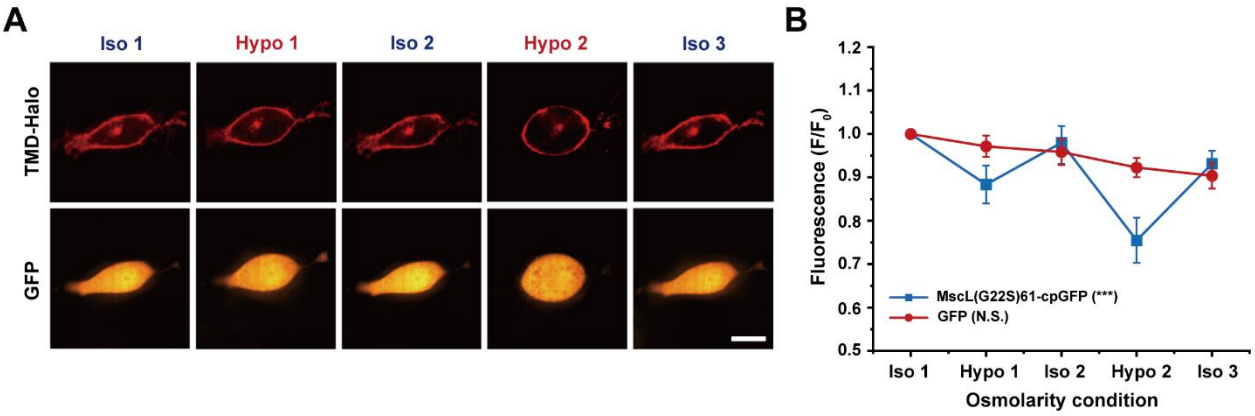

Figure 2-9: NIH3T3 cells expressing GFP in response to cyclic pressure. (A) Confocal images showing the NIH3T3 cells transfected with the GFP-P2A-MscL(G22S) construct as a control in response to the cyclic pressure test, which was carried out by alternating between iso-osmotic and hypo-osmotic conditions. Transfected cells were cultured in iso-osmotic condition for 2 days. DI water was first added to the cell culture media to create hypo-osmotic environments and then 10X PBS solution was added back to the media to increase the osmolarity back to iso-osmotic environments. The osmolarity of the media is ~330 mOsm for iso-osmotic conditions and ~165 mOsm for hypo-osmotic conditions. Each confocal image was taken four minutes after the addition of DI water or PBS solution. (B) Normalized fluorescence intensities of the cell membranes of NIH3T3 cells transfected with the MscL tension reporter and GFP-P2A-MscL(G22S) construct corresponding to the cyclic pressure cycle test. Nine cells were analyzed from three independent experiments. Scale bars: 10 μm. ***: $p < 0.001$.

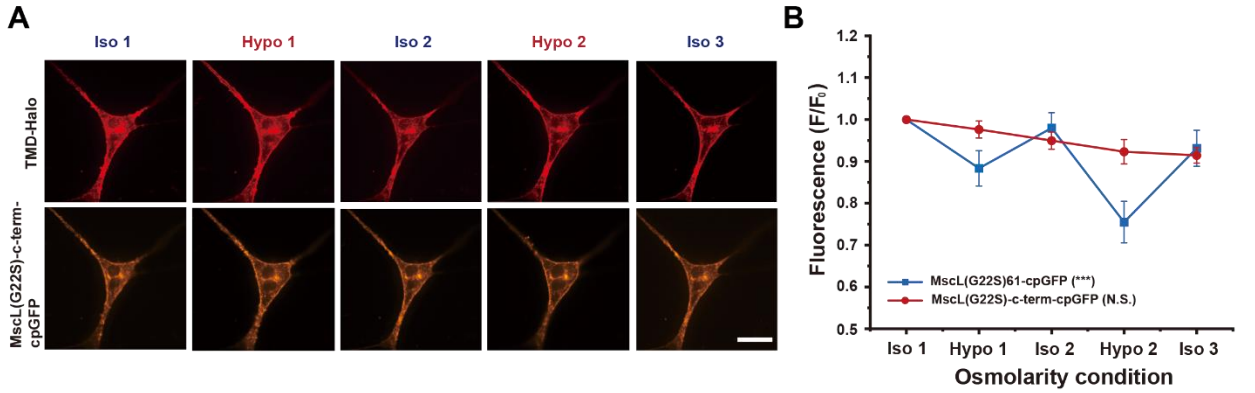

Figure 2-10: NIH3T3 cells expressing cpGFP connected to MscL G22S in response to cyclic pressure. (A) Confocal images showing the NIH3T3 cells transfected with the MscL(G22S)-c-term-cpGFP construct as a control in response to the cyclic pressure test, which was carried out by alternating between iso-osmotic and hypo-osmotic conditions. Transfected cells were cultured in iso-osmotic condition for 2 days. DI water was first added to the cell culture media to create hypo-osmotic environments and then 10X PBS solution was added back to the media to increase the osmolarity back to iso-osmotic environments. The osmolarity of the media is ~330 mOsm for iso-osmotic conditions and ~165 mOsm for hypo-osmotic conditions. Each confocal image was taken four minutes after the addition of DI water or PBS solution. (B) Normalized fluorescence intensities of the cell membranes of NIH3T3 cells transfected with the MscL tension reporter and MscL(G22S)-c-term-cpGFP construct corresponding to the cyclic pressure test. Nine cells were analyzed from three independent experiments. Scale bars: 10 μm. ***: $p < 0.001$.

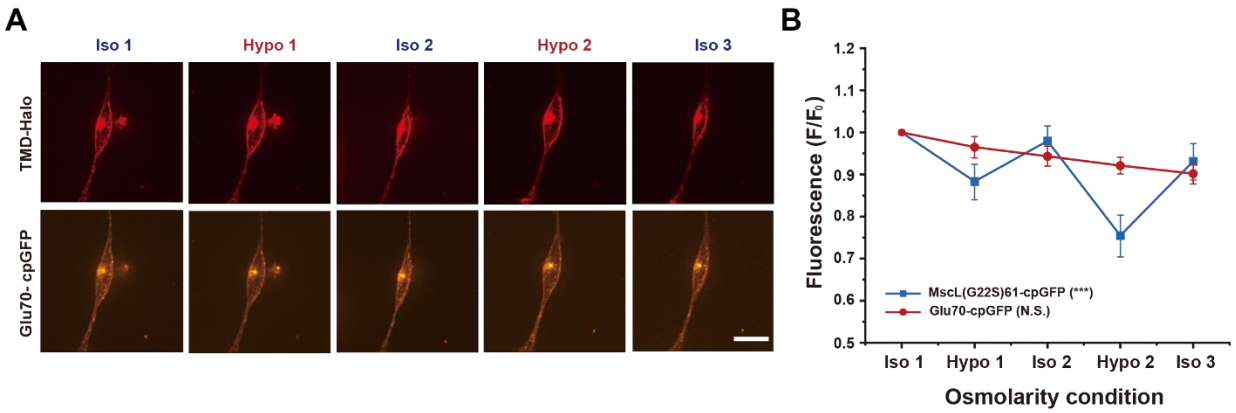

Figure 2-11: NIH3T3 cells expressing GluR0 with cpGFP inserted into its extracellular loop in response to cyclic pressure. (A) Confocal images showing the NIH3T3 cells transfected with the Glu70-cpGFP construct as a control in response to the cyclic pressure test, which was carried out by alternating between iso-osmotic and hypo-osmotic conditions. Transfected cells were cultured in iso-osmotic condition for 2 days. DI water was first added to the cell culture media to create hypo-osmotic environments and then 10X PBS solution was added back to the media to increase the osmolarity back to iso-osmotic environments. The osmolarity of the media is ~330 mOsm for iso-osmotic conditions and ~165 mOsm for hypo-osmotic conditions. Each confocal image was taken four minutes after the addition of DI water or PBS solution. (B) Normalized fluorescence intensities of the cell membranes of NIH3T3 cells transfected with the MscL tension reporter and Glu70-cpGFP construct corresponding to the cyclic pressure cycle test. Nine cells were analyzed in each independent experiment with three in total. Scale bars: 10 μm. ***: $p < 0.001$.

2.4.3 Volume and Membrane Fluorescence Dynamics of Cells Expressing the MscL Membrane Tension Reporter under Hypotonic Conditions

All our osmotic shock measurements so far have been conducted at 4 min after the onsets of osmotic shocks. Nonetheless, it is well appreciated that cells have the ability to accommodate and recover from rapid changes in cell volume during osmotic shocks to regulate membrane tension[282]. Therefore, we sought to correlate the cell recovery dynamics from osmotic shocks to the corresponding membrane fluorescence of the MscL tension reporter. We performed cell volume measurements every 1 min after hypo-osmotic shocks (with ~165 mOsm osmotic difference between the cells and the medium) in the first 5 min and continued tracking at 10, 20, and 30 min, respectively, by using 3D reconstruction of the side view of cells analyzed with Limeseg (**Figure 2-12**A). In separate experiments, we acquired MscL tension reporter

fluorescence under the same condition. We observed a significant increase in cell volume (~61%) and decrease in tension reporter fluorescence (~21%) in the first 2 min after exposure of cells to hypotonic medium, which is followed by a gradual decrease in the average cell volume from 2 to 10 min. During this same period, the corresponding fluorescence of the tension reporter increased from 2 to 10 min (**Figure 2-12**B), showing a positive correlation between the cell volume and membrane tension changes during the dynamic cell recovery under hypotonic condition.

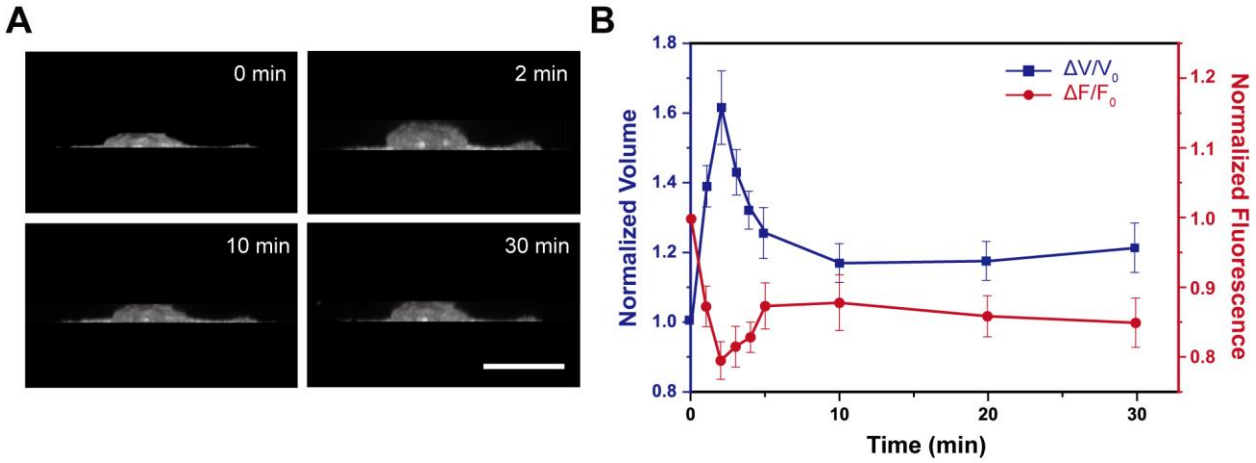

Figure 2-12: Volume and membrane fluorescence dynamics of NIH 3T3 cells expressing the MscL membrane tension reporter (MscL(G22S)61-cpGFP) exposed to a hypotonic (~165mOsm) solution. (A) 3D reconstruction of cell volume using ImageJ 3D projection. (B) Normalized volume change and cpGFP fluorescence change under hypotonic shock of 165 mOsm. Confocal images were captured every 1 min after osmotic shocks for the first 5 min followed by once every 5 min. Ten cells were analyzed for each condition from three independent experiments. Scale bars: 10 μm. The error bars denote standard error.

2.4.4 Fluorescence Response of the MscL Tension Reporter Expressed in Cells in Response to Different Substrate Rigidities

Finally, we used polydimethylsiloxane (PDMS) micropost arrays to further demonstrate the applicability of the MscL membrane tension sensor in cells under different spreading conditions. Micropost array technologies have been widely used to study the mechanosensitive behaviors of cells. Cells attached to fibronectin-coated microposts with different post heights,

therefore stiffnesses, experience different degrees of cell spreading[276,283,284]. Cells attached to shorter microposts have greater membrane tension as they spread more on more rigid substrates. Conversely, longer microposts cause lower plasma membrane tension due to limited cell spreading on softer substrates. For our assay, fibronectin (50 μg/mL) was microcontact printed onto micropost arrays to create an adhesive surface. Human mesenchymal stem cells (hMSCs) co-transfected with the MscL tension reporter and TMD-Halo were seeded at a density of around 1,500 cells/cm2 on micropost arrays with posts of 1.83 μm diameter and 2.3 or 6.4 μm height. We observed successful expression and membrane localization of the MscL tension reporter, and cells seeded on short microposts exhibited lower cpGFP membrane fluorescence than those attached to longer microposts (**Figure 2-13**A), consistent with the data from the osmotic pressure experiments in Figure 2Ai. We should note that cells were transfected prior to seeding them on short vs long microposts, so differences in membrane tension reporter fluorescence intensity in cells on short vs long microposts could not have resulted from different expression levels. As expected, cells spread more on short microposts than on long microposts, irrespective of the constructs expressed (**Figure 2-13**B).

While cells expressing the MscL tension sensor responded to changes in cell spreading, with ~33% reduction in average of membrane fluorescent intensity from longer to shorter microposts, the control MscL(G22S)-c-term-GFP expressing cells showed no difference in GFP membrane fluorescence under the same conditions (**Figure 2-13**C).

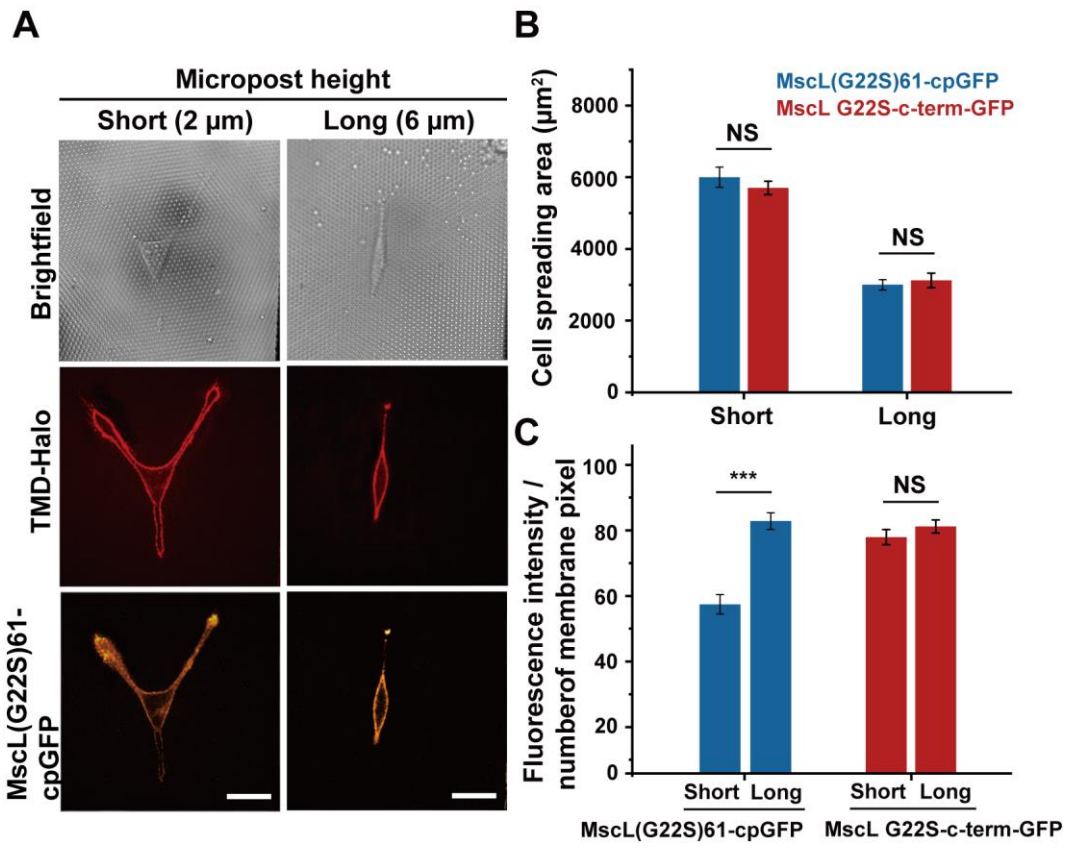

Figure 2-13: Fluorescence response of the MscL tension reporter expressed in hMSCs attached to micropost arrays with different rigidities. (A) Confocal images showing the expression of the MscL tension reporter in hMSCs spreading on short (left) or long (right) microposts. (B) Cell spreading areas of hMSCs on microposts with different heights. (C) Average fluorescence intensity of cpGFP or GFP signals localized to the cell membranes in response to different substrate rigidities. Nine cells were analyzed for each post height from three independent experiments. Scale bars: 50 μm. The error bars denote standard error. NS denotes not significant. ***: $p < 0.001$.

2.5 Conclusion

Our study demonstrates that the MscL tension reporter can be expressed efficiently on cell membranes and used in different cell types for membrane tension measurement. However, one drawback is the limitation that the reporter only measures membrane tension in hypotonic conditions due to intact MscL structure under iso- and hypertonic conditions. Another potential concern is that MscL expression may exert major physiological effects on the cells and alter innate cell membrane tension and volume regulation, given MscL's large opening. To what extent MscL

opening regulates membrane tension is debatable and remains to be tested. In bacteria, MscL serves as an emergency release valve for tensional homeostasis. Bacteria have significantly higher surface area-to-volume ratios compared to mammalian cells, so it is not apparent to what degree MscL opening alters membrane tension in mammalian cells. Previously, our lab has expressed MscL in mammalian cells and introduced membrane-impermeable small molecules into cells following a 2–3 min hypo-osmotic shock[281]. We did not find MscL expression and their activation had an adverse effect on cell viability. In another more recent work, we examined migration of MscL-expressing cells in confining microfluidic channels and found that migration velocity was not affected once they entered the microfluidic channel but that MscL-expressing cells were stuck more at the entrance than were the control cells[275]. Nevertheless, the effect of MscL activation on cell physiology should be further examined to ensure the use of the reporter does not adversely impact cell physiology. As alluded to earlier, our MscL tension reporter is both a tension sensor and an actuator since its opening can lead to upregulated transmembrane transport. In this context, it is perhaps worth speculating that the cpGFP inserted into the extracellular loop may reduce MscL conductance. Finally, it will be desirable to perform a detailed analysis of membrane tension and fluorescence from the reporter. Membrane tension response to hypo-osmotic shock likely varies significantly across cell types and such calibration, in each experimental system, would be necessary for quantitative assessment of membrane tension and would be the subject of future research. Given our goal was to establish a membrane tension reporter based on MscL, we believe our current data support the use of this reporter.

In summary, we successfully developed an optical membrane tension reporter by repurposing MscL through insertion of cpGFP. As an OFF sensor, fluorescence of the MscL tension reporter is negatively correlated to membrane tension. The MscL membrane tension

reporter is user-friendly, thus offering a useful approach for detailed investigations of spatial and temporal dynamics of membrane tension, which will help advance research in cell mechanics, mechanotransduction, and cell signaling in a variety of cell types (e.g., mammalian, plant, and archaea) and subcellular organellar membranes including the membranes of the nucleus and the endoplasmic reticulum.

Chapter 3 Investigation of Osmoregulation and Mechanosensitivity of Pkd2 Using Synthetic Cells with Encapsulated Cell-Free Expression System

The results of this chapter have been published in Poddar, Hsu et al. *Molecular Biology of Cell*, 2022. A.P, Y.Y.H., Q.C., and A.P.L. contributed to the conception and design of the conceived of the study. Y.Y.H. designed and carried out all *in vitro* experiments/ encapsulation experiments in liposomes shown in Figures 3.1- 3.6. A.P., F.Z., A.S., Z.K., C.M., M.M., and A.R. designed and carried out all *in vivo* experiments/cell culture shown in Figures 3.7 and 3.8. A.P, Y.Y.H. wrote the paper. All authors contributed to the manuscript revision and approved the final version. Q.C. and A.P.L. provided supervision and administered the project.

3.1 Abstract

Pkd2 is the fission yeast homologue of human polycystins. This putative ion channel localizes to the plasma membrane and is required for the expansion of cell volume during interphase growth and cytokinesis, the last step of cell division. However, the channel activity of Pkd2 remains untested. Here, we examined the calcium permeability and mechanosensitivity of Pkd2 through *in vitro* reconstitution and calcium imaging of Pkd2 mutant cells. Pkd2 was translated and inserted into the lipid bilayers of giant unilamellar vesicles using a cell-free expression system. The reconstituted Pkd2 permeated calcium when the membrane was stretched via hypo-osmotic shock. *In vivo*, inactivation of Pkd2 through a temperature-sensitive mutation *pkd2-B42* reduced the average intracellular calcium level by 34%. Compared with the wild type, the hypomorphic mutation *pkd2-81KD* reduced the amplitude of hypo-osmotic shock–triggered

calcium spikes by 59%. During cytokinesis, mutations of *pkd2* reduced the calcium spikes, accompanying cell separation and the ensuing membrane stretching, by 60%. We concluded that fission yeast polycystin Pkd2 allows calcium influx when activated by membrane stretching, representing a likely mechanosensitive channel that contributes to the cytokinetic calcium spikes.

3.2 Introduction

Force plays a pivotal role in separation of daughter cells during cell division in eukaryotes[285,286]. Fission yeast cytokinesis, in particular, relies on mechanical contributions from various sources, such as the contractile ring, the septum, and turgor pressure[287–289]. The tension generated by the actomyosin contractile ring has been identified as a crucial initiator of cell separation, with studies revealing its significance in the molecular mechanism of fission yeast cytokinesis[290]. The assembly of the actomyosin contractile ring, a process shared with animal cells, involves essential proteins like Myo2p, Cdc12p, and cofilin, along with continuous actin filament polymerization[291–294]. Subsequent to ring assembly, closure is orchestrated by the activities of both type II and type V myosins[295,296]. The final step of cytokinesis is cell separation encompassing septum biosynthesis and cell wall degradation[297–300]. Importantly, the mechanical cue provided by the ring guides septum biosynthesis[301], and the pressure applied by the expanding septum aids cleavage furrow ingression and anchors the furrow at the division plane[302].

Turgor pressure also plays a significant role in yeast cell morphogenesis including separation of daughter cells[303,304]. Despite the critical roles of these forces, understanding how these mechanical stimuli are sensed and modulated during fission yeast cytokinesis remains a challenge. Some propose the force sensitivity of myosin II[305,306], a motor protein in the ring, but the mechanism remains unclear. Additionally, few studies have explored alternative mechanisms

for force sensing during cytokinesis, including the potential involvement of mechanosensitive (MS) channels[41].

In our investigation, we delved into the functions of MS channels in cytokinesis using the fission yeast *Schizosaccharomyces pombe*. Specifically, we examined the role of the putative transient receptor potential (TRP) channel Pkd2 in fission yeast cytokinesis. TRP channels, known for their mechanical activation, respond to various environmental stimuli through signaling cascades that modify membrane lipid composition, alter plasma membrane conformation, and gate the TRPs via membrane stretch. Consisting of seven subfamilies, this family of nonselective cation channels has been found in most eukaryotes and many eukaryotic MS channels including human polycystin PKD2. Polycystins are evolutionarily conserved calcium-permissive cation channels. Loss-of-function mutations of human polycystins lead to one of the most common genetic disorders, autosomal dominant polycystic kidney disorder (ADPKD), which is diagnosed in 1 in 1000 live births[307,308]. Homologues of polycystins have been found in most metazoans, including fruit flies and worms[309,310], as well as unicellular organisms such as social amoebae[311], green algae[312], and fission yeast[313].

The fission yeast polycystin homologue Pkd2 is an essential protein required for both cell division and growth. Pkd2 localizes to the plasma membrane throughout the cell cycle[314]. During interphase, Pkd2 is enriched at the cell tips, where the putative channel promotes the extension of cylindrical fission yeast cells[315]. During cytokinesis, Pkd2 moves to the equatorial plane, regulating contractile ring constriction and cell separation[314]. The importance of Pkd2 is proved by the failure of separation between daughter cells in the absence of Pkd2. Additionally, Pkd2 antagonizes the activity of the yeast Hippo signaling pathway SIN (septation initiation network) by modulating its activity and localization during cytokinesis[315]. Although fission yeast

cytokinesis is accompanied by a temporary increase in intracellular calcium concentration through cytokinetic calcium spikes[316], it remains unclear If Pkd2 Is related to the regulation of calcium levels in this process and how it is activated.

Although numerous MS channels have been well-studied in living cells, there are still many limitations to investigate their molecular mechanism in response to mechanical force due to the intrinsic complexity of their protein structures and interactions with other endogenous cellular components in the passive cytoplasm. Therefore, reconstitution experiments using bottom-up *in vitro* expression of transmembrane proteins, including ion channels, have become a powerful approach to investigating their functions, compared with using purified proteins expressed from cells. For expression of certain proteins in cells, growth retardation or lysis of the host cells and low endogenous expression levels contribute to poor production of heterologous recombinant proteins[317]. Despite advances in protein purification, several limitations exist with in vitro reconstitution of membrane proteins with complicated structures, such as improper protein function, compromised membrane integrity due to residual detergents, and poor control over the orientation of protein insertion[208,318–321]. Cell-free expression(CFE) systems coupling transcription and translation reactions outside the cellular environment have shown the potential to overcome the barriers mentioned above and can be a robust strategy for protein synthesis and investigation[234,322–325]. For example, the bacterial mechanosensitive channel MscL is expressed by encapsulating CFE reactions in giant unilamellar vesicles (GUVs) and has been shown to sense physical stimuli[326,327]. Since bacterial lysate lacks membranous components, eukaryotic CFE systems are gaining increasing attention for in vitro production of membrane proteins[327]. Their innate endogenous microsomal structures enable newly synthesized membrane proteins to insert directly into the natural endoplasmic reticulum (ER)–based lipid bilayers without detergents. This

eukaryotic CFE-based approach significantly reduces the potential for membrane protein denaturation and favors their proper folding in vitro.

In this study, we examined the calcium permeability and mechanosensitivity of Pkd2 through *in vitro* reconstitution using eukaryotic cell-free protein expression platform. We first expressed the putative channel Pkd2 in a HeLa-based CFE system and reconstituted it in a lipid bilayer. To determine the orientation of Pkd2 in the membrane, we used a pronase digestion assay with *Streptomyces griseus*–derived pronase[328]. To determine whether Pkd2 can be force-activated to regulate calcium influx, we applied different osmotic pressures to GUVs co-expressing Pkd2 and G-GECO, a fluorescent calcium-sensitive reporter, and monitored the fluorescence changes inside GUVs. The functions of the Pkd2 channel were also investigated *in vivo* by observing the calcium spikes in response to fast expansion of the plasma membrane under microfluidics-applied osmotic shock using a GcaMP-based calcium indicator in the *pkd2* mutant yeast cells in comparison to the wild type cells. Overall, our study demonstrated Pkd2 as a likely MS channel that promotes calcium influx during cytokinesis.

3.3 Materials and Methods

3.3.1 DNA Constructs

Pkd2-sfGFP was constructed through High-Fi DNA Assembly (NEB). All PCR reactions were carried out with Q5 High-Fidelity DNA Polymerase (NEB #M0491). The cDNA of Pkd2 was amplified from the plasmid Pkd2-EGFP-N1 (Lab stock) using the forward primer AACCCTCAAAAGACAAGACCATGAGGCTTTGGAGAAGCCC and the reverse primer AAGAATTCGTCGACCTCGAGACGAAAA-GCATTGTTAGGTA. The vector pAV0714 (Vjestica et al., 2020) was amplified using the forward primer TACCTAACAATGCTTTTCGT-CTC-GAGGTCGACGAATTCTT and the reverse primer

GGGCTTCT-CCAAAGCCTCATGGTCTTGTCTTTTGAGGGTT. The PCR products were then digested with DpnI for 1 h at 37°C and purified with Macherey-Nagel NucleoSpin Gel and PCR Clean-Up kit (NC0389463). The purified fragments were assembled through HiFi DNA Assembly (NEB, E2621S) to generate the Pkd2-sfGFP construct (QC-V199).

To generate Pkd2-His6 and Pkd2-sfGFP-His6 for the HeLa CFE reaction, the SUN1FL-His6 construct in pT7-CFE1-Chis[255] was used as a template for Gibson assembly cloning. Initially, Pkd2 was amplified from QC-V199 using the primers Pkd2–Forward: CCACCACCCATATGGGATCCGAATTCATGAGGCTTTGGAGAAGCCC and Pkd2–Reverse: CTCGAGTGCGGCCGCGTCGACTTAACGAAAAGCATTGTTAGGTAATGG with Phusion High-Fidelity DNA Polymerase. The DNA of Pkd2–sfGFP was amplified from QC-V199 using the primers Pkd2–sfGFP–Forward: CACCC-ATATGGGATCCGAATTCATGAGGCTTTGGAGAAGCCCAC and Pkd2–sfGFP–Reverse: CGAGTGCGGCCGCGTCGACCTTATAAAGCTCGTCCATTCCGTGAG. The next step was to insert Pkd2 or Pkd2-sfGFP into pT7-CFE1-Chis downstream from the T7 promoter construct by replacing SUN1FL with Pkd2 in the pT7-CFE1-Chis construct (Thermo Fisher Scientific). To remove SUN1FL from the pT7-CFE1-SUN1FL-His6 construct (Majumder et al., 2018) as the backbone, we used primers pT7–CFE–Forward: GAATGGACGAGCTTTATAAGGTCGACGCGGCCGCACTC and pT7–CFE–Reverse: GCTTCTCCAAAGCCTCATGAATTCGGATCCCATATGGGTGGTG with Phusion High-Fidelity DNA Polymerase for PCR amplification. Afterward, the resulting PCR products, Pkd2, Pkd2-sfGFP, and pT7CFE-Chis, were digested with DpnI for 1 h at 37°C and subsequently purified with a QIAquick Gel Extraction Kit (Qiagen #28704). They were ligated with homemade

Gibson Master Mix (**Table 3-1**) to create pT7-CFE1-Pkd2-Chis and pT7-CFE1-Pkd2-sfGFP-Chis constructs.

Table 3-1: 2X homemade Gibson master mix for 20 reactions. The mixture is split in 5 µl aliquots for each reaction and should be froze immediately with liquid nitrogen. The reactions can be stored at -80°C for up to 3 months.

5X isothermal reaction buffer	40 µl
10U/µl T5 exonuclease	0.1µl
2U/µl Phusion polymerase	2.5 µl
40U/µl Taq DNA ligase	20 µl
UltraPure Dnase/Rnase-Free Distilled Water	37.4µl
Total	100 µl

3.3.2 CFE Reactions

We used the 1-Step Human Coupled IVT Kit (Thermo Fisher Scientific #88881) to produce Pkd2 protein in vitro. The reaction was carried out based on the manufacturer's protocol. Briefly, 1 µl plasmid DNA (~500 ng/µl) was used for one 10-µl reaction. G-GECO plasmid was used in a previous study[182]. CFE reactions were carried out at 30°C for 3 h. Pkd2-sfGFP expression was measured on a fluorescence plate reader (Biotek Synergy H1).

3.3.3 SUPER Template Generation

SUPER templated beads were generated following a published protocol[329]. For SUPER template formation, 25 µl of small unilamellar vesicle (SUV) solution was fused with 2 µl of 5-µm silica beads (Bangs Laboratories) in the presence of 1 M NaCl. The final SUPER templated beads were washed with PBS twice by centrifuging at 200 × g for 2 min and then resuspended in 30 µl of milli-Q water at a final concentration of ~9.6 × 106 beads/ml. The SUPER template stock can be stored at room temperature for 3 h.

For SUV generation, 75% 1,2-dioleoyl-sn-glycero-3-phosphatidylcholine (DOPC), 24.9% cholesterol, and 0.1% Rhod-PE for a final concentration of 1 mM were mixed and dried under vacuum for 1 h. One milliliter of milli-Q water was then added, and the tube was thoroughly vortexed. The mixture was then passed through a liposome extruder (T&T Scientific, Knoxville, TN) with a 100-nm porous membrane 11 times to generate SUVs.

3.3.4 Vesicle Encapsulation System

Vesicles were generated by modifying the continuous droplet interface crossing encapsulation (cDICE) method. The device contains a rotor chamber made with clear resin using a 3D printer (Formlabs) mounted on the servo motor of a benchtop stir plate. The procedure involves an inner solution (IS), outer solution (OS), and lipid-in-oil solution (LOS). HeLa-based CFE reactions with the addition of 5% OptiPrep (to increase the density to aid sedimentation of GUVs) were prepared as the IS. OS stock (115 mM HEPES, 23 mM MgCl2, 1.15 M KCl, 770 mM glucose) was diluted with Milli-Q water to the same osmolarity matching that of the IS. The LOS consists of 40% DOPC, 30% DOPE, 29.9% cholesterol, and 0.1% Rhod-PE in mole percentage with a total lipid concentration of 0.4 mM thoroughly mixed with the desired volume of 1:4 mineral oil: silicone oil by vortexing for at least 10 s. The water-in-oil emulsion was first generated by vigorously pipetting CFE reactions in 500 µl of LOS ~10 times. Then 700 µl of aqueous OS, 5 ml of LOS, and the water-in-oil emulsion were sequentially added into the cDICE chamber rotating at 700 rpm. After 2 min of rotation, vesicles accumulating in the OS near the chamber wall could be gently collected from the capped hole near the outer edge of the chamber.

3.3.5 Airfuge Fractionation Assay

After the CFE reaction was completed, it was collected in a 1.5-ml microcentrifuge tube and then mixed well with 30 µl of extraction buffer (20 mM HEPES-KOH, pH 7.5, 45 mM potassium acetate, 45 mM KCl, 1.8 mM magnesium acetate, 1 mM dithiothreitol [DTT]). Then 40 µl of the mixture was transferred to an ultracentrifuge tube and centrifuged at around 100,000 × g for 15 min at room temperature using an airfuge (Beckman Coulter). After the centrifugation, 20 µl of the supernatant was carefully recovered and transferred to a 1.5-ml microcentrifuge tube without disturbing the pellet, and the remaining 20 µl of pellet fraction was resuspended by pipetting up and down to thoroughly mix before transferring to another microcentrifuge tube. The centrifugation cycles mentioned above can be repeated multiple times, as shown in **Figure 3-3**. To investigate the protein incorporation, 2 µl of SUPER templated beads were added and incubated with the supernatant and pellet fractions respectively for 30 min at room temperature and then centrifuged at 300 × g for 3 min. After the centrifugation, SUPER templated beads were visible as a small white pellet, and the remaining supernatant was collected as the final pellet fraction. The SUPER template pellets were washed twice with PBS by centrifuging at 200 × g for 2 min and then resuspended in 30 µl of milli-Q water at a final concentration of ~9.6 × 106 beads/ml. Following the recovery of fractions, the amount of cell-free expressed Pkd2 in each fraction can be determined by visualizing fluorescence proteins on an SDS–PAGE gel.

3.3.6 Pronase Digestion Assay

Lyophilized S. griseus pronase (Roche) was dissolved in Milli-Q water to a stock concentration of 6 mg/ml and stored at 4°C for a maximum of 3 d. After 1 h of incubation of CFE reactions with SUPER templates, the beads were pelleted by centrifugation at 300 g for 3 min. The supernatant was then gently removed and collected for fluorescence gel imaging. The remaining bead pellets were washed twice with 1 ml of PBS (Ca2+ and Mg2+-free, pH 7.5) by centrifugation

at 200 × g for 2 min, followed by resuspension in 20 µl of PBS. Next, 10 µl of the SUPER templated beads in PBS was incubated with 5 µl of pronase stock solution (6 mg/ml) at room temperature for 15 min. The final concentration of pronase was 2 mg/ml, and the other 10 µl of beads were used for observing the protein incorporation as a control. Confocal fluorescence images were taken 15 min after the addition of pronase.

3.3.7 Confocal Fluorescence Microscopy and In-Gel Imaging of In Vitro Reconstituted Pkd2

All images were acquired using an oil immersion 60×/1.4 NA Plan-Apochromat objective with an Olympus IX-81 inverted fluorescence microscope (Olympus, Japan) controlled by MetaMorph software (Molecular Devices, USA) equipped with a CSU-X1 spinning disk confocal head (Yokogawa, Japan), AOTF-controlled solid-state lasers (Andor, Ireland), and an iXON3 EMCCD camera (Andor). Images of sfGFP and lipid fluorescence were acquired with 488-nm laser excitation at an exposure time of 500 ms and with 561-nm laser excitation at an exposure time of 100 ms, respectively. Each acquired image contained ∼5 lipid bilayer vesicles or ∼10 lipid-coated beads that had settled upon a 96-well glass-bottom plate or a coverslip, respectively. Three images were taken at different locations across a well or coverslip for an individual experiment. Three independent repeats were carried out for each experimental condition. Samples were always freshly prepared before each experiment.

FluoroTect Green lysine-tRNA (green lysine) was purchased from Promega. In-gel imaging of Pkd2-sfGFP or Pkd2 was carried out on a Sapphire biomolecular imager (Azure Biosystems). Samples were not heated to retain in-gel sfGFP and green lysine fluorescence.

3.3.8 Image Analysis

To quantify the fluorescence inside the lipid bilayer vesicles, all images were analyzed using MATLAB. All data was included for analysis without blinding. Since all the vesicles were labeled with rhodamine PE, the edges/boundaries of vesicles were first detected and isolated, corresponding to the red fluorescence rings using the function "imfindcircles" embedded in MATLAB. Averaged background–intensity measurements were then performed for each image by the average fluorescence (of all pixels), excluding the area of vesicles defined by the code in MATLAB from the previous step. For quantification, the final fluorescence intensity of each vesicle was obtained by averaging the fluorescence of all the pixels inside the vesicles after subtracting the average background intensity. For the box plots marking the first and third quartile and the median in **Figure 3-5**F, each data point represents the fluorescence of one vesicle after normalization with respect to the average background subtracted fluorescence intensity of vesicles corresponding to the cell-free expressed proteins at time zero under each condition. Since there are two independent variables, time and osmotic condition/osmolarity, statistical analysis was performed using two-way ANOVA followed by Dunnett's post-hoc test for all data among all groups throughout the whole experiment. The quantitative data was compared/analyzed between the individual groups at a certain time followed by a two-tailed t-test with a significance level of 0.05. $p < 0.05$ was considered statistically significant. P values are indicated as * $p < 0.05$; ** $p < 0.01$; *** $p < 0.001$.

3.3.9 Yeast Genetics and Cell Cultures

We followed the standard protocols for yeast cell culture and genetics (Moreno et al., 1991). Tetrads were dissected with a Spore+ micromanipulator (Singer, UK). All the fission yeast strains used in this study are listed in **Table 3-2**.

Table 3-2: List of fission yeast strains

Strains	Genotype	Source
QC-Y941	*h-leu1::kanMX6-Padh1-GcaMP6s-Tadh1 ura4-D18 his3- D1 ade6-M216*	Lab Stock
QC-Y949	*h-leu1::kanMX6-Padh1-GcaMP6s-Tadh1 ura4-D18 his3- D1 ade6-M216*	This study
QC-Y1004	*h+rlc1-tdTomato-natMX6 leu1::kanMX6-Padh1- GcaMP6s-Tadh1 ura4-D18 ade6-M216*	Lab Stock
QC-Y1027	*h?kanMX6-81xnmt1-pkd2 rlc1-tdTomato-natMX6 leu1::kanMX6-Padh1-GcaMP6s-Tadh1 ura4-D18 his3-D1 ade6-M216*	This study
QC-Y1064	*h-leu1::kanMX6-Padh1-GcaMP6s-mCherry-ura4+ his3- D1 ade6-M216*	Lab Stock
QC-Y1182	*h?pkd2::pkd2-B42-ura4+-his5+ leu1:: kanMX6-Padh1- GcaMP6s-Tadh1 his3-D1 ade6-M216*	This study
QC-Y1343	*h?leu1::kanMX6-Padh1-GcaMP6s-mCherry-ura4+ kanMX6-81xnmt1-pkd2 his3-D1*	This study
QC-Y1365	*h? pkd2::pkd2-B42-ura4+-his5+ leu1::kanMX6-Padh1- GcaMP6s-mCherry-ura4+ his3-D1*	This study
QC-Y1425	*h? sid2-250 ura4-D18 ade-M21X leu1-32 leu1::kanMX6- Padh1-GcaMP6s-mCherry-ura4+ his3-D1 ade6-M216*	This study
QC-Y1426	*h? orb6-25 ade-M21X leu1::kanMX6-Padh1-GcaMP6smCherry-ura4+ his3-D1*	This study
QC-Y1436	*h? pkd2::pkd2-B42-ura4+-his5+ rlc1-tdTomato-NatMX6 leu1::kanMX6-Padh1-GcaMP6s-Tadh1 ade6-M216*	This study
QC-Y1457	*h? kanMX6-P3nmt1-pkd2 leu1::kanMX6-Padh1- GcaMP6s-mCherry-ura4+ his3-D1 ade6-M216*	This study
QC-Y1586	*h? leu1::Pbip1-mCherry-ADEL leu1+ his+ ade6-M216 ura4-D18*	This study

3.3.10 Microscopy of Fission Yeast Cells

For microscopy, fission yeast cells were first inoculated in a YE5S medium for 2 days at 25°C. Then 1 ml of the exponentially growing cell culture, at a density between 5×10^6/ml and 1.0×10^7/ml, was harvested by centrifugation at 4000 rpm for 1 min. It was washed three times with synthetic EMM medium ($[Ca^{2+}] = 10^7$ μM) and resuspended in 1 ml of EMM before proceeding for microscopy. Then 20 μl of the resuspended cells were spotted in a 10-mm Petri dish with a glass coverslip (#1.5) at the bottom (D35-10-1.5N, Cellvis). The coverslip was

precoated with 50 µl of 50 µg/ml lectin (Sigma, L2380) and allowed to dry overnight at 4°C. The cells were allowed to attach to the coverslip for 10 min at room temperature before addition of another 2 ml EMM in the Petri dish.

We employed a spinning-disk confocal microscope for fluorescence microscopy using an Olympus IX71 unit equipped with a CSU-X1 spinning-disk unit (Yokogawa, Japan). The motorized stage (ASI, USA) included a Piezo Z Top plate for acquiring Z-series. The images were captured on an EMCCD camera (IXON-897, Andor) controlled by iQ3.0 (Andor). Solid-state lasers of 488 and 561 nm were used at a power of no more than 2.5 mW. Unless specified, we used a 60× objective lens (Olympus, Plan Apochromat, NA = 1.40). A Z-series of eight slices at a spatial distance of 1 µm was captured at each time point. The microscopy was carried out in a designated room maintained at 22 ± 2°C. To minimize environmental variations, we typically imaged both control and experimental groups in randomized order on the same day.

We employed a CellASIC ONIX2 system controlled by a desktop computer through ONIX software (EMD Millipore) to apply osmotic shock. Using a yeast haploid microfluidics plate (Y04C, EMD Millipore), we pushed the cells into the imaging chamber at a pressure of 34–55 kPa for a minimum of 2 min using EMM media. The trapped cells were equilibrated in EMM for 10 min at a pressure of 10 kPa. The same perfusion pressure was applied afterward for the media exchange (EMM, EMM-calcium and EMM+2 mM EGTA).

3.3.11 Calcium Imaging of Fission Yeast Cells and Data Analysis

To measure the intracellular calcium level of single fission yeast cells, we quantified the fluorescence intensity of cells expressing GcaMP-mCherry[316]. GcaMP and mCherry fluorescence were calculated from the average intensity projection of Z-series after the background subtraction. To measure the intracellular calcium level, we quantified the average fluorescence intensity on a

line drawn along the long axis of a cell. GcaMP-to-mCherry fluorescence ratio gave a more accurate measurement than GcaMP alone for quantifying the calcium levels because it took into consideration the intracellular concentration of the calcium reporter. A small fraction of the pkd2 mutant cells appeared to be deflated temporarily, as we reported previously[314,315]. They were included in our measurements as well. Whenever a temperature shift was required, cells were imaged at 36°C for 4 h after incubation.

For time-lapse measurement of calcium spikes, we quantified the fluorescence intensity of cells expressing GcaMP. The GcaMP fluorescence was quantified from the average intensity projection of the Z-series on a line along the long axis of a cell throughout osmotic shock. The fluorescence intensities were background-subtracted and normalized to the average value before application of osmotic shock. Amplitudes of a calcium spike were defined as ΔF/F0. ΔF equals Fmax, the maximum value during the first 10 min after osmotic shock, minus the baseline value F0, calculated as the average of the five data points before osmotic shock.

3.3.12 Computation-Assisted Quantification of Cytokinetic Calcium Spikes

We applied custom-written software to extract the parameters of cytokinetic calcium spikes from time-lapse microscopy. Specifically, the analysis of the separation spikes was performed in two separate segments, before and after cell separation. The first step of this analysis involves removal of background noise to increase the signal to noise ratio (SNR) by preprocessing the image sequences extracted from the videos. The images were passed through a median filter, which smoothed them while preserving their spatiotemporal resolution. The background fluorescence was removed by subtracting the temporal average of each median-filtered pixel value from the median-filtered images at each time point. A binary mask was generated by further subtracting the average pixel value of each frame and binarizing the images using Otsu's thresholding method.

The signal from individual cells were identified by applying the binary mask on the median-filtered background-subtracted images and the average fluorescence intensity value per pixel was calculated for each frame. For postcell separation, the two daughter cells were analyzed separately. The aforementioned steps were also applied on the daughter cells separately, that is, median filtering followed by background subtraction and application of the binary mask. Additionally, we applied a size-based filter to digitally eliminate any other fragments of cells that may be present within the field of view and interfere with the analysis. This filtering was done by detecting the objects (cells) and calculating their area. Any object with size below a preset cutoff was eliminated from Analysis. The cutoff size was manually calculated based on the average of more than 20 different cells.

The time-dependent average fluorescence intensity (per pixel in each frame) was recorded for each cell both before and after the cell separation. Temporal averaging of the signal was performed in order to eliminate any minute fluctuations within the data and intensity values lower than a threshold value was nullified. The locations of the peaks are defined by the point of inversion of the derivative from positive to negative. These locations (frame number/timepoint) and the average fluorescence intensity values corresponding to these time points were recorded and used for analysis.

The temporal average of the baseline fluorescence Intensity value (per pixel) was calculated by applying the binary mask on the original images without any preprocessing. The baseline for the parent cell and the two daughter cells were calculated separately. The video processing and analysis was performed by implementing our custom developed code in MATLAB (MathWorks, MA).

3.4 Results

3.4.1 Synthesis of Pkd2 Using Mammalian Cell-Free Expression

We used a CFE system to synthesize this putative channel Pkd2 *in vitro*. We expressed full-length Pkd2 tagged with superfold GFP (sfGFP) at the C-terminus in a HeLa cell extract–based CFE system. To monitor expression yield, we quantified the fluorescence of Pkd2-sfGFP over 3 h (**Figure 3-1**). The fluorescence increased gradually and reached a plateau after 2 h. We concluded that Pkd2 is efficiently expressed in our cell-free system.

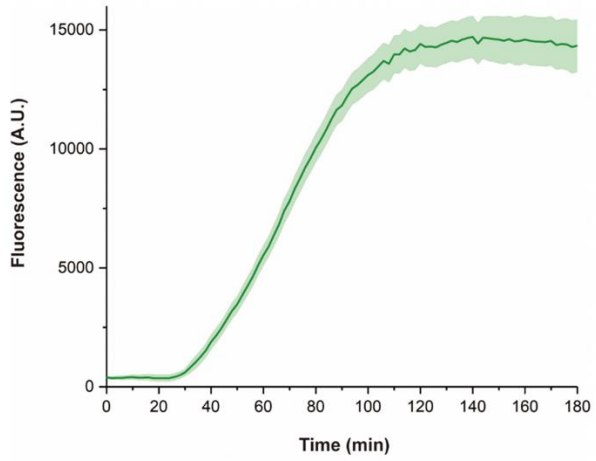

Figure 3-1: Synthesis of Pkd2 using a mammalian CFE system. Time course of the expression of Pkd2-sfGFP using HeLa-based CFE reaction by monitoring sfGFP fluorescence. Error bands represent the standard deviation calculated from three independent reactions.

We then determined if the *in vitro* synthesized Pkd2 can be reconstituted as a transmembrane protein in supported lipid bilayers with extra reservoir (SUPER) templates (A). The excess lipid bilayer membranes were generated on silica beads by the rupture and fusion of small unilamellar vesicles (SUVs) carrying lipids with negative charges at high ionic strength[326,330]. We incubated SUPER templates with the in vitro translated Pkd2-sfGFP and isolated them by low-speed centrifugation. The supernatant fraction contained most of the CFE reaction, while the pellet fraction included the SUPER templates for different assays (**Figure**

3-2A). The expressed protein appeared as a single band of ~105 kDa on an SDS–PAGE gel (**Figure 3-2**B), which was consistent with the predicted molecular weight of the fusion protein (MW_{Pkd2} = 80 kDa and MW_{GFP} = 27 kDa). The yield was roughly 15 µg from a 10 µl reaction. The lipid-coated beads incubated with the pellet fraction became fluorescent after being washed with PBS (**Figure 3-2**C), thus confirming that Pkd2-sfGFP was incorporated into the SUPER templates.

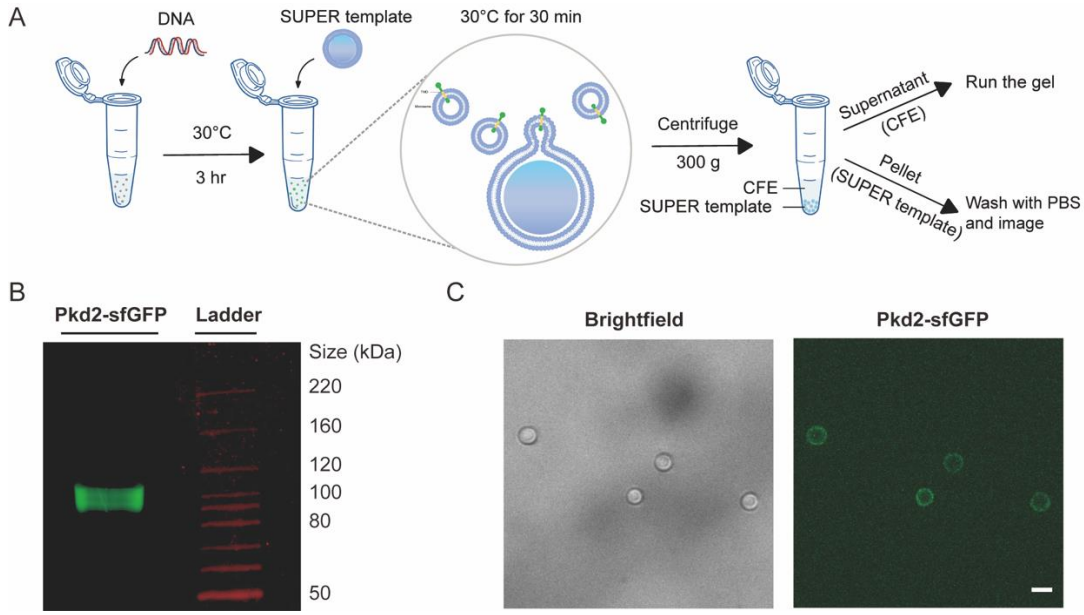

Figure 3-2: Localization of cell-free expressed Pkd2 in SUPER template. (A) Schematic illustrating the use of CFE for in vitro protein production and testing the incorporation of membrane proteins using SUPER templates. SUPER templated beads are added to the CFE reaction expressing Pkd2 protein fused to sfGFP at the C-terminus and incubated together. CFE reaction and SUPER templates are then isolated by low-speed centrifugation for running a gel or imaging, respectively. (B) Fluorescence gel image of cell-free expressed Pkd2-sfGFP added to SUPER templates. (C) Brightfield and fluorescence micrograph of SUPER templates incubated with cell-free expressed Pkd2-sfGFP. Beads were washed with PBS before imaging. Scale bar: 5 µm.

Since several Pkd2 homologues, including the human polycystins, localize to the ER and the plasma membrane of the cilia[307,331,332], we investigated whether Pkd2 similarly translocates into endogenous microsomal structures. We applied a high-speed airfuge assay to CFE-expressed Pkd2, labeled with fluorescently tagged lysine, Green lysine, to isolate supernatant and pellet

fractions; the latter presumably contained microsomes (**Figure 3-3**A). Green lysine is a lysine-charged tRNA labeled with the fluorophore BODIPY-FL at the epsilon amino group and can be incorporated into synthesized proteins during in vitro translation reactions. We found that the majority of Pkd2 was in the pellet, while the amount of Pkd2 in the supernatant decreased as the washing cycles increased (**Figure 3-3**B). This indicated that ER fragments might recognize translocons and membrane protein chaperones to promote Pkd2 insertion into microsomes. When the pellet or supernatant fractions were added to the SUPER templates, only the beads incubated with the pellet fraction were fluorescent (**Figure 3-3**C). We concluded that *in vitro*–expressed Pkd2 translocates into microsomal fragments, which subsequently fuse with the SUPER templates.

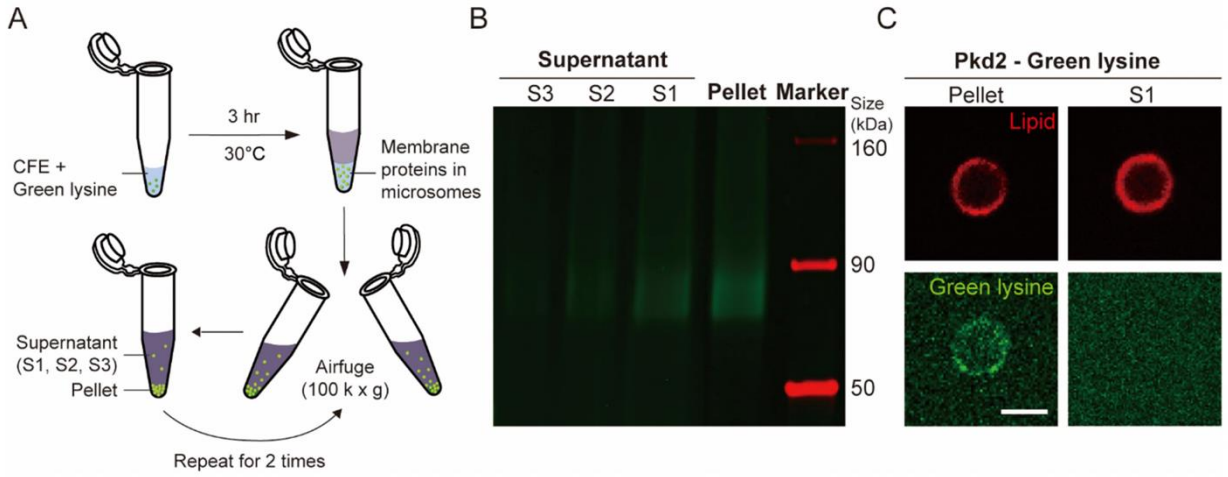

Figure 3-3: Application of a fractionation assay for reconstitution of Pkd2 into SUPER templates. (A) Schematics illustrating the fractionation assay. Cell-free expressed membrane proteins, including Pkd2, were translocated into microsomes after three hours of incubation. The CFE reaction was then centrifuged by using an airfuge three times. Membrane proteins incorporated into microsomes become concentrated as pellets while the remaining CFE reaction remains as supernatant. 10 nM green lysine was added to the CFE reaction before incubation to label Pkd2 for observation. (B) Fluorescent gel image of pellet and supernatant fractions of a CFE reaction. S1-S3 represent the supernatant with increasing number of washing cycles using an airfuge. (C) Representative confocal images of pellet fractions incorporating into SUPER templates using the same approach mentioned in Fig. 1A. Pkd2 did not localize in the supernatant fraction of SUPER templates. Scale bar: 5 µm.

3.4.2 Reconstituted Pkd2 responds to osmotic pressure to permeate calcium

We next determined the orientation of Pkd2 in the lipid bilayer membranes on SUPER templates using an image-based pronase protection assay. Unlike the human polycystins, the

structure of fission yeast Pkd2 has not been experimentally determined. AlphaFold[333] and other transmembrane helices projection software predicted that Pkd2 possesses an N-terminal extracellular domain and a putative C-terminal cytoplasmic tail (**Figure 3-4**A). Depending on the orientation of Pkd2-sfGFP in the lipid bilayer, sfGFP will either be exposed to pronase or be protected from degradation (**Figure 3-4**B). Based on our previous work on reconstituting the nuclear envelope proteins SUN1 and SUN2 in SUPER templates[326], we predicted that Pkd2 would insert into the excess lipid bilayer membranes with its C-terminus orienting outward. We observed that the fluorescence of *in vitro*–translated Pkd2-sfGFP disappeared following pronase treatment (**Figure 3-4**C). We concluded that Pkd2 might be inserted into microsomal fragments in an orientation that positions its C-terminus on the cytosolic side. For the GUVs used in our experiment, the C-terminus of Pkd2-sfGFP would be in the lumen of the vesicle, an orientation consistent with their predicted topology in cells (**Figure 3-5**A), since CFE reactions were encapsulated in vesicles.

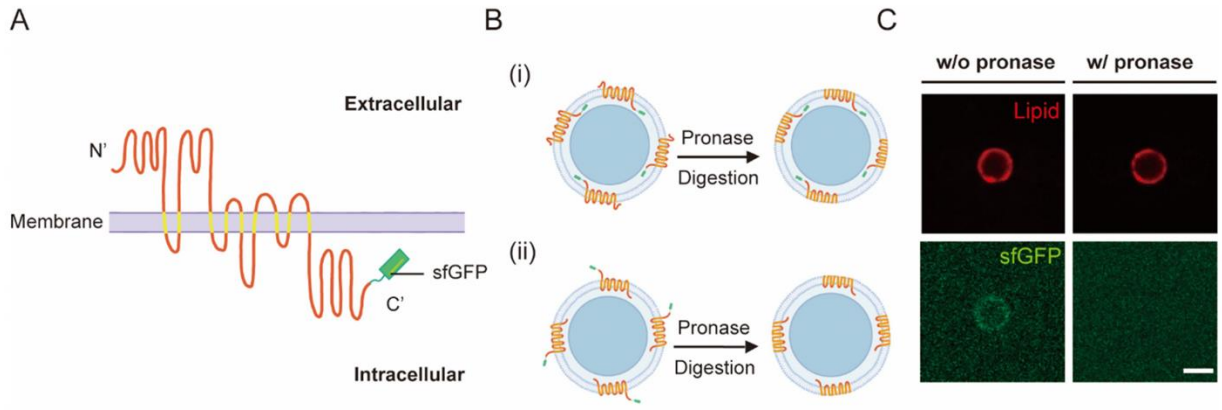

Figure 3-4: Application of a pronase digestion assay to determine the orientation of CFE-synthesized Pkd2 in SUPER templates. (A) Illustration of the putative topology of Pkd2 channel with sfGFP fused to its C-terminus. (B) Schematic illustrating the principle of using pronase digestion to determine the orientation of inserted cell-free expressed Pkd2 into SUPER templates. If Pkd2 proteins were oriented with their N-termini exposed to the solution, sfGFP would be protected from degradation (i). On the other hand, if Pkd2 proteins were oriented with their C-termini protruding away from the lipid-coated bead, then sfGFP would be degraded by pronase (ii). (C) Confocal fluorescence images of SUPER templates (red) incorporating cell-free expressed Pkd2-sfGFP (green) with and without the addition of pronase. Scale bar: 5 μm.

Next, to determine whether reconstituted Pkd2 alone is calcium-permissive, we encapsulated CFE-expressed Pkd2 in GUVs generated using continuous droplet interface crossing encapsulation (cDICE)[334,335] and monitored calcium entry into GUVs (**Figure 3-5**B). A genetically encoded calcium fluorescent reporter, G-GECO, was used to detect calcium entry into vesicles[182]. There was no G-GECO fluorescence in GUVs under iso-osmotic conditions with or without Pkd2 expression (**Figure 3-5**C), indicating that CFE-expressed Pkd2 is mostly nonpermeable to calcium without a stimulus.

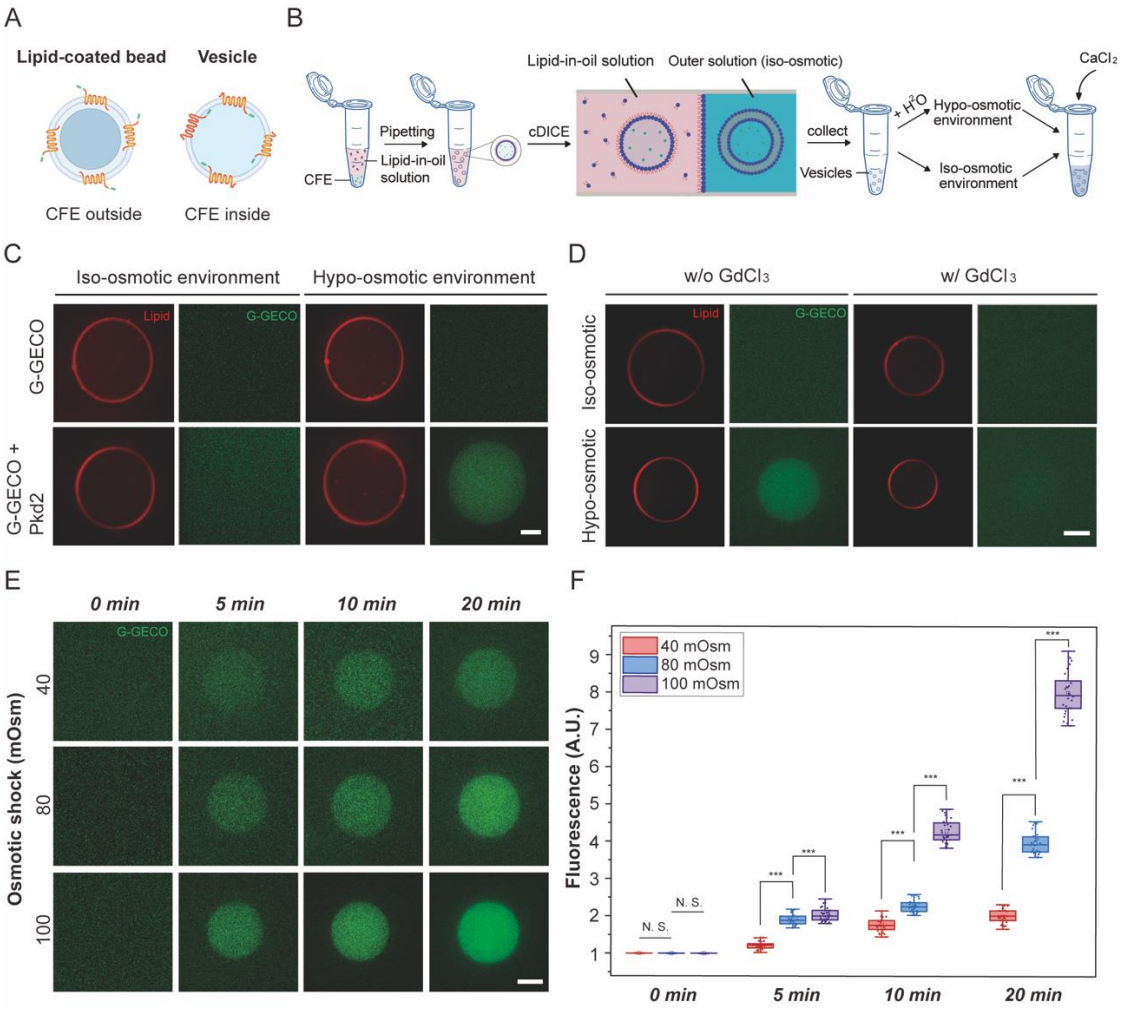

Figure 3-5: Pkd2 reconstituted in GUVs responds to osmotic pressure. (A) Schematic illustrating the directional insertion of cell-free expressed Pkd2 protein into the lipid bilayer membrane of SUPER templated beads and GUVs. Pkd2 channels are oriented with their C-termini protruding away from the lipid-coated beads and with their C-termini pointing inside the vesicles. (B) Schematic illustrates the formation of vesicles encapsulating cell-free expressed proteins using cDICE, followed by applying osmotic shock to Pkd2-containing GUVs. Vesicles were formed under

iso-osmotic conditions and then milli-Q water was added to the outer solution to create a hypo-osmotic environment. A 100-mM $CaCl_2$ stock solution was added to the hypo-osmotic external solution to a final concentration of 10 mM. (C) Representative fluorescence micrographs of vesicles encapsulating 1-mM EGTA and cell-free expressed Pkd2 and G-GECO at t = 10 min after osmotic shock. Plasmid concentrations of Pkd2 and G-GECO were fixed at 1 nM. The final concentration of Ca^{2+} in the hypo-osmotic external solution was 10 mM. The aqueous external solution was made by diluting the external solution stock (HEPES: MgCl2: KCl: glucose [in mM] = 15:3:150:50) with milli-Q water. The osmolarity difference between iso-osmotic and hypo-osmotic solutions was kept at 100 mOsm. (D) Representative fluorescence micrographs of vesicles expressing Pkd2 and G-GECO with addition of $GdCl_3$ for blocking the force-activated function of Pkd2 channels under osmotic shock. $GdCl_3$ was added to the outer solution with the final concentration fixed at 1 mM. The same method and solutions/conditions described in C were used to apply osmotic presure to the vesicles. The images were taken 15 min after the application of osmotic shock. Vesicles expressing Pkd2 and G-GECO without the addition of $GdCl_3$ served as a control. (E) Representative fluorescence micrographs of vesicles encapsulating cell-free expressed Pkd2 and G-GECO under different hypo-osmotic environments at specified time points. The concentrations of EGTA, Pkd2, G-GECO, and Ca^{2+} were the same as indicated in C. (F) Box plot depicting the fluorescence intensities of vesicles under different osmotic conditions and at different times. At least 30 vesicles were analyzed for each condition. All experiments were repeated three times under identical conditions. Scale bars: 10 μm. *** $p < 0.001$.

To determine whether Pkd2 can become calcium-permeable upon mechanical stimulus, we stretched the membrane of Pkd2-expressing GUVs with hypo-osmotic shock. We added water to the external solution of the GUVs. The G-GECO fluorescence in Pkd2-embedded GUVs gradually increased under a hypo-osmotic condition of 100 mOsm (**Figure 3-5**C). In comparison, the fluorescence changed very little under the similar condition in those GUVs without Pkd2 (**Figure 3-5**C). The fluorescence increase was proportional to calcium concentrations in the external solution (**Figure 3-6**). When gadolinium chloride ($GdCl_3$), a nonspecific stretch-activated ion channel blocker, was added to the external solution, it blocked the fluorescence increase of G-GECO inside those Pkd2-expressing GUVs under the same conditions (**Figure 3-5**D). As expected, the peak fluorescence intensities of GUVs increased proportionally to the strength (40–100 mOsm) and duration (0–20 min) of hypo-osmotic shock (**Figure 3-5**E and F). We concluded that Pkd2 is calcium-permeable under the mechanical stimulus of membrane stretching.

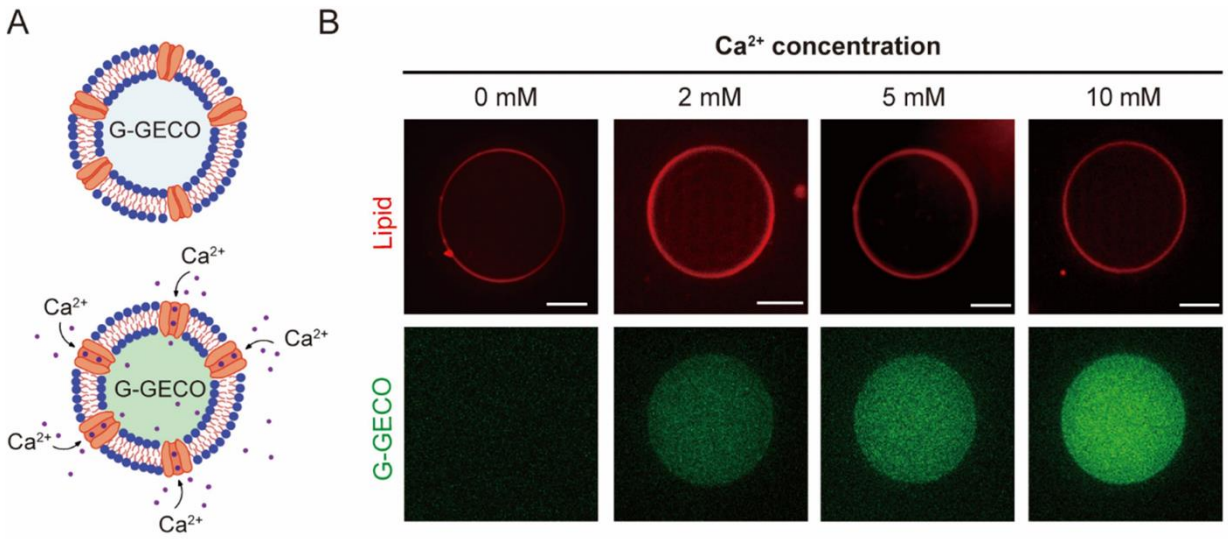

Figure 3-6: Pkd2 mediates calcium influx in response to osmotic pressure in GUVs. (A) Schematic illustrating the function of G-GECO in a Pkd2-expressing GUV. (B) Representative confocal fluorescence images of GUVs encapsulating G-GECO in a hypo-osmotic solution with different external calcium concentrations as indicated. Plasmid concentration of G-GECO was fixed at 1 nM. GUVs were subjected to a hypo-osmotic medium after encapsulation following 3 hours of incubation. The osmolarity difference between internal CFE reactions and external hypo-osmotic solutions was 100 mOsm. Scale bars: 20 μm.

3.4.3 In vivo investigation: Intracellular calcium level and osmotic shock–induced calcium spikes were reduced in pkd2 mutants

Since the human polycystin PC-2 is found in the ER[336], Pkd2 might also localize to the fission yeast ER. However, as a putative MS channel, Pkd2 is supposed to localize to the plasma membrane. To determine the localization, we examined the cells expressing both Pkd2-GFP and the ER marker mCherry-ADEL with fluorescence microscopy and found that Pkd2 localizes to plasma membranes but not ER by the evidence that Pkd2-GFP localized to the equatorial plane during cytokinesis, while the ER marker did not (**Figure 3-7**A). Moreover, Pkd2-GFP was absent from the perinuclear ER and the ER tethers. Therefore, we concluded that the Pkd2 primarily localizes to the plasma membrane.

To further determine if the plasma membrane–bound Pkd2 regulates calcium homeostasis in fission yeast cells, we measured the intracellular calcium level of a novel temperature-sensitive *pkd2* mutant at the restrictive temperature using the ratiometric indicator GCaMP-mCherry [315]. At 36°C, the average calcium level of *pkd2-B42* cells was 34% lower than that of wild type cells (**Figure 3-7**B and C). The possibility that reduced calcium concentration was an indirect result of either cytokinesis or growth defects was ruled out by the results of other Pkd2 mutants that are defective in cell growth and cytokinesis including *pkd2-81KD*, *sid2-250* and *orb6-25*[314]. Therefore, we concluded that Pkd2 plays an important role in maintaining intracellular calcium levels.

Next, we examined whether Pkd2 promotes calcium spikes triggered by plasma membrane stretching *in vivo*. In yeast, an abrupt drop in extracellular osmolarity triggers a sharp increase in intracellular calcium levels[337] and such calcium spikes, accompanied by cell volume expansion, raise the intracellular calcium level by up to 5-folds[316]. For testing, the wild type cells were first trapped in a microfluidic imaging chamber infused with the isosmotic EMM media, which was changed to EMM plus 1.2 M sorbitol for 30 min. Hypo-osmotic shock was then applied to cells by dropping the extracellular osmolarity more than 1300 mOsm via switching back to EMM (**Figure 3-8**A). This shock caused the average width of wild type cells to increase significantly (**Figure 3-8**B) and was accompanied by calcium spikes (**Figure 3-8**C). To determine whether Pkd2 contributes to osmotic shock–induced calcium spikes, we measured the spikes in *pkd2* mutant cells stimulated with hypo-osmotic shock. Peak amplitudes of the calcium spikes in *pkd2-81KD* and *pkd2-B42* cells were 59% and 62% lower than in wild type cells respectively (**Figure 3-8**C, D and E), which indicates that Pkd2 contributes significantly to calcium influx triggered by hypo-osmotic shock in vivo. Beyond this, we also found that Pkd2 contributes significantly to the

separation calcium spikes accompanied by cell separation at the end of cytokinesis, which is a process requiring stretching of the plasma membrane, with the evidence that the average peak amplitude of the separation spikes of *pkd2-81KD* and *pkd2-B42* mutant cells decreased by 45% and 60%, respectively, compared with those of the wild-type cells (**Figure 3-8**F, G).

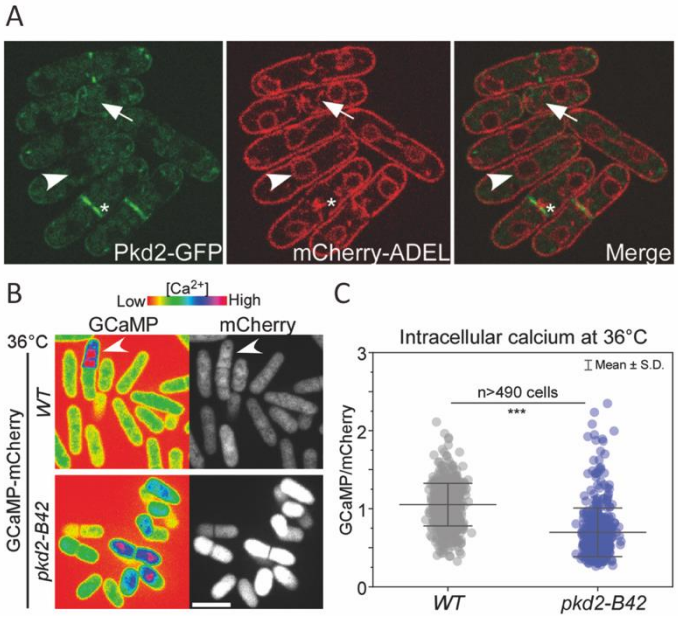

Figure 3-7: Intracellular calcium level was reduced in pkd2 mutant cells. (A) Pkd2 primarily localizes to the plasma membrane. Fluorescence micrograph of the cells expressing both Pkd2-GFP (green) and the ER marker mCherry-ADEL (red). Only the center slice of the Z-series is shown. Asterisk: Equatorial plane localization, Arrowhead: Perinuclear ER, Arrow: Membrane tethers. (B, C) The intracellular calcium level of wild type (WT) and *pkd2* mutant cells at restrictive temperature of 36°C. (B) Representative fluorescence micrographs of wild type (top) and *pkd2* mutant (bottom) cells expressing GCaMP-mCherry. Arrowhead: a cell with elevated calcium level. (C) Scatter interval plots of intracellular calcium level of the wild type and the pkd2 mutant cells. The average calcium level of *pkd2-B42* cells was 34% lower than that of the wild type at 36°C. All data are pooled from three biological repeats. N.S.: no significant difference ($p > 0.05$), *** $p < 0.001$. Two-tailed Student's t tests with unequal variance were used. Scale bars: 10 μm.

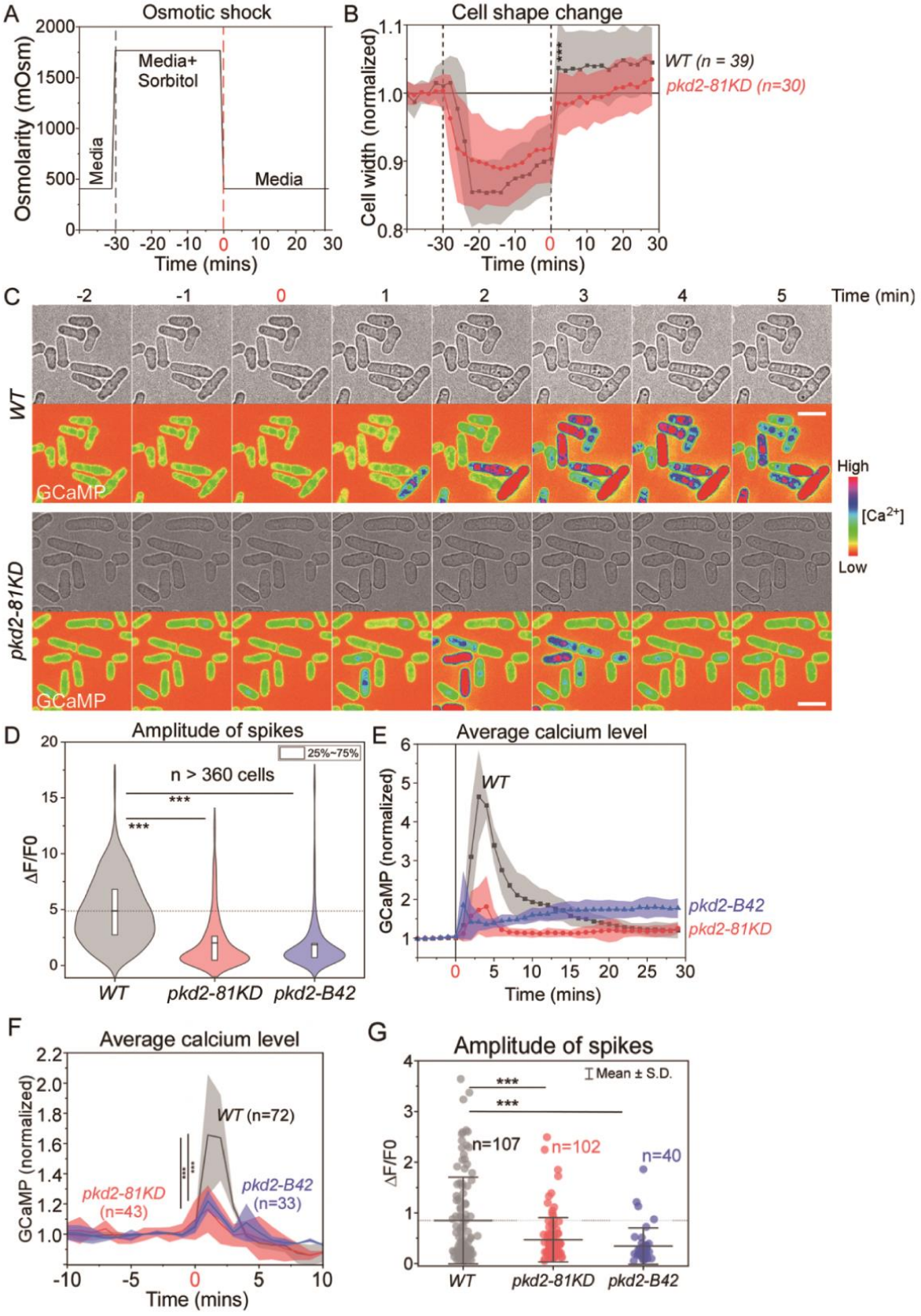
A
Osmotic shock
Osmolarity (mOsm)
Media
Media+
Sorbitol
Media
Time (mins)
B
Cell shape change
Cell width (normalized)
WT (n = 39)
pkd2-81KD (n=30)
Time (mins)
C
Time (min)
WT
pkd2-81KD
GCaMP
High
[Ca2+]
Low
D
Amplitude of spikes
25%~75%
n > 360 cells
ΔF/F0
WT
pkd2-81KD
pkd2-B42
E
Average calcium level
GCaMP (normalized)
WT
pkd2-B42
pkd2-81KD
Time (mins)
F
Average calcium level
GCaMP (normalized)
WT (n=72)
pkd2-81KD
(n=43)
pkd2-B42
(n=33)
Time (mins)
G
Amplitude of spikes
Mean ± S.D.
ΔF/F0
n=107
n=102
n=40
WT
pkd2-81KD
pkd2-B42

Figure 3-8: Pkd2 mutations reduced calcium spikes triggered by hypo-osmotic shock. (A) Time course of the osmolarity of the extracellular environment in the microfluidics chamber. Time zero: application of hypo-osmotic shock through replacing EMM plus 1.2-M sorbitol with EMM media. (B) Time course of the cell width changes during the hypo-osmotic shock. Cloud represents standard deviations. Both wild type (WT) and *pkd2-81KD* cells expanded their cell width significantly after shock, but the wild type expanded more than the pkd2-81KD mutant. (C) Time-lapse micrographs of wild type and *pkd2-81KD* cells expressing GCaMP. The hypo-osmotic shock triggered calcium spikes. (D) Violin plot comparing calcium spikes amplitude of wild type, *pkd2-81KD*, and *pkd2-B42* cells. (E) Time course of normalized GCaMP fluorescence during hypo-osmotic shock. Cloud represents standard deviations. (F) Time course of the average GCaMP fluorescence of the wild type and two pkd2 mutants (pkd2-81KD and pkd2-B42) cells. Cloud represents SD. (G) Dot plot of the peak amplitude of the separation calcium spikes. Line: average. All data are pooled from at least three biological repeats. *** $p < 0.001$. Two-tailed Student's t tests with unequal variance were used. Scale bars: 10 μm.

3.5 Discussion

In this study, we determined the calcium permeability and activation mechanism of the putative fission yeast channel Pkd2. *In vitro* reconstitution established Pkd2 as calcium-permeable under membrane tension. Calcium imaging of *pkd2* mutant cells demonstrated this essential protein's critical role in regulating calcium homeostasis and adaptation to hypo-osmotic shock. Most importantly, our results identified Pkd2 as the first channel that promotes the calcium transients during fission yeast cytokinesis.

In vitro reconstituted Pkd2 in GUVs allowed the passage of calcium ions in a force-dependent manner. Mechanical activation of Pkd2 was proportional to the extent of membrane stretching, suggesting that only a small fraction of the transmembrane protein was activated at the lower applied force. Compared with calcium spikes in the yeast cells, the calcium influx mediated by Pkd2 in vitro was relatively slow. This is likely due to the small amount of reconstituted Pkd2 in the membrane, which slows the calcium influx. Nevertheless, our minimal system demonstrated that Pkd2 is calcium-permeable in response to membrane stretching.

The calcium permeability of reconstituted Pkd2 is consistent with the significantly reduced intracellular level of calcium in *pkd2* mutant cells. Our *in vivo* data have provided the first line of evidence that Pkd2 mediates calcium homeostasis in fission yeast cells. Consistent with the

mechanosensitivity *in vitro*, Pkd2 also plays a critical role in adaptation to hypo-osmotic shock for fission yeast cells when the tension of the plasma membrane increases. There has been a long-standing hypothesis that stretch-activated yeast channels likely contribute to osmotic adaptation, whose identities nevertheless remained unknown[337]. Considering its localization on the plasma membrane and its force sensitivity, Pkd2 likely allows the direct influx of calcium that contributes to adaptation after hypo-osmotic shock. However, it is worth noting that mutations of *pkd2* reduced calcium spikes even more than the removal of external calcium following hypo-osmotic shock. This strongly suggests that Pkd2 regulates not only calcium influx, but also internal release of calcium during the spiking events.

The function of Pkd2 in regulating osmotic adaptation bears some similarities to that of mechanosensitive MscS channels, but there are some critical differences. Msy1 and Msy2 are fission yeast homologues of the small bacterial conductance mechanosensitive channel MscS[316,338]. Like Pkd2, Msy1 and Msy2 play a crucial role in adaptation to hypo-osmotic shock. However, unlike Pkd2, they localize to the ER[338]. More surprisingly, deletion of both fission yeast MscS channels leads to enhanced calcium spikes following hypo-osmotic shock[338], contrary to the phenotype of *pkd2-81KD* mutant cells. The potential interlinks between polycystin and MscS channels will require further analysis. The calcium permeability of Pkd2 is similar to that of mammalian polycystins, but its mechanosensitivity is different. Like Pkd2, human polycystin channels also regulate intracellular calcium levels[339,340]. Moreover, between the two mammalian homologues, polycystin-1 is sensitive to mechanical stimulus[341]. However, the mammalian polycystin channels mostly localize to primary cilia, where they are activated by mechanical force from fluid flow[342].

The force-sensitive nature of the putative channel Pkd2, combined with its localization on the plasma membrane, makes it an ideal candidate to sense membrane tension and regulate turgor pressure homeostasis during cell growth. The key phenotype of pkd2 mutants is their failure to maintain turgor pressure required for both tip extension and cell separation[315]. This putative channel could play a critical role in maintaining turgor pressure during cell growth as the cell volume expands. Pkd2 is a potential candidate for the known mechanosensitive channel regulating the turgor pressure of fission yeast[343].

3.6 Conclusion

In summary, our results support the hypothesis that Pkd2 is a calcium-permissible ion channel activated by membrane stretching. It mediates calcium influx in response to osmotic shock, which requires temporary increase of cell volume and concurrent plasma membrane stretching. This likely activates the putative Pkd2 channel and allows the calcium influx. The mechanosensitivity of Pkd2 and its calcium permeability may underlie its essential function during both cell growth and cytokinesis, which we discovered in our previous studies[314,315]. Nevertheless, further single-channel electrophysiology studies will be required to determine the ion channel activity of Pkd2 and its gating mechanism. Moreover, it remains to be determined whether fission yeast Pkd2 is also permeable to other cations such as potassium, sodium, and organic cations similar to human polycystins[339,344–346] .

Chapter 4 Reconstitution of Calcium-Dependent Artificial Exocytosis Through DNA-Mediated Membrane Fusion in Synthetic Cells

Part of this chapter has been published in Hsu, Chen et al. *Chemical Communications*, 2023. The author implemented the design platform, carried out the experiments presented and generated figures in the manuscript. A.P.L. conceived the study. Y.Y.H., S.J.C., and A.P.L. designed the experiments. Y.Y.H., S.J.C., J.B.C., B.S., and H.M. performed the experiments. Y.Y.H, S.J.C., J.B.C., H.M., and A.P.L. wrote the paper. All authors contributed to the manuscript revision and approved the final version. A.P.L. provided supervision and administered the project.

4.1 Abstract

In cells, membrane fusion is mediated by soluble N-ethylmaleimide-sensitive factor attachment protein receptor (SNARE) proteins, whose activities are calcium-dependent. While several non-native membrane fusion mechanisms have been demonstrated, few can respond to external stimuli. Here, we develop a calcium-triggered DNA-mediated membrane fusion strategy where fusion is regulated using surface-bound PEG chains that are cleavable by the calcium-activated protease calpain-1. Such strategy is then used in a vesicle-in-vesicle (SUV-in-GUV) system for reconstitution of calcium-dependent synthetic exocytosis. To capacitate the synthetic system with mechanosensing, MS channel MscL is further expressed on GUV membranes to perform force-activated secretion and communication with natural cells.

4.2 Introduction

Exocytosis, a process for transporting large molecules or proteins out of the cells into extracellular space through fusion of intracellular secretory vesicles with the plasma membrane, is essential for cell-cell communication in multicellular organisms and is important for numerous biological functions. For instance, glucose homeostasis in blood is regulated by secretion of hormones insulin and glucagon produced by pancreas islets through exocytosis when signals are received. High glucose level causes release of insulin from pancreatic beta cells while low glucose concentration leads to secretion of glucagon from pancreatic alpha cells [347]. Another example is the synaptic transmission in neurons. A synaptic vesicle filled with neurotransmitters in the pre-synaptic neuron fuses with the pre-synaptic membrane, releasing neurotransmitters into the synaptic cleft. The neurotransmitters can then bind to receptors on the post-synaptic neuron for excitation or inhibition [348]. Activated platelets also release the contents of different types of preformed intracellular vesicles, including dense granules, lysosomes, and alpha granules, through exocytosis. For example, proteins from alpha granule membranes localize to the platelet surface upon granule release and contribute to platelet adhesion and activation. A large number of soluble mediators from alpha granules can also promote inflammation, both positively and negatively regulate the coagulation cascade, and facilitate wound healing to help resolve tissue damage[349]. Other examples include transportation of protein-filled vesicles from T cells to virus-infected cells[350] and granule release by leukocytes for destroying pathogens [351].

In eukaryotic cells, membrane fusion is the key mechanism that underpins exocytosis, and this intricate mechanism lies in the orchestration of SNARE proteins, comprising both v-SNAREs on vesicle membranes and t-SNAREs on target membranes. Coiled-coil interactions between these proteins on opposing membranes help overcome the kinetic and energetic barriers to induce

membrane fusions [348]. A key feature of SNARE-mediated membrane fusion is its calcium dependency, which serves as a key trigger for the initiation of exocytosis, enabling precise spatiotemporal control over exocytosis. For example, calcium-bound synaptotagmin interacts with the SNARE complex and other proteins, leading to the stabilization of the SNARE complex in a partially zippered state. This interaction primes the vesicle for fusion with the target membrane. The calcium-dependent activation of synaptotagmin also promotes the formation of a fusion pore between the vesicle and target membranes, allowing the release of vesicular contents into the extracellular space[352]. The specificity and precision exhibited by SNARE proteins in mediating calcium-dependent membrane fusion make them pivotal players in cellular communication and homeostasis.

Despite the elegant mechanism of SNARE-mediated fusion, SNARE motifs require multiple post-translational modifications[351], which introduces challenges for *in vitro* reconstitution. While SNARE-mediated membrane fusion has been demonstrated in a synthetic system[195,353], *in vitro* membrane fusions have utilized many other artificial fusion strategies, including peptide-mediated[199,354,355] and DNA oligonucleotide-mediated[356–358] approaches. Most peptide-mediated membrane fusion designs contain the minimal peptide sequence required to induce membrane fusion from the SNARE motif[354], which are commonly denoted as peptide E and peptide K. On the other hand, modifying the vesicles with complementary single stranded DNA can bring opposing membranes into close proximity with each other enabling favorable conditions for fusion[356]. While robust, both strategies on their own allow fusion to occur spontaneously, with no mechanisms to regulate the process through external stimuli. In addition, few studies have demonstrated spatiotemporal control over membrane fusion by exploiting specific external signals, such as the presence of certain ions or pH levels[199], to trigger membrane

fusion. Crucially, the calcium-dependent nature of SNARE-mediated membrane fusion has yet to be demonstrated in a synthetic system. Incorporating a stimulus-responsive membrane fusion mechanism in synthetic cells would enable the next generation of smart drug delivery vehicles. Consequently, we devise a calcium-triggered membrane fusion strategy, building upon a previously developed DNA-mediated membrane fusion strategy[356]. We further apply this strategy to a small vesicle-in-large vesicle system and capacitate the system with mechanosensing by expressing mechanosensitive channel MscL, which provides a potential for reconstitution synthetic calcium-dependent exocytosis that can be triggered by mechanical stimuli.

4.3 Materials and Methods

4.3.1 Reagents and Materials

Fmoc-protected amino acids for peptide synthesis were purchased from EDM Millipore. Fmoc-NH-PEG12-COOH was purchased from Biopharma PEG Scientific Inc. Cholesteryl Hemisuccinate was purchased from Cayman Chemical. Dichloromethane (DCM) was purchased from Millipore Sigma. Dimethylformamide (DMF) and diethyl ether were purchased from Oakwood Chemical Inc. Piperidine was purchased from Alfa Aesar. Oxyma and N,N'-Diisopropylcarbodiimide (DIC) were purchased from ChemImpex. TFA was purchased from Oakwood, and Rink Amide resin was purchased from Novabiochem. All lipids (1,2-dioleoyl-sn-glycero-3-phosphati-dylcholine (DOPC), 1,2-dioleoyl-sn-glycero-3-phosphoethanolamine (18:1 (Δ9-Cis) PE (DOPE)), cholesterol, 1,2-dioleoyl-sn-glycero-3-phosphoethanolamine-N-(lissamine rhodamine B sulfonyl) (Rhod-PE), 1,2-dioleoyl-sn-glycero-3-phosphoethanolamine-N-(7-nitro-2-1,3-benzoxadiazol-4-yl) (NBD-PE)) were purchased from Avanti Polar Lipids. Cholesterol-conjugated oligonucleotides were purchased from Integrated DNA Technologies and cholesterol-conjugated PEG chains were purchased from Creative PEGWorks. EDANS/DABCYL FRET

reporter for calpain-1 was purchased from GenScript. 16.5% Mini-PROTEAN® Tris-Tricine Gel and Precision Plus TM Protein Unstained Protein Standards were purchased from Bio-Rad Laboratories. All chemicals were purchased from Sigma unless otherwise noted. Peptides were custom synthesized and listed in Table S1 (more details below).

4.3.2 Cloning and Preparation DNA Constructs for His-tagged Fluorescent Protein (His_6-BFP)

A plasmid for bacterial expression of mTagBFP with a C-terminal 6xHis tag was generated by cloning the sequence encoding mTagBFP into a pET28b vector. The backbone fragment was amplified from a pET28b vector (a gift from Tobias Pirzer, Technical University of Munich, Germany) with forward primer: CACCACCACCACCACCAC and reverse primer: AAAAAACCTCCTTACTTTCTAGTCTCAAG. Similarly, the insert fragment was amplified from sTag-BFP plasmid (Addgene #186905) using forward primer: TCTTGAGACTAGAAAGTAAGGAGGTTTTTTATGTACACCATCGTGGAGCAGTAC and reverse primer: AGCCGGATCTCAGTGGTGGTGGTGGTGGTGCAGATCCTCTTCTGAGATGAG. The fragments were assembled using Gibson Assembly, and the cloning sequences were verified using Sanger sequencing (Eurofins).

4.3.3 Bacterial Expression and Purification

Protein expression and purification from bacteria were performed following the conventional His-purification reported elsewhere1. pET28b-mTagBFP construct was transformed into BL21-DE3-pLysS cells (Agilent). A single colony was picked from the LB plate and grown in 5 mL LB supplied with 50 μg/mL kanamycin at 37 ºC shaking at 220 rpm overnight. Next day,

the culture was diluted in 1 L LB supplemented with 0.8% w/v glucose and 50 μg/mL kanamycin. The culture was grown at 37 ºC shaking at 220 rpm and was induced with 0.42 mM isopropyl β-D-1-thiogalactopyranoside (IPTG) once the A600 reached 0.5-0.6. After induction, the culture was incubated at 30 ºC shaking at 200 rpm for 4-5 h. The cells were then harvested through centrifugation at 5000 g for 10 min. The cell pellet was resuspended in 30 mL of lysis buffer (50 mM Tris-HCl (pH 7.4), 300 mM NaCl, and 1 mM 4-(2-aminoethyl) benzenesulfonyl fluoride hydrochloride (AEBSF)). The cells were then lysed using a tip sonicator (Branson Sonifier 450) and the lysate was centrifuged at 30000 g for 25 min. Next, the supernatant was run through an equilibrated HisTrap column (Cytiva) in an AKTA start fast protein liquid chromatography system. The column was washed with 15 column volumes of washing buffer (50 mM Tris-HCl (pH 7.4), 300 mM NaCl, and 50 mM imidazole) before the purified protein was eluted with 10 column volumes of elution buffer (50 mM Tris-HCl (pH 7.4), 300 mM NaCl, and 400 mM imidazole) and collected in 1 mL fractions. The purification quality was assessed for each fraction by SDS-PAGE, and the fractions with high concentration of the protein were pooled and dialyzed against 1 L PBS overnight at 4 ºC. The protein concentration was measured with NanoDrop (Thermo Fisher Scientific) (extinction coefficients predicted by Benchling) before it was aliquoted and stored at −80 ºC until use.

4.3.4 Preparation of GUVs

GUVs were generated via electroformation following a published protocol[359] for all membrane interaction experiments, due to the method's ability to reliably produce high GUV yield. GUVs were formed by the droplet transfer approach (i.e., inverted emulsion-based method)[360,361] for all membrane fusion experiments and reconstitution of cell-free expressed MscL. 0.5 mM lipid dissolved in chloroform was mixed in molar ratios specified in **Table 4-1** and **Table**

4-2 for different experiments. The lipid mixture was evaporated under a stream of nitrogen to remove any remaining chloroform in a glass vial. 1 ml of mineral oil (Sigma-Aldrich) was then added to the glass vial and then mixed with the dried lipid film by vigorous vertexing. The lipid-in-oil solution was placed in the oven at 60°C for 20 minutes. During incubation, the outer solution was prepared by mixing the desired amount of glucose solution into 1X PBS solution to match the osmolarity of the inner solution to be encapsulated inside the GUVs. For membrane interaction experiments, the inner solution was 300 mM sucrose solution in milli-Q water. For membrane fusion experiments, the inner solution contains His_6-BFP with 5% OptiPrep. For the preparation of vesicle-in-vesicle (SUV-in-GUV) system, the inner solution becomes the mixture of SUV and calpain with 5% OptiPrep. In a 1.5 ml epitube, 300 µl of lipid-in-oil solution was carefully added on top of 400 µl of outer solution and incubated at room temperature for 1 hr to form a lipid monolayer at the interface, followed by carefully adding to the top water-in-oil single emulsion droplets generated by vigorously pipetting 20 µl of inner solution with 600 µl of lipid-in-oil solution. After centrifugation at a speed of 2.5 k RCF for 10 mins, the oil on top was carefully removed and the pellet fraction was gently resuspended and transferred to a new epitube.

Table 4-1. GUV lipid compositions

Experiment	Lipid composition for GUVs (molar ratio)
Membrane interaction w/o Chol-CCS-PEG	DOPC: DOPE: cholesterol: NBD-PE = 74.9: 5: 20: 0.1
Membrane interaction w/ Chol-CCS-PEG	DOPC: DOPE: cholesterol: NBD-PE:Chol-CCS-PEG2K = 69.9: 5: 20: 0.1: 5
Membrane fusion w/o Chol-CCS-PEG	POPC: DOPE: NBD-PE = 94.9: 5: 20: 0.1
Membrane fusion w/ Chol-CCS-PEG	POPC: DOPE: NBD-PE: Chol-CCS-PEG2K = 89.9: 5: 20: 0.1: 5

Table 4-2. Lipid compositions of GUVs expressing/ with reconstituted MscL

Experiment	Lipid composition for GUVs (molar ratio)
Insertion of MscL (Encapsulation of FITC)	DOPC: Chol: Rhod = 69.9: 30: 0.1

Insertion of MscL (Encapsulation of Cy5)	DOPC: Chol =70: 30
Insertion of MscL to asymmetrical lipid bilayer containing CCS-PEG2K (10 μM DNA A in inner leaf)	(i) Outer leaflet: DOPC: DOPE: Chol: Chol-CCS-PEG2K= 73.2: 5: 20: 1.8 Inner leaflet: DOPC: DOPE: Chol: Chol-CCS-PEG2K= 73.2: 5: 20: 1.8 (ii) Outer leaflet: DOPC: DOPE: Chol = 75: 5: 20 Inner leaflet: DOPC: DOPE: Chol: Chol-CCS-PEG2K= 73.2: 5: 20: 1.8 (iii) Outer leaflet: DOPC: DOPE: Chol = 75: 5: 20 Inner leaflet: DOPC: DOPE: Chol: Chol-CCS-PEG2K= 74.1: 5: 20: 0.9 (iv) Outer leaflet: DOPC: DOPE: Chol = 75: 5: 20 Inner leaflet: DOPC: DOPE: Chol = 75: 5: 20
Calcium-activated membrane interaction	Outer leaflet: DOPC: DOPE: Chol = 75:5:20 Inner leaflet: DOPC: DOPE: Chol = 75:5:20 + 10 μM DNA A

4.3.5 Preparation of SUVs

SUVs were prepared by using a thin film hydration method followed by extrusion. 1 mM lipids dissolved in chloroform were mixed in molar ratios specified in **Table 4-3**. The lipid was dried under vacuum for 1 h to create a uniform lipid film and remove any remaining chloroform in a glass vial. 1 ml of 1X PBS was then added to the film and thoroughly vortexed. The mixture was then passed through a liposome extruder (Avanti Polar Lipids) with a 100-nm porous membrane 15 times to generate SUVs. For calcium-dependent membrane fusion experiment, calpain-1 cleavable PEG chains (Chol-CCS-PEG2K) were added to the lipid mixture at a final concentration of 1 mM so the lipid composition becomes DOPC: DOPE: cholesterol: Chol-CCS-PEG2K: Rhod-PE/NBD-PE = 63.9: 5: 29:5: 0.1.

Table 4-3. **SUV lipid compositions**

Experiment	**Lipid composition for SUVs (molar ratio)**
Membrane interaction w/o Chol-CCS-PEG_{2K}	DOPC: DOPE: cholesterol: Rhod-PE = 69.9:10: 20: 0.1
Membrane interaction w/ Chol-CCS-PEG_{2K}	DOPC: DOPE: cholesterol: Rhod-PE:Chol-CCS-PEG_{2K} = 64.9:10: 20: 0.1: 5
Membrane fusion w/o Chol-CCS-PEG_{2K}	DOPC: cholesterol: Rhod-PE: DGS-NTA (Ni) = 34.9: 15: 0.1: 50
Membrane fusion w/ Chol-CCS-PEG_{2K}	DOPC: cholesterol: Rhod-PE: DGS-NTA (Ni): Chol-CCS-PEG_{2K} = 34.9: 10: 0.1: 50: 5

4.3.6 Generation of SUPER Templates

SUPER templated beads were generated following a published protocol.5 For SUPER template formation, 25 µl of SUV solution was fused with 5 µl of 5-µm silica beads (Bangs Laboratories) in the presence of 1 M NaCl. The final SUPER templated beads were washed with PBS twice by centrifuging at 200 × g for 2 min and then resuspended in 30 µl of milli-Q water at a final concentration of ~2.4 × 107 beads/ml. The SUPER template stock can be stored at room temperature for 3 hr.

4.3.7 Peptide Synthesis and Characterization

Peptides mentioned in **Table 4-4** were obtained using solid phase peptide synthesis (SPPS) on a CEM Liberty Blue instrument. Synthesis was performed on a solid phase Rink-Amide resin (0.78 mmol/g) at a 0.1 mmol scale, using a standard Fmoc protocol and deprotected in 20% piperidine in DMF. Amino acids, PEG blocks, cholesterol hemisuccinate, coupling agents, DIC and Oxyma, were added in a 10-fold molar excess. Crude peptides were cleaved by shaking the resin in a solution containing trifluoroacetic acid (TFA), triisopropylsilane (TIPS), and water in a ratio of 95:2.5:2.5 for 3.5 h. The resin was washed with TFA and concentrated under nitrogen. The solution was then added to 40 mL of cold diethyl ether to precipitate the peptide. The solution was centrifuged at 4200 rpm for 10 min, the supernatant was removed, and the pellet was allowed to dry overnight. The dried pellet was dissolved in a mixture of water and acetonitrile (50:50) and 0.1% TFA. Peptides were purified via reverse phase chromatography on a Waters HPLC using a Phenomenex column with C18 resin. A linear gradient was generated using water/acetonitrile + 0.1% TFA, from 10% to 100% acetonitrile over 50 minutes. Peak fractions were collected based upon their absorbance at 230 nm and tested for purity by MALDI-TOF mass spectrometry on

Bruker microflex LRF MALDI using α-cyano-4-hydroxycinnamic acid matrix (Sigma). Pure fractions were pooled and lyophilized, and peptides were stored at -20 °C until use.

Table 4-4. Synthesized peptides

Peptide	Description	Sequence	Molecular weight (Da)
P1	Cholesterol-PEG_4-K Coil	Cholesterol-$(PEG)_4$KLNKWWYKRKELAAIEKELAAIEKELAAIEKELAAIK	5022
P2	Cholesterol-PEG_4-K Coil-PEG_{24}	Cholesterol-$(PEG)_4$KIAALKEKIAALKEKIAALKEKIAALKE$(PEG)_{24}$	4917
P3	Cholesterol-PEG_4-K Coil-CCS-PEG_{24}	Cholesterol-$(PEG)_4$KIAALKEKIAALKEKIAALKEKIAALKEEPLFAERK$(PEG)_{24}$	5885
P4	Cholesterol-PEG_4-E Coil	Cholesterol-$(PEG)_4$KKRRAKSQEKLAAIKEKLAAIKEKLAAIWEKLAAIK	4757
P5	Cholesterol-PEG_4-E Coil-PEG_{24}	Cholesterol-$(PEG)_4$EIAALEKEIAALEKEIAALEKEIAALEK$(PEG)_{24}$	4918
P6	Cholesterol-PEG_4-E Coil-CCS-PEG_{24}	Cholesterol-$(PEG)_4$EIAALEKEIAALEKEIAALEKEIAALEKEPLFAERK$(PEG)_{24}$	5925
P7	Cholesterol-CCS-PEG_{48}	Cholesterol-GGSEPLFAERK$(PEG)_{48}$	4123

* Block diagram of peptides can be found in **Figure 4-19**.

4.3.8 Membrane Interaction Assay

To functionalize vesicles with DNA oligonucleotides, SUVs consisted of 1 mM lipids with mole percentage of 69.9% DOPC, 10% DOPE, 20% cholesterol and either 0.1% Rhod-PE or NBD-PE were functionalized with ~200 oligos per vesicle (calculated following formulas given in Peruzzi *et al.*)[356] by incubating SUVs with 10 μM cholesterol-conjugated DNA strand A or B for 30 mins. SUVs containing NBD-PE were later used for generating lipid-coated beads. Similarly, GUVs were functionalized with 10 μM of cholesterol-conjugated DNA strand A' or B' for 30 mins. To prevent close contact between vesicle membranes, 40 μM of cholesterol-conjugated PEG

chains were added to SUVs, GUVs, and SUPER templates and incubated for 30 minutes. For calcium-dependent membrane interaction experiment, a lipid composition of 64.9% DOPC, 10% DOPE, 20% cholesterol, 0.1% Rhod-PE or NBD-PE and 5% Chol-CCS-PEG2K was used instead. For the SUV-SUPER template experiment, SUVs and SUPER templates labeled with complementary DNA oligos were mixed in a 1:4 volume ratio and incubated together for 30 minutes. Afterwards, SUPER templates were washed with 1X PBS twice by centrifuging at 200 g for 2 mins and then resuspended in 30 µl of PBS. The solution containing SUPER template was then deposited onto a coverslip chamber and imaged using a 60x oil objective. For the SUV-GUV experiment, SUVs and GUVs labeled with complementary DNA strands were mixed in a 1:4 molar ratio (~0.83 mM final lipid concentration) and incubated together for 30 minutes. The mixture was then transferred to a 96-well glass-bottom plate and imaged on a confocal microscope using a 60x objective.

4.3.9 Membrane Fusion Assay

To visualize membrane fusion triggered by calcium, GUVs with 94.9% POPC, 5% DOPE, and 0.1% NBD-PE and encapsulating 6.25 µM His6-BFP were made via the inverted emulsion method outlined above. SUVs consisting of 1 mM lipids with 34.9% DOPC, 15% cholesterol, 0.1% Rhod-PE and 50% DGS-NTA (Ni) were extruded 15x through a 400 nm filter. GUVs were functionalized with 10 µM of DNA-oligos while SUVs were functionalized with ~200 oligos per vesicle using the method described above. GUVs and SUVs were mixed in a 1 to 4 molar ratio and incubated for 30 mins. The vesicle solution was then deposited into a 96-well plate chamber and imaged on a confocal microscope using a 60x objective.

4.3.10 Confocal Fluorescence Microscopy

All images were acquired using an oil immersion 60×/1.4 NA Plan-Apochromat objective with an Olympus IX-81 inverted fluorescence microscope (Olympus) controlled by MetaMorph software (Molecular Devices) equipped with a CSU-X1 spinning disk confocal head (Yokogawa), a custom laser launch with solid-state lasers (Solamere Technology Group), and an iXON3 EMCCD camera (Andor). Images of BFP and lipid fluorescence were acquired with 405-nm and 488-nm laser excitation at an exposure time of 500 ms, and with 561-nm laser excitation at an exposure time of 200 ms, respectively. Each acquired image contained ~10 lipid bilayer vesicles or ~10 lipid-coated beads that had settled upon a 96-well glass-bottom plate or a coverslip, respectively. Three images were taken at different locations across a well or coverslip for an individual experiment. Three independent repeats were carried out for each experimental condition. Samples were always freshly prepared before each experiment.

4.3.11 Detection of Calpain Activity through FRET-Based Assay Using Plate Reader

250 nM FRET-pair calpain-1 biosensor & 450 nM calpain-1 were combined with 2 μL OptiPrep and 2 μL reaction buffer, which consists of 50 mM KOH & 10 mM dithiothreitol (DTT), and then DI water was added to a total reaction volume of 20 μL. Each reaction is loaded into a 384-well glass-bottomed well plate and the corresponding EDANS fluorescence intensity was measured at 336/455 nm wavelength using a Synergy H1 plate reader (BioTek). After baseline fluorescence measurements, 5 mM $CaCl_2$ was added to the reaction. The reaction is then immediately imaged with the same settings for 1 h.

4.3.12 Bulk Reaction and Gel Electrophoresis of Peptides with Calpain Cleavage Site

Peptides P3 & P6 were taken from the stock solution, which was dissolved in chloroform. Peptides were dried under a stream of Argon gas, and then desiccated for 30 min. Peptides were

then rehydrated in reaction buffer to a working concentration of 10 μM. For bulk reactions, a combination of peptides (10 μM), calpain-1 (225 nM), or $CaCl_2$ (3 mM) was mixed to a total reaction volume of 15 μL in a microcentrifuge tube. Reactions were then incubated at 37 ºC for 30 min. After completion, reactions were mixed with tricine sample buffer (1:1 mix ratio) and 2% β-mercaptoethanol, and then heated at 90 ºC for 5 min. SDS-PAGE gels were run in a 16.5% polyacrylamide tris-tricine precast gel at 100V. After electrophoresis, the gel was stained with Coomassie G-250 stain for 1 h on a rocking shaker, and then washed overnight in DI water. Gel images were acquired in a Sapphire Biomolecular Imager (Azure Biosystems).

4.3.13 Image and Data Analysis

All images were analyzed in MATLAB and in a nonblinded manner. Since all the GUVs were labeled with green fluorescence from NBD-PE, the edges/boundaries of vesicles were first detected and isolated using the built-in MATLAB function "imfindcircles". The areas that GUVs cover were marked. Next, the red fluorescence images, which portray SUVs, were analyzed. The average background intensity of red fluorescence was measured by averaging the fluorescent intensity measurements of all locations across one image except areas where the GUVs were located. Then, the average red fluorescence along the GUV perimeter (i.e., all pixels that fall on a one-pixel wide line, which traces the GUV perimeter) was compared to the average background intensity. If the red fluorescence along the perimeter was at least 1.2x greater than the background, then co-localization of SUV and GUV membrane fluorescence was observed. Consequently, GUV-SUV interactions were implied. Lastly, the ratio of GUVs that had interactions with SUVs could be quantified by comparing the number of GUVs with GUV-SUV interactions with the total number of GUVs detected.

Taking the GUVs that were identified earlier that had membrane interactions with SUVs, we then quantified if membrane fusion occurred. For each image, we averaged its background fluorescence (blue) using the same method conducted on red fluorescence images. Next, the blue fluorescence on and inside the GUV was subtracted by the average background fluorescence. All the subtracted values were averaged and defined as the average GUV lumen fluorescence. Furthermore, still using the subtracted fluorescent values, the GUV membrane fluorescence was quantified using the method for membrane fluorescence quantification of red (i.e., from SUV) fluorescence. Lastly, the GUV lumen and membrane fluorescence were compared; recruitment of His6-BFP from GUV lumen to membrane was quantified when the GUV membrane fluorescence was at least 2x greater than the GUV lumen fluorescence. By comparing the GUVs with membrane fusion and the ones with membrane interactions, the percentage of GUVs experiencing membrane interactions, as well as membrane fusion could be calculated.

4.3.14 PEG Conformation Calculation

D is the distance between PEG graft and R_f is the Flory radius of the PEG graft. A is the area occupied per PEG chain, a is the monomer length of the PEG chain (0.35 nm), N is the degree of polymerization (i.e., number of PEG repeats, which is 48 repeats for PEG2K).

For Chol-CCS-PEG2K construct, assuming the PEG conformation only depends on the PEG chain in the construct, we can use the equations below to compute D and R_f values,6 which will help us predict the expected PEG conformation on SUV membranes.

$$\boldsymbol{D = 2\left(\frac{A}{\pi}\right)^{\frac{1}{2}}; \quad R_f = aN^{3/5}}$$

Specifically, if the R_f/D ratio is below 1, PEG chains are in the "mushroom" conformation. If R_f/D is greater than 1, PEG chains are in the "brush" conformation[356]. For PEG2K, the Flory

radius is 3.57 nm. With the addition of 5% PEG by count (mole), and since all the PEG is on the outer membrane PEG will account for 10% of the composition of the outer membrane assuming both inner and outer membrane of the SUV have the same surface area. Based on the 100 nm size of the SUVs, the surface area of SUVs is approx. 31,400 nm^2. Assuming that a phospholipid molecule takes up around 65 $Å^2$ (0.65 nm^2), each SUV will contain around 48,000 molecules on its outer membrane. Of which, Chol-CCS-PEG2K will account for around 4,800 of them. Thus, on average, each PEG chain will occupy an area of 6.54 nm^2. Thus, the distance between PEG grafts can be calculated to be 2.89 nm. As a result, the R_f/D ratio is 1.24, which predicts that PEG exhibits a "brush" conformation.

4.3.15 Reconstitution of cell-free expressed MscL on vesicle/ GUV membranes

SUVs labeled with complementary DNA (**Table 4-5**) were encapsulated inside GUVs composed of asymmetrical lipid bilayer, with different (lipid) compositions between outer and inner membrane (**Table 4-6**) using cDICE method. GUVs solution was then incubated with PURE reaction in 1:1 volume ratio. We used the cell-free protein synthesis kit PUREfrex 2.0 (COSMO BIO USA # GFK-PF201-0.25-EX) to produce MscL-sfGFP protein in vitro. The reaction was carried out based on the manufacturer's protocol. Briefly, 1 µl plasmid DNA (~50 ng/µl) was used for one 20-µl reaction. CFE reactions were carried out at 37°C for 2 h. MscL-sfGFP expression was measured on a fluorescence plate reader (Biotek Synergy H1) (**Figure 4-1**). Insertion of MscL-sfGFP into GUV membranes, defined as green fluorescence rings, was observed using fluorescence confocal microscope.

Table 4-5. Lipid compositions of SUVs encapsulated inside GUVs expressing/ with reconstituted MscL

Experiment	Lipid composition for GUVs (molar ratio)
Insertion of MscL to asymmetrical lipid bilayer containing CCS-PEG2K	DOPC: DOPE: Chol: Rhod PE: Chol-CCS-PEG2K= 67.9: 5: 20: 0.1: 5: 2 + 10 μM DNA A'
Calcium-activated membrane interaction	DOPC: DOPE: Chol: Rhod PE: Chol-CCS-PEG2K= 67.9: 5: 20: 0.1: 5: 2 + 10 μM DNA A'

Table 4-6. Lipid compositions of GUVs expressing/ with reconstituted MscL

Experiment	Lipid composition for GUVs (molar ratio)
Insertion of MscL (Encapsulation of FITC)	DOPC: Chol: Rhod = 69.9: 30: 0.1
Insertion of MscL (Encapsulation of Cy5)	DOPC: Chol =70: 30
Insertion of MscL to asymmetrical lipid bilayer containing CCS-PEG2K (10 μM DNA A in inner leaf)	(v) Outer leaflet: DOPC: DOPE: Chol: Chol-CCS-PEG2K= 73.2: 5: 20: 1.8 Inner leaflet: DOPC: DOPE: Chol: Chol-CCS-PEG2K= 73.2: 5: 20: 1.8 (vi) Outer leaflet: DOPC: DOPE: Chol = 75: 5: 20 Inner leaflet: DOPC: DOPE: Chol: Chol-CCS-PEG2K= 73.2: 5: 20: 1.8 (vii) Outer leaflet: DOPC: DOPE: Chol = 75: 5: 20 Inner leaflet: DOPC: DOPE: Chol: Chol-CCS-PEG2K= 74.1: 5: 20: 0.9 (viii) Outer leaflet: DOPC: DOPE: Chol = 75: 5: 20 Inner leaflet: DOPC: DOPE: Chol = 75: 5: 20
Calcium-activated membrane interaction	Outer leaflet: DOPC: DOPE: Chol = 75:5:20 Inner leaflet: DOPC: DOPE: Chol = 75:5:20 + 10 μM DNA A

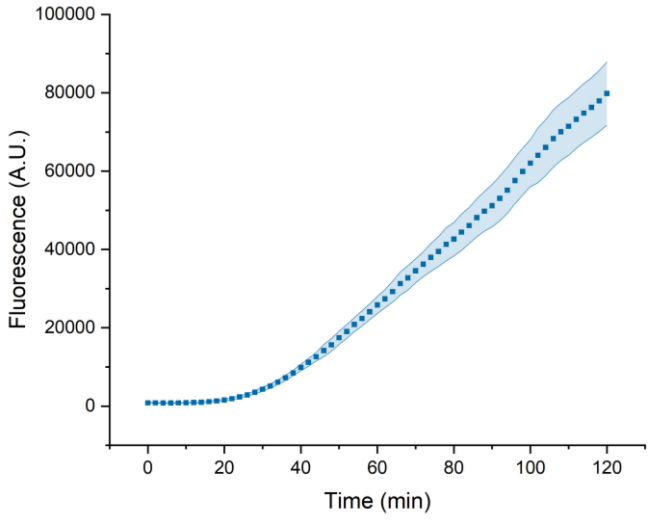

Figure 4-1. Synthesis of MscL using a mammalian CFE system. Time course of the expression of MscL-sfGFP using PURE CFE reaction by monitoring sfGFP fluorescence.

4.4 Results

4.4.1 Calcium-Dependent Membrane Interactions Between SUVs and SUPER Templates Mediated by Cholesterol-Conjugated DNA oligos and PEG Chains

To develop a membrane fusion system triggered by calcium, our general methodology is to shield opposing vesicle membranes with surface-bound polyethylene glycol (PEG) chains for blocking membrane interactions in the absence of calcium. These surface-bound PEG chains physically prevent complementary DNA oligos on each surface from hybridizing. A cleavage site for the protease calpain-1 is placed between the membrane-facing cholesterol and the outward-facing PEG chain (**Figure 4-2**). Since calpain is calcium-activated, in the presence of calcium ions, the PEG chains are cleaved off from vesicle membranes by the activated calpain, abrogating their shielding effect and resulting in the exposure and interaction of the complementary DNA oligos for membrane fusion (**Figure 4-2**).

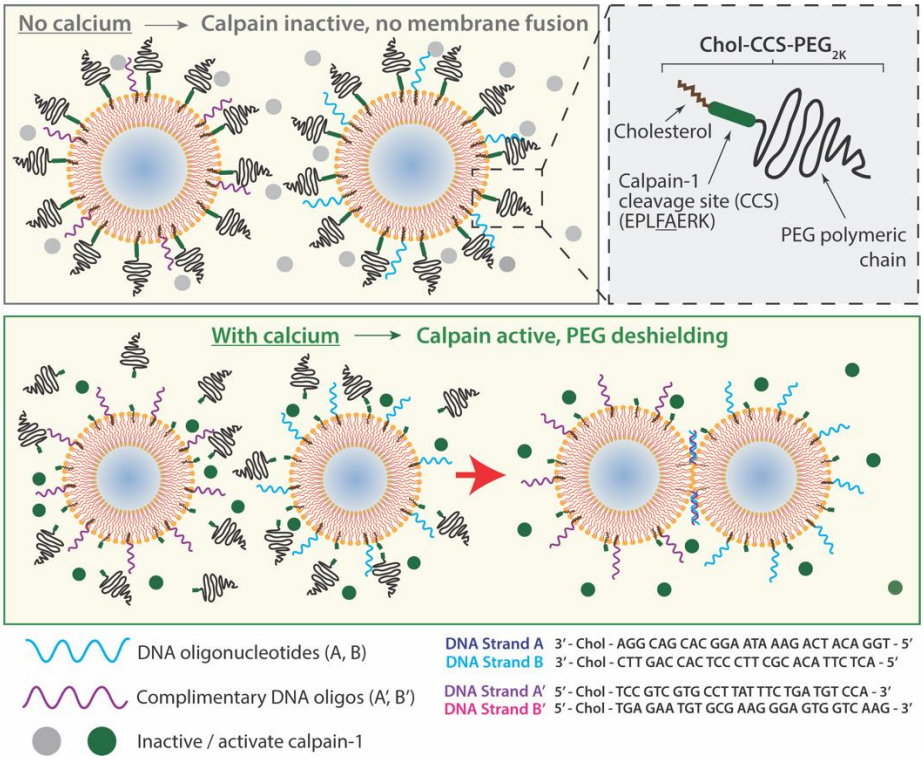

Figure 4-2: Schematic of DNA-mediated membrane fusion induced by calcium. Complementary single-strand DNA oligonucleotides form double helices in a minimal model for membrane fusion. Without calcium, surface-bound PEG chains linked with a calpain cleavage site physically prevent DNA oligos on opposing membranes from interacting with their complementary DNA oligos. In the presence of calcium, protease calpain-1 activates and cleaves off the PEG chains, which then allows bundle formation between complementary oligos on opposing membranes mediating membrane fusion.

To validate this strategy, we started by establishing robust DNA-mediated fusion using cholesterol-conjugated single-stranded DNA oligo pairs developed in Peruzzi et al[356]. Membrane fusion was first tested between supported bilayers with excess membrane reservoir (SUPER) templates and small unilamellar vesicles (SUVs) (**Figure 4-3**A). DNA oligo strands A or B decorate SUPER template membranes and strands A' or B' decorate SUV membranes with ~200 oligos per SUV based on a calculation. With strand A on SUPER templates and stand A' on SUVs, localization of SUV with fluorescently labelled lipids on SUPER templates membranes were observed across 92.8 ± 2% of near all fully formed SUPER templates (**Figure 4-3**B, **Figure 4-4**A), suggesting membrane interactions between SUVs and SUPER templates. Similar interactions were observed between SUPER templates and SUVs when strands A and A' were exchanged for strands

B and B' (**Figure 4-3**C, **Figure 4-4**A). Conversely, with oligos (strand A) only on the membranes of SUPER templates, no co-localization of SUVs on SUPER template membranes was observed in the vast majority of cases (**Figure 4-3**B, **Figure 4-4**A), which indicates membrane interactions between SUVs and SUPER templates are DNA-mediated. Furthermore, when SUV membranes were functionalized with strand A, while SUPER template membranes were functionalized with strand B, no interactions between SUVs and SUPER templates were observed in the vast majority of cases (**Figure 4-3**C, **Figure 4-4**A), which confirms the binding specificity of the complementary oligo pairs.

Following the demonstration of DNA-mediated membrane interactions, we next established the mechanism to regulate these interactions with surface-bound PEG chains (**Figure 4-6**A). With SUPER templates and SUVs decorated with oligos A and A', respectively, cholesterol conjugated with PEG chains of various sizes (PEG1K, PEG2K, and PEG5K) were added to SUPER templates and SUVs (**Figure 4-4**B). We found that SUVs and SUPER templates largely did not interact in the presence of surface-bound PEG2K (**Figure 4-4**B, **Figure 4-6**B), or PEG5K (**Figure 4-4**B, **Figure 4-5**). However, surface-bound PEG1K was not sufficient to block DNA-mediated membranes interactions (**Figure 4-4**B, **Figure 4-6**B). Furthermore, having PEG2K on the surface of either SUVs or SUPER templates was also not sufficient to block membrane fusion. In sum, functionalizing opposing membranes with PEG2K is minimally required to prevent membrane interactions mediated by DNA oligos.

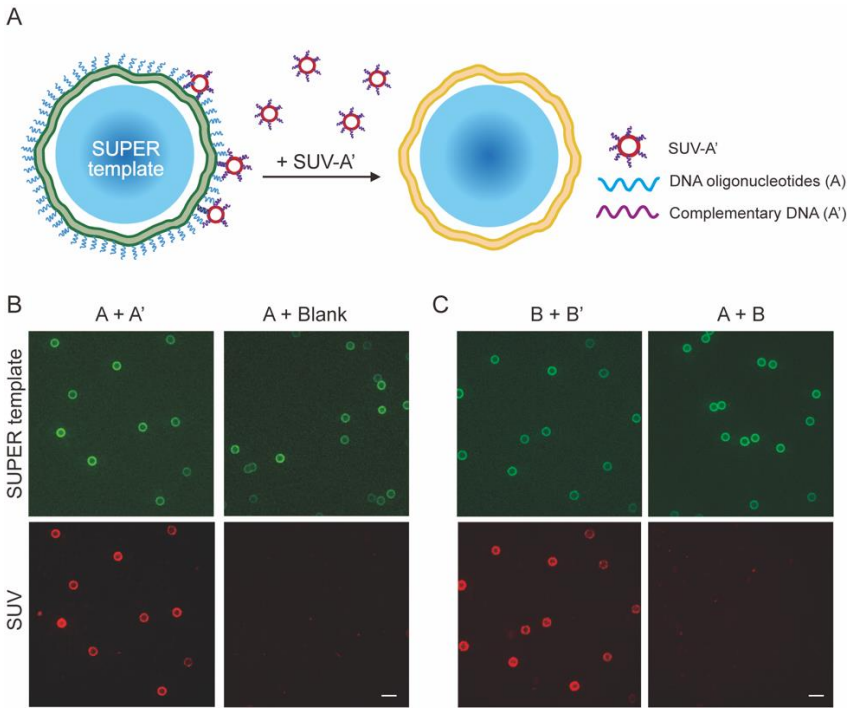

Figure 4-3: Cholesterol-conjugated DNA oligos mediate membrane interactions between SUVs and SUPER templates. (A) Schematic of DNA-mediated interactions between SUVs and SUPER templates. When mixed together, interactions occur between SUPER templates decorated with strand A and labelled with green fluorescence and SUVs decorated with DNA strand A' and labelled with red fluorescence. (B) SUPER templates functionalized with strand A interact with SUVs functionalized with strand A', but not with SUVs without strand A'. (C) Different oligo pair strands B and B' also induce interactions between SUPER templates (labelled with NBD-PE, green) and SUVs (labelled with Rhod-PE, red) (i.e., strand B on SUPER template and strand on SUV. No membrane interactions between with mismatched oligos (i.e., strand B on SUPER templates and strand A on SUVs). Scale bar: 10 µm.

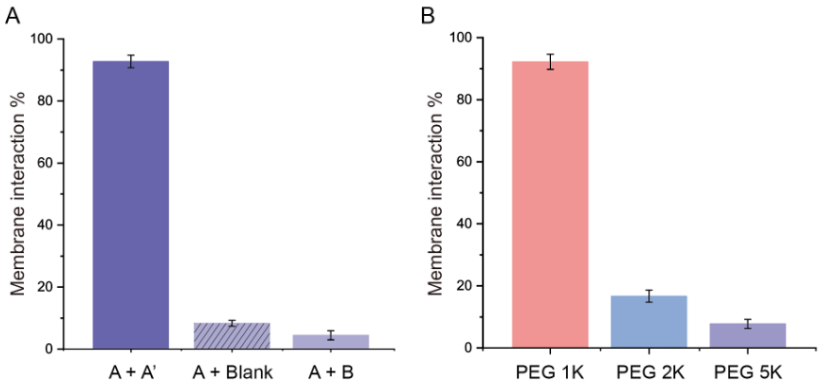

Figure 4-4: Quantification of DNA-mediated membrane interactions between SUPER templates and SUVs. (A) SUPER templates labeled with NBD-PE are functionalized with DNA strand A while SUVs labeled with Rhod-PE are functionalized with either DNA strand A', no DNA, or DNA strand B. The bar graphs represent the percentage of SUPER templates showing membrane interaction with SUVs by the red fluorescence detected on SUPER template membranes. (B) Both SUPER templates and SUVs membranes were covered with complementary DNA and PEG chains. The bar graphs display the percentage of lipid-coated beads showing red fluorescence observed on SUPER templates to the total number of lipid-coated beads. At least 60 lipid-coated beads were analyzed for each condition. All experiments were repeated three times under identical conditions. The error bars represent standard errors.

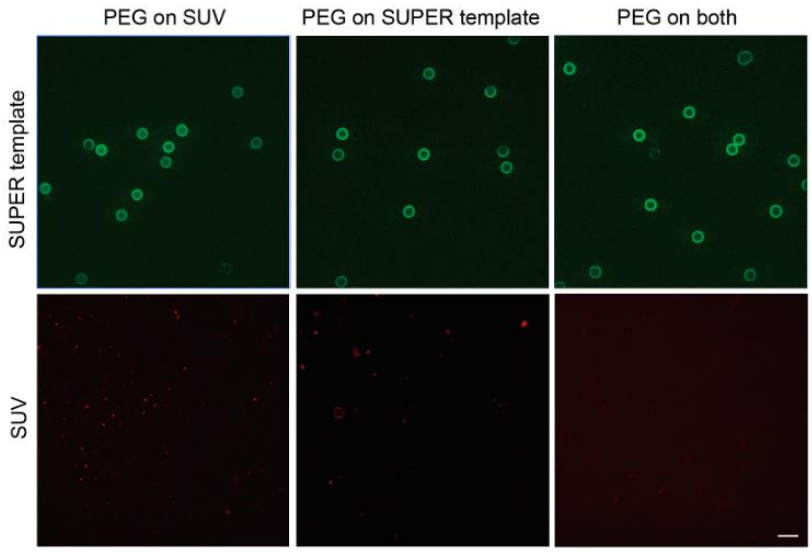

Figure 4-5: Blocking DNA-mediated interaction between SUVs and SUPER templates using surface-bound PEG5K. Functionalizing cholesterol-conjugated PEG5K on either SUV membranes or SUPER templates was sufficient to block the interaction between SUVs and GUVs labeled with complementary oligos (SUVs with strand A and SUPER templates with strand A'). SUVs and SUPER templates both labeled with surface-bound PEG5K showed no membrane interaction. Scale bar: 10 μm.

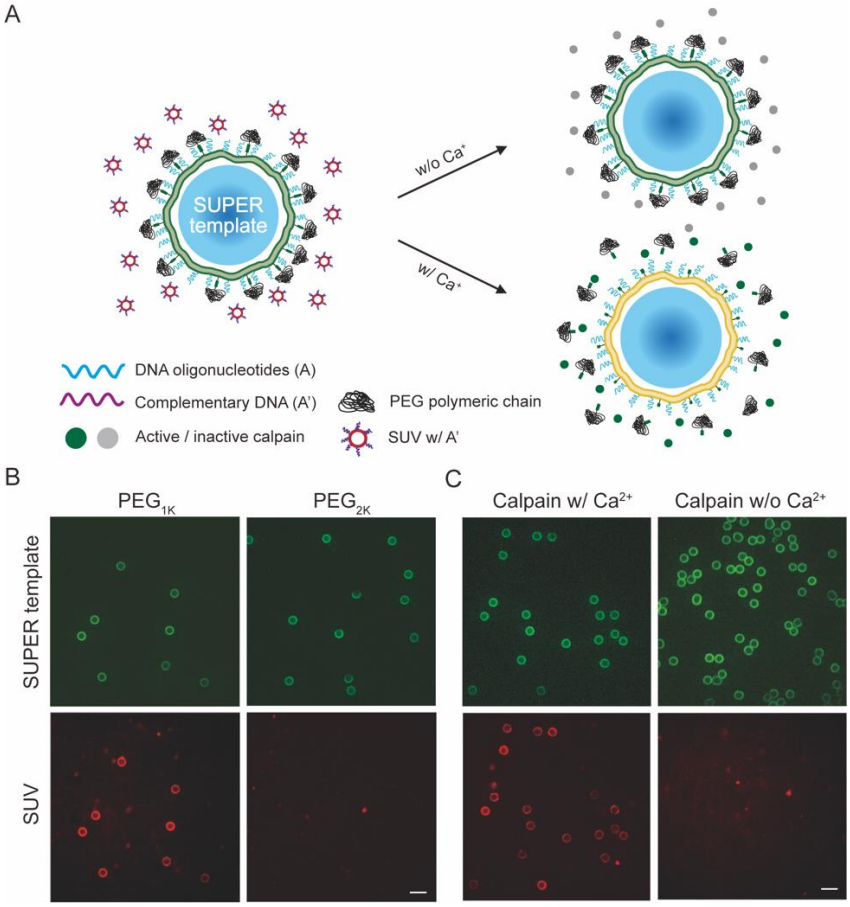

Figure 4-6: Cholesterol-functionalized PEG chains regulate DNA-mediated membrane interactions. (A) Schematic of calcium dependent regulation of DNA-mediated membrane interactions with Chol-CCS-PEG2K. Similar to **Figure 4-3**, SUPER templates (labelled with NBD-PE, green) and SUVs (labelled with Rhod-PE) are functionalized with complementary DNA oligos of their respective surfaces. (B) Surface-bound PEG2K on both SUPER template and SUV membranes effectively blocks DNA-mediated interactions, but not PEG1K. (C) With Chol-CCS-PEG2K on SUPER template and SUV membranes, membrane interactions are only observed when 225 nM calpain-1 is activated with 5 mM $CaCl_2$. Scale bar: 10 μm.

Next, a custom peptide construct, denoted as P7 in **Table 4-4**, was synthesized with a cholesterol molecule on one side, the calpain-1 cleavage site (CCS) EPLFAERK in the middle, and PEG2K on the other side (Chol-CCS-PEG2K). Successful synthesis of the desired peptide (molecular weight: 4.1 kDa) was confirmed by MALDI-TOF mass spectrometry (**Figure 4-7**). The ability to cleave CCS was validated first by conjugating it to a fluorescence resonance energy transfer (FRET) dye pair (DABCYL and EDANS)[362–364]. When mixed with calpain-1 and $CaCl_2$

in a bulk reaction, the CCS was cleaved, leading to a 2.5-fold increase in EDANS fluorescence over the control condition (**Figure 4-8**A). Calpain cleavage was also visualized in an encapsulated system. When calpain FRET reporter, calpain-1, and $CaCl_2$ were encapsulated into a giant unilamellar vesicle (GUV), strong fluorescence was observed (**Figure 4-8**B). In addition, shuttling calcium across the GUV membrane via ionophores also caused significant EDANS fluorescence in GUVs encapsulating calpain-1 and calpain FRET reporter (**Figure 4-8**B). Besides using a calpain FRET reporter, we also confirmed calpain cleavage by gel electrophoresis (Figure 4-9).

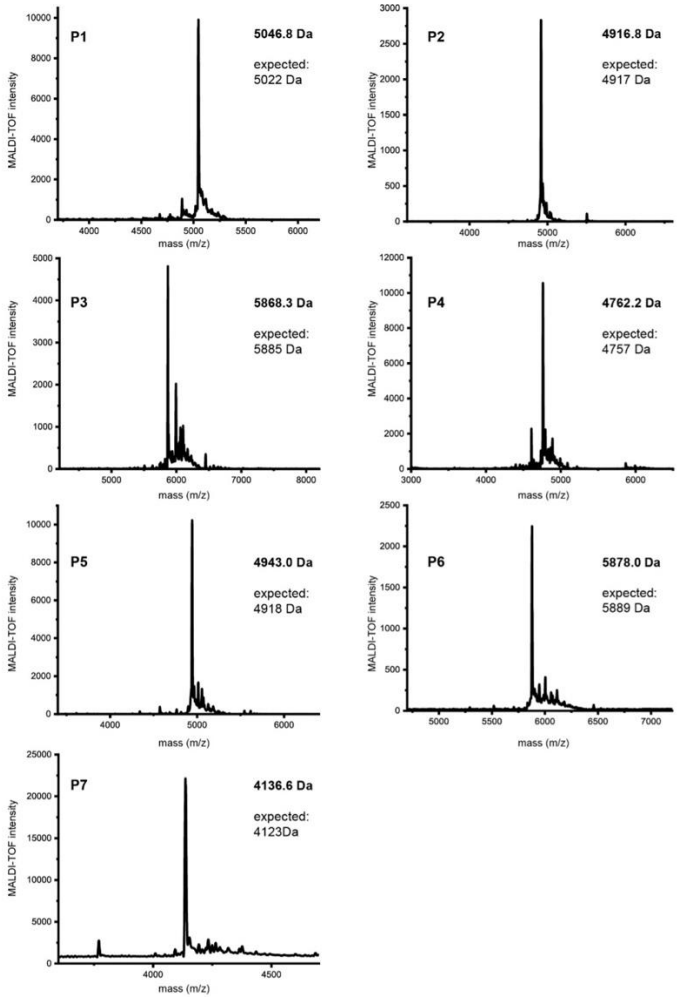

Figure 4-7: MALDI-TOF MS spectra of indicated peptides. Peaks of synthesized peptides match the expected molecular weights. See **Table 4-4** for specific details on peptides P1-7.

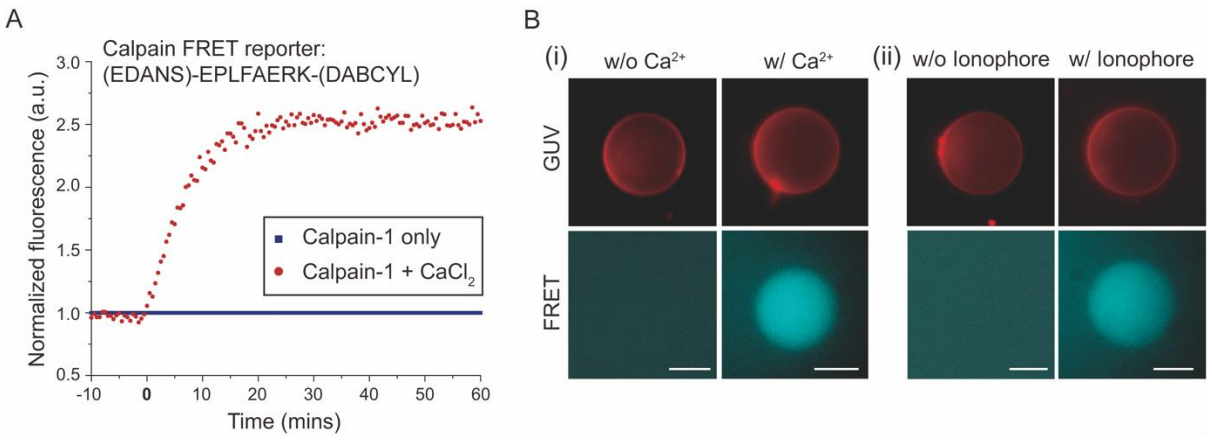

Figure 4-8: Calcium-dependent calpain-1 activity tested by EDANS/DABCYL FRET pair. (A) Time course of the calpain-1 activity of EDANS/DABCY FRET pair connected with calpain cleavage site by monitoring EDANS fluorescence by using a fluorescence plate reader. 5 mM $CaCl_2$ was added to the solution at T = 0 min. (B) Encapsulation of 250 nM calpain-cleavable EDANS/DABCYL FRET reporters inside GUVs. EDANS fluorescence was observed in GUVs co-encapsulating EDANS/DABCYL FRET pair and 3 mM $CaCl_2$ while GUVs without Ca^{2+} inside exhibited low/no fluorescence (i). In the presence of 3 mM $CaCl_2$ in the outer solution, EDANS fluorescence was detected inside GUVs encapsulating EDANS/DABCYL FRET pair following the addition of 2 μM calcium ionophore A23187 in the outer solution (ii). Scale bars are 10 μm.

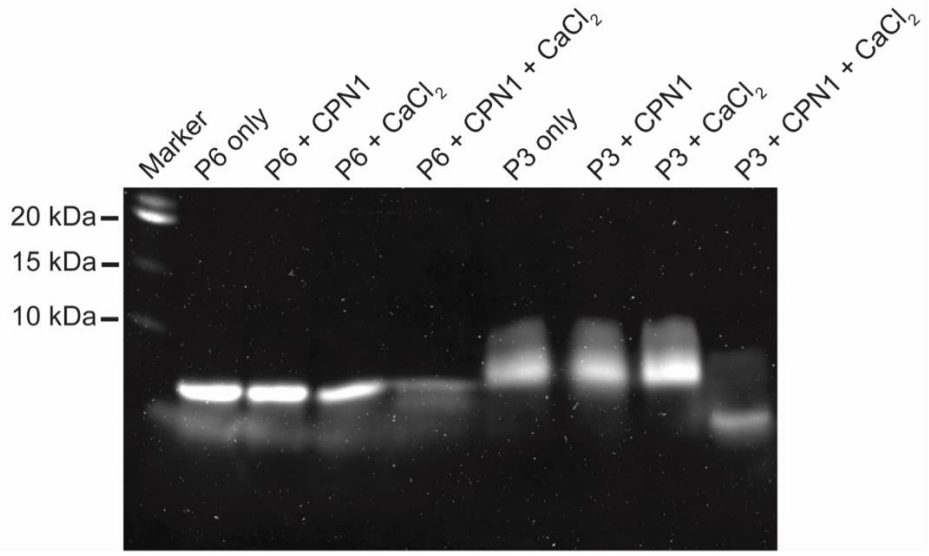

Figure 4-9: **Sodium dodecyl sulfate–polyacrylamide gel electrophoresis (SDS-PAGE) analysis to validate the calpain cleavage site (CCS) in bulk reaction.** For peptides P3 & P6, which contain CCS between peptide K or E and PEG24 (around 1 kDa), only the addition of both 450 nM calpain-1 (CPN1) and 3 mM $CaCl_2$ in bulk reaction resulted in a significant decrease in the size of peptide, which suggests cleavage of the peptide at the CCS.

Following this, Chol-CCS-PEG2K were added to SUPER template and SUV membranes at a surface density that should induce the PEG chains to exhibit "brush" conformation. This will allow PEG to extend further from the membrane surface, potentially enhancing the blockage of

fusion of SUPER templates and SUVs concurrently decorated with oligos A and A', respectively. Minimal membrane interactions were observed when Chol-CCS-PEG2K containing SUPER templates and SUVs were mixed with inactive calpain (**Figure 4-6**C, **Figure 4-10**). However, with the addition of 5 mM $CaCl_2$ to the mixture, membrane interactions were observed across 85.2 ± 1.8% of fully formed SUPER templates indicating the successful cleavage of membrane-bound PEG chains by calpain-1 (**Figure 4-6**C, **Figure 4-10**).

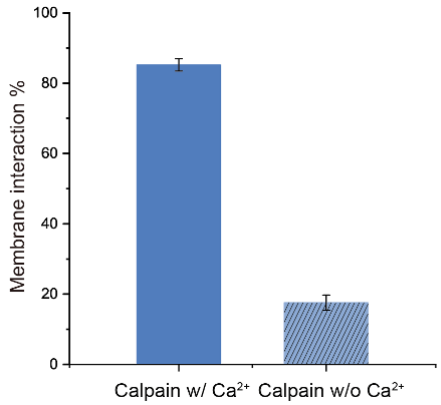

Figure 4-10: Quantification of calcium-activated membrane interactions between SUPER templates and SUVs mediated by DNA oligonucleotides. SUPER templates labeled with NBD-PE are functionalized with DNA strand A while SUVs labeled with Rhod-PE are functionalized with DNA strand A'. In the presence of 225 nM calpain-1, the bar graphs display the percentage of lipid-coated beads showing membrane interaction with SUVs by the red fluorescence detected on SUPER templates membranes with or without the addition of 5 mM $CaCl_2$. At least 60 lipid-coated beads were analyzed for each condition. All experiments were repeated three times under identical conditions. The error bars represent standard errors.

4.4.2 DAN-Mediated Membrane Fusions Between SUVs and GUVs Triggered by Calcium

In addition to the successful demonstration of DNA-meditated membrane interaction between SUVs and SUPER templates, we also tested the interactions between SUVs and GUVs, where we decorated GUV membranes with strand A or B, and SUV membranes with strand A' or B'. DNA-mediated membrane interactions were observed consistently on the surfaces of 80.9 ± 5.7 % (A+A') and 77.6 ± 6.8 % (B+B') of the observed GUVs (**Figure 4-11**A, **Figure 4-12**A).

Consistent with the earlier result, both PEG2K and PEG5K effectively blocked the DNA-mediated interactions between GUVs and SUVs, while PEG1K did not (**Figure 4-11**B, **Figure**

4-12B). To test calpain-mediated membrane fusion, Chol-CCS-PEG2K was incorporated into DNA-decorated GUV and SUV membranes. When GUVs were combined with SUVs and inactive calpain-1, minimal interactions were observed. However, with the addition of 5mM $CaCl_2$, membrane interactions between GUV and SUVs were observed across 75.8 ± 5.5% of imaged GUVs (**Figure 4-11**C, **Figure 4-13**A).

However, with the goal of calcium-triggered membrane fusion, the previous experiments are not sufficient to prove the fusion of GUV membranes with SUV membranes. Due to the small size of SUVs, which are below the diffraction limit of confocal microscopy, co-localization of SUV membrane fluorescence with SUPER template or GUV membrane fluorescence does not necessarily indicate membrane fusion. Thus, additional experiments like content mixing assays have been used to prove membrane fusion[354–356]. Content mixing assays seek to find evidence that contents encapsulated in SUVs can be delivered and found inside GUVs. However, the detection of content mixing can be challenging, especially since most content-mixing assays rely on fluorescence readouts. This is largely due to the huge volume disparity between GUVs and SUVs; furthermore, the process for generating SUVs leads to the same contents inside and outside the vesicles. Thus, encapsulating SUVs with fluorescent dyes like calcein or fluorescein will require the removal of the dye in the solution containing SUVs, which might be not complete. Thus, the high background fluorescence caused by incomplete dye removal dominates the already weak fluorescent signal inside of GUVs, which results from the substantial dilution of dye when SUVs fuse with GUVs that are approximately a million times larger by volume.

To combat these detection challenges, we developed a novel membrane fusion assay based on the localization of an encapsulated fluorescence protein. Here, SUVs are made with a lipid composition containing DGS-NTA-Ni, a synthetic diacyl lipid carrying a nickel ion with a His-tag

binding head group. GUVs encapsulating a histidine-tagged blue fluorescent protein (His_6-BFP) are prepared by an inverted emulsion-based method[360,365], which ensures the contents inside GUVs are completely separate from the outside. When SUVs fuse with GUVs, the Ni-NTA in SUVs become incorporated into GUV membranes, causing the translocation of His_6-BFP from the GUV lumen to the GUV membrane. When SUVs with strand A' and Chol-CCS-PEG2K were mixed with GUVs encapsulating His_6-BFP and decorated with strand A and Chol-CCS-PEG2K, BFP fluorescence inside GUVs localized to the membrane, in a manner that is dependent on calpain-1 activity (**Figure 4-11**D). We found 45.7 ± 6 % of GUVs showed membrane interaction with SUVs and BFP translocation to the GUV membrane (**Figure 4-13**B). This result strongly supports that DNA-mediated membrane fusion occurs between SUVs and GUVs. The lower efficiency compared with the membrane fusion results in **Figure 4-6** could be caused by Ni-NTA being positively charged, which limits the amount of Ni-NTA in SUVs. Thus, a significant number of SUVs are required to fuse with each GUV for BFP translocation to be observed. In addition, DNA-mediated membrane fusion is not 100% efficient. Nevertheless, these results demonstrate the initiation of DNA-mediated membrane fusion between SUVs and GUVs in response to calcium-dependent calpain-1 activity.

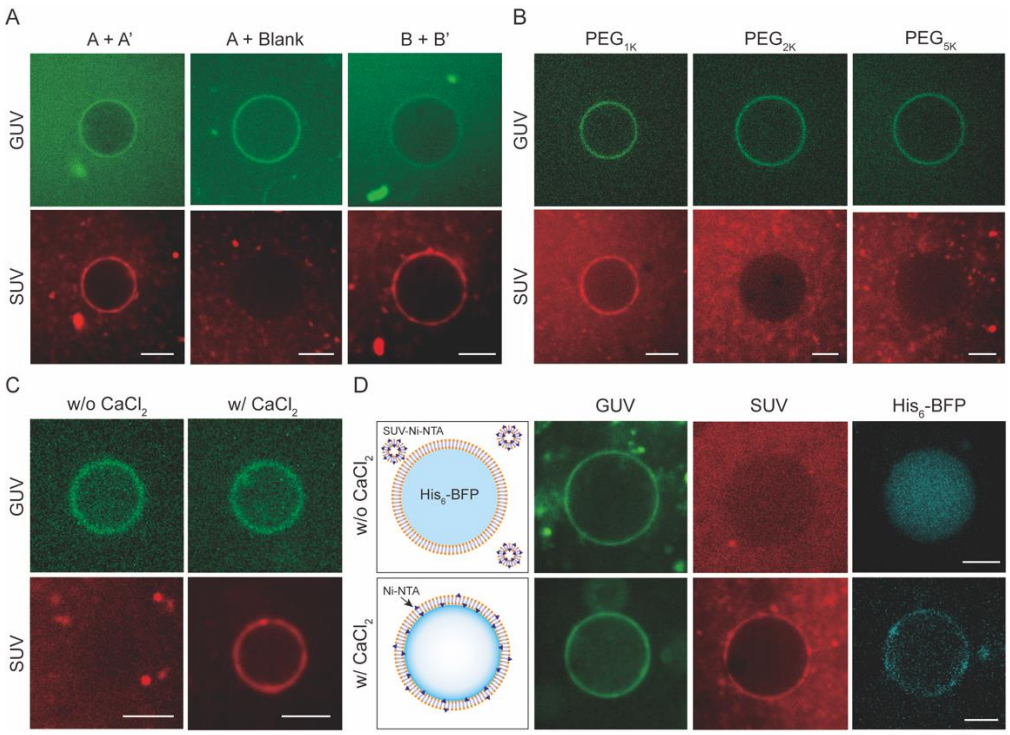

Figure 4-11: Chol-CCS-PEG2K enables calcium-triggered, DNA-mediated membrane fusion between SUVs and GUVs. (A) Membrane interactions between GUVs (labelled with NBD-PE, green) and SUVs (labelled with Rhod-PE, red) only occur when opposing membranes are decorated with complementary DNA oligos (i.e., GUV with strand A or B, and SUV with strand A' or B'). (B) PEG2K or PEG5K on both GUV and SUV membranes effectively blocks DNA-mediated interactions, while PEG1K does not. (C) Calcium regulates DNA-mediated membrane interaction between GUVs and SUVs, in the presence of calpain-1. (D) Membrane fusion between GUVs and SUVs. SUVs made with Ni-NTA and decorated with Chol-CCS-PEG2K and strand A' are mixed with GUVs encapsulating His6-BFP and decorated with Chol-CCS-PEG2K and strand A and in the presence of 225 nM calpain-1, with and without 5 mM $CaCl_2$. Scale bars: 10 μm.

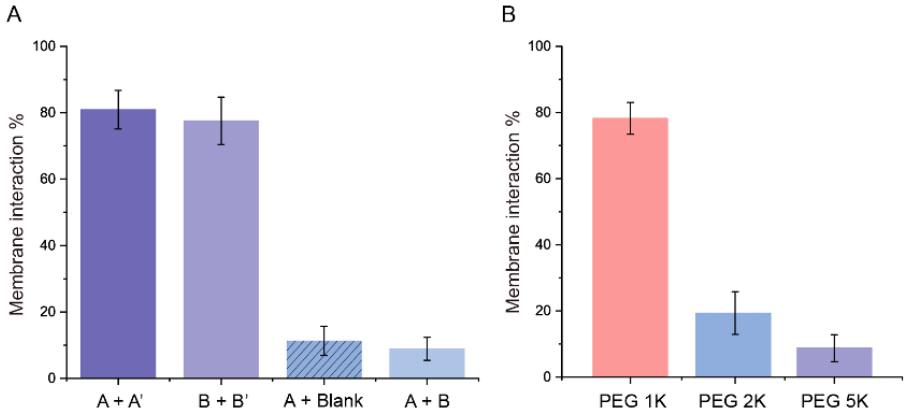

Figure 4-12: Quantification of DNA-mediated membrane interactions between GUVs and SUVs. (A) GUVs labeled with NBD-PE are functionalized with DNA strand A or B respectively while SUVs labeled with Rhod-PE are functionalized with DNA strand A', B', or no DNA. The bar graphs represent the percentage of GUVs showing membrane interaction with SUVs by the red fluorescence GUV membranes. (B) Both GUVs and SUVs membranes were covered with complementary DNA and PEG chains. The bar graphs display the percentage of GUVs showing

red fluorescence rings to the total number of GUVs. At least 30 vesicles were analyzed for each condition. All experiments were repeated three times under identical conditions. The error bars represent standard errors.

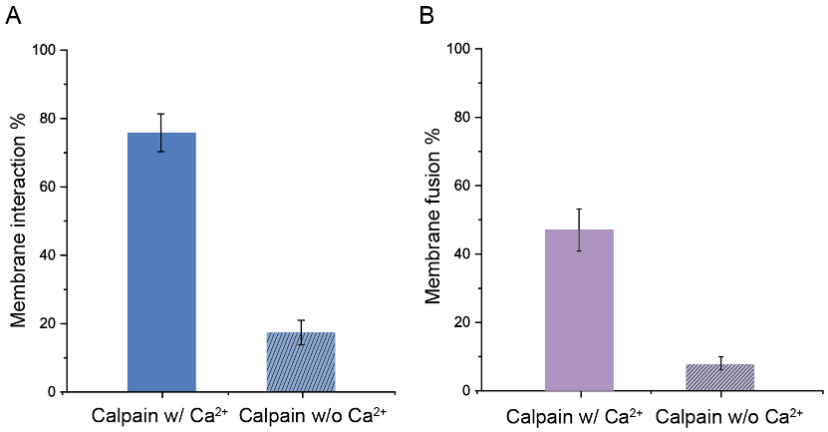

Figure 4-13: Quantification of calcium-activated membrane interactions and membrane fusions between GUVs and SUVs mediated by DNA oligonucleotides. GUVs labeled with NBD-PE were covered with DNA strand A and calpain-cleavable PEG2k while SUVs labeled with Rhod-PE were covered with DNA strand A' and calpain-cleavable PEG2k. (A) The blue bars represent the percentage of GUVs showing membrane interaction with SUVs by the red fluorescence on GUV membranes. (B) The purple bars represent the percentage GUVs showing membrane interactions with SUVs that also show GUV membrane fusion with SUVs. At least 30 vesicles were analyzed for each condition. All experiments were repeated three times under identical conditions. The error bars represent standard errors.

The strategy for regulating fusion with calpain-cleavable, membrane-bound PEG chains is in theory not limited to DNA-mediated membrane fusion approaches. We believe this strategy can also work for peptide K/E-based membrane fusion[354,355]. To test this hypothesis, SUPER templates and SUVs were decorated with membrane-bound peptides K and E, respectively. Membrane interactions were only inhibited when surface-bound PEG2K was functionalized on both SUPER template and SUV membranes (**Figure 4-14**). While not demonstrated here, we strongly suspect the Chol-CCS-PEG2K construct can also regulate peptide-mediated membrane fusion.

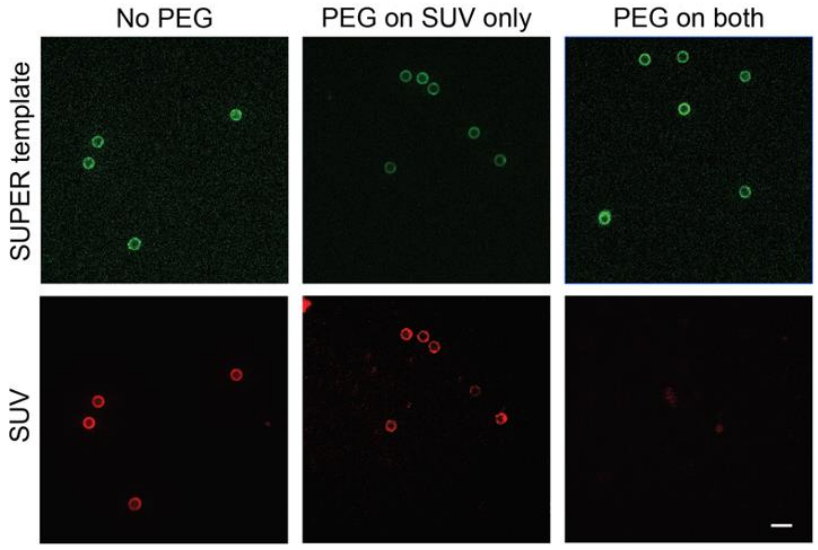

Figure 4-14: Inhibition of peptide-mediated membrane interactions with surface-bound PEG2K. SUPER templates and SUVs decorated with membrane-bound peptides K (peptide P1) and E (peptide P1), respectively. Membrane interactions were observed when no surface-bound PEG2K polymers were present (No PEG) and when PEG2K polymers were only on the SUV membrane (PEG on SUV only). When PEG2K chains are conjugated to both membrane surfaces, no membrane interactions are seen. Scale bar: 10 μm.

4.4.3 DNA-Mediated Membrane Fusions in GUV-in-SUV System Triggered by Calcium

Having demonstrated DNA-mediated calcium-triggered membrane fusion, I next wanted to establish this synthetic exocytosis scheme in a vesicle-in-vesicle system. In this case, calpain and SUVs labeled with complementary DNA strand A' and calpain cleavable PEG shield (Chol-CCS-PEG2K) were encapsulated inside GUVs labeled with DNA strand A. To demonstrate the feasibility, I utilized the previously developed membrane fusion assay on the SUV-in-GUV system. The only difference is that this time the His_6-BFP is present outside the GUVs instead of being encapsulated inside. In the absence of calcium, no binding of His_6-BFP from the outer solution to GUV membranes was observed. On the other hand, membrane fusion was observed by the localization of His_6-BFP on GUV membranes in the presence of encapsulated calcium (**Figure 4-15**). In addition, this was observed only in GUVs with red fluorescence rings, which further confirmed the delivery of Ni-NTA from SUVs to GUV membranes through the membrane fusion.

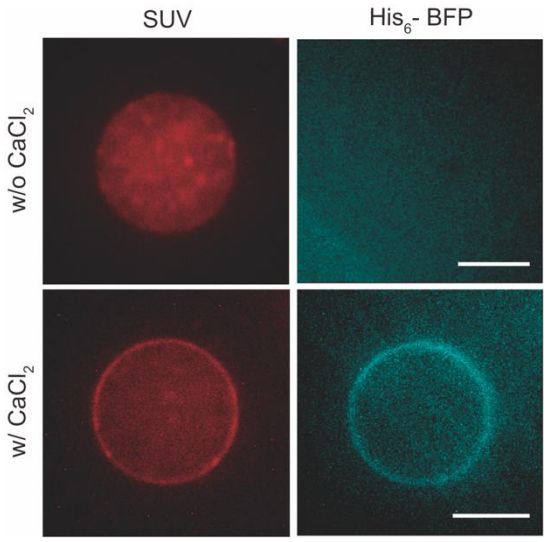

Figure 4-15: Recruitment of His_6-BFP to GUV membranes through DNA-mediated membrane fusion in SUV-in-GUV system triggered by calcium. GUVs functionalized with DNA strand B encapsulating 225 nM calpain-1, SUVs decorated with DNA strand B' and Chol-CCS-PEG2K were placed in the solution with 5 uM His_6-BFP. Accumulation of His_6-BFP on GUV membranes was detected only when 5 mM $CaCl_2$ was co-encapsulated inside GUVs. Scale bars: 10 μm

4.4.4 Reconstitution of functional cell-free expressed MscL on GUV membranes

As introduced in Chapter 2, MscL is a well-known mechanosensitive channel that allows molecules and ions to transport across membranes under elevated membrane tension. To control membrane fusion in a calcium-dependent manner by mechanical force, I capacitate the GUVs with mechanosensing abilities by reconstituting MscL in the lipid bilayer. In this way, when GUVs are subjected to mechanical stimuli, MscL will open its channel pore to induce calcium influx. The external calcium will then activate calpain inside GUVs and deshield the PEG chains, which then trigger membrane fusion between SUVs and GUVs.

To demonstrate that the cell-free expressed MscL can be reconstituted and be functional in the GUV membranes, I encapsulated fluorescein (FITC) and Cyanine5 (Cy5) respectively inside GUVs, followed by incubating with CFE reaction for expressing MscL channels. As MscL is being produced, GUV membranes provide an appropriate substrate for MscL insertion. After 3 hours of incubation, localization of MscL-sfGFP as green fluorescence rings was observed on GUV

membranes, which implies the insertion of MscL into lipid bilayer membranes (**Figure 4-16**). To confirm whether the inserted MscL was functional, osmotic pressure was applied to GUVs by adding water to the outer solution. Under hypo-osmotic conditions, I observed that both FITC and Cy5 were released from GUVs (**Figure 4-16**), respectively, indicating MscL was functionally reconstituted on GUV membranes.

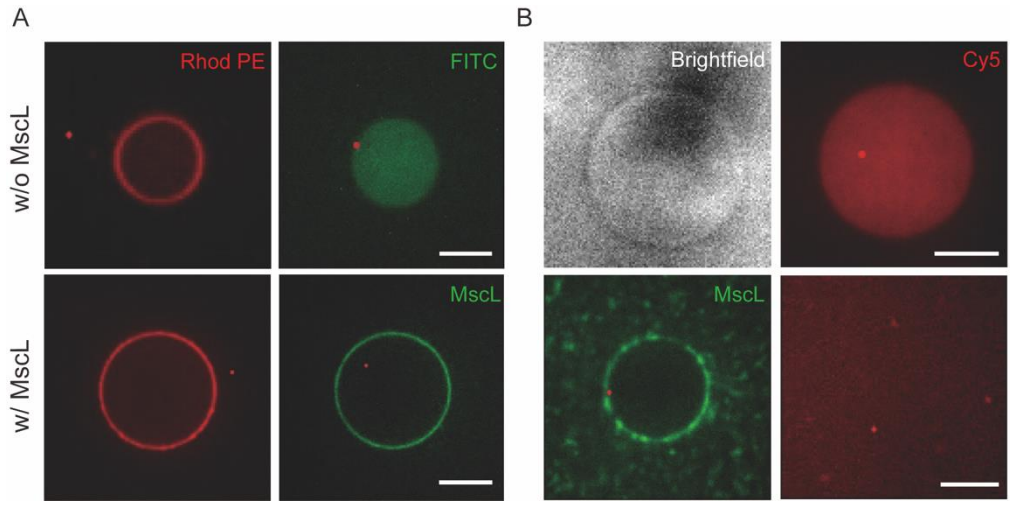

Figure 4-16: Release of fluorescence dye controlled by cell-free expressed MscL reconstituted on GUV membranes. (A) 5mM of fluorescein (FITC) was encapsulated within GUVs with and without MscL expressed by the PURE system. With application of hypo-osmotic pressure, where the osmolarity difference between the outer and inner solution is ~100 mOsm, FITC was released only from the vesicles expressing MscL rather than the ones without MscL. (B) 5mM of Cyanine5 (Cy5) dye was encapsulated within GUVs with and without MscL expressed by the PURE system. Only vesicles expressing MscL released Cy5 under hypo-osmotic environment while the ones without MscL did not. The osmolarity difference between iso-osmotic and hypo-osmotic solutions was measured at 100 mOsm. Scale bar: 10 μm.

After the demonstration of successful insertion of MscL into GUV membrane with a simple lipid composition (DOPC and cholesterol, more details in **Table 4-2**) as shown above, I next tested membrane fusion of SUVs with GUVs containing more complex lipid components (DOPC, DOPE, cholesterol, Chol-CCS-PEG2K and DNA, more details in **Table 4-5**, **Table 4-6**) in order to establish calcium-dependent membrane fusion. When PEG chains existed in both the outer and inner membranes of GUVs, MscL-sfGFP did not localize to the GUV membranes at all as no green fluorescence rings were observed (**Figure 4-17**). Poor insertion of MscL might be caused by the PEG chains pointed outwards from the outer GUV membranes, which prevents MscL from

incorporating into GUV membranes. To increase the insertion efficiency, Chol-CCS-PEG2K was removed from the outer membranes of GUVs. However, insertion of MscL was still not observed. A possible reason could be the asymmetry of lipid bilayer caused by the different lipid composition between the inner and outer membranes of GUVs since Chol-CCS-PEG2K was also added to the inner GUV solution. Therefore, I reduced the amount of Chol-CCS-PEG2K in the inner GUV membranes and found a negative correlation between PEG concentration and MscL insertion efficiency (**Figure 4-17**).

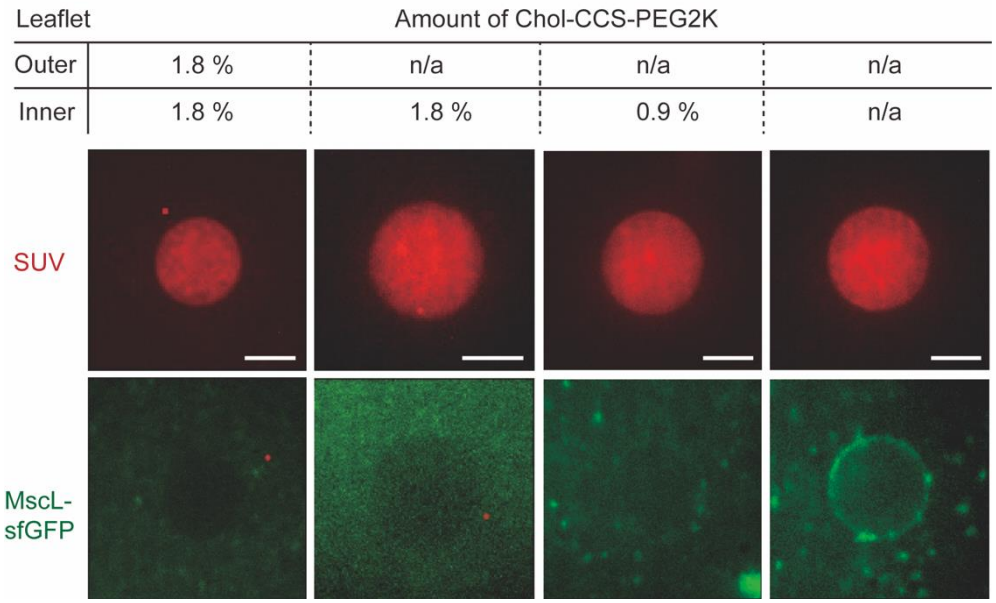

Figure 4-17: Insertion of cell-free expressed MscL into GUV membranes. GUVs encapsulating SUVs labeled with 2% CCS-PEG2K and Rhod PE (red) were incubated with PURE system for expressing MscL-sfGFP. Different amounts of CCS-PEG2K were added on the outer and inner leaf of GUV membranes respectively. No insertion was observed when CCS-PEG2K existed in the outer membranes. Insertion efficiency of MscL increased as the amount of CCS-PEG2K existed in the inner membranes. Scale bar: 10 μm.

After optimizing the concentration of PEG2K in inner membranes for good localization of MscL on GUVs, I further confirmed the function of reconstituted MscL for transporting ions across lipid bilayer membranes by testing calcium-activated membrane interaction between GUVs and SUVs. GUVs, which encapsulate SUVs labeled with complementary DNA (strand A') and CCS-

PEG2K, were labeled with DNA (strand A) and CCS-PEG2K for their inner membranes and were incubated with PURE expressed MscL under iso-osmotic condition. No red fluorescence rings were observed on GUVs placed in the iso-osmotic solution with 10 mM $CaCl_2$ after 2 hours of incubation, which indicates no calcium was detected inside GUVs for inducing membrane interactions between GUVs and SUVs (**Figure 4-18**). After applying osmotic pressure on GUVs by adding water into outer solution for generating hypo-osmotic environment, GUVs expressing MscL showed red fluorescence rings, implying the detection of calcium influx caused by the opening of MscL channel for triggering calcium-dependent membrane interactions (**Figure 4-18**).

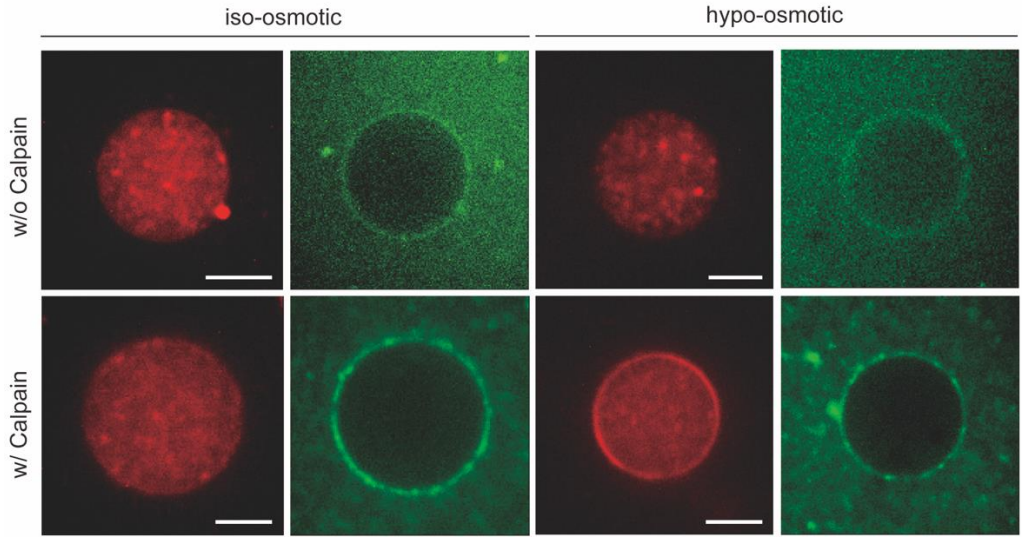

Figure 4-18: Calcium-activated membrane interaction between GUVs and SUVs controlled by cell-free expressed MscL. Vesicles with cell-free expressed MscL encapsulating SUVs labeled with 2% CCS-PEG2K and Rhod PE (red) were formed under iso-osmotic conditions and then milli-Q water was added to the outer solution to create a hypo-osmotic environment. A 100mM CaCl2 stock solution was added to the hypo-osmotic external solution to a final concentration of 10 mM. No membrane interactions were observed between SUVs and GUVs under iso-osmotic condition. Under hypo-osmotic condition/ when osmotic pressure was applied, interactions between GUVs and SUVs shown by red fluorescent rings were detected only when 225nM calpain was co-encapsulated inside vesicles. Scale bar: 10 μm.

For the next step, to further verify if membrane fusion actually occurs following the above-mentioned calcium dependent membrane interactions triggered by mechanical stimuli, our newly developed membrane fusion assay[366] can be applied to this system. Using the same experimental setup mentioned before in **Figure 4-11**, where the GUV containing SUVs containing Ni-NTA are

placed in the solution with His_6-BFP proteins, membrane fusion inside the SUV-in-GUV system can be detected by the translocation of BFP fluorescence signal in response to hypo-osmotic shocks. The success of the mechanically activated membrane fusion strategy depending on calcium can be further explored for reconstitution of mechanically controlled synthetic exocytosis.

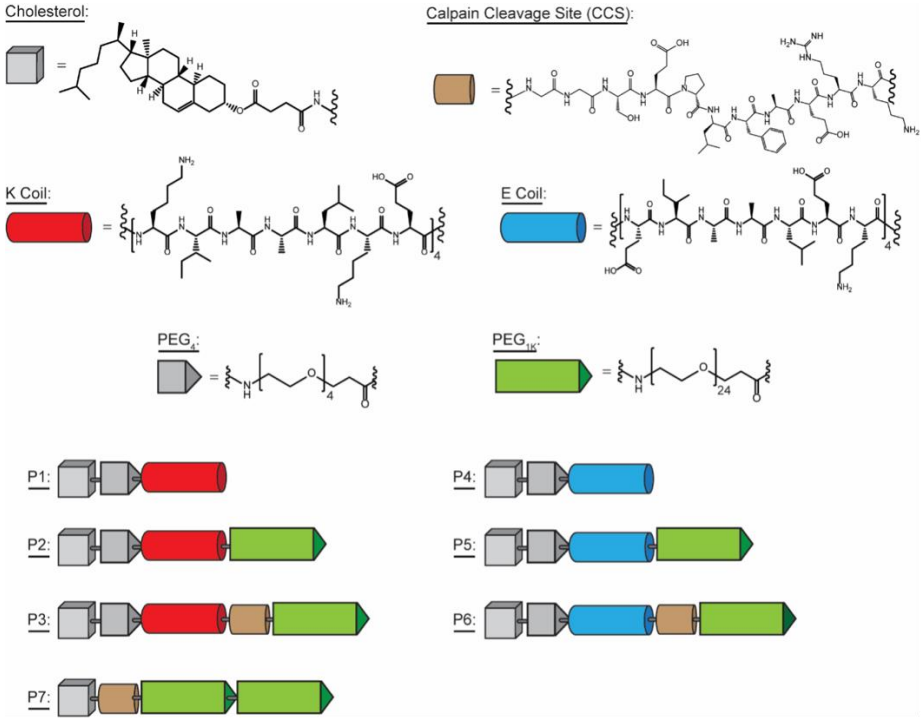

Figure 4-19: Schematics of synthesized peptides. All seven peptides synthesized are graphically represented above. This figure complements the peptide details listed in **Table 4-4**.

4.5 Conclusion

In summary, we have developed a strategy that mimics *in vivo* SNARE-mediated membrane fusion by recapitulating the calcium-dependent nature and demonstrated the feasibility using different synthetic membrane systems including SUPER templates, GUVs, and SUVs. I further demonstrated calcium-induced membrane fusion in a vesicle-in-vesicle system (i.e., SUVs inside GUV) with the potential for synthetic exocytosis. Successful reconstitution of functional

mechanosensitive channel MscL on GUV membranes provides a means for mechanically controlled exocytosis only when calcium, a common secondary messenger molecule[256,367,368], is shuttled inside the synthetic cell, in response to a mechanical stimulus. Such development would enable communication between synthetic cells and natural cells in the future.

Chapter 5 Conclusion and Future Work

5.1 Summary

Mechanosensitive ion channels underlie a variety of fundamental physiological processes that require sensation of mechanical force. They adapt distinctive structures and mechanotransduction mechanisms to fit their biological roles. However, their complex protein structures and sophisticated purification processes hamper in-depth investigation of their functions and molecular identifications. Recent advances in cell-free expression (CFE) systems and the development of cell membrane models have enabled the studies of a wide variety of membrane proteins. In this dissertation, I have reconstituted a newly found putative mechanosensitive channel Pkd2 found in fission yeast in lipid bilayer vesicles using cell-free protein expression and verified that it can sense and respond to increased membrane stretching by changing its channel permeability to calcium ions.

In addition to the investigation of mechanosensitive channel functions through *in vitro* platforms, I also explored their application in living cells. In Chapter 3, I developed a genetically encoded optical membrane tension sensor using a well-studied bacterial mechanosensitive channel MscL with insertion of circularly permuted green fluorescent protein (cpGFP) in the periplasmic loop. As an OFF sensor, the fluorescence intensity reduces with increasing tension, due to conformation changes of the channel that disrupts cpGFP conformation. To demonstrate the feasibility, I transfected different cell types with this membrane tension sensor and demonstrated the reversibility of the fluorescence shift on the plasma membrane under cyclic osmotic pressure.

I also showed the fluorescence changes of the sensor signal localized to the cell membranes in response to different substrate rigidity that is known to alter membrane tension.

The applications of the mechanosensitive channels are not limited to living cells but can be explored in synthetic cells as well. By reconstituting these channels on lipid bilayer membranes, synthetic cells can be capacitated with mechanosensitivity and their behaviors can be regulated by mechanical force. In Chapter 4, I successfully reconstituted cell-free expressed MscL on GUV membranes from the outside and demonstrated that it can be activated via membrane stretching under hypo-osmotic conditions, subsequently releasing lumenal contents. The force-sensitive synthetic cells can be used as a drug delivery/release system that can perform exocytosis activated by mechanical stimuli.

Common in all eukaryotes, calcium-dependent membrane fusion is the key process observed in exocytosis. Therefore, with the goal of developing mechanosensitive synthetic cells capable of secretion, I developed a DNA-mediated membrane fusion strategy that can be triggered by calcium ions. By using surface-bound PEG chains that are cleavable by the calcium-activated protease calpain-1 on vesicle membranes, I demonstrated that membrane interactions and fusions between vesicles (e.g., SUVs - SUPER templates and SUVs – GUVs) only occurred in the presence of calcium ions. I further demonstrated the calcium-dependent membrane fusion strategy can be used in a vesicle-in-vesicle (i.e., SUVs-in-GUV) system, which can be functionalized with mechanosensitivity by the addition of reconstituted MscL on GUV membranes. In the future, the success of force-activated exocytosis can be used for communication between synthetic cells and natural cells, which will be discussed more in future work and perspective section.

5.2 Future work and perspective

While considerable progress has been made in confirming the localization and mechanosensitivity of recently discovered mechanosensitive channels through initial investigations into ion permeabilities during membrane stretching, a plethora of unanswered inquiries persist regarding their intricate molecular mechanisms, mechanotransduction pathways, and potential multifaceted functions. The elucidation of these aspects stands as a critical frontier in understanding the complex interplay between mechanical stimuli and cellular responses. Furthermore, the optimization and thorough assessment of the feasibility and efficacy of the MscL membrane tension sensor represent promising avenues for future research endeavors. The refinement of this sensor holds the potential to unlock deeper insights into the dynamic interplay between membrane tension and cellular signaling, offering invaluable tools for both in vivo and in vitro studies. Through meticulous experimentation and optimization, it is plausible to enhance the sensor's precision and sensitivity, thereby enabling more accurate and reliable detection of subtle changes in membrane tension dynamics. Such advancements not only bolster our fundamental understanding of mechanotransduction processes but also hold promising implications for various fields, including biophysics, cellular physiology, and biomedical engineering. Consequently, in the forthcoming section, I aim to delineate a comprehensive roadmap outlining potential future directions emanating from the culmination of my findings, encompassing both theoretical inquiries and practical applications.

5.2.1 In vitro investigation of different mutants of fission yeast polycystin Pkd2p

As an ion channel, Pkd2p has been confirmed to function as a calcium-permeable mechanosensitive channel when being activated under physical force in both *in vivo* and *in vitro* systems[256,314]. My research has shown that *in vit*ro-reconstituted Pkd2 on GUVs can be activated

by membrane stretching caused by osmotic pressure. For *in vivo* studies, the mechanosensitivity of Pkd2 allows it to direct the Ca^{2+} influx during osmotic adaption and the separation of daughter cells during cytokinesis. As a putative TRP channel, it is also very important to understand how Pkd2 is targeted to the plasma membrane, where it can sense changes in membrane tension and function as a gate for ion transport. Therefore, conducting a deeper investigation of the mechanistic structure-based studies to understand which parts of the protein structure affect membrane targeting and mechanosensitivity or functions of Pkd2 is necessary. In the previous studies, different domains of Pkd2, the lipid-binding domain (LBD), the transmembrane domain (TMD), and C-the terminal cytoplasmic domain (CCD) were examined in fission yeast cells for their contribution to intracellular localization and function[369]. The results show that both the LBD and TMD domains are essential for membrane localization and function of Pkd2 as truncation mutants with deletion of either LBD or TMD made fission yeast cells unviable. Removal of one or more transmembrane helices caused Pkd2 mutants to be retained in the endothelial reticulum and unable to reach the plasma membranes. There is also evidence showing that the cytoplasmic tail or CCD plays a crucial role in regulating the internalization of Pkd2 and its distribution in the plasma membranes, where the truncation mutant with the removal of CCD clusters in eisosomes in the plasma membrane and become depolarized on the cell surface[369]. In spite of these *in vivo* findings in fission yeast, how the protein structure affects the functionality and localization of Pkd2 remains elusive and can be explored through investigation of calcium membrane permeability and protein insertion using *in vitro* bottom-up reconstitution.

Pkd2 plasmids with deletion or mutation in LBD, TMD, and CCD will be used to produce mutant proteins using cell-free expression systems and be further reconstituted on artificial membranes respectively. SUPER templates or lipid-coated beads will be used to test if mutant

Pkd2 has a defect in its localization and insertion into the lipid bilayer. The mechanosensitivity will also be examined by testing whether these mutant Pkd2 expressed on GUV membranes can cause calcium influx when they are subjected to mechanical stimuli. By carrying out these *in vitro* studies, the role of the extracellular and transmembrane domain, and the cytoplasmic tail in the function of Pkd2p can be revealed. In the future, the function of different mutants sensitive to diverse environmental stimuli, such as temperature, light, or electrical impulse could be tested using the synthetic cell platform through bottom-up reconstitution.

5.2.2 In vitro application of the MscL tension biosensor expressed on GUV membranes

We have demonstrated the application of the MscL membrane tension biosensor in both fibroblast cells (NIH3T3) and stem cells (hMSCs). The tension sensor also shows changes in fluorescence intensity when cells are attached to micropost arrays with different rigidity, and reversibility of fluorescence intensity when cells are subjected to cyclic osmotic pressures, with lower fluorescence in hypotonic environments while higher fluorescence in isotonic conditions. Besides plasma membranes in mammalian cells, the MscL membrane tension reporter may offer a useful approach for detailed investigations of spatial and temporal dynamics of membrane tension and cell signaling in subcellular organellar membranes including the membranes of the nucleus and the endoplasmic reticulum.

Besides testing in *in vivo* systems, the relationship between the fluorescence to tension response could be further calibrated using *in vitro* platforms. CFE systems allow simultaneous expression of multiple proteins with high efficiency, which is ideally suited for the reconstitution of multiple proteins without the need for more complicated and time-consuming purification steps. Leveraging CFE systems, the development of synthetic cells that recapitulate gene expression with encapsulated CFE reactions capable of synthesizing desired proteins of interest has gained

popularity as an approach to characterize biological functions in isolation. The lipid bilayer membranes of synthetic cells and microsomes from different organelle membranes that are present in cell-free lysates also provide suitable substrates for proper membrane protein folding and insertion during synthesis. For example, bacterial membrane protein MscL has been successfully reconstituted on GUV membranes with good membrane localization and functionality using CFE systems[182]. In light of these advantages, utilizing synthetic cell membranes, cell-free expressing MscL tension reporter holds significant promise as a robust experimental platform, poised to facilitate extensive exploration and comprehensive evaluation of the membrane tension sensor's performance. The MscL membrane tension reporter can be expressed using CFE systems and be reconstituted on GUV membranes. When GUVs are subject to mechanical stimulus through diversity of experimental methods, such as pressure suction applied by micropipette aspiration[370], osmotic stress caused by sudden change in the solute concentration[371], mechanical force applied by atomic force microscopy[372], microindentation or parallel microplate stretcher[373], or shear stress produced in flow chamber [374], changes in membrane tension can be detected through the fluorescence intensity of the MscL tension sensor. The exact membrane tension can be measured after the calibration of the relationship between membrane fluorescence and membrane tension (by using micropipette aspiration). Broader application of the user-friendly MscL membrane tension reporter to a variety of cell types (e.g., plant, and archaea) will help advance research in membrane biophysics and cell mechanics and mechanotransduction.

5.2.3 Building force-activated communication between synthetic cells and natural cells through artificial exocytosis

Although synthetic cells provide a powerful platform to study protein functions or reconstitute cellular mechanisms in isolation, the fact is that living systems generally do not

operate independently but are often connected with others as collaborators or competitors. Intercellular communication is critical to coordinate the behaviors of individual cells in multicellular communities or organisms. Chemical substances, which are secreted by cells, can act as signals on other cells. Cells can also signal directly to others by engaging cell surface receptors or through cell junction structures. For chemical signals, they can act as local mediators in paracrine signaling to affect nearby target cells. By using a variety of signaling processes, cells can exchange information with each other to organize, synchronize and differentiate their specialized tissues. Therefore, the utilization of synthetic cells has been extended to the area of intercellular communication. For instance, allosteric amplification of a low molecular signal, adenosine 5'-monophosphate (AMP), through synthetic enzymatic cascades to high metabolite output, NADH, has been demonstrated by communication between sender vesicles encapsulating enzyme apyrase, generating AMP from ADP or ATP, and receiver vesicles loading with glycogen phosphorylase b (GPb), an enzyme that can be activated by the binding of AMP, and other two downstream enzymes from the pentose phosphate pathway (phosphoglucomutase; PGM, and glucose-6-phosphate dehydrogenase; G6PDH) for producing NADH[375]. Although research has shown advances in encapsulation methods by successfully building Intercellular communication between synthetic cells, interaction between synthetic cells and natural cells remains limited. Recently, emerging work has begun exploring the communication between synthetic cells and natural cells. Even so, the studies have mostly been limited to communication between bacterial-sized synthetic cells and bacteria[376]. Therefore, developing a mammalian cell-sized synthetic cell capable of direct communication with nearby natural cells will significantly advance our engineering capability of synthetic cells for applications in human health. In the past, we have successfully established calcium-dependent activation of membrane fusion using calpain cleavable

PEG chains mediated by complementary DNA oligonucleotides *in vitro* between vesicles[366]. We have also successfully reconstituted functional MscL using CFE systems on vesicle membranes and demonstrated its activity by showing calcium and fluorescent dye transport in vesicles under hypo-osmotic stress[182]. These two successes can be integrated to engineer a mechanical force-sensitive synthetic cell system for secreting bioactive molecules.

Reconstitute exocytosis of encapsulated SUVs in large lipid bilayer vesicles can be reconstituted by leveraging calcium-sensitive vesicle fusion. The calcium-dependent DNA-mediated membrane fusion strategy can be applied to a vesicle-in-vesicle system, with cargo-containing SUVs within a larger vesicle, and MscL can be expressed on the larger vesicle membranes for force-sensing. By applying mechanical stimuli on synthetic cells, MscL can be activated and allow calcium influx to trigger exocytosis, thereby eliciting biological effects on living cells depending on the secreting factors. The biological effects can be quite diverse ranging from proliferation to cell death. Engineered extracellular matrix (ECM) as a biomaterial are generally designed to promote cell growth and proliferation as they are important for tissue engineering applications[374,377,378]. Although engineered ECM materials can respond to various chemical and physical environmental cues, they have mainly been used to direct responses of cells that attach to them. Therefore, I envision this mechanosensitive synthetic cell system as a novel biomaterial that when attached to cells and experiencing mechanical force would secrete chemical substances to communicate distinct signals to target cells.

Although there are multiple ways to activate MscL including applying osmotic shocks or micropipette suction, as long as it creates sufficiently high membrane tension (e.g., membrane tension threshold for MscL gating is ~7-12 mN/m tension threshold)[379,380], the proposed concept is to use shear stress which takes advantage of the shear-sensitive environment present in our

bodies, in particular in the cardiovascular and cerebrovascular contexts[381–383], as many physiological functions are highly-related to disturbed fluid flow. For instance, the initiation and progression of atherosclerotic lesions are known to be associated with localized disturbed flow, and disturbed flow alters endothelial cell morphology, proliferation, migration, and cytoskeletal organization[383–385]. Hence, building a shear force-sensitive vesicle system that can communicate with endothelial cells, which respond to changes in shear forces based on the pattern of blood flow, can largely benefit and advance the application of synthetic cells as a drug delivery system in human health for multiple disease treatments. Studies have shown that vascular endothelial growth factor (VEGF) plays a major role in controlling proliferation, cell migration, and wound healing in endothelial cells[386,387]. By encapsulating VEGF-A inside the shear force-sensitive vesicle system, we can control upregulation of VEGF-A/VEGFR2 signaling network[388], where exocytosed VEGF-A can initiate VEGF signaling by activating VEGFR2 and then trigger a proliferation signaling pathway mediated by extracellular signal-regulated protein kinases 1 and 2 (ERK 1/2)[389], under different shear stress. By observing real-time ERK activity using a kinase translocation reporter (KTR)[390] based on nucleocytoplasmic shuttling equilibrium, we can monitor cell proliferation rate in response to VEGF-A release caused by different shear activating flow rates (**Figure 5-1**).

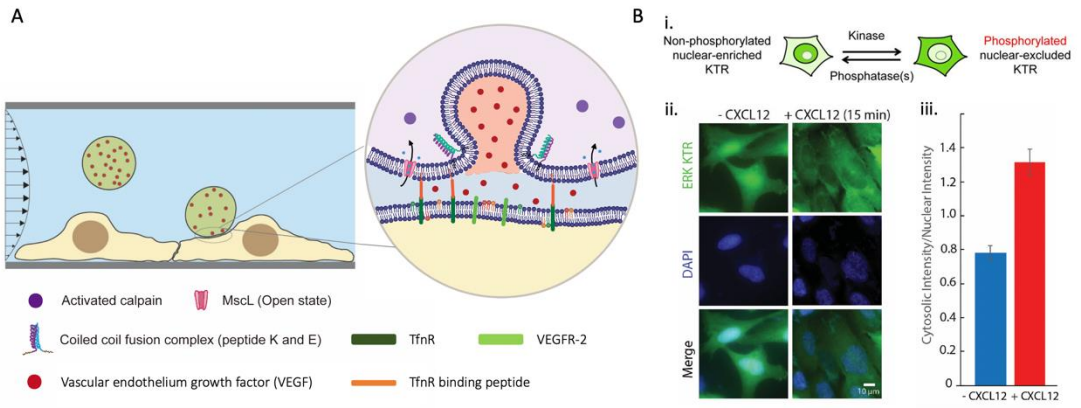

Figure 5-1: Schematic of intercellular communication between a synthetic cell and a natural cell. A synthetic cell is bound to TfnR and activated by shear stress to secrete VEGF. (B) Mechanism of KTR for reporting kinase activities. The ERK KTR is stably expressed in SUM159 cells and treated with 50 nM of chemokine CXCL12 for 15 min. These preliminary data are from Jophin Joseph.

To further demonstrate the versatility of the vesicle-in-vesicle system performing synthetic exocytosis, the application of this shear force-sensitive vesicle system can be explored on inflammatory response. It is known that extracellular ATP is an important inflammatory signaling molecule and major pathway to release cytoplasmic ATP is through connexin hemichannels Cx43[391,392]. Blockade of Cx43 has been shown to reduce inflammation and improve healing[392]. Recent evidence shows that synthetic peptide JM2 can promote interaction of Cx43 and β-tubulin, which reduce trafficking of Cx43 to the cell surfaces. In addition, JM2 prevents ATP release induced by low calcium and subsequently attenuates neutrophil response[391,393]. Hence, JM2 can be encapsulated inside SUVs and then exocytosed by synthetic cells activated with shear force for regulation of inflammatory response. Binding of Cx43 and beta tubulin caused by releasing JM2 can be monitored using duolink proximity ligation assay. We anticipate that the shear-sensitive synthetic cells will deliver chemical substances locally to cells very much like how chemical signals are communicated between cells in our bodies. The secretion of different types of signals from the synthetic cells can directly affect cells that are in close proximity (i.e., attached to the cells). By having specific control over the size of synthetic cells and cell-free expression, activation

at specific shear flow rates can be achieved aimed at targeting cells in different flow geometries. This novel synthetic cell platform with force-activated triggered exocytosis inspired by cell secretion in intercellular communication will be the first synthetic cells that can communicate with natural living mammalian cells and provide a great degree of flexibility in the type of chemical substances that can be secreted and target cells. If successful, other sensing mechanisms beyond mechanosensing can be envisioned in the construction of more sophisticated synthetic cells as cell-based therapeutics.

5.2.4 Developing mechanosensitive synthetic cells for controlled drug release

Recent advances in synthetic cell technologies as drug carriers have benefitted drug delivery systems with effective and controlled release of a variety of therapeutics for different diseases[394]. For example, artificial cell-based drug carriers encapsulating chemotherapeutic or antibiotic drugs such as doxorubicin[395], daunorubicin[396], or paclitaxel[397], with the addition of certain surface-bound molecules with affinity to specific receptors on cancer cells, have been shown to improve tumor-targeting and reduce toxicity and side effects to healthy tissues[398,399]. The development of a cationic liposome system and biodegradable polymeric carriers facilitates the delivery of various forms of nucleic acids into target cells for long-term administration[398,399]. Finally, liposomes as carriers encapsulating components of weakened or inactivated forms of disease-causing agents can effectively prevent enzymatic degradation of antigenic proteins and reduce toxicity or allergic responses by reducing the required dose[400]. In spite of these successful application, few of them are capacitated with sensing and responding mechanism, which hampers the advance in controlling drug release and building more sophisticated cell-like systems. As one of the most essential molecular force sensors and transducers found in cell membranes, MS channels can convert mechanical inputs into biochemical or electrical signals to mediate a variety

of sensations[158]. By reconstituting MS channels in the synthetic lipid bilayers, we envision using different mechanical stimuli such as ultrasound, shear stress to activate drug release from mechanosensitive synthetic cells for different disease treatments.

The first concept is to build acoustically controlled drug release system in blood vessels using mechanosensing GUVs. In the human vascular system, white blood cells and platelets stay in circulation until activated. Platelets, for example, are activated upon reaching the area of vascular injury. Then, they immediately adhere to exposed collagen or immobilized von Willebrand factor, externalize phosphatidylserine, and activate prothrombinase, which activates thrombin[401]. Inspired by this elegant system, we theorize a synthetic cell-based drug delivery system could offer the potential to mimic native physiology and make controlled drug delivery vehicles smart with the ability to decide when to release drugs based on their surroundings. Previously, synthetic platelets have been conceived by others using microgels or nanoparticles, as alternatives to natural platelets[402,403]. Here, GUVs are a great candidate since they are roughly cell-sized and can easily encapsulate drug payloads. In addition, they are biocompatible and do not provoke immune responses, due to their phospholipid membrane[404]. However, the main challenge to use them as drug delivery system is the retention of circulating GUVs in the blood flow[405]. To improve the survival rate, one potential solution is to adhere to blood vessel walls, which has not been explored in any study. Interestingly, recent advancements in acoustic trapping have demonstrated non-invasive and precise spatial manipulation of GUVs with ultrasound[406,407]. Taken together, bio-inspired drug delivery can be realized by using acoustic trapping to manipulate GUVs in circulation facilitating them to adhere to blood vessel walls. In this scheme, drug-encapsulating GUVs could be intravenously injected into the bloodstream and allowed to reach the site of interest. One or more pairs of ultrasound transducers could be placed around the site of interest in

contact with the patient's skin. These transducers produce precise pressure waves, which concentrate at the site of interest along the vessel wall. For vessel adhesion, the surface of GUVs could be decorated with collagen-binding peptides or other adhesion-mediating constructs[326]. Inspired by the phenomenon of blood cell margination *in vivo*, we propose that acoustic pressure waves can pull GUVs in circulation towards the surface of the blood vessel providing favorable proximity for adhesion (**Figure 5-2**A). However, since GUVs are filled with an aqueous solution and submerged in liquid, they are largely transparent to acoustic pressure waves. Thus, the force acoustic waves exert on circulating GUVs may not be sufficient to facilitate adhesion. In that case, commercially available microbubbles or gas vesicles may be used [408,409]. Specifically, avidin-coated microbubbles/gas vesicles bind to biotin-conjugated cholesterol, which immobilizes them on the inner surface of GUVs. When GUVs are immobilized, they can then deliver drugs of interest in response to local cue(s) utilizing established or emergent artificial cell-based biosensing mechanisms, for example, a mechanosensitive GUV using MscL (**Figure 5-2**B)[405]. The success of the system can overcome many hindrances of the current acoustically controlled intravenous drug delivery approaches, including precision limited to millimeter-scale, side effects when using higher intensity ultrasound, such as skin burns and blood clots, and limitations in tailoring drug delivery based on real-time local environmental cues, achieving adaptive, intelligent response at the microscale. Most importantly, the ultrasound-induced system can be used to treat a wide range of diseases when the target locations are known.

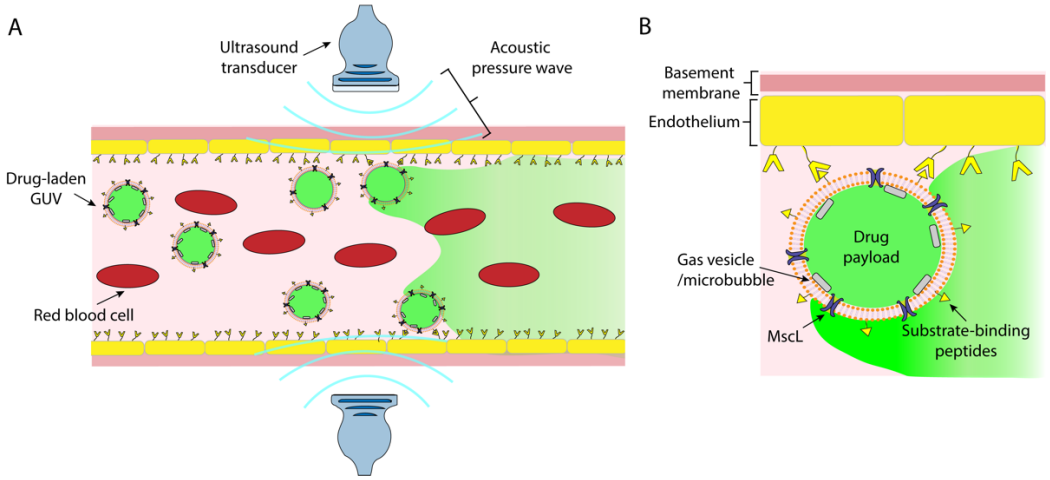

Figure 5-2: (A) Overall schematic of acoustically controlled GUV manipulation and subsequent drug delivery. (B) Closeup schematic of an adhered GUV whose drug delivery is gated by changes in the GUV's membrane tension using the MS channel MscL. The schematic is courtesy of Samuel Chen.

Besides using ultrasound, we propose a promising strategy by focusing on the distinctive mechanical feature of the stenotic blood vessels, which is an increase in shear stress. Therefore, the second concept is to target stenotic blood vessels with mechanosensitive synthetic cells. It is known that the shear stress in the stenotic or obstructed regions can increase up to >1000 dyne/cm^2, while that of normal blood vessels is in the tight range of 1–70 dyne/cm^2 under a dynamic regulatory controlling system[410–412]. Using this difference, developing a drug delivery system that can respond to increased shear stress can be a solution to the current challenge, which is the high risk of bleeding caused by thrombolytic or anticoagulant drugs spreading throughout the body. Thus, there is an increasing need for developing a targeted drug delivery system capable of concentrating drugs only in locally constricted vessels. To develop such a system, we propose to use mechanosensitive synthetic cells harboring MscL as drug carriers. Recent theoretical studies have shown that the MscL reconstituted on GUV membranes can be activated when GUVs are flowing through a narrowing constriction channel and deformed under the shear stress, which cause the increase in membrane tension[413,414]. Based on such theoretical predictions, one can

envision loading small molecule thrombolytic or anticoagulant drugs, such as orniplabin[415–417], into mechanosensitive synthetic cells and expect the release of drugs through activated MscL when synthetic cells are exposed to elevated shear stress in the stenotic region (**Figure 5-3**). The development of such a system will not only reduce the risk of current treatments but also provide pre-hospital treatment for emergency use, which may contribute to reduced mortality of stenosis.

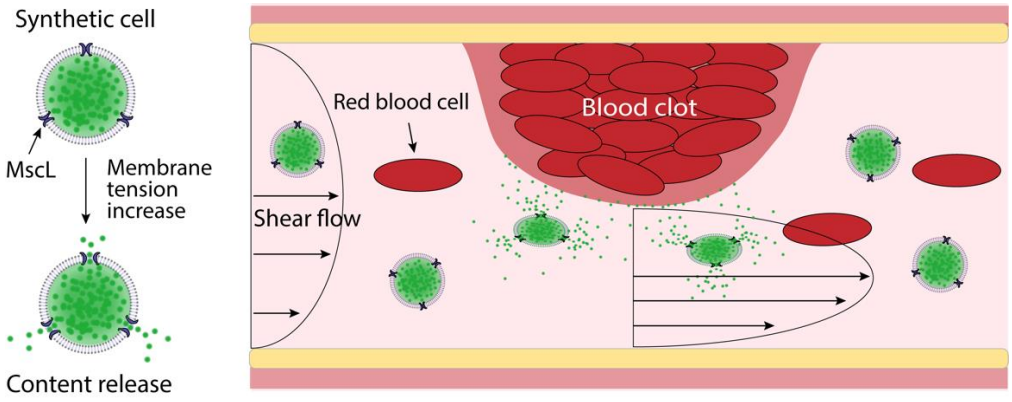

Figure 5-3: Schematics of concept of shear stress-responsive drug delivery system using synthetic cells as drug carrier. Increased shear stress in the stenotic vessel activates MscL and leads to the release of thrombolytic or anticoagulant drugs in a controlled manner. The schematic is courtesy of Sung-Won Hwang.

5.3 Conclusion

In this dissertation, I have repurposed the MS channel MscL as an optical membrane tension reporter, representing a significant leap forward in our ability to study the dynamic interplay of membrane mechanics, mechanotransduction, and cell signaling. By developing a genetically encoded tension sensor, I have introduced a non-invasive, user-friendly tool that empowers researchers to delve deeply into the spatial-temporal dynamics of membrane tension with unprecedented precision and versatility. This breakthrough promises to catalyze advancements across diverse fields, from cell biology to biophysics, by providing a platform for elucidating the intricate biophysical properties of cellular membranes. Moreover, the versatility of this sensor

extends beyond its initial application, offering utility across a spectrum of cell types and intracellular membranes. From the nucleus to the endoplasmic reticulum, Golgi apparatus, mitochondria, and beyond, the sensor opens doors to unraveling the mysteries of membrane biophysics within subcellular organelles. Its adaptability facilitates exploration in both prokaryotic and eukaryotic organisms, amplifying its impact and potential contributions to fundamental research endeavors.

Beyond its application in vivo, this dissertation presents a novel platform for in vitro investigations of mechanosensitive channels and complex membrane proteins using artificial cells with encapsulated CFE reactions. These modular tools offer unprecedented flexibility, enabling researchers to modify and control reaction conditions with ease, without the constraints imposed by living organisms. Combined with the development of the novel membrane fusion strategy triggered by calcium ions, bottom-up reconstitution of MS channels on GUV membranes lays the groundwork for the development of mechanosensitive artificial cells capable of calcium-dependent exocytosis, holding promise as smart drug delivery/release systems regulated by mechanical forces for biomedical applications. The envisioned trajectory extends further, with potential for exploring intercellular communication between synthetic and natural cells through synthetic exocytosis. This ambitious endeavor could yield groundbreaking outcomes, potentially leading to the realization of synthetic cells capable of seamlessly interfacing with living mammalian cells. Such synthetic platforms offer unparalleled flexibility in targeting cells and modulating chemical release, heralding a new era in cell-based therapeutics and biomedical research.

Looking ahead, the foundation laid in this dissertation paves the way for exploring sensing mechanisms beyond mechanosensing, facilitating the development of even more sophisticated synthetic cells for diverse therapeutic applications. By embracing innovation and interdisciplinary

collaboration, the future holds immense promise for advancing our understanding of mechanobiology and harnessing synthetic biology to address pressing healthcare challenges.

Bibliography

(1) Song, D.; Yang, D.; Powell, C. A.; Wang, X. Cell–Cell Communication: Old Mystery and New Opportunity. *Cell Biology and Toxicology*. 2019. https://doi.org/10.1007/s10565-019-09470-y.

(2) Sanz-Ezquerro, J. J.; Münsterberg, A. E.; Stricker, S. Editorial: Signaling Pathways in Embryonic Development. *Frontiers in Cell and Developmental Biology*. 2017. https://doi.org/10.3389/fcell.2017.00076.

(3) Hara, M. R.; Snyder, S. H. Cell Signaling and Neuronal Death. *Annual Review of Pharmacology and Toxicology*. 2007. https://doi.org/10.1146/annurev.pharmtox.47.120505.105311.

(4) Leung, P. C. K.; Choi, J. H. Endocrine Signaling in Ovarian Surface Epithelium and Cancer. *Human Reproduction Update*. 2007. https://doi.org/10.1093/humupd/dml002.

(5) Cho, W.; Stahelin, R. V. Membrane-Protein Interactions in Cell Signaling and Membrane Trafficking. *Annual Review of Biophysics and Biomolecular Structure*. 2005. https://doi.org/10.1146/annurev.biophys.33.110502.133337.

(6) Martinac, B. Mechanosensitive Ion Channels: Molecules of Mechanotransduction. *J Cell Sci* **2004**, *117* (12), 2449–2460. https://doi.org/10.1242/jcs.01232.

(7) Jin, P.; Jan, L. Y.; Jan, Y. N. Mechanosensitive Ion Channels: Structural Features Relevant to Mechanotransduction Mechanisms. *Annual Review of Neuroscience*. 2020. https://doi.org/10.1146/annurev-neuro-070918-050509.

(8) Korenbrot, J. I. Speed, Sensitivity, and Stability of the Light Response in Rod and Cone Photoreceptors: Facts and Models. *Progress in Retinal and Eye Research*. 2012. https://doi.org/10.1016/j.preteyeres.2012.05.002.

(9) Rutter, G. A.; Pullen, T. J.; Hodson, D. J.; Martinez-Sanchez, A. Pancreatic β-Cell Identity, Glucose Sensing and the Control of Insulin Secretion. *Biochemical Journal*. 2015. https://doi.org/10.1042/BJ20141384.

(10) Schwartz, M. A.; DeSimone, D. W. Cell Adhesion Receptors in Mechanotransduction. *Current Opinion in Cell Biology*. 2008. https://doi.org/10.1016/j.ceb.2008.05.005.

(11) Li, X.; Egervari, G.; Wang, Y.; Berger, S. L.; Lu, Z. Regulation of Chromatin and Gene Expression by Metabolic Enzymes and Metabolites. *Nature Reviews Molecular Cell Biology*. 2018. https://doi.org/10.1038/s41580-018-0029-7.

(12) Hughes, C. E.; Nibbs, R. J. B. A Guide to Chemokines and Their Receptors. *FEBS Journal*. 2018. https://doi.org/10.1111/febs.14466.

(13) SenGupta, S.; Parent, C. A.; Bear, J. E. The Principles of Directed Cell Migration. *Nature Reviews Molecular Cell Biology*. 2021. https://doi.org/10.1038/s41580-021-00366-6.

(14) You, M.; Xie, Z.; Zhang, N.; Zhang, Y.; Xiao, D.; Liu, S.; Zhuang, W.; Li, L.; Tao, Y. Signaling Pathways in Cancer Metabolism: Mechanisms and Therapeutic Targets. *Signal Transduction and Targeted Therapy*. 2023. https://doi.org/10.1038/s41392-023-01442-3.

(15) Ohashi, P. S. T-Cell Signalling and Autoimmunity: Molecular Mechanisms of Disease. *Nature Reviews Immunology*. 2002. https://doi.org/10.1038/nri822.

(16) Corneth, O. B. J.; Neys, S. F. H.; Hendriks, R. W. Aberrant B Cell Signaling in Autoimmune Diseases. *Cells*. 2022. https://doi.org/10.3390/cells11213391.

(17) Berridge, M. J. Module 12: Signalling Defects and Disease. *Cell Signalling Biology* **2014**, *6*. https://doi.org/10.1042/csb0001012.

(18) Albert Basson, M. Signaling in Cell Differentiation and Morphogenesis. *Cold Spring Harb Perspect Biol* **2012**, *4* (6). https://doi.org/10.1101/cshperspect.a008151.

(19) Berridge, M. J. Unlocking the Secrets of Cell Signaling. *Annual Review of Physiology*. 2005. https://doi.org/10.1146/annurev.physiol.67.040103.152647.

(20) Wymann, M. P.; Schneiter, R. Lipid Signalling in Disease. *Nature Reviews Molecular Cell Biology*. 2008. https://doi.org/10.1038/nrm2335.

(21) Sunshine, H.; Iruela-Arispe, M. L. Membrane Lipids and Cell Signaling. *Current Opinion in Lipidology*. 2017. https://doi.org/10.1097/MOL.0000000000000443.

(22) Bondos, S. E.; Dunker, A. K.; Uversky, V. N. Intrinsically Disordered Proteins Play Diverse Roles in Cell Signaling. *Cell Communication and Signaling*. 2022. https://doi.org/10.1186/s12964-022-00821-7.

(23) Paudel, S.; Wu, G.; Wang, X. Amino Acids in Cell Signaling: Regulation and Function. In *Advances in Experimental Medicine and Biology*; 2021; Vol. 1332. https://doi.org/10.1007/978-3-030-74180-8_2.

(24) Giuliani, A. L.; Sarti, A. C.; Di Virgilio, F. Extracellular Nucleotides and Nucleosides as Signalling Molecules. *Immunology Letters*. 2019. https://doi.org/10.1016/j.imlet.2018.11.006.

(25) Hodo, T. W.; de Aquino, M. T. P.; Shimamoto, A.; Shanker, A. Critical Neurotransmitters in the Neuroimmune Network. *Frontiers in Immunology*. 2020. https://doi.org/10.3389/fimmu.2020.01869.

(26) Falomir-Lockhart, L. J.; Cavazzutti, G. F.; Giménez, E.; Toscani, A. M. Fatty Acid Signaling Mechanisms in Neural Cells: Fatty Acid Receptors. *Frontiers in Cellular Neuroscience*. 2019. https://doi.org/10.3389/fncel.2019.00162.

(27) Snyder, S. H.; Jaffrey, S. R.; Zakhary, R. Nitric Oxide and Carbon Monoxide: Parallel Roles as Neural Messengers. In *Brain Research Reviews*; 1998; Vol. 26. https://doi.org/10.1016/S0165-0173(97)00032-5.

(28) Pandey, S.; Zhang, W.; Assmann, S. M. Roles of Ion Channels and Transporters in Guard Cell Signal Transduction. *FEBS Letters*. 2007. https://doi.org/10.1016/j.febslet.2007.04.008.

(29) Newton, A. C.; Bootman, M. D.; Scott, J. Second Messengers. *Cold Spring Harb Perspect Biol* **2016**, *8* (8). https://doi.org/10.1101/cshperspect.a005926.

(30) Richards, J. A. S.; Ascoli, M. Endocrine, Paracrine, and Autocrine Signaling Pathways That Regulate Ovulation. *Trends in Endocrinology and Metabolism*. 2018. https://doi.org/10.1016/j.tem.2018.02.012.

(31) Doğaner, B. A.; Yan, L. K. Q.; Youk, H. Autocrine Signaling and Quorum Sensing: Extreme Ends of a Common Spectrum. *Trends in Cell Biology*. 2016. https://doi.org/10.1016/j.tcb.2015.11.002.

(32) Rohr, S. Role of Gap Junctions in the Propagation of the Cardiac Action Potential. *Cardiovascular Research*. 2004. https://doi.org/10.1016/j.cardiores.2003.11.035.

(33) Ogunshola, O. O.; Antic, A.; Donoghue, M. J.; Fan, S. Y.; Kim, H.; Stewart, W. B.; Madri, J. A.; Ment, L. R. Paracrine and Autocrine Functions of Neuronal Vascular Endothelial Growth Factor (VEGF) in the Central Nervous System. *Journal of Biological Chemistry* **2002**, *277* (13). https://doi.org/10.1074/jbc.M111085200.

(34) Rodriguez-Diaz, R.; Menegaz, D.; Caicedo, A. Neurotransmitters Act as Paracrine Signals to Regulate Insulin Secretion from the Human Pancreatic Islet. *Journal of Physiology* **2014**, *592* (16). https://doi.org/10.1113/jphysiol.2013.269910.

(35) Tan, M. I. Cell and Molecular Biology for Diagnostic and Therapeutic Technology. In *Journal of Physics: Conference Series*; 2016; Vol. 694. https://doi.org/10.1088/1742-6596/694/1/012001.

(36) Mora-Garcia, P.; Sakamoto, K. M. Cell Signaling Defects and Human Disease. *Mol Genet Metab* **1999**, *66* (3). https://doi.org/10.1006/mgme.1998.2798.

(37) Sebastian-Leon, P.; Vidal, E.; Minguez, P.; Conesa, A.; Tarazona, S.; Amadoz, A.; Armero, C.; Salavert, F.; Vidal-Puig, A.; Montaner, D.; Dopazo, J. Understanding Disease Mechanisms with Models of Signaling Pathway Activities. *BMC Syst Biol* **2014**, *8*. https://doi.org/10.1186/s12918-014-0121-3.

(38) Zhang, H.; Labouesse, M. Signalling through Mechanical Inputs - A Coordinated Process. *Journal of Cell Science*. 2012. https://doi.org/10.1242/jcs.093666.

(39) Happe, C. L.; Engler, A. J. Mechanical Forces Reshape Differentiation Cues That Guide Cardiomyogenesis. *Circulation Research*. 2016. https://doi.org/10.1161/CIRCRESAHA.115.305139.

(40) Chien, S.; Li, S.; Shyy, J. Y. J. Effects of Mechanical Forces on Signal Transduction and Gene Expression in Endothelial Cells. In *Hypertension*; 1998; Vol. 31. https://doi.org/10.1161/01.hyp.31.1.162.

(41) Ranade, S. S.; Syeda, R.; Patapoutian, A. Mechanically Activated Ion Channels. *Neuron*. 2015. https://doi.org/10.1016/j.neuron.2015.08.032.

(42) Sun, Z.; Guo, S. S.; Fässler, R. Integrin-Mediated Mechanotransduction. *Journal of Cell Biology*. 2016. https://doi.org/10.1083/jcb.201609037.

(43) Shyy, J. Y. J.; Chien, S. Role of Integrins in Cellular Responses to Mechanical Stress and Adhesion. *Curr Opin Cell Biol* **1997**, *9* (5). https://doi.org/10.1016/S0955-0674(97)80125-1.

(44) Dehkhoda, F.; Lee, C. M. M.; Medina, J.; Brooks, A. J. The Growth Hormone Receptor: Mechanism of Receptor Activation, Cell Signaling, and Physiological Aspects. *Frontiers in Endocrinology*. 2018. https://doi.org/10.3389/fendo.2018.00035.

(45) Miller, B.; Sewell-Loftin, M. K. Mechanoregulation of Vascular Endothelial Growth Factor Receptor 2 in Angiogenesis. *Frontiers in Cardiovascular Medicine*. 2021. https://doi.org/10.3389/fcvm.2021.804934.

(46) Eliceiri, B. P. Integrin and Growth Factor Receptor Crosstalk. *Circulation Research*. 2001. https://doi.org/10.1161/hh2401.101084.

(47) Wagh, K.; Ishikawa, M.; Garcia, D. A.; Stavreva, D. A.; Upadhyaya, A.; Hager, G. L. Mechanical Regulation of Transcription: Recent Advances. *Trends in Cell Biology*. 2021. https://doi.org/10.1016/j.tcb.2021.02.008.

(48) Mendez, M. G.; Janmey, P. A. Transcription Factor Regulation by Mechanical Stress. *International Journal of Biochemistry and Cell Biology*. 2012. https://doi.org/10.1016/j.biocel.2012.02.003.

(49) Syeda, R.; Florendo, M. N.; Cox, C. D.; Kefauver, J. M.; Santos, J. S.; Martinac, B.; Patapoutian, A. Piezo1 Channels Are Inherently Mechanosensitive. *Cell Rep* **2016**, *17* (7), 1739–1746. https://doi.org/10.1016/j.celrep.2016.10.033.

(50) Zhang, M.; Ma, Y.; Ye, X.; Zhang, N.; Pan, L.; Wang, B. TRP (Transient Receptor Potential) Ion Channel Family: Structures, Biological Functions and Therapeutic Interventions for Diseases. *Signal Transduction and Targeted Therapy*. 2023. https://doi.org/10.1038/s41392-023-01464-x.

(51) Inoue, R.; Jian, Z.; Kawarabayashi, Y. Mechanosensitive TRP Channels in Cardiovascular Pathophysiology. *Pharmacology and Therapeutics*. 2009. https://doi.org/10.1016/j.pharmthera.2009.05.009.

(52) Beech, D. J.; Kalli, A. C. Force Sensing by Piezo Channels in Cardiovascular Health and Disease. *Arteriosclerosis, thrombosis, and vascular biology*. 2019. https://doi.org/10.1161/ATVBAHA.119.313348.

(53) Umar Shinge, S. A.; Zhang, D.; Din, A. U.; Yu, F.; Nie, Y. M. Emerging Piezo1 Signaling in Inflammation and Atherosclerosis; a Potential Therapeutic Target. *International Journal of Biological Sciences*. 2022. https://doi.org/10.7150/IJBS.63819.

(54) Mukherjee, P.; Rahaman, S. G.; Goswami, R.; Dutta, B.; Mahanty, M.; Rahaman, S. O. Role of Mechanosensitive Channels/Receptors in Atherosclerosis. *American Journal of Physiology - Cell Physiology*. 2022. https://doi.org/10.1152/ajpcell.00396.2021.

(55) Albarrán-Juárez, J.; Iring, A.; Wang, S. P.; Joseph, S.; Grimm, M.; Strilic, B.; Wettschureck, N.; Althoff, T. F.; Offermanns, S. Piezo1 and Gq/G11 Promote Endothelial Inflammation Depending on Flow Pattern and Integrin Activation. *Journal of Experimental Medicine* **2018**, *215* (10). https://doi.org/10.1084/JEM.20180483.

(56) Zhang, Y.; Ying, F.; Tian, X.; Lei, Z.; Li, X.; Lo, C. Y.; Li, J.; Jiang, L.; Yao, X. TRPM2 Promotes Atherosclerotic Progression in a Mouse Model of Atherosclerosis. *Cells* **2022**, *11* (9). https://doi.org/10.3390/cells11091423.

(57) Randhawa, P. K.; Jaggi, A. S. TRPV1 Channels in Cardiovascular System: A Double Edged Sword? *International Journal of Cardiology*. 2017. https://doi.org/10.1016/j.ijcard.2016.11.205.

(58) Zhang, C.; Ye, L.; Zhang, Q.; Wu, F.; Wang, L. The Role of TRPV1 Channels in Atherosclerosis. *Channels*. 2020. https://doi.org/10.1080/19336950.2020.1747803.

(59) Falcón, D.; Galeano-Otero, I.; Calderón-Sánchez, E.; Toro, R. Del; Martín-Bórnez, M.; Rosado, J. A.; Hmadcha, A.; Smani, T. TRP Channels: Current Perspectives in the Adverse Cardiac Remodeling. *Front Physiol* **2019**, *10* (MAR). https://doi.org/10.3389/fphys.2019.00159.

(60) Earley, S.; Brayden, J. E. Transient Receptor Potential Channels in the Vasculature. *Physiol Rev* **2015**, *95* (2). https://doi.org/10.1152/physrev.00026.2014.

(61) Gonzalez-Cobos, J. C.; Trebak, M. TRPC Channels in Smooth Muscle Cells. *Frontiers in Bioscience*. 2010. https://doi.org/10.2741/3660.

(62) Pereira da Silva, E. A.; Martín-Aragón Baudel, M.; Navedo, M. F.; Nieves-Cintrón, M. Ion Channel Molecular Complexes in Vascular Smooth Muscle. *Frontiers in Physiology*. 2022. https://doi.org/10.3389/fphys.2022.999369.

(63) Chen, X.; Wanggou, S.; Bodalia, A.; Zhu, M.; Dong, W.; Fan, J. J.; Yin, W. C.; Min, H. K.; Hu, M.; Draghici, D.; Dou, W.; Li, F.; Coutinho, F. J.; Whetstone, H.; Kushida, M. M.; Dirks, P. B.; Song, Y.; Hui, C. chung; Sun, Y.; Wang, L. Y.; Li, X.; Huang, X. A Feedforward Mechanism Mediated by Mechanosensitive Ion Channel PIEZO1 and Tissue Mechanics Promotes Glioma Aggression. *Neuron* **2018**, *100* (4). https://doi.org/10.1016/j.neuron.2018.09.046.

(64) Dombroski, J. A.; Hope, J. M.; Sarna, N. S.; King, M. R. Channeling the Force: Piezo1 Mechanotransduction in Cancer Metastasis. *Cells*. 2021. https://doi.org/10.3390/cells10112815.

(65) Luo, M.; Cai, G.; Ho, K. K. Y.; Wen, K.; Tong, Z.; Deng, L.; Liu, A. P. Compression Enhances Invasive Phenotype and Matrix Degradation of Breast Cancer Cells via Piezo1 Activation. *BMC Mol Cell Biol* **2022**, *23* (1). https://doi.org/10.1186/s12860-021-00401-6.

(66) Thoppil, R. J.; Adapala, R. K.; Cappelli, H. C.; Kondeti, V.; Dudley, A. C.; Gary Meszaros, J.; Paruchuri, S.; Thodeti, C. K. TRPV4 Channel Activation Selectively Inhibits Tumor Endothelial Cell Proliferation. *Sci Rep* **2015**, *5*. https://doi.org/10.1038/srep14257.

(67) Thoppil, R. J.; Cappelli, H. C.; Adapala, R. K.; Kanugula, A. K.; Paruchuri, S.; Thodeti, C. K. TRPV4 Channels Regulate Tumor Angiogenesis via Modulation of Rho/Rho Kinase Pathway. *Oncotarget* **2016**, *7* (18). https://doi.org/10.18632/oncotarget.8405.

(68) Ma, Z.; Finkel, T. H. T Cell Receptor Triggering by Force. *Trends Immunol* **2010**, *31* (1). https://doi.org/10.1016/j.it.2009.09.008.

(69) Noguchi, S.; Saito, A.; Nagase, T. YAP/TAZ Signaling as a Molecular Link between Fibrosis and Cancer. *International Journal of Molecular Sciences*. 2018. https://doi.org/10.3390/ijms19113674.

(70) Kim, C. L.; Choi, S. H.; Mo, J. S. Role of the Hippo Pathway in Fibrosis and Cancer. *Cells*. 2019. https://doi.org/10.3390/cells8050468.

(71) Dupont, S.; Morsut, L.; Aragona, M.; Enzo, E.; Giulitti, S.; Cordenonsi, M.; Zanconato, F.; Le Digabel, J.; Forcato, M.; Bicciato, S.; Elvassore, N.; Piccolo, S. Role of YAP/TAZ in Mechanotransduction. *Nature* **2011**, *474* (7350). https://doi.org/10.1038/nature10137.

(72) Schwartz, M. A. Integrins and Extracellular Matrix in Mechanotransduction. *Cold Spring Harbor perspectives in biology*. 2010. https://doi.org/10.1101/cshperspect.a005066.

(73) Streuli, C. H. Integrins as Architects of Cell Behavior. *Molecular Biology of the Cell*. 2016. https://doi.org/10.1091/mbc.E15-06-0369.

(74) Singh, P.; Schwarzbauer, J. E. Fibronectin and Stem Cell Differentiation - Lessons from Chondrogenesis. *J Cell Sci* **2012**, *125* (16). https://doi.org/10.1242/jcs.095786.

(75) Di, X.; Gao, X.; Peng, L.; Ai, J.; Jin, X.; Qi, S.; Li, H.; Wang, K.; Luo, D. Cellular Mechanotransduction in Health and Diseases: From Molecular Mechanism to Therapeutic Targets. *Signal Transduction and Targeted Therapy*. 2023. https://doi.org/10.1038/s41392-023-01501-9.

(76) Novoseletskaya, E. S.; Evdokimov, P. V.; Efimenko, A. Y. Extracellular Matrix-Induced Signaling Pathways in Mesenchymal Stem/Stromal Cells. *Cell Communication and Signaling*. 2023. https://doi.org/10.1186/s12964-023-01252-8.

(77) Fennen, M.; Pap, T.; Dankbar, B. Smad-Dependent Mechanisms of Inflammatory Bone Destruction. *Arthritis Research and Therapy*. 2016. https://doi.org/10.1186/s13075-016-1187-7.

(78) Saito, A.; Horie, M.; Nagase, T. TGF-β Signaling in Lung Health and Disease. *International Journal of Molecular Sciences*. 2018. https://doi.org/10.3390/ijms19082460.

(79) Biernacka, A.; Dobaczewski, M.; Frangogiannis, N. G. TGF-β Signaling in Fibrosis. *Growth Factors* **2011**, *29* (5). https://doi.org/10.3109/08977194.2011.595714.

(80) Liu, J.; Wang, F.; Luo, F. The Role of JAK/STAT Pathway in Fibrotic Diseases: Molecular and Cellular Mechanisms. *Biomolecules*. 2023. https://doi.org/10.3390/biom13010119.

(81) Benveniste, E. N.; Liu, Y.; McFarland, B. C.; Qin, H. Involvement of the Janus Kinase/Signal Transducer and Activator of Transcription Signaling Pathway in Multiple Sclerosis and the Animal Model of Experimental Autoimmune Encephalomyelitis. *Journal of Interferon and Cytokine Research*. 2014. https://doi.org/10.1089/jir.2014.0012.

(82) Zhou, Y.; Wang, T.; Hamilton, J. L.; Chen, D. Wnt/β-Catenin Signaling in Osteoarthritis and in Other Forms of Arthritis. *Current Rheumatology Reports*. 2017. https://doi.org/10.1007/s11926-017-0679-z.

(83) Tan, R. J.; Zhou, D.; Zhou, L.; Liu, Y. Wnt/β-Catenin Signaling and Kidney Fibrosis. *Kidney International Supplements*. 2014. https://doi.org/10.1038/kisup.2014.16.

(84) Zou, M.; Zhang, G.; Zou, J.; Liu, Y.; Liu, B.; Hu, X.; Cheng, Z. Inhibition of the ERK1/2-Ubiquitous Calpains Pathway Attenuates Experimental Pulmonary Fibrosis in Vivo and in Vitro. *Exp Cell Res* **2020**, *391* (1). https://doi.org/10.1016/j.yexcr.2020.111886.

(85) Hu, Y.; Fu, J.; Liu, X.; Xue, X. ERK1/2 Signaling Pathway Activated by EGF Promotes Proliferation, Transdifferentiation, and Migration of Cultured Primary Newborn Rat Lung Fibroblasts. *Biomed Res Int* **2020**, *2020*. https://doi.org/10.1155/2020/7176169.

(86) Boyer, J. G.; Prasad, V.; Song, T.; Lee, D.; Fu, X.; Grimes, K. M.; Sargent, M. A.; Sadayappan, S.; Molkentin, J. D. ERK1/2 Signaling Induces Skeletal Muscle Slow Fiber-Type Switching and Reduces Muscular Dystrophy Disease Severity. *JCI Insight* **2019**, *4* (10). https://doi.org/10.1172/jci.insight.127356.

(87) Esteller, M. Epigenetics in Cancer. *New England Journal of Medicine* **2008**, *358* (11). https://doi.org/10.1056/nejmra072067.

(88) Park, J. W.; Han, J. W. Targeting Epigenetics for Cancer Therapy. *Archives of Pharmacal Research*. 2019. https://doi.org/10.1007/s12272-019-01126-z.

(89) Yang, J.; Xu, J.; Wang, W.; Zhang, B.; Yu, X.; Shi, S. Epigenetic Regulation in the Tumor Microenvironment: Molecular Mechanisms and Therapeutic Targets. *Signal Transduction and Targeted Therapy*. 2023. https://doi.org/10.1038/s41392-023-01480-x.

(90) Saul, D.; Kosinsky, R. L. Epigenetics of Aging and Aging-Associated Diseases. *International Journal of Molecular Sciences*. 2021. https://doi.org/10.3390/ijms22010401.

(91) Wang, K.; Liu, H.; Hu, Q.; Wang, L.; Liu, J.; Zheng, Z.; Zhang, W.; Ren, J.; Zhu, F.; Liu, G. H. Epigenetic Regulation of Aging: Implications for Interventions of Aging and Diseases. *Signal Transduction and Targeted Therapy*. 2022. https://doi.org/10.1038/s41392-022-01211-8.

(92) Felisbino, M. B.; McKinsey, T. A. Epigenetics in Cardiac Fibrosis: Emphasis on Inflammation and Fibroblast Activation. *JACC: Basic to Translational Science*. 2018. https://doi.org/10.1016/j.jacbts.2018.05.003.

(93) Shao, J.; Liu, J.; Zuo, S. Roles of Epigenetics in Cardiac Fibroblast Activation and Fibrosis. *Cells*. 2022. https://doi.org/10.3390/cells11152347.

(94) Primakoff, P.; Myles, D. G. Cell-Cell Membrane Fusion during Mammalian Fertilization. *FEBS Letters*. 2007. https://doi.org/10.1016/j.febslet.2007.02.021.

(95) Gadella, B. M.; Evans, J. P. Membrane Fusions during Mammalian Fertilization. *Adv Exp Med Biol* **2011**, *713*. https://doi.org/10.1007/978-94-007-0763-4_5.

(96) Harrison, S. C. Viral Membrane Fusion. *Nature Structural and Molecular Biology*. 2008. https://doi.org/10.1038/nsmb.1456.

(97) White, J. M.; Delos, S. E.; Brecher, M.; Schornberg, K. Structures and Mechanisms of Viral Membrane Fusion Proteins: Multiple Variations on a Common Theme. *Critical*

Reviews in Biochemistry and Molecular Biology. 2008. https://doi.org/10.1080/10409230802058320.

(98) Palade, G. E. Membrane Biogenesis: An Overview. *Methods Enzymol* **1983**, *96* (C). https://doi.org/10.1016/S0076-6879(83)96004-4.

(99) Jahn, R. Principles of Exocytosis and Membrane Fusion. *Annals of the New York Academy of Sciences*. 2004. https://doi.org/10.1196/annals.1294.018.

(100) Gerst, J. E. SNAREs and SNARE Regulators in Membrane Fusion and Exocytosis. *Cellular and Molecular Life Sciences*. 1999. https://doi.org/10.1007/s000180050328.

(101) Jena, B. P. Cell Secretion and Membrane Fusion. In *Domestic Animal Endocrinology*; 2005; Vol. 29. https://doi.org/10.1016/j.domaniend.2005.02.039.

(102) Sauvola, C. W.; Littleton, J. T. SNARE Regulatory Proteins in Synaptic Vesicle Fusion and Recycling. *Frontiers in Molecular Neuroscience*. 2021. https://doi.org/10.3389/fnmol.2021.733138.

(103) Woodman, P. G. Biogenesis of the Sorting Endosome: The Role of Rab5. *Traffic* **2000**, *1* (9). https://doi.org/10.1034/j.1600-0854.2000.010902.x.

(104) Christoforidis, S.; McBride, H. M.; Burgoyne, R. D.; Zerial, M. The Rab5 Effector EEA1 Is a Core Component of Endosome Docking. *Nature* **1999**, *397* (6720). https://doi.org/10.1038/17618.

(105) Martens, S.; McMahon, H. T. Mechanisms of Membrane Fusion: Disparate Players and Common Principles. *Nature Reviews Molecular Cell Biology*. July 2008, pp 543–556. https://doi.org/10.1038/nrm2417.

(106) Krämer, L.; Ungermann, C. HOPS Drives Vacuole Fusion by Binding the Vacuolar SNARE Complex and the Vam7 PX Domain via Two Distinct Sites. *Mol Biol Cell* **2011**, *22* (14). https://doi.org/10.1091/mbc.E11-02-0104.

(107) Coonrod, E. M.; Graham, L. A.; Carpp, L. N.; Carr, T. M.; Stirrat, L.; Bowers, K.; Bryant, N. J.; Stevens, T. H. Homotypic Vacuole Fusion in Yeast Requires Organelle Acidification and Not the V-ATPase Membrane Domain. *Dev Cell* **2013**, *27* (4). https://doi.org/10.1016/j.devcel.2013.10.014.

(108) Song, Z.; Ghochani, M.; McCaffery, J. M.; Frey, T. G.; Chan, D. C. Mitofusins and OPA1 Mediate Sequential Steps in Mitochondrial Membrane Fusion. *Mol Biol Cell* **2009**, *20* (15). https://doi.org/10.1091/mbc.E09-03-0252.

(109) Benard, G.; Karbowski, M. Mitochondrial Fusion and Division: Regulation and Role in Cell Viability. *Seminars in Cell and Developmental Biology*. 2009. https://doi.org/10.1016/j.semcdb.2008.12.012.

(110) Ramachandran, R. Mitochondrial Dynamics: The Dynamin Superfamily and Execution by Collusion. *Seminars in Cell and Developmental Biology*. 2018. https://doi.org/10.1016/j.semcdb.2017.07.039.

(111) Önel, S. F.; Rust, M. B.; Jacob, R.; Renkawitz-Pohl, R. Tethering Membrane Fusion: Common and Different Players in Myoblasts and at the Synapse. *Journal of Neurogenetics*. 2014. https://doi.org/10.3109/01677063.2014.936014.

(112) Kim, J. H.; Chen, E. H. The Fusogenic Synapse at a Glance. *J Cell Sci* **2019**, *132* (18). https://doi.org/10.1242/JCS.213124.

(113) Lee, D. M.; Chen, E. H. Drosophila Myoblast Fusion: Invasion and Resistance for the Ultimate Union. *Annual Review of Genetics*. 2019. https://doi.org/10.1146/annurev-genet-120116-024603.

(114) Rout, P.; Preußner, M.; Önel, S. F. Drosophila Melanogaster: A Model System to Study Distinct Genetic Programs in Myoblast Fusion. *Cells*. 2022. https://doi.org/10.3390/cells11030321.

(115) Deneke, V. E.; Pauli, A. The Fertilization Enigma: How Sperm and Egg Fuse. *Annual Review of Cell and Developmental Biology*. 2021. https://doi.org/10.1146/annurev-cellbio-120219-021751.

(116) Klinovska, K.; Sebkova, N.; Dvorakova-Hortova, K. Sperm-Egg Fusion: A Molecular Enigma of Mammalian Reproduction. *International Journal of Molecular Sciences*. 2014. https://doi.org/10.3390/ijms150610652.

(117) Martens, S.; Kozlov, M. M.; McMahon, H. T. How Synaptotagmin Promotes Membrane Fusion. *Science (1979)* **2007**, *316* (5828). https://doi.org/10.1126/science.1142614.

(118) Martens, S.; McMahon, H. T. *C2 Domains and Membrane Fusion*; 2011; Vol. 68. https://doi.org/10.1016/B978-0-12-385891-7.00006-4.

(119) Martens, S. Role of C2 Domain Proteins during Synaptic Vesicle Exocytosis. *Biochem Soc Trans* **2010**, *38* (1). https://doi.org/10.1042/BST0380213.

(120) MacLauchlan, S.; Skokos, E. A.; Meznarich, N.; Zhu, D. H.; Raoof, S.; Shipley, J. M.; Senior, R. M.; Bornstein, P.; Kyriakides, T. R. Macrophage Fusion, Giant Cell Formation, and the Foreign Body Response Require Matrix Metalloproteinase 9. *J Leukoc Biol* **2009**, *85* (4). https://doi.org/10.1189/jlb.1008588.

(121) Vignery, A. Osteoclasts and Giant Cells: Macrophage-Macrophage Fusion Mechanism. *International Journal of Experimental Pathology*. 2000. https://doi.org/10.1046/j.1365-2613.2000.00164.x.

(122) Melloy, P.; Shen, S.; White, E.; McIntosh, J. R.; Rose, M. D. Nuclear Fusion during Yeast Mating Occurs by a Three-Step Pathway. *Journal of Cell Biology* **2007**, *179* (4). https://doi.org/10.1083/jcb.200706151.

(123) Hall, A. E.; Rose, M. D. Cell Fusion in Yeast Is Negatively Regulated by Components of the Cell Wall Integrity Pathway. *Mol Biol Cell* **2019**, *30* (4). https://doi.org/10.1091/mbc.E18-04-0236.

(124) Sieber, B.; Coronas-Serna, J. M.; Martin, S. G. A Focus on Yeast Mating: From Pheromone Signaling to Cell-Cell Fusion. *Seminars in Cell and Developmental Biology*. 2023. https://doi.org/10.1016/j.semcdb.2022.02.003.

(125) Renaud, S. J.; Jeyarajah, M. J. How Trophoblasts Fuse: An in-Depth Look into Placental Syncytiotrophoblast Formation. *Cellular and Molecular Life Sciences*. 2022. https://doi.org/10.1007/s00018-022-04475-z.

(126) White, J. M.; Whittaker, G. R. Fusion of Enveloped Viruses in Endosomes. *Traffic*. 2016. https://doi.org/10.1111/tra.12389.

(127) Halldorsson, S.; Li, S.; Li, M.; Harlos, K.; Bowden, T. A.; Huiskonen, J. T. Shielding and Activation of a Viral Membrane Fusion Protein. *Nat Commun* **2018**, *9* (1). https://doi.org/10.1038/s41467-017-02789-2.

(128) Sriwilaijaroen, N.; Suzuki, Y. Molecular Basis of the Structure and Function of H1 Hemagglutinin of Influenza Virus. *Proceedings of the Japan Academy Series B: Physical and Biological Sciences*. 2012. https://doi.org/10.2183/pjab.88.226.

(129) Pabis, A.; Rawle, R. J.; Kasson, P. M. Influenza Hemagglutinin Drives Viral Entry via Two Sequential Intramembrane Mechanisms. *Proc Natl Acad Sci U S A* **2020**, *117* (13). https://doi.org/10.1073/pnas.1914188117.

(130) Borisevich, S. S.; Zarubaev, V. V.; Shcherbakov, D. N.; Yarovaya, O. I.; Salakhutdinov, N. F. Molecular Modeling of Viral Type I Fusion Proteins: Inhibitors of Influenza Virus Hemagglutinin and the Spike Protein of Coronavirus. *Viruses*. 2023. https://doi.org/10.3390/v15040902.

(131) Zierath, J. R.; Lendahl, U. Scientific Background: Machinery Regulating Vesicle Traffic, A Major Transport System in Our Cells. *Nobelförsamlingen. The Nobel Assembly at Karolinska Institutet* **2013**, *14* (4).

(132) Knothe Tate, M. L. Top down and Bottom up Engineering of Bone. *J Biomech* **2011**, *44* (2). https://doi.org/10.1016/j.jbiomech.2010.10.019.

(133) Connon, C. J. Approaches to Corneal Tissue Engineering: Top-down or Bottom-Up? In *Procedia Engineering*; 2015; Vol. 110. https://doi.org/10.1016/j.proeng.2015.07.004.

(134) Weisenberger, M. S.; Deans, T. L. Bottom-up Approaches in Synthetic Biology and Biomaterials for Tissue Engineering Applications. *Journal of Industrial Microbiology and Biotechnology*. 2018. https://doi.org/10.1007/s10295-018-2027-3.

(135) Galle, J.; Hoffmann, M.; Aust, G. From Single Cells to Tissue Architecture-a Bottom-up Approach to Modelling the Spatio-Temporal Organisation of Complex Multi-Cellular Systems. *J Math Biol* **2009**, *58* (1–2). https://doi.org/10.1007/s00285-008-0172-4.

(136) Bausch, A. R.; Kroy, K. A Bottom-up Approach to Cell Mechanics. *Nat Phys* **2006**, *2* (4). https://doi.org/10.1038/nphys260.

(137) Simpson, M. L. Cell-Free Synthetic Biology: A Bottom-up Approach to Discovery by Design. *Molecular Systems Biology*. 2006. https://doi.org/10.1038/msb4100104.

(138) Fletcher, D. A.; Mullins, R. D. Cell Mechanics and the Cytoskeleton. *Nature*. 2010. https://doi.org/10.1038/nature08908.

(139) Halbleib, J. M.; Nelson, W. J. Cadherins in Development: Cell Adhesion, Sorting, and Tissue Morphogenesis. *Genes and Development*. 2006. https://doi.org/10.1101/gad.1486806.

(140) Ganzinger, K. A.; Schwille, P. More from Less – Bottom-up Reconstitution of Cell Biology. *Journal of Cell Science*. 2019. https://doi.org/10.1242/jcs.227488.

(141) Lopes dos Santos, R.; Campillo, C. Studying Actin-Induced Cell Shape Changes Using Giant Unilamellar Vesicles and Reconstituted Actin Networks. *Biochemical Society Transactions*. 2022. https://doi.org/10.1042/BST20220900.

(142) Liu, A. P.; Richmond, D. L.; Maibaum, L.; Pronk, S.; Geissler, P. L.; Fletcher, D. A. Membrane-Induced Bundling of Actinfilaments. *Nat Phys* **2008**, *4* (10). https://doi.org/10.1038/nphys1071.

(143) Dürre, K.; Keber, F. C.; Bleicher, P.; Brauns, F.; Cyron, C. J.; Faix, J.; Bausch, A. R. Capping Protein-Controlled Actin Polymerization Shapes Lipid Membranes. *Nat Commun* **2018**, *9* (1). https://doi.org/10.1038/s41467-018-03918-1.

(144) Matsuoka, K.; Orci, L.; Amherdt, M.; Bednarek, S. Y.; Hamamoto, S.; Schekman, R.; Yeung, T. COPII-Coated Vesicle Formation Reconstituted with Purified Coat Proteins and Chemically Defined Liposomes. *Cell* **1998**, *93* (2). https://doi.org/10.1016/S0092-8674(00)81577-9.

(145) Lee, M. C. S.; Orci, L.; Hamamoto, S.; Futai, E.; Ravazzola, M.; Schekman, R. Sar1p N-Terminal Helix Initiates Membrane Curvature and Completes the Fission of a COPII Vesicle. *Cell* **2005**, *122* (4). https://doi.org/10.1016/j.cell.2005.07.025.

(146) Sorre, B.; Callan-Jones, A.; Manzi, J.; Goud, B.; Prost, J.; Bassereau, P.; Roux, A. Nature of Curvature Coupling of Amphiphysin with Membranes Depends on Its Bound Density. *Proc Natl Acad Sci U S A* **2012**, *109* (1). https://doi.org/10.1073/pnas.1103594108.

(147) Pokorny, D.; Truebestein, L.; Fleming, K. D.; Burke, J. E.; Leonard, T. A. In Vitro Reconstitution of Sgk3 Activation by Phosphatidylinositol 3-Phosphate. *Journal of Biological Chemistry* **2021**, *297* (2). https://doi.org/10.1016/j.jbc.2021.100919.

(148) Fujii, H.; Chinnusamy, V.; Rodrigues, A.; Rubio, S.; Park, S.; Cutler, S. R.; Sheen, J.; Rodriguez, P. L. In Vitro Reconstitution of an ABA Signaling Pathway. *Nature* **2010**, *462* (7273).

(149) Fujii, H.; Chinnusamy, V.; Rodrigues, A.; Rubio, S.; Antoni, R.; Park, S. Y.; Cutler, S. R.; Sheen, J.; Rodriguez, P. L.; Zhu, J. K. In Vitro Reconstitution of an Abscisic Acid Signalling Pathway. *Nature* **2009**, *462* (7273). https://doi.org/10.1038/nature08599.

(150) Su, X.; Ditlev, J. A.; Rosen, M. K.; Vale, R. D. Reconstitution of TCR Signaling Using Supported Lipid Bilayers. In *Methods in Molecular Biology*; 2017; Vol. 1584. https://doi.org/10.1007/978-1-4939-6881-7_5.

(151) Varma, R.; Campi, G.; Yokosuka, T.; Saito, T.; Dustin, M. L. T Cell Receptor-Proximal Signals Are Sustained in Peripheral Microclusters and Terminated in the Central Supramolecular Activation Cluster. *Immunity* **2006**, *25* (1). https://doi.org/10.1016/j.immuni.2006.04.010.

(152) Yokosuka, T.; Sakata-Sogawa, K.; Kobayashi, W.; Hiroshima, M.; Hashimoto-Tane, A.; Tokunaga, M.; Dustin, M. L.; Saito, T. Newly Generated T Cell Receptor Microclusters Initiate and Sustain T Cell Activation by Recruitment of Zap70 and SLP-76. *Nat Immunol* **2005**, *6* (12). https://doi.org/10.1038/ni1272.

(153) Mossman, K. D.; Campi, G.; Groves, J. T.; Dustin, M. L. Immunology: Altered TCR Signaling from Geometrically Repatterned Immunological Synapses. *Science (1979)* **2005**, *310* (5751). https://doi.org/10.1126/science.1119238.

(154) Chang, V. T.; Fernandes, R. A.; Ganzinger, K. A.; Lee, S. F.; Siebold, C.; McColl, J.; Jönsson, P.; Palayret, M.; Harlos, K.; Coles, C. H.; Jones, E. Y.; Lui, Y.; Huang, E.; Gilbert, R. J. C.; Klenerman, D.; Aricescu, A. R.; Davis, S. J. Initiation of T Cell Signaling by CD45 Segregation at "Close Contacts." *Nat Immunol* **2016**, *17* (5). https://doi.org/10.1038/ni.3392.

(155) Mukhopadhyay, H.; De Wet, B.; Clemens, L.; Maini, P. K.; Allard, J.; Van Der Merwe, P. A.; Dushek, O. Multisite Phosphorylation Modulates the T Cell Receptor ζ-Chain Potency but Not the Switchlike Response. *Biophys J* **2016**, *110* (8). https://doi.org/10.1016/j.bpj.2016.03.024.

(156) Rohrs, J. A.; Zheng, D.; Graham, N. A.; Wang, P.; Finley, S. D. Computational Model of Chimeric Antigen Receptors Explains Site-Specific Phosphorylation Kinetics. *Biophys J* **2018**, *115* (6). https://doi.org/10.1016/j.bpj.2018.08.018.

(157) Payne, S.; Li, B.; Cao, Y.; Schaeffer, D.; Ryser, M. D.; You, L. Temporal Control of Self-Organized Pattern Formation without Morphogen Gradients in Bacteria. *Mol Syst Biol* **2013**, *9* (1). https://doi.org/10.1038/msb.2013.55.

(158) Haswell, E. S.; Phillips, R.; Rees, D. C. Mechanosensitive Channels: What Can They Do and How Do They Do It? *Structure*. 2011. https://doi.org/10.1016/j.str.2011.09.005.

(159) Rasmussen, T. How Do Mechanosensitive Channels Sense Membrane Tension? *Biochem Soc Trans* **2016**, *44* (4). https://doi.org/10.1042/BST20160018.

(160) Bootha, I. R.; Blount, P. The MscS and MscL Families of Mechanosensitive Channels Act as Microbial Emergency Release Valves. *Journal of Bacteriology*. 2012. https://doi.org/10.1128/JB.00576-12.

(161) Levina, N.; Tötemeyer, S.; Stokes, N. R.; Louis, P.; Jones, M. A.; Booth, I. R. Protection of Escherichia Coli Cells against Extreme Turgor by Activation of MscS and MscL Mechanosensitive Channels: Identification of Genes Required for MscS Activity. *EMBO Journal* **1999**, *18* (7). https://doi.org/10.1093/emboj/18.7.1730.

(162) Perozo, E.; Cortes, D. M.; Sompornpisut, P.; Kloda, A.; Martinac, B. Open Channel Structure of MscL and the Gating Mechanism of Mechanosensitive Channels. *Nature* **2002**, *418* (6901). https://doi.org/10.1038/nature00992.

(163) O'Hagan, R.; Chalfie, M.; Goodman, M. B. The MEC-4 DEG/ENaC Channel of Caenorhabditis Elegans Touch Receptor Neurons Transduces Mechanical Signals. *Nat Neurosci* **2005**, *8* (1). https://doi.org/10.1038/nn1362.

(164) Liedtke, W.; Friedman, J. M. Abnormal Osmotic Regulation in Trpv4-/- Mice. *Proc Natl Acad Sci U S A* **2003**, *100* (23). https://doi.org/10.1073/pnas.1735416100.

(165) Garry, A.; Fromy, B.; Blondeau, N.; Henrion, D.; Brau, F.; Gounon, P.; Guy, N.; Heurteaux, C.; Lazdunski, M.; Saumet, J. L. Altered Acetylcholine, Bradykinin and Cutaneous Pressure-Induced Vasodilation in Mice Lacking the TREK1 Potassium

Channel: The Endothelial Link. *EMBO Rep* **2007**, *8* (4). https://doi.org/10.1038/sj.embor.7400916.

(166) Lolicato, M.; Riegelhaupt, P. M.; Arrigoni, C.; Clark, K. A.; Minor, D. L. Transmembrane Helix Straightening and Buckling Underlies Activation of Mechanosensitive and Thermosensitive K2P Channels. *Neuron* **2014**, *84* (6). https://doi.org/10.1016/j.neuron.2014.11.017.

(167) Mathie, A.; Veale, E. L. Two-Pore Domain Potassium Channels: Potential Therapeutic Targets for the Treatment of Pain. *Pflugers Archiv European Journal of Physiology*. 2015. https://doi.org/10.1007/s00424-014-1655-3.

(168) Oh, S. J.; Lee, J. M.; Kim, H. B.; Lee, J.; Han, S.; Bae, J. Y.; Hong, G. S.; Koh, W.; Kwon, J.; Hwang, E. S.; Woo, D. H.; Youn, I.; Cho, I. J.; Bae, Y. C.; Lee, S.; Shim, J. W.; Park, J. H.; Lee, C. J. Ultrasonic Neuromodulation via Astrocytic TRPA1. *Current Biology* **2019**, *29* (20). https://doi.org/10.1016/j.cub.2019.08.021.

(169) Albuisson, J.; Murthy, S. E.; Bandell, M.; Coste, B.; Louis-Dit-Picard, H.; Mathur, J.; Fénéant-Thibault, M.; Tertian, G.; De Jaureguiberry, J. P.; Syfuss, P. Y.; Cahalan, S.; Garçon, L.; Toutain, F.; Simon Rohrlich, P.; Delaunay, J.; Picard, V.; Jeunemaitre, X.; Patapoutian, A. Dehydrated Hereditary Stomatocytosis Linked to Gain-of-Function Mutations in Mechanically Activated PIEZO1 Ion Channels. *Nat Commun* **2013**, *4*. https://doi.org/10.1038/ncomms2899.

(170) Nikolaev, Y. A.; Dosen, P. J.; Laver, D. R.; Van Helden, D. F.; Hamill, O. P. Single Mechanically-Gated Cation Channel Currents Can Trigger Action Potentials in Neocortical and Hippocampal Pyramidal Neurons. *Brain Res* **2015**, *1608*. https://doi.org/10.1016/j.brainres.2015.02.051.

(171) Zhang, X.; Wang, J.; Feng, Y.; Ge, J.; Li, W.; Sun, W.; Iscla, I.; Yu, J.; Blount, P.; Li, Y.; Yang, M. Structure and Molecular Mechanism of an Anion-Selective Mechanosensitive Channel of Small Conductance. *Proc Natl Acad Sci U S A* **2012**, *109* (44). https://doi.org/10.1073/pnas.1207977109.

(172) Edwards, M. D.; Bartlett, W.; Booth, I. R. Pore Mutations of the Escherichia Coli MscS Channel Affect Desensitization but Not Ionic Preference. *Biophys J* **2008**, *94* (8). https://doi.org/10.1529/biophysj.107.123448.

(173) Gamini, R.; Sotomayor, M.; Chipot, C.; Schulten, K. Cytoplasmic Domain Filter Function in the Mechanosensitive Channel of Small Conductance. *Biophys J* **2011**, *101* (1). https://doi.org/10.1016/j.bpj.2011.05.042.

(174) Bass, R. B.; Strop, P.; Barclay, M.; Rees, D. C. Crystal Structure of Escherichia Coli MscS, a Voltage-Modulated and Mechanosensitive Channel. *Science (1979)* **2002**, *298* (5598). https://doi.org/10.1126/science.1077945.

(175) Nomura, T.; Sokabe, M.; Yoshimura, K. Interaction between the Cytoplasmic and Transmembrane Domains of the Mechanosensitive Channel MscS. *Biophys J* **2008**, *94* (5). https://doi.org/10.1529/biophysj.107.114785.

(176) Cox, C. D.; Nomura, T.; Ziegler, C. S.; Campbell, A. K.; Wann, K. T.; Martinac, B. Selectivity Mechanism of the Mechanosensitive Channel MscS Revealed by Probing Channel Subconducting States. *Nat Commun* **2013**, *4*. https://doi.org/10.1038/ncomms3137.

(177) Price, C. E.; Kocer, A.; Kol, S.; Van Der Berg, J. P.; Driessen, A. J. M. In Vitro Synthesis and Oligomerization of the Mechanosensitive Channel of Large Conductance, MscL, into

a Functional Ion Channel. *FEBS Lett* **2011**, *585* (1). https://doi.org/10.1016/j.febslet.2010.11.057.

(178) Berrier, C.; Guilvout, I.; Bayan, N.; Park, K. H.; Mesneau, A.; Chami, M.; Pugsley, A. P.; Ghazi, A. Coupled Cell-Free Synthesis and Lipid Vesicle Insertion of a Functional Oligomeric Channel MscL: MscL Does Not Need the Insertase YidC for Insertion in Vitro. *Biochim Biophys Acta Biomembr* **2011**, *1808* (1). https://doi.org/10.1016/j.bbamem.2010.09.018.

(179) Blain, J. C.; Szostak, J. W. Progress toward Synthetic Cells. *Annual Review of Biochemistry*. 2014. https://doi.org/10.1146/annurev-biochem-080411-124036.

(180) Gaut, N. J.; Adamala, K. P. Reconstituting Natural Cell Elements in Synthetic Cells. *Advanced Biology*. 2021. https://doi.org/10.1002/adbi.202000188.

(181) Goers, R.; Thoma, J.; Ritzmann, N.; Di Silvestro, A.; Alter, C.; Gunkel-Grabole, G.; Fotiadis, D.; Müller, D. J.; Meier, W. Optimized Reconstitution of Membrane Proteins into Synthetic Membranes. *Commun Chem* **2018**, *1* (1). https://doi.org/10.1038/s42004-018-0037-8.

(182) Majumder, S.; Garamella, J.; Wang, Y. L.; Denies, M.; Noireaux, V.; Liu, A. P. Cell-Sized Mechanosensitive and Biosensing Compartment Programmed with DNA. *Chemical Communications* **2017**. https://doi.org/10.1039/c7cc03455e.

(183) Wilson, D. W.; Whiteheart, S. W.; Orci, L.; Rothman, J. E. Intracellular Membrane Fusion. *Trends Biochem Sci* **1991**, *16* (C). https://doi.org/10.1016/0968-0004(91)90138-L.

(184) Weissenhorn, W.; Hinz, A.; Gaudin, Y. Virus Membrane Fusion. *FEBS Letters*. 2007. https://doi.org/10.1016/j.febslet.2007.01.093.

(185) Hutagalung, A. H.; Novick, P. J. Role of Rab GTPases in Membrane Traffic and Cell Physiology. *Physiological Reviews*. 2011. https://doi.org/10.1152/physrev.00059.2009.

(186) Ungermann, C.; Kümmel, D. Structure of Membrane Tethers and Their Role in Fusion. *Traffic*. 2019. https://doi.org/10.1111/tra.12655.

(187) Homma, Y.; Hiragi, S.; Fukuda, M. Rab Family of Small GTPases: An Updated View on Their Regulation and Functions. *FEBS Journal*. 2021. https://doi.org/10.1111/febs.15453.

(188) Duman, J. G.; Forte, J. G. What Is the Role of SNARE Proteins in Membrane Fusion? *American Journal of Physiology - Cell Physiology*. 2003. https://doi.org/10.1152/ajpcell.00091.2003.

(189) Wickner, W.; Schekman, R. Membrane Fusion. *Nature Structural and Molecular Biology*. 2008. https://doi.org/10.1038/nsmb.1451.

(190) Yoon, T. Y.; Munson, M. SNARE Complex Assembly and Disassembly. *Current Biology*. 2018. https://doi.org/10.1016/j.cub.2018.01.005.

(191) Gaisano, H. Y. Recent New Insights into the Role of SNARE and Associated Proteins in Insulin Granule Exocytosis. *Diabetes, Obesity and Metabolism*. 2017. https://doi.org/10.1111/dom.13001.

(192) Urbina, F. L.; Gupton, S. L. SNARE-Mediated Exocytosis in Neuronal Development. *Frontiers in Molecular Neuroscience*. 2020. https://doi.org/10.3389/fnmol.2020.00133.

(193) Brunger, A. T.; Cipriano, D. J.; Diao, J. Towards Reconstitution of Membrane Fusion Mediated by SNAREs and Other Synaptic Proteins. *Critical Reviews in Biochemistry and Molecular Biology*. 2015. https://doi.org/10.3109/10409238.2015.1023252.

(194) Kiessling, V.; Liang, B.; Tamm, L. K. Reconstituting SNARE-Mediated Membrane Fusion at the Single Liposome Level. *Methods Cell Biol* **2015**, *128*. https://doi.org/10.1016/bs.mcb.2015.02.005.

(195) Weber, T.; Zemelman, B. V.; McNew, J. A.; Westermann, B.; Gmachl, M.; Parlati, F.; Söllner, T. H.; Rothman, J. E. SNAREpins: Minimal Machinery for Membrane Fusion. *Cell* **1998**, *92* (6). https://doi.org/10.1016/S0092-8674(00)81404-X.

(196) Hay, J. C. Calcium: A Fundamental Regulator of Intracellular Membrane Fusion? *EMBO Reports*. 2007. https://doi.org/10.1038/sj.embor.7400921.

(197) Yoon, T. Y.; Lu, X.; Diao, J.; Lee, S. M.; Ha, T.; Shin, Y. K. Complexin and Ca2+ Stimulate SNARE-Mediated Membrane Fusion. *Nat Struct Mol Biol* **2008**, *15* (7). https://doi.org/10.1038/nsmb.1446.

(198) Tucker, W. C.; Weber, T.; Chapman, E. R. Reconstitution of Ca2+-Regulated Membrane Fusion by Synaptotagmin and SNAREs. *Science (1979)* **2004**, *304* (5669). https://doi.org/10.1126/science.1097196.

(199) Chen, Z.; Wang, J.; Sun, W.; Archibong, E.; Kahkoska, A. R.; Zhang, X.; Lu, Y.; Ligler, F. S.; Buse, J. B.; Gu, Z. Synthetic Beta Cells for Fusion-Mediated Dynamic Insulin Secretion. *Nat Chem Biol* **2018**, *14* (1). https://doi.org/10.1038/nchembio.2511.

(200) Kumar, P.; Sharma, S. M. An Overview of Purification Methods for Proteins. *Ijar* **2015**, *1* (12).

(201) Walls, D.; Walker, J. M. Protein Chromatography. *Protein Chromatography* **2017**, *1485*. https://doi.org/10.1007/978-1-4939-6412-3.

(202) Kar, U. K.; Simonian, M.; Whitelegge, J. P. Integral Membrane Proteins: Bottom-up, Top-down and Structural Proteomics. *Expert Review of Proteomics*. 2017. https://doi.org/10.1080/14789450.2017.1359545.

(203) Orwick-Rydmark, M.; Arnold, T.; Linke, D. The Use of Detergents to Purify Membrane Proteins. *Curr Protoc Protein Sci* **2016**, *2016*. https://doi.org/10.1002/0471140864.ps0408s84.

(204) Seddon, A. M.; Curnow, P.; Booth, P. J. Membrane Proteins, Lipids and Detergents: Not Just a Soap Opera. *Biochimica et Biophysica Acta - Biomembranes*. 2004. https://doi.org/10.1016/j.bbamem.2004.04.011.

(205) Le Maire, M.; Champeil, P.; Møller, J. V. Interaction of Membrane Proteins and Lipids with Solubilizing Detergents. *Biochimica et Biophysica Acta - Biomembranes*. 2000. https://doi.org/10.1016/S0304-4157(00)00010-1.

(206) Asenjo, J. A.; Andrews, B. A. Protein Purification Using Chromatography: Selection of Type, Modelling and Optimization of Operating Conditions. *Journal of Molecular Recognition* **2009**, *22* (2). https://doi.org/10.1002/jmr.898.

(207) Palanirajan, S. K.; Govindasamy, P.; Gummadi, S. N. Polystyrene Adsorbents: Rapid and Efficient Surrogate for Dialysis in Membrane Protein Purification. *Sci Rep* **2020**, *10* (1). https://doi.org/10.1038/s41598-020-73522-1.

(208) Wingfield, P. T. Overview of the Purification of Recombinant Proteins. *Curr Protoc Protein Sci* **2015**, *80* (1). https://doi.org/10.1002/0471140864.ps0601s80.

(209) Mancia, F.; Love, J. High-Throughput Expression and Purification of Membrane Proteins. *J Struct Biol* **2010**, *172* (1). https://doi.org/10.1016/j.jsb.2010.03.021.

(210) Janson, J. C. *Protein Purification: Principles, High Resolution Methods, and Applications: Third Edition*; 2011. https://doi.org/10.1002/9780470939932.

(211) Shimizu, Y.; Inoue, A.; Tomari, Y.; Suzuki, T.; Yokogawa, T.; Nishikawa, K.; Ueda, T. Cell-Free Translation Reconstituted with Purified Components. *Nat Biotechnol* **2001**. https://doi.org/10.1038/90802.

(212) Noireaux, V.; Liu, A. P. The New Age of Cell-Free Biology. *Annual Review of Biomedical Engineering*. 2020, pp 51–77. https://doi.org/10.1146/annurev-bioeng-092019-111110.

(213) Lu, Y. Cell-Free Synthetic Biology: Engineering in an Open World. *Synthetic and Systems Biotechnology*. 2017. https://doi.org/10.1016/j.synbio.2017.02.003.

(214) Brookwell, A.; Oza, J. P.; Caschera, F. Biotechnology Applications of Cell-Free Expression Systems. *Life*. 2021. https://doi.org/10.3390/life11121367.

(215) Swartz, J. Developing Cell-Free Biology for Industrial Applications. In *Journal of Industrial Microbiology and Biotechnology*; 2006; Vol. 33. https://doi.org/10.1007/s10295-006-0127-y.

(216) Kigawa, T.; Yabuki, T.; Matsuda, N.; Matsuda, T.; Nakajima, R.; Tanaka, A.; Yokoyama, S. Preparation of Escherichia Coli Cell Extract for Highly Productive Cell-Free Protein Expression. *J Struct Funct Genomics* **2004**, *5* (1–2). https://doi.org/10.1023/B:JSFG.0000029204.57846.7d.

(217) Dondapati, S. K.; Kreir, M.; Quast, R. B.; Wüstenhagen, D. A.; Brüggemann, A.; Fertig, N.; Kubick, S. Membrane Assembly of the Functional KcsA Potassium Channel in a Vesicle-Based Eukaryotic Cell-Free Translation System. *Biosens Bioelectron* **2014**, *59*. https://doi.org/10.1016/j.bios.2014.03.004.

(218) Takai, K.; Sawasaki, T.; Endo, Y. Practical Cell-Free Protein Synthesis System Using Purified Wheat Embryos. *Nat Protoc* **2010**, *5* (2). https://doi.org/10.1038/nprot.2009.207.

(219) Madin, K.; Sawasaki, T.; Ogasawara, T.; Endo, Y. A Highly Efficient and Robust Cell-Free Protein Synthesis System Prepared from Wheat Embryos: Plants Apparently Contain a Suicide System Directed at Ribosomes. *Proc Natl Acad Sci U S A* **2000**, *97* (2). https://doi.org/10.1073/pnas.97.2.559.

(220) Tarui, H.; Murata, M.; Tani, I.; Imanishi, S.; Nishikawa, S.; Hara, T. Establishment and Characterization of Cell-Free Translation/Glycosylation in Insect Cell (Spodoptera Frugiperda 21) Extract Prepared with High Pressure Treatment. *Appl Microbiol Biotechnol* **2001**, *55* (4). https://doi.org/10.1007/s002530000534.

(221) Hancock, J. F. Reticulocyte Lysate Assay for in Vitro Translation and Posttranslational Modification of Ras Proteins. *Methods Enzymol* **1995**, *255* (C). https://doi.org/10.1016/S0076-6879(95)55009-7.

(222) Suzuki, T.; Ito, M.; Ezure, T.; Shikata, M.; Ando, E.; Utsumi, T.; Tsunasawa, S.; Nishimura, O. Protein Prenylation in an Insect Cell-Free Protein Synthesis System and Identification of Products by Mass Spectrometry. *Proteomics* **2007**, *7* (12). https://doi.org/10.1002/pmic.200700237.

(223) Suzuki, T.; Ito, M.; Ezure, T.; Shikata, M.; Ando, E.; Utsumi, T.; Tsunasawa, S.; Nishimura, O. N-Terminal Protein Modifications in an Insect Cell-Free Protein Synthesis System and Their Identification by Mass Spectrometry. *Proteomics* **2006**, *6* (16). https://doi.org/10.1002/pmic.200600126.

(224) Safer, B.; Jagus, R. Control of EIF-2 Phosphatase Activity in Rabbit Reticulocyte Lysate. *Proc Natl Acad Sci U S A* **1979**, *76* (3). https://doi.org/10.1073/pnas.76.3.1094.

(225) Suzuki, T.; Ezure, T.; Ando, E.; Nishimura, O.; Utsumi, T.; Tsunasawa, S. Preparation of Ubiquitin-Conjugated Proteins Using an Insect Cell-Free Protein Synthesis System. *J Biotechnol* **2010**, *145* (1). https://doi.org/10.1016/j.jbiotec.2009.10.009.

(226) Shields, D.; Blobel, G. Efficient Cleavage and Segregation of Nascent Presecretory Proteins in a Reticulocyte Lysate Supplemented with Microsomal Membranes. *Journal of Biological Chemistry* **1978**, *253* (11). https://doi.org/10.1016/s0021-9258(17)34748-8.

(227) Iizuka, N.; Najita, L.; Franzusoff, A.; Sarnow, P. Cap-Dependent and Cap-Independent Translation by Internal Initiation of MRNAs in Cell Extracts Prepared from Saccharomyces Cerevisiae. *Mol Cell Biol* **1994**, *14* (11). https://doi.org/10.1128/mcb.14.11.7322.

(228) Wang, X.; Liu, J.; Zheng, Y.; Li, J.; Wang, H.; Zhou, Y.; Qi, M.; Yu, H.; Tang, W.; Zhao, W. M. An Optimized Yeast Cell-Free System: Sufficient for Translation of Human Papillomavirus 58 L1 MRNA and Assembly of Virus-like Particles. *J Biosci Bioeng* **2008**, *106* (1). https://doi.org/10.1263/jbb.106.8.

(229) Brödel, A. K.; Kubick, S. Developing Cell-Free Protein Synthesis Systems: A Focus on Mammalian Cells. *Pharm Bioprocess* **2014**, *2* (4). https://doi.org/10.4155/pbp.14.30.

(230) Brödel, A. K.; Wüstenhagen, D. A.; Kubick, S. Cell-Free Protein Synthesis Systems Derived from Cultured Mammalian Cells. In *Structural Proteomics: High-Throughput Methods: Second Edition*; 2014; pp 129–140. https://doi.org/10.1007/978-1-4939-2230-7_7.

(231) Heide, C.; Buldum, G.; Moya-Ramirez, I.; Ces, O.; Kontoravdi, C.; Polizzi, K. M. Design, Development and Optimization of a Functional Mammalian Cell-Free Protein Synthesis Platform. *Front Bioeng Biotechnol* **2021**, *8*. https://doi.org/10.3389/fbioe.2020.604091.

(232) Moghimianavval, H.; Hsu, Y. Y.; Groaz, A.; Liu, A. P. In Vitro Reconstitution Platforms of Mammalian Cell-Free Expressed Membrane Proteins. In *Methods in Molecular Biology*; 2022; Vol. 2433. https://doi.org/10.1007/978-1-0716-1998-8_6.

(233) Majumder, S.; Hsu, Y. Y.; Moghimianavval, H.; Andreas, M.; Giessen, T. W.; Luxton, G. W. G.; Liu, A. P. In Vitro Synthesis and Reconstitution Using Mammalian Cell-Free Lysates Enables the Systematic Study of the Regulation of LINC Complex Assembly. *Biochemistry* **2022**, *61* (14). https://doi.org/10.1021/acs.biochem.2c00118.

(234) Lu, Y. Cell-Free Synthetic Biology: Engineering in an Open World. *Synth Syst Biotechnol* **2017**, *2* (1). https://doi.org/10.1016/j.synbio.2017.02.003.

(235) Cho, E.; Lu, Y. Compartmentalizing Cell-Free Systems: Toward Creating Life-like Artificial Cells and Beyond. *ACS Synthetic Biology*. 2020. https://doi.org/10.1021/acssynbio.0c00433.

(236) Zhu, Y.; Guo, X.; Liu, J.; Li, F.; Yang, D. Emerging Advances of Cell-Free Systems toward Artificial Cells. *Small Methods*. 2020. https://doi.org/10.1002/smtd.202000406.

(237) Shin, J.; Noireaux, V. An E. Coli Cell-Free Expression Toolbox: Application to Synthetic Gene Circuits and Artificial Cells. *ACS Synth Biol* **2012**, *1* (1). https://doi.org/10.1021/sb200016s.

(238) Yoshida, A.; Kohyama, S.; Fujiwara, K.; Nishikawa, S.; Doi, N. Regulation of Spatiotemporal Patterning in Artificial Cells by a Defined Protein Expression System. *Chem Sci* **2019**, *10* (48). https://doi.org/10.1039/c9sc02441g.

(239) Yue, K.; Li, Y.; Cao, M.; Shen, L.; Gu, J.; Kai, L. Bottom-Up Synthetic Biology Using Cell-Free Protein Synthesis. In *Advances in Biochemical Engineering/Biotechnology*; 2023; Vol. 185. https://doi.org/10.1007/10_2023_232.

(240) Scott, A.; Noga, M. J.; De Graaf, P.; Westerlaken, I.; Yildirim, E.; Danelon, C. Cell-Free Phospholipid Biosynthesis by Gene-Encoded Enzymes Reconstituted in Liposomes. *PLoS One* **2016**, *11* (10). https://doi.org/10.1371/journal.pone.0163058.

(241) Tabuchi, T.; Yokobayashi, Y. High-Throughput Screening of Cell-Free Riboswitches by Fluorescence-Activated Droplet Sorting. *Nucleic Acids Res* **2022**, *50* (6). https://doi.org/10.1093/nar/gkac152.

(242) Adamala, K. P.; Martin-Alarcon, D. A.; Guthrie-Honea, K. R.; Boyden, E. S. Engineering Genetic Circuit Interactions within and between Synthetic Minimal Cells. *Nat Chem* **2017**, *9* (5). https://doi.org/10.1038/nchem.2644.

(243) Li, J.; Haas, W.; Jackson, K.; Kuru, E.; Jewett, M. C.; Fan, Z. H.; Gygi, S.; Church, G. M. Cogenerating Synthetic Parts toward a Self-Replicating System. *ACS Synth Biol* **2017**, *6* (7). https://doi.org/10.1021/acssynbio.6b00342.

(244) Jewett, M. C.; Fritz, B. R.; Timmerman, L. E.; Church, G. M. In Vitro Integration of Ribosomal RNA Synthesis, Ribosome Assembly, and Translation. *Mol Syst Biol* **2013**, *9* (1). https://doi.org/10.1038/msb.2013.31.

(245) Van Nies, P.; Westerlaken, I.; Blanken, D.; Salas, M.; Mencía, M.; Danelon, C. Self-Replication of DNA by Its Encoded Proteins in Liposome-Based Synthetic Cells. *Nat Commun* **2018**, *9* (1). https://doi.org/10.1038/s41467-018-03926-1.

(246) Sun, Y.; Ma, X.; Zhou, D.; Vacek, I.; Sun, A. M. Normalization of Diabetes in Spontaneously Diabetic Cynomologus Monkeys by Xenografts of Microencapsulated Porcine Islets without Immunosuppression. *Journal of Clinical Investigation* **1996**, *98* (6). https://doi.org/10.1172/JCI118929.

(247) Calafiore, R.; Basta, G.; Luca, G.; Boselli, C.; Bufalari, A.; Bufalari, A.; Cassarani, M. P.; Giustozzi, G. M.; Brunetti, P. Transplantation of Pancreatic Islets Contained in Minimal Volume Microcapsules in Diabetic High Mammalians. In *Annals of the New York Academy of Sciences*; 1999; Vol. 875. https://doi.org/10.1111/j.1749-6632.1999.tb08506.x.

(248) De Vos, P.; Hamel, A. F.; Tatarkiewicz, K. Considerations for Successful Transplantation of Encapsulated Pancreatic Islets. In *Diabetologia*; 2002; Vol. 45. https://doi.org/10.1007/s00125-001-0729-x.

(249) Bloch, J.; Bachoud-Lévi, A. C.; Déglon, N.; Lefaucheur, J. P.; Winkel, L.; Palfi, S.; Nguyen, J. P.; Bourdet, C.; Gaura, V.; Remy, P.; Brugières, P.; Boisse, M. F.; Baudic, S.; Cesaro, P.; Hantraye, P.; Aebischer, P.; Peschanski, M. Neuroprotective Gene Therapy for Huntington's Disease, Using Polymer-Encapsulated Cells Engineered to Secrete Human Ciliary Neurotrophic Factor: Results of a Phase I Study. *Hum Gene Ther* **2004**, *15* (10). https://doi.org/10.1089/hum.2004.15.968.

(250) Basic, D.; Vacek, I.; Sun, A. M. Microencapsulation and Transplantation of Genetically Engineered Cells: A New Approach to Somatic Gene Therapy. *Artif Cells Blood Substit Immobil Biotechnol* **1996**, *24* (3). https://doi.org/10.3109/10731199609117437.

(251) Löhr, M.; Hoffmeyer, A.; Kröger, J. C.; Freund, M.; Hain, J.; Holle, A.; Karle, P.; Knöfel, W. T.; Liebe, S.; Müller, P.; Nizze, H.; Renner, M.; Saller, R. M.; Wagner, T.; Hauenstein, K.; Günzburg, W. H.; Salmons, B. Microencapsulated Cell-Mediated Treatment of Inoperable Pancreatic Carcinoma. *Lancet* **2001**, *357* (9268). https://doi.org/10.1016/S0140-6736(00)04749-8.

(252) Krinsky, N.; Kaduri, M.; Zinger, A.; Shainsky-Roitman, J.; Goldfeder, M.; Benhar, I.; Hershkovitz, D.; Schroeder, A. Synthetic Cells Synthesize Therapeutic Proteins inside Tumors. *Adv Healthc Mater* **2018**, *7* (9). https://doi.org/10.1002/adhm.201701163.

(253) Sachse, R.; Dondapati, S. K.; Fenz, S. F.; Schmidt, T.; Kubick, S. Membrane Protein Synthesis in Cell-Free Systems: From Bio-Mimetic Systems to Bio-Membranes. *FEBS Letters*. 2014. https://doi.org/10.1016/j.febslet.2014.06.007.

(254) Junge, F.; Haberstock, S.; Roos, C.; Stefer, S.; Proverbio, D.; Dötsch, V.; Bernhard, F. Advances in Cell-Free Protein Synthesis for the Functional and Structural Analysis of Membrane Proteins. *N Biotechnol* **2011**, *28* (3). https://doi.org/10.1016/j.nbt.2010.07.002.

(255) Majumder, S.; Willey, P. T.; DeNies, M. S.; Liu, A. P.; Luxton, G. A Synthetic Biology Platform for the Reconstitution and Mechanistic Dissection of LINC Complex Assembly. *J Cell Sci* **2019**, *132* (4). https://doi.org/10.1242/jcs.219451.

(256) Poddar, A.; Hsu, Y.-Y.; Zhang, F.; Shamma, A.; Kreais, Z.; Muller, C.; Malla, M.; Ray, A.; Liu, A.; Chen, Q. Membrane Stretching Activates Calcium Permeability of a Putative Channel Pkd2 during Fission Yeast Cytokinesis. *Mol Biol Cell* **2022**, *33* (14).

(257) Diz-Muñoz, A.; Fletcher, D. A.; Weiner, O. D. Use the Force: Membrane Tension as an Organizer of Cell Shape and Motility. *Trends in Cell Biology*. 2013, pp 47–53. https://doi.org/10.1016/j.tcb.2012.09.006.

(258) Masters, T. A.; Pontes, B.; Viasnoff, V.; Li, Y.; Gauthier, N. C. Plasma Membrane Tension Orchestrates Membrane Trafficking, Cytoskeletal Remodeling, and Biochemical Signaling during Phagocytosis. *Proc Natl Acad Sci U S A* **2013**, *110* (29). https://doi.org/10.1073/pnas.1301766110.

(259) Shi, Z.; Graber, Z. T.; Baumgart, T.; Stone, H. A.; Cohen, A. E. Cell Membranes Resist Flow. *Cell* **2018**, *175* (7). https://doi.org/10.1016/j.cell.2018.09.054.

(260) Gauthier, N. C.; Fardin, M. A.; Roca-Cusachs, P.; Sheetz, M. P. Temporary Increase in Plasma Membrane Tension Coordinates the Activation of Exocytosis and Contraction during Cell Spreading. *Proc Natl Acad Sci U S A* **2011**, *108* (35). https://doi.org/10.1073/pnas.1105845108.

(261) Joseph, J. G.; Liu, A. P. Mechanical Regulation of Endocytosis: New Insights and Recent Advances. *Adv Biosyst* **2020**, *4* (5), 1900278. https://doi.org/10.1002/adbi.201900278.

(262) Raucher, D.; Sheetz, M. P. Cell Spreading and Lamellipodial Extension Rate Is Regulated by Membrane Tension. *Journal of Cell Biology* **2000**, *148* (1). https://doi.org/10.1083/jcb.148.1.127.

(263) Houk, A. R.; Jilkine, A.; Mejean, C. O.; Boltyanskiy, R.; Dufresne, E. R.; Angenent, S. B.; Altschuler, S. J.; Wu, L. F.; Weiner, O. D. Membrane Tension Maintains Cell Polarity by Confining Signals to the Leading Edge during Neutrophil Migration. *Cell* **2012**, *148* (1–2). https://doi.org/10.1016/j.cell.2011.10.050.

(264) Nambiar, R.; McConnell, R. E.; Tyska, M. J. Control of Cell Membrane Tension by Myosin-I. *Proc Natl Acad Sci U S A* **2009**, *106* (29). https://doi.org/10.1073/pnas.0901641106.

(265) Patel, A.; Sharif-Naeini, R.; Folgering, J. R. H.; Bichet, D.; Duprat, F.; Honoré, E. Canonical TRP Channels and Mechanotransduction: From Physiology to Disease States. *Pflugers Archiv European Journal of Physiology*. 2010. https://doi.org/10.1007/s00424-010-0847-8.

(266) Ridone, P.; Vassalli, M.; Martinac, B. Piezo1 Mechanosensitive Channels: What Are They and Why Are They Important. *Biophysical Reviews*. 2019, pp 795–805. https://doi.org/10.1007/s12551-019-00584-5.

(267) Hochmuth, R. M. Micropipette Aspiration of Living Cells. *Journal of Biomechanics*. 2000. https://doi.org/10.1016/S0021-9290(99)00175-X.

(268) Nussenzveig, H. M. Cell Membrane Biophysics with Optical Tweezers. *European Biophysics Journal* **2018**, *47* (5). https://doi.org/10.1007/s00249-017-1268-9.

(269) Kirmizis, D.; Logothetidis, S. Atomic Force Microscopy Probing in the Measurement of Cell Mechanics. *International Journal of Nanomedicine*. 2010. https://doi.org/10.2147/ijn.s5787.

(270) Wang, Y.; Wang, N. FRET and Mechanobiology. *Integrative Biology*. 2009, pp 565–573. https://doi.org/10.1039/b913093b.

(271) Liu, L.; He, F.; Yu, Y.; Wang, Y. Application of FRET Biosensors in Mechanobiology and Mechanopharmacological Screening. *Frontiers in Bioengineering and Biotechnology*. 2020. https://doi.org/10.3389/fbioe.2020.595497.

(272) Cost, A. L.; Ringer, P.; Chrostek-Grashoff, A.; Grashoff, C. How to Measure Molecular Forces in Cells: A Guide to Evaluating Genetically-Encoded FRET-Based Tension Sensors. *Cell Mol Bioeng* **2015**, *8* (1). https://doi.org/10.1007/s12195-014-0368-1.

(273) Boyd, M. A.; Kamat, N. P. Visualizing Tension and Growth in Model Membranes Using Optical Dyes. *Biophys J* **2018**, *115* (7). https://doi.org/10.1016/j.bpj.2018.08.021.

(274) Colom, A.; Derivery, E.; Soleimanpour, S.; Tomba, C.; Molin, M. D.; Sakai, N.; González-Gaitán, M.; Matile, S.; Roux, A. A Fluorescent Membrane Tension Probe. *Nat Chem* **2018**, *10* (11). https://doi.org/10.1038/s41557-018-0127-3.

(275) Heureaux-Torres, J.; Luker, K. E.; Haley, H.; Pirone, M.; Lee, L. M.; Herrera, Y.; Luker, G. D.; Liu, A. P. The Effect of Mechanosensitive Channel MscL Expression in Cancer Cells on 3D Confined Migration. *APL Bioeng* **2018**, *2* (3). https://doi.org/10.1063/1.5019770.

(276) Fu, J.; Wang, Y. K.; Yang, M. T.; Desai, R. A.; Yu, X.; Liu, Z.; Chen, C. S. Mechanical Regulation of Cell Function with Geometrically Modulated Elastomeric Substrates. *Nat Methods* **2010**, *7* (9), 733–736. https://doi.org/10.1038/nmeth.1487.

(277) Rosholm, K. R.; Baker, M. A. B.; Ridone, P.; Nakayama, Y.; Rohde, P. R.; Cuello, L. G.; Lee, L. K.; Martinac, B. Activation of the Mechanosensitive Ion Channel MscL by Mechanical Stimulation of Supported Droplet-Hydrogel Bilayers. *Sci Rep* **2017**, *7*. https://doi.org/10.1038/srep45180.

(278) St-Pierre, F.; Marshall, J. D.; Yang, Y.; Gong, Y.; Schnitzer, M. J.; Lin, M. Z. High-Fidelity Optical Reporting of Neuronal Electrical Activity with an Ultrafast Fluorescent Voltage Sensor. *Nat Neurosci* **2014**, *17* (6). https://doi.org/10.1038/nn.3709.

(279) Hofherr, A.; Fakler, B.; Klöcker, N. Selective Golgi Export of Kir2.1 Controls the Stoichiometry of Functional Kir2.x Channel Heteromers. *J Cell Sci* **2005**, *118* (9), 1935–1943. https://doi.org/10.1242/jcs.02322.

(280) Soloperto, A.; Boccaccio, A.; Contestabile, A.; Moroni, M.; Hallinan, G. I.; Palazzolo, G.; Chad, J.; Deinhardt, K.; Carugo, D.; Difato, F. Mechano-Sensitization of Mammalian Neuronal Networks through Expression of the Bacterial Large-Conductance Mechanosensitive Ion Channel. *J Cell Sci* **2018**, *131* (5). https://doi.org/10.1242/jcs.210393.

(281) Heureaux, J.; Chen, D.; Murray, V. L.; Deng, C. X.; Liu, A. P. Activation of a Bacterial Mechanosensitive Channel in Mammalian Cells by Cytoskeletal Stress. *Cell Mol Bioeng* **2014**, *7* (3), 307–319. https://doi.org/10.1007/s12195-014-0337-8.

(282) Gonzalez, N. P.; Tao, J.; Rochman, N. D.; Vig, D.; Chiu, E.; Wirtz, D.; Sun, S. X. Cell Tension and Mechanical Regulation of Cell Volume. *Mol Biol Cell* **2018**, *29* (21). https://doi.org/10.1091/mbc.E18-04-0213.

(283) Liu, A. P.; Chaudhuri, O.; Parekh, S. H. New Advances in Probing Cell-Extracellular Matrix Interactions. *Integrative Biology (United Kingdom)*. 2017, pp 383–405. https://doi.org/10.1039/c6ib00251j.

(284) Yang, M. T.; Fu, J.; Wang, Y. K.; Desai, R. A.; Chen, C. S. Assaying Stem Cell Mechanobiology on Microfabricated Elastomeric Substrates with Geometrically Modulated Rigidity. *Nat Protoc* **2011**, *6* (2). https://doi.org/10.1038/nprot.2010.189.

(285) Pollard, T. D. Mechanics of Cytokinesis in Eukaryotes. *Current Opinion in Cell Biology*. 2010. https://doi.org/10.1016/j.ceb.2009.11.010.

(286) Srivastava, V.; Iglesias, P. A.; Robinson, D. N. Cytokinesis: Robust Cell Shape Regulation. *Seminars in Cell and Developmental Biology*. 2016. https://doi.org/10.1016/j.semcdb.2015.10.023.

(287) Straight, A. F.; Cheung, A.; Limouze, J.; Chen, I.; Westwood, N. J.; Sellers, J. R.; Mitchison, T. J. Dissecting Temporal and Spatial Control of Cytokinesis with a Myosin II Inhibitor. *Science (1979)* **2003**, *299* (5613). https://doi.org/10.1126/science.1081412.

(288) De Lozanne, A.; Spudich, J. A. Disruption of the Dictyostelium Myosin Heavy Chain Gene by Homologous Recombination. *Science (1979)* **1987**, *236* (4805). https://doi.org/10.1126/science.3576222.

(289) Sanger, J. M.; Sanger, J. W. Banding and Polarity of Actin Filaments in Interphase and Cleaving Cells. *Journal of Cell Biology* **1980**, *86* (2). https://doi.org/10.1083/jcb.86.2.568.

(290) Pollard, T. D.; Wu, J. Q. Understanding Cytokinesis: Lessons from Fission Yeast. *Nature Reviews Molecular Cell Biology*. 2010. https://doi.org/10.1038/nrm2834.

(291) Chen, Q.; Pollard, T. D. Actin Filament Severing by Cofilin Is More Important for Assembly than Constriction of the Cytokinetic Contractile Ring. *Journal of Cell Biology* **2011**, *195* (3). https://doi.org/10.1083/jcb.201103067.

(292) Balasubramanian, M. K.; McCollum, D.; Chang, L.; Wong, K. C. Y.; Naqvi, N. I.; He, X.; Sazer, S.; Gould, K. L. Isolation and Characterization of New Fission Yeast Cytokinesis Mutants. *Genetics* **1998**, *149* (3). https://doi.org/10.1093/genetics/149.3.1265.

(293) Chang, F.; Drubin, D.; Nurse, P. Cdc12p, a Protein Required for Cytokinesis in Fission Yeast, Is a Component of the Cell Division Ring and Interacts with Profilin. *Journal of Cell Biology* **1997**, *137* (1). https://doi.org/10.1083/jcb.137.1.169.

(294) Wu, J. Q.; Kuhn, J. R.; Kovar, D. R.; Pollard, T. D. Spatial and Temporal Pathway for Assembly and Constriction of the Contractile Ring in Fission Yeast Cytokinesis. *Dev Cell* **2003**, *5* (5). https://doi.org/10.1016/S1534-5807(03)00324-1.

(295) Laplante, C.; Berro, J.; Karatekin, E.; Hernandez-Leyva, A.; Lee, R.; Pollard, T. D. Three Myosins Contribute Uniquely to the Assembly and Constriction of the Fission Yeast Cytokinetic Contractile Ring. *Current Biology* **2015**, *25* (15). https://doi.org/10.1016/j.cub.2015.06.018.

(296) Mishra, M.; Kashiwazaki, J.; Takagi, T.; Srinivasan, R.; Huang, Y.; Balasubramanian, M. K.; Mabuchi, I. In Vitro Contraction of Cytokinetic Ring Depends on Myosin II but Not on Actin Dynamics. *Nat Cell Biol* **2013**, *15* (7). https://doi.org/10.1038/ncb2781.

(297) Dekker, N.; Speijer, D.; Grün, C. H.; Van Den Berg, M.; De Haan, A.; Hochstenbach, F. Role of the α-Glucanase Agn1p in Fission-Yeast Cell Separation. *Mol Biol Cell* **2004**, *15* (8). https://doi.org/10.1091/mbc.E04-04-0319.

(298) Muñoz, J.; Cortés, J. C. G.; Sipiczki, M.; Ramos, M.; Clemente-Ramos, J. A.; Moreno, M. B.; Martins, I. M.; Pérez, P.; Ribas, J. C. Extracellular Cell Wall β(1,3)Glucan Is Required to Couple Septation to Actomyosin Ring Contraction. *Journal of Cell Biology* **2013**, *203* (2). https://doi.org/10.1083/jcb.201304132.

(299) García Cortés, J. C.; Ramos, M.; Osumi, M.; Pérez, P.; Ribas, J. C. The Cell Biology of Fission Yeast Septation. *Microbiology and Molecular Biology Reviews* **2016**, *80* (3). https://doi.org/10.1128/mmbr.00013-16.

(300) Sipiczki, M. Splitting of the Fission Yeast Septum. *FEMS Yeast Research*. 2007. https://doi.org/10.1111/j.1567-1364.2007.00266.x.

(301) Zhou, Z.; Munteanu, E. L.; He, J.; Ursell, T.; Bathe, M.; Huang, K. C.; Chang, F. The Contractile Ring Coordinates Curvature-Dependent Septum Assembly during Fission Yeast Cytokinesis. *Mol Biol Cell* **2015**, *26* (1). https://doi.org/10.1091/mbc.E14-10-1441.

(302) Thiyagarajan, S.; Munteanu, E. L.; Arasada, R.; Pollard, T. D.; O'Shaughnessy, B. The Fission Yeast Cytokinetic Contractile Ring Regulates Septum Shape and Closure. *J Cell Sci* **2015**, *128* (19). https://doi.org/10.1242/jcs.166926.

(303) Proctor, S. A.; Minc, N.; Boudaoud, A.; Chang, F. Contributions of Turgor Pressure, the Contractile Ring, and Septum Assembly to Forces in Cytokinesis in Fission Yeast. *Current Biology* **2012**, *22* (17). https://doi.org/10.1016/j.cub.2012.06.042.

(304) Abenza, J. F.; Couturier, E.; Dodgson, J.; Dickmann, J.; Chessel, A.; Dumais, J.; Carazo Salas, R. E. Wall Mechanics and Exocytosis Define the Shape of Growth Domains in Fission Yeast. *Nat Commun* **2015**, *6*. https://doi.org/10.1038/ncomms9400.

(305) Pinheiro, D.; Hannezo, E.; Herszterg, S.; Bosveld, F.; Gaugue, I.; Balakireva, M.; Wang, Z.; Cristo, I.; Rigaud, S. U.; Markova, O.; Bellaïche, Y. Transmission of Cytokinesis Forces via E-Cadherin Dilution and Actomyosin Flows. *Nature* **2017**, *545* (7652). https://doi.org/10.1038/nature22041.

(306) Effler, J. C.; Kee, Y. S.; Berk, J. M.; Tran, M. N.; Iglesias, P. A.; Robinson, D. N. N. Mitosis-Specific Mechanosensing and Contractile-Protein Redistribution Control Cell Shape. *Current Biology* **2006**, *16* (19). https://doi.org/10.1016/j.cub.2006.08.027.

(307) Hughes, J.; Ward, C. J.; Peral, B.; Aspinwall, R.; Clark, K.; Millán, J. L. S.; Gamble, V.; Harris, P. C. The Polycystic Kidney Disease 1 (PKD1) Gene Encodes a Novel Protein with Multiple Cell Recognition Domains. *Nat Genet* **1995**, *10* (2). https://doi.org/10.1038/ng0695-151.

(308) Mochizuki, T.; Wu, G.; Hayashi, T.; Xenophontos, S. L.; Veldhuisen, B.; Saris, J. J.; Reynolds, D. M.; Cai, Y.; Gabow, P. A.; Pierides, A.; Kimberling, W. J.; Breuning, M. H.; Deltas, C. C.; Peters, D. J. M.; Somlo, S. PKD2, a Gene for Polycystic Kidney Disease That Encodes an Integral Membrane Protein. *Science (1979)* **1996**, *272* (5266). https://doi.org/10.1126/science.272.5266.1339.

(309) Barr, M. M.; Sternberg, P. W. A Polycystic Kidney-Disease Gene Homologue Required for Male Mating Behaviour in C. Elegans. *Nature* **1999**, *401* (6751). https://doi.org/10.1038/43913.

(310) Gao, Z.; Ruden, D. M.; Lu, X. PKD2 Cation Channel Is Required for Directional Sperm Movement and Male Fertility. *Current Biology* **2003**, *13* (24). https://doi.org/10.1016/j.cub.2003.11.053.

(311) Lima, W. C.; Vinet, A.; Pieters, J.; Cosson, P. Role of PKD2 in Rheotaxis in Dictyostelium. *PLoS One* **2014**, *9* (2). https://doi.org/10.1371/journal.pone.0088682.

(312) Huang, K.; Diener, D. R.; Mitchell, A.; Pazour, G. J.; Witman, G. B.; Rosenbaum, J. L. Function and Dynamics of PKD2 in Chlamydomonas Reinhardtii Flagella. *Journal of Cell Biology* **2007**, *179* (3). https://doi.org/10.1083/jcb.200704069.

(313) Palmer, C. P.; Aydar, E.; Djamgoz, M. B. A. A Microbial TRP-like Polycystic-Kidney-Disease-Related Ion Channel Gene. *Biochemical Journal* **2005**, *387* (1). https://doi.org/10.1042/BJ20041710.

(314) Morris, Z.; Sinha, D.; Poddar, A.; Morris, B.; Chen, Q. Fission Yeast TRP Channel Pkd2p Localizes to the Cleavage Furrow and Regulates Cell Separation during Cytokinesis. *Mol Biol Cell* **2019**. https://doi.org/10.1091/mbc.E18-04-0270.

(315) Sinha, D.; Ivan, D.; Gibbs, E.; Chetluru, M.; Goss, J.; Chen, Q. Fission Yeast Polycystin Pkd2p Promotes Cell Size Expansion and Antagonizes the Hippo-Related SIN Pathway. *J Cell Sci* **2022**, *135* (4). https://doi.org/10.1242/jcs.259046.

(316) Poddar, A.; Sidibe, O.; Ray, A.; Chen, Q. Calcium Spikes Accompany Cleavage Furrow Ingression and Cell Separation during Fission Yeast Cytokinesis. *Mol Biol Cell* **2021**, *32* (1). https://doi.org/10.1091/MBC.E20-09-0609.

(317) Laohakunakorn, N.; Grasemann, L.; Lavickova, B.; Michielin, G.; Shahein, A.; Swank, Z.; Maerkl, S. J. Bottom-Up Construction of Complex Biomolecular Systems With Cell-

Free Synthetic Biology. *Frontiers in Bioengineering and Biotechnology*. 2020. https://doi.org/10.3389/fbioe.2020.00213.

(318) Knol, J.; Sjollema, K.; Poolman, B. Detergent-Mediated Reconstitution of Membrane Proteins. *Biochemistry* **1998**. https://doi.org/10.1021/bi981596u.

(319) Rigaud, J.-L.; Lévy, D. Reconstitution of Membrane Proteins into Liposomes; 2003. https://doi.org/10.1016/S0076-6879(03)72004-7.

(320) Jia, B.; Jeon, C. O. High-Throughput Recombinant Protein Expression in Escherichia Coli: Current Status and Future Perspectives. *Open Biology*. 2016. https://doi.org/10.1098/rsob.160196.

(321) Shen, P. S.; Yang, X.; DeCaen, P. G.; Liu, X.; Bulkley, D.; Clapham, D. E.; Cao, E. The Structure of the Polycystic Kidney Disease Channel PKD2 in Lipid Nanodiscs. *Cell* **2016**, *167* (3). https://doi.org/10.1016/j.cell.2016.09.048.

(322) Rigaud, J. L.; Pitard, B.; Levy, D. Reconstitution of Membrane Proteins into Liposomes: Application to Energy-Transducing Membrane Proteins. *BBA - Bioenergetics*. 1995. https://doi.org/10.1016/0005-2728(95)00091-V.

(323) Chong, S. Overview of Cell-Free Protein Synthesis: Historic Landmarks, Commercial Systems, and Expanding Applications. *Curr Protoc Mol Biol* **2014**. https://doi.org/10.1002/0471142727.mb1630s108.

(324) Gregorio, N. E.; Levine, M. Z.; Oza, J. P. A User's Guide to Cell-Free Protein Synthesis. *Methods and Protocols*. 2019. https://doi.org/10.3390/mps2010024.

(325) Khambhati, K.; Bhattacharjee, G.; Gohil, N.; Braddick, D.; Kulkarni, V.; Singh, V. Exploring the Potential of Cell-Free Protein Synthesis for Extending the Abilities of

Biological Systems. *Frontiers in Bioengineering and Biotechnology*. 2019. https://doi.org/10.3389/fbioe.2019.00248.

(326) Majumder, S.; Liu, A. P. Bottom-up Synthetic Biology: Modular Design for Making Artificial Platelets. *Phys Biol* **2018**, *15* (1). https://doi.org/10.1088/1478-3975/aa9768.

(327) Dondapati, S. K.; Lübberding, H.; Zemella, A.; Thoring, L.; Wüstenhagen, D. A.; Kubick, S. Functional Reconstitution of Membrane Proteins Derived from Eukaryotic Cell-Free Systems. *Front Pharmacol* **2019**, *10* (JULY). https://doi.org/10.3389/fphar.2019.00917.

(328) Xu, S.; Cramer, W. A.; Peterson, A. A.; Hermodson, M.; Montecucco, C. Dynamic Properties of Membrane Proteins: Reversible Insertion into Membrane Vesicles of a Colicin E1 Channel-Forming Peptide. *Proc Natl Acad Sci U S A* **1988**, *85* (20). https://doi.org/10.1073/pnas.85.20.7531.

(329) Neumann, S.; Pucadyil, T. J.; Schmid, S. L. Analyzing Membrane Remodeling and Fission Using Supported Bilayers with Excess Membrane Reservoir. *Nat Protoc* **2013**, *8* (1), 213–222. https://doi.org/10.1038/nprot.2012.152.

(330) Pucadyil, T. J.; Schmid, S. L. Real-Time Visualization of Dynamin-Catalyzed Membrane Fission and Vesicle Release. *Cell* **2008**, *135* (7). https://doi.org/10.1016/j.cell.2008.11.020.

(331) González-Perrett, S.; Kim, K.; Ibarra, C.; Damiano, A. E.; Zotta, E.; Batelli, M.; Harris, P. C.; Reisin, I. L.; Arnaout, M. A.; Cantiello, H. F. Polycystin-2, the Protein Mutated in Autosomal Dominant Polycystic Kidney Disease (ADPKD), Is a Ca2+-Permeable Nonselective Cation Channel. *Proc Natl Acad Sci U S A* **2001**. https://doi.org/10.1073/pnas.98.3.1182.

(332) Protchenko, O.; Rodriguez-Suarez, R.; Androphy, R.; Bussey, H.; Philpott, C. C. A Screen for Genes of Heme Uptake Identifies the FLC Family Required for Import of FAD into the Endoplasmic Reticulum. *Journal of Biological Chemistry* **2006**, *281* (30). https://doi.org/10.1074/jbc.M512812200.

(333) Jumper, J.; Evans, R.; Pritzel, A.; Green, T.; Figurnov, M.; Ronneberger, O.; Tunyasuvunakool, K.; Bates, R.; Žídek, A.; Potapenko, A.; Bridgland, A.; Meyer, C.; Kohl, S. A. A.; Ballard, A. J.; Cowie, A.; Romera-Paredes, B.; Nikolov, S.; Jain, R.; Adler, J.; Back, T.; Petersen, S.; Reiman, D.; Clancy, E.; Zielinski, M.; Steinegger, M.; Pacholska, M.; Berghammer, T.; Bodenstein, S.; Silver, D.; Vinyals, O.; Senior, A. W.; Kavukcuoglu, K.; Kohli, P.; Hassabis, D. Highly Accurate Protein Structure Prediction with AlphaFold. *Nature* **2021**, *596* (7873). https://doi.org/10.1038/s41586-021-03819-2.

(334) Bashirzadeh, Y.; Wubshet, N.; Litschel, T.; Schwille, P.; Liu, A. P. Rapid Encapsulation of Reconstituted Cytoskeleton inside Giant Unilamellar Vesicles. *Journal of Visualized Experiments* **2021**, No. 177. https://doi.org/10.3791/63332.

(335) Van De Cauter, L.; Fanalista, F.; Van Buren, L.; De Franceschi, N.; Godino, E.; Bouw, S.; Danelon, C.; Dekker, C.; Koenderink, G. H.; Ganzinger, K. A. Optimized CDICE for Efficient Reconstitution of Biological Systems in Giant Unilamellar Vesicles. *ACS Synth Biol* **2021**, *10* (7). https://doi.org/10.1021/acssynbio.1c00068.

(336) Cai, Y.; Maeda, Y.; Cedzich, A.; Torres, V. E.; Wu, G.; Hayashi, T.; Mochizuki, T.; Park, J. H.; Witzgall, R.; Somlo, S. Identification and Characterization of Polycystin-2, the PKD2 Gene Product. *Journal of Biological Chemistry* **1999**, *274* (40). https://doi.org/10.1074/jbc.274.40.28557.

(337) Batiza, A. F.; Schulz, T.; Masson, P. H. Yeast Respond to Hypotonic Shock with a Calcium Pulse. *Journal of Biological Chemistry* **1996**, *271* (38). https://doi.org/10.1074/jbc.271.38.23357.

(338) Nakayama, Y.; Yoshimura, K.; Iida, H. Organellar Mechanosensitive Channels in Fission Yeast Regulate the Hypo-Osmotic Shock Response. *Nat Commun* **2012**, *3*. https://doi.org/10.1038/ncomms2014.

(339) Liu, X.; Vien, T.; Duan, J.; Sheu, S. H.; DeCaen, P. G.; Clapham, D. E. Polycystin-2 Is an Essential Ion Channel Subunit in the Primary Cilium of the Renal Collecting Duct Epithelium. *Elife* **2018**. https://doi.org/10.7554/eLife.33183.

(340) Wang, Z.; Ng, C.; Liu, X.; Wang, Y.; Li, B.; Kashyap, P.; Chaudhry, H. A.; Castro, A.; Kalontar, E. M.; Ilyayev, L.; Walker, R.; Alexander, R. T.; Qian, F.; Chen, X.; Yu, Y. The Ion Channel Function of Polycystin-1 in the Polycystin-1/Polycystin-2 Complex. *EMBO Rep* **2019**, *20* (11). https://doi.org/10.15252/embr.201948336.

(341) Forman, J. R.; Qamar, S.; Paci, E.; Sandford, R. N.; Clarke, J. The Remarkable Mechanical Strength of Polycystin-1 Supports a Direct Role in Mechanotransduction. *J Mol Biol* **2005**, *349* (4). https://doi.org/10.1016/j.jmb.2005.04.008.

(342) Nauli, S. M.; Alenghat, F. J.; Luo, Y.; Williams, E.; Vassilev, P.; Li, X.; Elia, A. E. H.; Lu, W.; Brown, E. M.; Quinn, S. J.; Ingber, D. E.; Zhou, J. Polycystins 1 and 2 Mediate Mechanosensation in the Primary Cilium of Kidney Cells. *Nat Genet* **2003**, *33* (2), 129–137. https://doi.org/10.1038/ng1076.

(343) Zhou, X. L.; Kung, C. A Mechanosensitive Ion Channel in Schizosaccharomyces Pombe. *EMBO J* **1992**, *11* (8). https://doi.org/10.1002/j.1460-2075.1992.tb05355.x.

(344) Anyatonwu, G. I.; Ehrlich, B. E. Organic Cation Permeation through the Channel Formed by Polycystin-2. *Journal of Biological Chemistry* **2005**, *280* (33). https://doi.org/10.1074/jbc.M504359200.

(345) Kleene, S. J.; Kleene, N. K. The Native TRPP2-Dependent Channel of Murine Renal Primary Cilia. *Am J Physiol Renal Physiol* **2017**, *312* (1). https://doi.org/10.1152/ajprenal.00272.2016.

(346) Ha, K.; Nobuhara, M.; Wang, Q.; Walker, R. V.; Qian, F.; Schartner, C.; Cao, E.; Delling, M. The Heteromeric Pc-1/Pc-2 Polycystin Complex Is Activated by the Pc-1 n-Terminus. *Elife* **2020**, *9*. https://doi.org/10.7554/eLife.60684.

(347) Thurmond, D. C.; Gaisano, H. Y. Recent Insights into Beta-Cell Exocytosis in Type 2 Diabetes. *Journal of Molecular Biology*. 2020. https://doi.org/10.1016/j.jmb.2019.12.012.

(348) Südhof, T. C.; Rizo, J. Synaptic Vesicle Exocytosis. *Cold Spring Harb Perspect Biol* **2011**, *3* (12). https://doi.org/10.1101/cshperspect.a005637.

(349) Fitch-Tewfik, J. L.; Flaumenhaft, R. Platelet Granule Exocytosis: A Comparison with Chromaffin Cells. *Frontiers in Endocrinology*. 2013. https://doi.org/10.3389/fendo.2013.00077.

(350) Chitirala, P.; Ravichandran, K.; Galgano, D.; Sleiman, M.; Krause, E.; Bryceson, Y. T.; Rettig, J. Cytotoxic Granule Exocytosis from Human Cytotoxic T Lymphocytes Is Mediated by VAMP7. *Front Immunol* **2019**, *10* (AUG). https://doi.org/10.3389/fimmu.2019.01855.

(351) Cooper, S. T.; McNeil, P. L. Membrane Repair: Mechanisms and Pathophysiology. *Physiol Rev* **2015**, *95* (4). https://doi.org/10.1152/physrev.00037.2014.

(352) Chen, Y. A.; Scales, S. J.; Patel, S. M.; Doung, Y. C.; Scheller, R. H. SNARE Complex Formation Is Triggered by Ca2+ and Drives Membrane Fusion. *Cell* **1999**, *97* (2). https://doi.org/10.1016/S0092-8674(00)80727-8.

(353) Jahn, R.; Scheller, R. H. SNAREs - Engines for Membrane Fusion. *Nature Reviews Molecular Cell Biology*. 2006. https://doi.org/10.1038/nrm2002.

(354) Marsden, H. R.; Elbers, N. A.; Bomans, P. H. H.; Sommerdijk, N. A. J. M.; Kros, A. A Reduced SNARE Model for Membrane Fusion. *Angewandte Chemie - International Edition* **2009**, *48* (13). https://doi.org/10.1002/anie.200804493.

(355) Mora, N. L.; Boyle, A. L.; Kolck, B. J. van; Rossen, A.; Pokorná, Š.; Koukalová, A.; Šachl, R.; Hof, M.; Kros, A. Controlled Peptide-Mediated Vesicle Fusion Assessed by Simultaneous Dual-Colour Time-Lapsed Fluorescence Microscopy. *Sci Rep* **2020**, *10* (1). https://doi.org/10.1038/s41598-020-59926-z.

(356) Peruzzi, J. A.; Jacobs, M. L.; Vu, T. Q.; Wang, K. S.; Kamat, N. P. Barcoding Biological Reactions with DNA-Functionalized Vesicles. *Angewandte Chemie - International Edition* **2019**, *58* (51). https://doi.org/10.1002/anie.201911544.

(357) Stengel, G.; Zahn, R.; Höök, F. DNA-Induced Programmable Fusion of Phospholipid Vesicles. *J Am Chem Soc* **2007**, *129* (31). https://doi.org/10.1021/ja073200k.

(358) Insua, I.; Montenegro, J. Synthetic Supramolecular Systems in Life-like Materials and Protocell Models. *Chem*. 2020. https://doi.org/10.1016/j.chempr.2020.06.005.

(359) Angelova, M. I.; Dimitrov, D. S. Liposome Electroformation. *Faraday Discuss Chem Soc* **1986**, *81*. https://doi.org/10.1039/DC9868100303.

(360) Noireaux, V.; Libchaber, A. A Vesicle Bioreactor as a Step toward an Artificial Cell Assembly. *Proc Natl Acad Sci U S A* **2004**, *101* (51). https://doi.org/10.1073/pnas.0408236101.

(361) Eaglesfield, R.; Madsen, M. A.; Sanyal, S.; Reboud, J.; Amtmann, A. Cotranslational Recruitment of Ribosomes in Protocells Recreates a Translocon-Independent Mechanism of Proteorhodopsin Biogenesis. *iScience* **2021**, *24* (5). https://doi.org/10.1016/j.isci.2021.102429.

(362) McCartney, C. S. E.; MacLeod, J. A.; Greer, P. A.; Davies, P. L. An Easy-to-Use FRET Protein Substrate to Detect Calpain Cleavage in Vitro and in Vivo. *Biochim Biophys Acta Mol Cell Res* **2018**, *1865* (2). https://doi.org/10.1016/j.bbamcr.2017.10.013.

(363) McCartney, C. S. E.; Davies, P. L. FRET-Based Assays to Determine Calpain Activity. In *Methods in Molecular Biology*; 2019; Vol. 1915. https://doi.org/10.1007/978-1-4939-8988-1_4.

(364) Cuerrier, D.; Moldoveanu, T.; Davies, P. L. Determination of Peptide Substrate Specificity for μ-Calpain by a Peptide Library-Based Approach: The Importance of Primed Side Interactions. *Journal of Biological Chemistry* **2005**, *280* (49). https://doi.org/10.1074/jbc.M506870200.

(365) Altamura, E.; Milano, F.; Tangorra, R. R.; Trotta, M.; Omar, O. H.; Stano, P.; Mavelli, F. Highly Oriented Photosynthetic Reaction Centers Generate a Proton Gradient in Synthetic Protocells. *Proc Natl Acad Sci U S A* **2017**, *114* (15). https://doi.org/10.1073/pnas.1617593114.

(366) Hsu, Y. Y.; Chen, S. J.; Bernal-Chanchavac, J.; Sharma, B.; Moghimianavval, H.; Stephanopoulos, N.; Liu, A. P. Calcium-Triggered DNA-Mediated Membrane Fusion in

Synthetic Cells. *Chemical Communications* **2023**, *59* (57). https://doi.org/10.1039/d3cc02204h.

(367) Dalal, P. J.; Muller, W. A.; Sullivan, D. P. Endothelial Cell Calcium Signaling during Barrier Function and Inflammation. *American Journal of Pathology*. 2020. https://doi.org/10.1016/j.ajpath.2019.11.004.

(368) Ghibelli, L.; Cerella, C.; Diederich, M. The Dual Role of Calcium as Messenger and Stressor in Cell Damage, Death, and Survival. *International Journal of Cell Biology*. 2010. https://doi.org/10.1155/2010/546163.

(369) Malla, M.; Sinha, D.; Chowdhury, P.; Thomas Bisesi, B.; Chen, Q. The Cytoplasmic Tail of the Mechanosensitive Channel Pkd2 Regulates Its Internalization and Clustering in Eisosomes. *J Cell Sci* **2023**, *136* (12). https://doi.org/10.1242/jcs.260598.

(370) González-Bermúdez, B.; Guinea, G. V.; Plaza, G. R. Advances in Micropipette Aspiration: Applications in Cell Biomechanics, Models, and Extended Studies. *Biophysical Journal*. 2019. https://doi.org/10.1016/j.bpj.2019.01.004.

(371) Altendorf, K.; Booth, I. R.; Gralla, J.; Greie, J.-C.; Rosenthal, A. Z.; Wood, J. M. Osmotic Stress. *EcoSal Plus* **2009**, *3* (2). https://doi.org/10.1128/ecosalplus.5.4.5.

(372) Haase, K.; Pelling, A. E. Investigating Cell Mechanics with Atomic Force Microscopy. *Journal of the Royal Society Interface*. 2015. https://doi.org/10.1098/rsif.2014.0970.

(373) Guck, J.; Ananthakrishnan, R.; Mahmood, H.; Moon, T. J.; Cunningham, C. C.; Käs, J. The Optical Stretcher: A Novel Laser Tool to Micromanipulate Cells. *Biophys J* **2001**, *81* (2). https://doi.org/10.1016/S0006-3495(01)75740-2.

(374) Usami, S.; Chen, H. H.; Zhao, Y.; Chien, S.; Skalak, R. Design and Construction of a Linear Shear Stress Flow Chamber. *Ann Biomed Eng* **1993**, *21* (1). https://doi.org/10.1007/BF02368167.

(375) Buddingh', B. C.; Elzinga, J.; van Hest, J. C. M. Intercellular Communication between Artificial Cells by Allosteric Amplification of a Molecular Signal. *Nat Commun* **2020**, *11* (1). https://doi.org/10.1038/s41467-020-15482-8.

(376) Lentini, R.; Martín, N. Y.; Forlin, M.; Belmonte, L.; Fontana, J.; Cornella, M.; Martini, L.; Tamburini, S.; Bentley, W. E.; Jousson, O.; Mansy, S. S. Two-Way Chemical Communication between Artificial and Natural Cells. *ACS Cent Sci* **2017**, *3* (2). https://doi.org/10.1021/acscentsci.6b00330.

(377) Kim, B. S.; Park, I. K.; Hoshiba, T.; Jiang, H. L.; Choi, Y. J.; Akaike, T.; Cho, C. S. Design of Artificial Extracellular Matrices for Tissue Engineering. *Progress in Polymer Science (Oxford)*. 2011. https://doi.org/10.1016/j.progpolymsci.2010.10.001.

(378) Khanna, A.; Zamani, M.; Huang, N. F. Extracellular Matrix-Based Biomaterials for Cardiovascular Tissue Engineering. *Journal of Cardiovascular Development and Disease*. 2021. https://doi.org/10.3390/jcdd8110137.

(379) Sukharev, S. I.; Sigurdson, W. J.; Kung, C.; Sachs, F. Energetic and Spatial Parameters for Gating of the Bacterial Large Conductance Mechanosensitive Channel, MscL. *Journal of General Physiology* **1999**, *113* (4). https://doi.org/10.1085/jgp.113.4.525.

(380) Yoshimura, K.; Batiza, A.; Schroeder, M.; Blount, P.; Kung, C. Hydrophilicity of a Single Residue within MscL Correlates with Increased Channel Mechanosensitivity. *Biophys J* **1999**, *77* (4). https://doi.org/10.1016/S0006-3495(99)77037-2.

(381) DeStefano, J. G.; Xu, Z. S.; Williams, A. J.; Yimam, N.; Searson, P. C. Effect of Shear Stress on IPSC-Derived Human Brain Microvascular Endothelial Cells (DhBMECs). *Fluids Barriers CNS* **2017**, *14* (1). https://doi.org/10.1186/s12987-017-0068-z.

(382) Shojima, M. Magnitude and Role of Wall Shear Stress on Cerebral Aneurysm. Computational Fluid Dynamic Study of 20 Middle Cerebral Artery Aneurysms. *Stroke* **2004**. https://doi.org/10.1161/01.str.0000144648.89172.of.

(383) Davies, P. F.; Spaan, J. A.; Krams, R. Shear Stress Biology of the Endothelium. *Ann Biomed Eng* **2005**, *33* (12 SPEC. ISS.). https://doi.org/10.1007/s10439-005-8774-0.

(384) Davies, P. F. Hemodynamic Shear Stress and the Endothelium in Cardiovascular Pathophysiology. *Nature Clinical Practice Cardiovascular Medicine*. 2009. https://doi.org/10.1038/ncpcardio1397.

(385) Chiu, J. J.; Chien, S. Effects of Disturbed Flow on Vascular Endothelium: Pathophysiological Basis and Clinical Perspectives. *Physiological Reviews*. 2011. https://doi.org/10.1152/physrev.00047.2009.

(386) Bao, P.; Kodra, A.; Tomic-Canic, M.; Golinko, M. S.; Ehrlich, H. P.; Brem, H. The Role of Vascular Endothelial Growth Factor in Wound Healing. *Journal of Surgical Research*. 2009. https://doi.org/10.1016/j.jss.2008.04.023.

(387) Bernatchez, P. N.; Soker, S.; Sirois, M. G. Vascular Endothelial Growth Factor Effect on Endothelial Cell Proliferation, Migration, and Platelet-Activating Factor Synthesis Is Flk-1- Dependent. *Journal of Biological Chemistry* **1999**, *274* (43). https://doi.org/10.1074/jbc.274.43.31047.

(388) Shibuya, M. Vascular Endothelial Growth Factor (VEGF) and Its Receptor (VEGFR) Signaling in Angiogenesis: A Crucial Target for Anti- and Pro-Angiogenic Therapies. *Genes Cancer* **2011**, *2* (12). https://doi.org/10.1177/1947601911423031.

(389) Leppänen, V. M.; Prota, A. E.; Jeltsch, M.; Anisimov, A.; Kalkkinen, N.; Strandin, T.; Lankinen, H.; Goldman, A.; Ballmer-Hofer, K.; Alitalo, K. Structural Determinants of Growth Factor Binding and Specificity by VEGF Receptor 2. *Proc Natl Acad Sci U S A* **2010**, *107* (6). https://doi.org/10.1073/pnas.0914318107.

(390) de la Cova, C.; Townley, R.; Regot, S.; Greenwald, I. A Real-Time Biosensor for ERK Activity Reveals Signaling Dynamics during C. Elegans Cell Fate Specification. *Dev Cell* **2017**, *42* (5). https://doi.org/10.1016/j.devcel.2017.07.014.

(391) Calder, B. W.; Matthew Rhett, J.; Bainbridge, H.; Fann, S. A.; Gourdie, R. G.; Yost, M. J. Inhibition of Connexin 43 Hemichannel-Mediated ATP Release Attenuates Early Inflammation during the Foreign Body Response. *Tissue Eng Part A* **2015**, *21* (11–12). https://doi.org/10.1089/ten.tea.2014.0651.

(392) Diezmos, E. F.; Bertrand, P. P.; Liu, L. Purinergic Signaling in Gut Inflammation: The Role of Connexins and Pannexins. *Frontiers in Neuroscience*. 2016. https://doi.org/10.3389/fnins.2016.00311.

(393) Rhett, J. M.; Calder, B. W.; Fann, S. A.; Bainbridge, H.; Gourdie, R. G.; Yost, M. J. Mechanism of Action of the Anti-Inflammatory Connexin43 Mimetic Peptide JM2. *Am J Physiol Cell Physiol* **2017**, *313* (3). https://doi.org/10.1152/ajpcell.00229.2016.

(394) Lussier, F.; Staufer, O.; Platzman, I.; Spatz, J. P. Can Bottom-Up Synthetic Biology Generate Advanced Drug-Delivery Systems? *Trends in Biotechnology*. 2021. https://doi.org/10.1016/j.tibtech.2020.08.002.

(395) Goh, W. J.; Lee, C. K.; Zou, S.; Woon, E. C. Y.; Czarny, B.; Pastorin, G. Doxorubicin-Loaded Cell-Derived Nanovesicles: An Alternative Targeted Approach for Anti-Tumor Therapy. *Int J Nanomedicine* **2017**, *12*. https://doi.org/10.2147/IJN.S131786.

(396) Nadas, J.; Sun, D. Anthracyclines as Effective Anticancer Drugs. *Expert Opinion on Drug Discovery*. 2006. https://doi.org/10.1517/17460441.1.6.549.

(397) Narvekar, M.; Xue, H. Y.; Eoh, J. Y.; Wong, H. L. Nanocarrier for Poorly Water-Soluble Anticancer Drugs - Barriers of Translation and Solutions. *AAPS PharmSciTech*. 2014. https://doi.org/10.1208/s12249-014-0107-x.

(398) Felgner, P. L.; Gadek, T. R.; Holm, M.; Roman, R.; Chan, H. W.; Wenz, M.; Northrop, J. P.; Ringold, G. M.; Danielsen, M. Lipofection: A Highly Efficient, Lipid-Mediated DNA-Transfection Procedure. *Proc Natl Acad Sci U S A* **1987**, *84* (21). https://doi.org/10.1073/pnas.84.21.7413.

(399) Rytting, E.; Nguyen, J.; Wang, X.; Kissel, T. Biodegradable Polymeric Nanocarriers for Pulmonary Drug Delivery. *Expert Opinion on Drug Delivery*. 2008. https://doi.org/10.1517/17425247.5.6.629.

(400) Bookstaver, M. L.; Tsai, S. J.; Bromberg, J. S.; Jewell, C. M. Improving Vaccine and Immunotherapy Design Using Biomaterials. *Trends in Immunology*. 2018. https://doi.org/10.1016/j.it.2017.10.002.

(401) Li, Z.; Delaney, M. K.; O'Brien, K. A.; Du, X. Signaling during Platelet Adhesion and Activation. *Arterioscler Thromb Vasc Biol* **2010**, *30* (12). https://doi.org/10.1161/ATVBAHA.110.207522.

(402) Hickman, D. A.; Pawlowski, C. L.; Shevitz, A.; Luc, N. F.; Kim, A.; Girish, A.; Marks, J.; Ganjoo, S.; Huang, S.; Niedoba, E.; Sekhon, U. D. S.; Sun, M.; Dyer, M.; Neal, M. D.;

Kashyap, V. S.; Sen Gupta, A. Intravenous Synthetic Platelet (SynthoPlate) Nanoconstructs Reduce Bleeding and Improve “golden Hour” Survival in a Porcine Model of Traumatic Arterial Hemorrhage. *Sci Rep* **2018**, *8* (1). https://doi.org/10.1038/s41598-018-21384-z.

(403) Brown, A. C.; Stabenfeldt, S. E.; Ahn, B.; Hannan, R. T.; Dhada, K. S.; Herman, E. S.; Stefanelli, V.; Guzzetta, N.; Alexeev, A.; Lam, W. A.; Lyon, L. A.; Barker, T. H. Ultrasoft Microgels Displaying Emergent Platelet-like Behaviours. *Nat Mater* **2014**, *13* (12). https://doi.org/10.1038/nmat4066.

(404) Ma, H.; Jiang, Z.; Xu, J.; Liu, J.; Guo, Z. N. Targeted Nano-Delivery Strategies for Facilitating Thrombolysis Treatment in Ischemic Stroke. *Drug Deliv* **2021**, *28* (1). https://doi.org/10.1080/10717544.2021.1879315.

(405) Zhao, Y. Z.; Du, L. N.; Lu, C. T.; Jin, Y. G.; Ge, S. P. Potential and Problems in Ultrasound-Responsive Drug Delivery Systems. *International Journal of Nanomedicine*. 2013. https://doi.org/10.2147/IJN.S43589.

(406) Wang, X.; Tian, L.; Ren, Y.; Zhao, Z.; Du, H.; Zhang, Z.; Drinkwater, B. W.; Mann, S.; Han, X. Chemical Information Exchange in Organized Protocells and Natural Cell Assemblies with Controllable Spatial Positions. *Small* **2020**, *16* (27). https://doi.org/10.1002/smll.201906394.

(407) Silva, G. T.; Tian, L.; Franklin, A.; Wang, X.; Han, X.; Mann, S.; Drinkwater, B. W. Acoustic Deformation for the Extraction of Mechanical Properties of Lipid Vesicle Populations. *Phys Rev E* **2019**, *99* (6). https://doi.org/10.1103/PhysRevE.99.063002.

(408) Shapiro, M. G.; Goodwill, P. W.; Neogy, A.; Yin, M.; Foster, F. S.; Schaffer, D. V.; Conolly, S. M. Biogenic Gas Nanostructures as Ultrasonic Molecular Reporters. *Nat Nanotechnol* **2014**, *9* (4). https://doi.org/10.1038/nnano.2014.32.

(409) Lakshmanan, A.; Lu, G. J.; Farhadi, A.; Nety, S. P.; Kunth, M.; Lee-Gosselin, A.; Maresca, D.; Bourdeau, R. W.; Yin, M.; Yan, J.; Witte, C.; Malounda, D.; Foster, F. S.; Schröder, L.; Shapiro, M. G. Preparation of Biogenic Gas Vesicle Nanostructures for Use as Contrast Agents for Ultrasound and MRI. *Nat Protoc* **2017**, *12* (10). https://doi.org/10.1038/nprot.2017.081.

(410) Korin, N.; Kanapathipillai, M.; Matthews, B. D.; Crescente, M.; Brill, A.; Mammoto, T.; Ghosh, K.; Jurek, S.; Bencherif, S. A.; Bhatta, D.; Coskun, A. U.; Feldman, C. L.; Wagner, D. D.; Ingber, D. E. Shear-Activated Nanotherapeutics for Drug Targeting to Obstructed Blood Vessels. *Science (1979)* **2012**, *337* (6095). https://doi.org/10.1126/science.1217815.

(411) Xia, Y.; Shi, C.-Y.; Xiong, W.; Hou, X.-L.; Fang, J.-G.; Wang, W.-Q. Shear Stress-Sensitive Carriers for Localized Drug Delivery. *Curr Pharm Des* **2016**, *22* (38). https://doi.org/10.2174/1381612822666160628081419.

(412) Bark, D. L.; Ku, D. N. Wall Shear over High Degree Stenoses Pertinent to Atherothrombosis. *J Biomech* **2010**, *43* (15). https://doi.org/10.1016/j.jbiomech.2010.07.011.

(413) Peng, Z.; Pak, O. S.; Feng, Z.; Liu, A. P.; Young, Y. N. On the Gating of Mechanosensitive Channels by Fluid Shear Stress. *Acta Mechanica Sinica/Lixue Xuebao* **2016**, *32* (6). https://doi.org/10.1007/s10409-016-0606-y.

(414) Pak, O. S.; Young, Y. N.; Marple, G. R.; Veerapaneni, S.; Stone, H. A. Gating of a Mechanosensitive Channel Due to Cellular Flows. *Proc Natl Acad Sci U S A* **2015**, *112* (32). https://doi.org/10.1073/pnas.1512152112.

(415) Shibata, K.; Hashimoto, T.; Nobe, K.; Hasumi, K.; Honda, K. A Novel Finding of a Low-Molecular-Weight Compound, SMTP-7, Having Thrombolytic and Anti-Inflammatory Effects in Cerebral Infarction of Mice. *Naunyn Schmiedebergs Arch Pharmacol* **2010**, *382* (3). https://doi.org/10.1007/s00210-010-0542-5.

(416) Akamatsu, Y.; Saito, A.; Fujimura, M.; Shimizu, H.; Mekawy, M.; Hasumi, K.; Tominaga, T. Stachybotrys Microspora Triprenyl Phenol-7, a Novel Fibrinolytic Agent, Suppresses Superoxide Production, Matrix Metalloproteinase-9 Expression, and Thereby Attenuates Ischemia/Reperfusion Injury in Rat Brain. *Neurosci Lett* **2011**, *503* (2). https://doi.org/10.1016/j.neulet.2011.08.018.

(417) Hu, W.; Narasaki, R.; Nishimura, N.; Hasumi, K. SMTP (Stachybotrys Microspora Triprenyl Phenol) Enhances Clot Clearance in a Pulmonary Embolism Model in Rats. *Thromb J* **2012**, *10*. https://doi.org/10.1186/1477-9560-10-2.

.